Author:
Martin, David John

Title:
The effect of bypass lanes and sealing-strips in shell-and-tube heat exchangers.

THE EFFECT OF BYPASS LANES AND SEALING-STRIPS IN SHELL-AND-TUBE HEAT EXCHANGERS

BY

David John Martin

A dissertation submitted for the degree of Doctor of Philosophy at the University of Bristol, Department of Mechanical Engineering.

JULY 1989

SUMMARY

In shell-and-tube heat exchangers there is an unavoidable clearance between the tube bundle and the shell wall. This clearance has a relatively low flow resistance and hence a relatively large proportion of the shell-side flow will pass through it, bypassing the tube bundle and thus avoiding the heat transfer surface. The clearance can be blocked by sealing-strips, which eliminate the gap and divert the bypassing flow back into the tube bundle. This thesis details an investigation of bypass lanes in shell-and-tube heat exchangers and the use of sealing-strips.

A model exchanger was designed and built to represent a rectangular tube bank in which the bypass lane width could be varied, sealing-strips could be inserted at various positions along the bypass to block completely the bypass wall-to-tube bundle clearance. For four different tube arrays, the pressure drop and exit bypass mass flow fraction were found for isothermal air flow over a range of total flow rates. Three different tube bank geometries were investigated,

i) with no bypass lane (ideal bundle),
ii) for a range of bypass lane widths,
iii) for a range of bypass lane widths blocked by various numbers of sealing-strips.

For one tube array type, flow distributions upstream of the tube bank were found using a hot-wire anemometer; from these results the inlet bypass flow fractions were estimated. From these studies it was found that ESDU generally overestimates the pressure drop coefficients when bypassing is present. Bell's (1960) correction factor generally underestimates the pressure drop coefficient when bypassing is present and overestimates the effect of sealing-strips in increasing the pressure drop over the bank.

The rectangular tube bank model was modified to represent a section of a cylindrical exchanger. The effect on the pressure drop over a bank with a non-uniform bypass lane width, in the flow direction, was investigated. It was found that the inverse root mean square of the bypass clearances best characterised the "effective" bypass clearance of the whole bank.

Flow visualisation studies were undertaken of shell-side flow in a cylindrical exchanger made of glass in which all leakage flows, except bypassing, were eliminated. From the dye traces produced, the shell-side flow was seen to be highly complex. For the geometries examined it appeared that there was little interchange of flow between the bypass and crossflow stream over the crossflow section of the exchanger, but that the bypass stream became crossflow at each window region, with crossflow transferring into the bypass lane. Sealing-strips were seen to produce a thorough mixing of the bypass and crossflow streams.

for my parents

ACKNOWLEDGEMENTS

I would like to take this opportunity to thank Dr. Y. R. Mayhew and Dr. M. A. Hollingsworth for their supervision and assistance while at Bristol University, and the technicians in the Mechanical Engineering workshop, in particular Mr. D. Neale.

I would like to thank Dr. L. Haseler for his supervision during the time spent at UKAEA Harwell, Dr. P. Murray for familiarising me with the flow visualisation rig and Mr. A. Diaper for his help with the flow visualisation investigation.

I am grateful to the Science and Engineering Research Council for their financial support of this research project and to HTFS, Harwell for their sponsorship.

Finally, I would like to thank Miss A. Davies for help with the diagrams in this thesis and Mr. P. Pover for his patience in typing it.

MEMORANDUM

The accompanying dissertation entitled "The Effect of Bypass Lanes and Sealing-Strips in Shell-and-Tube Heat Exchangers", is submitted in support of an application for the degree of Doctor of Philosophy in Engineering at the University of Bristol.

The dissertation is based on independent work by the candidate and all contributions from others have been acknowledged fully within the dissertation.

None of the work described has been, or is being, submitted for any other degree or diploma at this or any other University.

I hereby declare that the above statements are true.

D. J. Martin

July 1989

CONTENTS

LIST OF TABLES

7.16 Data for 1.375 in-line square bank with 1½S bypass.

7.17 Upstream velocity data for a 1.25 equilateral-triangle bank.

8.1 Data for 15.9mm bypass lane with no flow transfer, no tubes.

8.2 Data for 23.8mm bypass lane with no flow transfer, no tubes.

8.3 Data for 31.8mm bypass lane with no flow transfer, no tubes.

8.4 Data for 15.9mm bypass lane with no flow transfer, equivalent to 1½T bypass in a 1.25 equilateral-triangle bank.

8.5 Data for 23.8mm bypass lane with no flow transfer, equivalent to 2½T bypass in a 1.25 equilateral-triangle bank.

8.6 Data for 31.8mm bypass lane with no flow transfer, equivalent to 3½T bypass in a 1.25 equilateral-triangle bank.

8.7 Data for 15.9mm bypass lane with no flow transfer, equivalent to ½S bypass in a 1.25 in-line square bank.

8.8 Data for 31.8mm bypass lane with no flow transfer, equivalent to 1½S bypass in a 1.25 in-line square bank.

9.1 Data for 1.25 equilateral-triangle bank with ½T bypass and one sealing-strip.

9.2 Data for 1.25 equilateral-triangle bank with ½T bypass and two sealing-strips.

9.3 Data for 1.25 equilateral-triangle bank with ½T bypass and four sealing-strips.

9.4 Data for 1.25 equilateral-triangle bank with 1½T bypass and one sealing-strip.

9.5 Data for 1.25 equilateral-triangle bank with 1½T bypass and two sealing-strips.

9.6 Data for 1.25 equilateral-triangle bank with 1½T bypass and four sealing-strips.

9.7 Data for 1.25 equilateral-triangle bank with 2½T bypass and one sealing-strip.

9.8 Data for 1.25 equilateral-triangle bank with 2½T bypass and two sealing-strips.

9.9 Data for 1.25 equilateral-triangle bank with 2½T bypass and four sealing-strips.

9.10 Data for 1.25 equilateral-triangle bank with 3½T bypass and one sealing-strip.

9.11 Data for 1.25 equilateral-triangle bank with 3½T bypass and two sealing-strips.

List of Figures

Figure Number

5.3 Pressure drop coefficients for 1.25 equilateral-triangle bank having a 2½T bypass with and without the exit flow divided by a splitter plate.

5.4 Pressure drop coefficients for 1.25 equilateral-triangle bank having a 3½T bypass with and without the exit flow divided by a splitter plate.

6.1 Pressure drop coefficient for an ideal equilateral-triangle bank with a pitch-diameter ratio of 1.25.

6.2 Pressure drop coefficient for an ideal equilateral-triangle bank with a pitch-diameter ratio of 1.375.

6.3 Pressure drop coefficient for an ideal in-line square bank with a pitch-diameter ratio of 1.25.

6.4 Pressure drop coefficient for an ideal in-line square bank with a pitch-diameter ratio of 1.375.

6.5 The effect of bank length. Pressure drop coefficients for an ideal in-line square bank, with a pitch-diameter ratio of 1.375, having N = 7, 10 and 13.

7.1 Pressure drop coefficient for a 1.25 equilateral-triangle bank with bypassing, compared with the predictions of ESDU (1974).

7.2 Pressure drop coefficient for a 1.25 equilateral-triangle bank with bypassing, compared with the results of Bell's (1960) bypassing correction factor.

7.3 Pressure drop coefficient for a 1.25 equilateral-triangle bank with bypassing, compared with Lee's (1983) data.

7.4 Pressure drop coefficient for a 1.375 equilateral-triangle bank with bypassing, compared with the predictions of ESDU (1974).

7.5 Pressure drop coefficient for a 1.375 equilateral-triangle bank with bypassing, compared with the results of Bell's (1960) bypassing correction factor.

7.6 Pressure drop coefficient for a 1.25 in-line square bank with bypassing, compared with the predictions of ESDU (1974).

7.7 Pressure drop coefficient for a 1.25 in-line square bank with bypassing, compared with the results of Bell's (1960) bypassing correction factor.

7.8 Pressure drop coefficient for a 1.25 in-line square bank with bypassing, compared with Lee's (1983) data.

7.9 Pressure drop coefficient for a 1.375 in-line square bank, compared with the predictions of ESDU (1974).

NOMENCLATURE

Symbol

A_B	Total area of bypass section of bank, Fig. 3.4.
A_{Bmin}	Minimum bypass flow area, Fig. 3.4.
A_C	Total area of crossflow section of bank, Fig. 3.4.
A_{Ceff}	Effective crossflow area.
A_{Cmin}	Minimum crossflow area, Fig. 3.4.
A_H	Total heat transfer surface area of tube bank.
A_{min}	Minimum flow area through tube bank.
A_T	Total cross-sectional area of duct, Fig. 3.4.
b	Bypass width.
B_C	Baffle cut.
C'	Pressure loss coefficient.
D	Tube diameter.
D_B	Bypass clearance width.
D_e	Hydraulic diameter
D_s	Transverse clearance between tubes.
D_{sh}	Internal shell diameter.
D_v	Equivalent volumetric diameter, Fig. 2.2.
F	The ratio of minimum bypass flow area to the total minimum flow area.
f	Friction factor.
f_B	Friction factor of bypass.
f_C	Friction factor of crossflow.
G	Mass velocity at minimum flow area.
G_B	Mass velocity of bypass flow.
G_S	Mass velocity of shell-side flow.

k	Flow conductivity.
K	Overall pressure loss coefficient.
ℓ	Tube length.
L	Length of bank in longitudinal, i.e. flow, direction.
L'	Tube flow length through bank.
L_B	Length of bypass stream.
$\dot{m}_B$	Mass flow rate of bypass stream.
$\dot{m}_{Beff}$	Effective mass flow rate of bypass stream.
$\dot{m}_{Bexit}$	Mass flow rate of bypass stream on exit from the tube bank.
$\dot{m}_C$	Mass flow rate of crossflow stream.
$\dot{m}_{Cexit}$	Mass flow rate of crossflow stream on exit from the tube bank.
$\dot{m}_T$	Total mass flow rate
n	Number of tubes in bank transverse to flow direction.
N_B	Number of baffles.
N_C	Number of tube rows of 'pure crossflow' equivalent to one sealing-strip, see 9.4 for full description.
N_S	Number of sealing-strips.
N_T	Total number of tubes in bank.
N_X	Number of constrictions in flow direction.
P_x	Longitudinal tube pitch, Fig. 1.4.
P_y	Transverse tube pitch, Fig. 1.4.
P_t	Tube pitch, Fig. 1.4.
Δp	Pressure drop across tube bank.
Δp_B	Pressure drop across bypass stream.
Δp_{BP}	Pressure drop across tube bank with bypass.
Δp_d	Inlet and exit duct pressure drop.
Δp_I	Pressure drop across ideal tube bank, with no bypass.
$\Delta p_{measured}$	Measured pressure drop across tube bank.
Δp_s	Total shell-side pressure drop.

ν	Kinematic viscosity.
ξ_b	Pressure drop coefficient of bypass lane.
ξ_p	Pressure drop coefficient.
$\xi_{p'}$	Pressure drop coefficient, definition proprietary to HTFS.
ρ_m	Mean fluid density in bank.
ρ_1	Fluid density at entry to bank.
ρ_N	Fluid density at exit from bank.
ϕ	Bypass exit mass flow ratio.
ϕ_{eff}	Effective bypass mass flow ratio.
ϕ_{in}	Bypass inlet mass flow ratio.
ϕ_s	Exit bypass mass flow ratio, obtained with one sealing-strip present.

1. INTRODUCTION

1.1 SHELL-AND-TUBE HEAT EXCHANGERS

The most commonly used heat exchanger is the shell-and-tube type. It has many applications in the power generation, chemical and process industries, for both single- and two-phase flows. Shell-and-tube heat exchangers are major capital items in industrial plant and if their effectiveness can be improved, by increasing the heat transfer for a given pressure drop and by refining the design process so that the operating characteristics of the exchanger may be more closely matched to the specifications required, there would be reductions in both capital and running costs.

There are many different designs of shell-and-tube heat exchanger and the dimensions and numbers of tubes used vary widely, depending on the application. A typical shell-and-tube heat exchanger is shown in Fig. 1.1. One flow stream passes through the tubes (tube-side flow) and the other flows outside the tubes (shell-side flow). Heat transfer between the streams occurs at the tube-wall boundary. An exchanger consists of several principal components. The shell is a cylinder containing the shell-side fluid which may be at a high pressure or at sub-atmospheric pressure. The shell-side fluid enters and leaves the shell via nozzles. Under the inlet nozzle an impingement plate is mounted which prevents the incoming fluid damaging the tube bundle. The tubes run longitudinally through the shell. They are supported along their length by baffles which are held in place by tie rods. The baffles also guide the shell-side fluid back and forth across the tube bundle. The tubes are welded at each end to tubesheets, to which the tie rods are also fixed. If the tube bundle need not be removeable, the tubesheet may be an integral part of the shell or extend beyond the internal diameter and bolt between flanges on the shell and end head. But if the bundle needs to be removeable for cleaning on the shell-side, a U-tube bundle which has only one tubesheet, or a floating head type closure is used, see Figs. 1.2 and 1.3.

The floating head enables the tubesheet to be drawn through the shell to allow the tube bundle to be removed.

The exchanger shell consists of three basic parts: the front end head, the shell itself and the rear end head. Figs. 1.1 and 1.2 show two types of exchanger; for a full description of the various combinations of tube-side and shell-side pass arrangements and shell types used,see TEMA (1978).

The shell-side flow may ideally be considered in two parts. In the baffle overlap region, see Fig. 1.1, the fluid flows normal to the tube bundle (crossflow). At the end of this region the fluid is turned around the baffle tip to flow through the window, formed between the baffle tip and the shell, into the next overlap region; this flow is termed the window flow. The window flow consists of the transition from pure crossflow to longitudinal flow and back to crossflow.

In practice the general pattern of flow is dependent on the baffle spacing and the baffle cut; baffle cut = (1 - baffle height / shell internal diameter). These parameters affect the amount by which the flow deviates from the ideal pattern; whether the flow in the overlap region is normal to the tubes, i.e. ideal crossflow, and how far this normal flow extends into the window region.

The tubes can be arranged in many different configurations, Fig. 1.4. Typically for single-phase flow a 30° triangular array is used if the flow is clean. However if fouling is likely to occur, a 90° array is often used for turbulent flow and a 45° array for laminar flow as these types allow easier access for external tube cleaning when the bundle is removed.

1.2 Bypassing of the Tube Bundle

Bypassing occurs where fluid from the crossflow stream avoids flowing through the tube bundle and is caused by the existence of alternative, low resistance flow routes.

There are several causes of bypassing. The commonest is due to the unavoidable manufacturing clearance between the shell and the tube bundle, which in the case of pull-through floating head types may be relatively large, as there must be a clearance to allow one tubesheet to be withdrawn through the length of the shell, see Fig. 1.5. The effects of this type of bypassing can be reduced by inserting sealing-strips between the tube bundle and the shell-wall to block the gap. Sealing-strips are sheet metal strips which are attached to the baffles and force the bypass stream back into the tube bundle.

Another type of bypassing is the deliberate use of access lanes created by removing one or more rows of tubes. This is particularly common in power condensers where they are used to prevent air blanketing of the tubes by increasing the flow velocity. This results in an increase in heat transfer.

The bypass lane, however it is formed, is a route of relatively low resistance to the flow. Therefore, even in cases where the bypass area is small in relation to the overall flow area, a relatively large proportion of the flow will pass through it. Where the bypass lane is formed next to the shell wall it leads to a reduction of heat transfer as the shell of the exchanger is not a heat transfer surface.

1.3 Nature of Pressure Losses

Prandtl (1904) suggested that the flow of a real fluid over a solid surface may be considered in two parts: the boundary layer where the fluid velocity increases from zero at the surface to the free stream velocity, and the region beyond the boundary layer where the velocity gradients are small so that the effect of viscosity is negligible. In this second region the flow is essentially that of an ideal inviscid fluid. In the boundary layer the presence of large velocity gradients leads to the effects of shear stresses dominating the flow. The total drag on the body consists of two components: the resultant force at the body surface caused by the tangential stresses, which is known as the skin friction drag, and the resultant in the main flow direction

of the pressure forces normal to the body surface, which is known as the pressure, or form, drag. In the presence of a positive pressure gradient along the surface over which the fluid is flowing, separation of the boundary layer from the body surface can occur. Downstream of this separation point the flow is disturbed by large-scale eddies, this region being known as the wake. As a result of energy dissipation in the wake by the highly turbulent motion, pressure is not recovered behind the body and consequently the pressure drag is increased. Therefore for flow over a bluff body, such as a circular tube, where there is a relatively large wake the pressure drag will predominate. The position of the separation point and the size of the wake depends on the nature of the flow, characterised by its Reynolds number. Turbulent boundary layers are more resistant to separation than laminar ones, thus separation occurs later, resulting in a smaller wake and less pressure drag in proportion to the total drag.

The flow around a tube in a bank is influenced by the presence of the surrounding tubes and is dependent upon the arrangement and geometrical parameters of the bank. The main factors which affect the flow are the repeated contractions and expansions of the flow area in the flow direction, leading to acceleration losses, and the presence of tubes upstream which dictate the pressure and velocity distribution of the approaching flow.

1.4 Flow Models and Design Methods

There are various ways of modelling the flow through a shell-and-tube heat exchanger. One is to consider the flow as a single flow stream. The earliest methods based the pressure drop on a "total" flow length through the exchanger but later methods differentiated between crossflow and window flow. These methods did not directly consider bypassing or leakage flows.

The idealised flow pattern of alternating crossflow and window flow is affected by various flow leakage paths. This leads to the shell-side flow through an

exchanger having a complex three-dimensional nature. The pattern may be described, however, in terms of a series of one-dimensional flow streams. This concept was first introduced by Tinker (1948). These flow streams are, Fig. 1.6:

(A) the leakage stream through the annular spaces between the tubes and baffle holes,

(B) the crossflow stream passing through the tube bundle,

(C) the bypass stream passing around the outside of the tube bundle,

(E) the leakage stream passing between the baffle and the shell,

(F) the pass partition bypass stream, first introduced by Palen and Taborek (1969) to account for bundles with a tube pass partition in the direction of the flow.

Latest multistream design methods model the complex shell-side flow as a network representing these various possible flow paths. Such a model is analogous to an electrical network with differing resistances for each of the flow paths. An example of a network model is shown in Fig. 1.7. There are many other possible network models. The more realistically the network attempts to model the flow the more potentially accurate the method becomes. However, it also increases the complexity and requires more precise information on the relative sizes, interactions and flow resistances of all the flow streams.

Network models are solved iteratively by balancing the pressure drops over each flow path between the nodes where the flows recombine. Therefore, even for quite simple networks the method requires the use of a computer.

Another design method which takes account of the leakage flows is the non-iterative "semi-analytical" method. This considers the crossflow and window flow to be the essential flow stream with the other leakage streams influencing it to various degrees. Correction factors dependent on the geometry are applied to the ideal crossflow pressure drop and to the heat transfer coefficient of an ideal tube bank.

1.5 PURPOSE OF CURRENT RESEARCH

All design methods rely on experimental data to derive the various flow resistances and correction factors used in their models. Much information has been published on ideal "homogeneous" tube banks but scarcely any on the isolated effects of bypassing, leakage flows and access lanes. An ideal "homogeneous" tube bank is a rectangular bank, i.e., having a constant bank width in which there is no bypass lane, access lane or leakage flow.

The main objectives of the current research were to investigate the effects of bypassing and the use of sealing-strips, in isolation from other leakage flow effects, on single-phase flow over tube banks. From this more detailed understanding, flow network models can be refined and a more precise relationship between flow resistance, exchanger geometry and flow conditions for the bypass stream can be established. One specific question the results might help to answer is whether the flow streams B and C, in Fig. 1.6, can be considered separately or if there is a significant interaction between them so that a more complex network model is required.

2. LITERATURE SURVEY

There is a considerable amount of reliable information published about pressure losses in single-phase flow over ideal tube banks. A review of this work is given here because it is at present used as the basis of pressure drop equations derived for non-homogeneous tube banks, including those with bypassing flow; it is also used as the basis for some pressure drop calculation methods for condensing flows. There has been some research carried out using real exchangers in which the effects of bypassing and the use of sealing-strips has been noted but there is very little published work on direct investigations of the effects of bypassing. Details of the terms used to describe the geometrical features of a shell-and-tube exchanger are given in Fig. 2.1.

2.1 Pressure Losses of Flow Over Ideal Tube Banks

Monrad (1932) investigated the heat transfer from hot gases to a staggered bank of tubes. He also correlated pressure drop equations given by Reiher (1925) and Walker et al.(1927) into a general Fanning-type equation. For staggered tube banks he gives the equation:

$$\frac{\Delta p}{\rho u_{av}^2} = \frac{cN}{BD}\left[\frac{\mu}{\rho u_{av} BD}\right]^{0.24} \qquad (2.1)$$

where $c = 0.052m$, $B = 1.6, 1.7, 2.0, 2.2$ for $N = 5, 10, 20, 30$ rows of tubes respectively.

Pigott (1933) examined the flow of fluids in closed ducts, including ducts containing bundles of tubes. He produced a correlation in the form of a Fanning-

type equation using a constant friction factor for all tube bank arrays, but based on the mean curved fluid flow distance through the bundle

$$\Delta p = \frac{0.054\rho U_{max}{}^2 L'}{D_s}$$

where L' is the curved flow path through the tube bank. For an equilateral-triangle array:

$$L' = \frac{\pi N P_x}{3}$$

Thus,

$$\Delta p = \frac{0.0565 N \rho U_{max}{}^2 P_x}{D_s} \qquad (2.2)$$

Chilton and Genereaux (1933) studied the literature covering previous work in the field and compared the results, and the pressure drop correlations derived from them, of seven investigators including those mentioned above. They produced correlations, using the published data, for the overall pressure drop for crossflow through ideal tube banks based on the Fanning equation

$$\Delta p = \frac{4 f \rho u^2 L}{2D} \qquad (2.3)$$

where $f = \Phi(Re)$, the form of Re depending on the nature of the flow.

For laminar flow through a staggered bank an equation based on the friction loss alone is recommended, using the equivalent volumetric diameter, D_v, as the flows characteristic dimension, Fig. 2.2, D_v being a measure of the ratio of tube surface

area to free flow volume. They concluded that

$$\Delta p = \frac{4f\rho u_{max}^2 L}{2D_v} \tag{2.4}$$

where $f = 26.5\ (D_v u_{max}/\nu)^{-1}$, which applies for $D_v u_{max}/\nu < 100$.

For turbulent flow a correlation is suggested which is based on a model of the bank as a series of orifices, such that the pressure drop is proportional to the number of contractions and expansions the flow experiences within the bank,

$$\Delta p = \frac{4f\rho u_{max}^2 N}{2} \tag{2.5}$$

where $f = 0.75\ (D_s u_{max}/\nu)^{-0.2}$ for staggered banks

and $f = 0.33\ (D_s u_{max}/\nu)^{-0.2}$ for in-line banks.

This correlation uses the transverse tube clearance, D_s, as the characteristic dimension in the Reynolds number.

Chilton and Genereaux compared these equations with the correlations cited in the literature and it was found that they deviated least from the published data, falling within ±25%, which was an improvement over all the previous correlations.

Pierson (1937) obtained pressure drop data for the isothermal crossflow of air through a tube bank which consisted of ten rows of tubes, N, with nine tubes per row, n. Tests were carried out for a range of Re_D of 2 000 to 40 000 using 7.9mm diameter tubes in 38 different configurations, both in-line and staggered. It was found that the flow resistance of the tube banks varied considerably with the tube arrangement but no simple conclusions could be drawn. The majority of the tube configurations tested by Pierson are not commonly used. Most commercial exchangers are built to TEMA standards which recommend the four arrays shown in Fig. 1.4. Huge (1937) expanded Pierson's work by collecting pressure drop data for larger tubes sizes (12.7mm, 17.5mm and 80.8mm diameters) for the same

configurations and tube pitch-diameter ratios under similar flow conditions. The results were found to be consistent with Pierson's data, thus confirming the validity of applying the principle of similarity to tube banks despite variations in the ratio of tube length to tube diameter, or to the inter-tube spacing, for the range of Re_D covered. Grimison (1937) correlated the data of Pierson and Huge to produce a general expression for the pressure drop across a homogeneous tube bank,

$$\Delta p = 2.30\, f N_x \rho u_{max}^2 \qquad (2.6)$$

This equation treats the bank as a series of orifices formed by the successive constrictions in the flow path. The friction factor, f, includes entrance and exit effects and therefore it only strictly applies to a tube bank ten rows deep. Correction factors are given for smaller banks and it is suggested that for larger banks the correction factors are small enough to be neglected. Curves are given for f over a range of Reynolds numbers for the different tube configurations used. In Jakob's (1938) discussion of the previous three papers he questioned the use of the tube diameter as the characteristic dimension and proposed the use of the transverse clearance between the tubes. He argued that since the behaviour of flow through a tube bank is similar to flow through a series of orifices, the size of the orifice must characterise the pressure drop. However, Jakob used the Reynolds number based on the tube diameter for practical reasons. He produced two general equations for the friction factor, f, of equation 2.6, based on the above work,

$$f = (Re_D)^{-0.16}\left[0.25 + \frac{0.175}{(P_y/D-1)^{1.08}}\right] \qquad (2.7)$$

for staggered arrangements, and

$$f = (Re_D)^{-0.15}\left[0.044 + \frac{0.08P_x/D}{(P_y/D-1)}\right] \qquad (2.8)$$

for in-line arrangements.

The first term in these equations shows the influence of Reynolds number. The second term is a sum, the first term of which represents the pressure drop in the contractions and expansions in the bank and the form drag caused by flow over the tubes; this is greater for staggered than for in-line arrangements. The last term in the sum shows the influence of the tube pitch-diameter ratios in both the transverse and longitudinal directions. Jakob made some general observations about the results of Pierson, Huge and Grimison:

(a) f decreases with increasing Re_D;

(b) f is generally greater for staggered than for in-line arrangements for the same P_y/D;

(c) f increases with decreasing P_y/D;

(d) for the configurations tested, the influence of P_x/D was found to be small for staggered arrangements but f increases with P_x/D for the in-line arrangements.

Wallis and White (1938) investigated the pressure drop for air flow over two tube bank configurations: one staggered and one in-line. The staggered bank consisted of 12.7mm diameter tubes in an equilateral triangle array with a tube pitch of 19.1mm. The bank had seven rows with six tubes per row. The in-line bank was created by removing alternate rows from the staggered bank, leaving four tube rows. The form drag of individual tubes was measured by rotating a tube with a pressure tapping in its surface to record the pressure distribution around the tube. Total and static pressures were also measured longitudinally through the bank. It was found that the static pressure falls during flow over each tube row but recovers slightly before reaching the next row and that the static pressure continues to recover after the last row for three tube diameters. For both configurations it was found that the form drag of the first row was more than double that of any other tube row and that the second row had the least drag of all. By subtracting the total form drag, found from the individual tube measurements, from the total resistance of the bank, found from the total pressure drop between tappings before and after the bundle, the drag

contribution due to skin friction could be found. In both cases the skin friction was less than 7% of the total drag. They produced correlations of their results in the form of a resistance factor,

$$C = \frac{\Delta p}{u_{max}^2 \rho} \tag{2.9}$$

where $C = 0.31\ Re_{max}^{0.031}$ (2.10)

for the first tube row in both arrangements, and,

$$C = 2.7\ Re_{max}^{-0.22} \tag{2.11}$$

for all but the first tube rows for the in-line array, and,

$$C = 3.9\ Re_{max}^{-0.29} \tag{2.12}$$

for all but the first tube rows for the staggered array. It is noted that these formulae are valid only for the tube bank configurations tested.

Wallis and White also examined the effect on the total measured bank pressure drop caused by varying the position of the downstream pressure tapping. It was found that if it was positioned too close to the rear of the bank the static pressure drop measured was up to 15% higher than if the tapping was placed further downstream, where the pressure had recovered.

Gunter and Shaw (1945) tried several methods of producing a single correlation of pressure drop data. They proposed that the use of the equivalent volumetric diameter, D_v, as the characteristic dimension and of geometric correction factors gives a satisfactory correlation for both staggered and in-line cases,

$$\Delta p = f\left[\frac{G^2 L}{2\rho D_v}\right]\left[\frac{D_v}{P_y}\right]^{0.4}\left[\frac{\mu}{\mu_w}\right]^{-0.14}\left[\frac{P_x}{P_y}\right]^{0.6} \tag{2.13}$$

where $f = 180(Re_v)^{-1}$ (2.14)

for laminar flow,

and $f = 1.82(Re_v)^{-0.146}$ (2.15)

for turbulent flow,

where the transition point occurs at approximately $Re_v = 200$.

The authors claimed that this equation gives reliable results for a Re_v range of 0.01 to 300 000, for tube pitch-diameter ratios of 1.25 to 5 and for tube diameters of 0.51mm to 50.8mm.

Boucher and Lapple (1948) reviewed the data and correlations for pressure drop across tube banks published up to that date. The authors questioned the single correlation of Gunter and Shaw for all tube arrangements because the nature of the losses through each configuration is different, and they state that any attempt to allow for tube configuration in a single equation is merely an empirical representation of the data. However, they suggest that their use of equivalent volumetric diameter is the more fundamentally correct way of correlating the results for the laminar flow regime, where the losses are predominantly due to skin friction, although it is not applicable to the turbulent regime where the losses are due mainly to kinetic energy changes and impact losses. Nevertheless the authors recommend the use of Chilton and Genereaux's method for the laminar region, as it best represents the data, but they note that it is based on a very limited number of results.

For turbulent flow they recommend the use of the graphical correlation by Grimison. Jakob's empirical expressions of these curves, equations 2.7 and 2.8, only apply with any accuracy for transverse tube pitch-diameter ratios of 1.5 to 4.0 and yield large over-estimates of pressure drop for smaller or larger pitch-diameter ratios, approximately 50% for the commonly used ratio, P_y/D, of 1.25.

Bergelin, Brown and Doberstein (1952) obtained pressure drop data for flow over ideal tube banks. They tested equilateral-triangle arrays and square arrays, both in-line and rotated, for tube pitch-diameter ratios of 1.25 and 1.5. The tests were mainly in the transitional flow regime but some data were obtained for turbulent flows. It was found that the data could be predicted accurately by Grimison's correlation.

Kays and London (1955) investigated the pressure drop of flow over tube banks. They used a variety of staggered and in-line banks covering a range of transverse tube pitch-diameter ratios of 1.25 to 2.5 and a range of longitudinal tube pitch-diameter ratios of 0.75 to 1.50. They carried out tests for Reynolds number, Re_R, from 500 to 2 000 where

$$Re_R = \frac{4R_h G}{\mu} \tag{2.16}$$

in which R_h is the hydraulic radius given by

$$R_h = \frac{A_{min} L}{A_T} \tag{2.17}$$

They suggested that the pressure drop over a tube bank can be broken down into its constituent parts: entrance and exit losses, losses within the tube bank due to friction and losses caused by flow acceleration. Hence

$$\Delta p = \frac{u_{max}^2 \rho_1}{2} \left[(1 + (A_{min}/A_T)^2) \left[\frac{\rho_1}{\rho_N} - 1 \right] + f \frac{A_H}{A_{min}} \frac{\rho_1}{\rho_m} \right] \tag{2.18}$$

where A_H is the total heat transfer surface area in the tube bundle,

$$A_H = \pi D \ell N_T \tag{2.19}$$

and ρ_m = mean fluid density within the bank.

The friction factor, f, includes the entrance and exit losses as well as the "friction" losses. Graphs of f against Re_R are given for all the tube arrangements tested.

Gram et al. (1958) obtained pressure drop data for a ten-row in-line tube bank over a range of Re_{max} of 600 to 40 000. Various tube arrangements were used with a transverse pitch-diameter ratio range of 1.25 to 6.0 and a longitudinal range of 1.0 to 6.0. By applying dimensional analysis to the flow system, the authors presented

the pressure drop through a tube bank as a function of the parameters which characterise the flow, viz. the bank geometry and flow conditions:

$$\frac{\Delta p}{\frac{1}{2}\rho u_{max}^{2} N} = \Phi\left(Re_{max}, \frac{P_y}{D}, \frac{P_x}{D}, \frac{\ell}{D}, \frac{P_y n}{D}, N\right) \qquad (2.20)$$

and $$f = \frac{\Delta p}{\frac{1}{2}\rho u_{max}^{2} N}$$

By making $P_y n/D$ and ℓ/D large it was assumed that duct wall effects were minimised so that the results from the model could be applied to larger scale tube banks. The pressure drop across the bank was broken down into its component parts as suggested by Kays and London. The results were presented as f plotted against P_y/D for various values of P_x/D and for a series of constant Re_{max}.

George (1967) investigated the air flow over a ten-row deep in-line tube bank with ten tubes per row for tube pitch-diameter ratios of 1.2 to 1.3 and over a range of Re_D of 8×10^4 to 8.5×10^5. The results were expressed as a loss coefficient, f, against Re_D. These data, obtained for high Reynolds number, were found to agree well with the extrapolated relations given by other investigators. The distribution of static pressure around tubes within the bank was also measured. It was found that there were large variations in the pressure differences between rows in the first part of the bundle but they were reasonably constant, for all values of Re_D, across the remaining rows. It was also found that for these close pitches the drops obtained with a non-uniform inlet velocity profile did not significantly vary from those with a uniform inlet profile.

Achenbach (1971) presented the results of an investigation into the effects of surface roughness on the pressure drop over various tube arrays. The first of these papers covers flow over single tubes for a range of Reynolds number, Re_D, of 6×10^4 to 10^7. At low Reynolds numbers, $Re_D < 10^5$, the effect of surface roughness was found to be negligible. At higher Re_D, for a smooth tube, a critical Re_D was

reached where the drag coefficient decreased to a minimum before rising again to a constant value, at approximately $Re_D = 5 \times 10^5$. It was found that surface roughness reduced this critical Reynolds number and increased the drag coefficient finally attained.

Achenbach reported in subsequent papers experiments using staggered and in-line tube banks, which consisted of five rows with three tubes per row with $P_y/D = 2.04$ and $P_x/D = 1.4$, over a Re_{max} range of 4×10^4 to 10^7. It was found that there was no effect of surface roughness for $Re_{max} < 10^5$. Above this value of Re_{max}, opposite effects were observed in the in-line and staggered banks.

For staggered banks the pressure drop coefficient, ζ, where

$$\zeta = \frac{\Delta P}{\frac{1}{2}\rho u_{max}^2} \tag{2.21}$$

behaved like the drag coefficient in the single tube case, falling to a minimum value before increasing to a constant value. Increasing the surface roughness also had the same effect as for a single tube.

For the in-line array increasing the surface roughness lowered the final pressure drop coefficient attained when the Reynolds number increased above the critical value, i.e. opposite to its effect in the staggered case. It is suggested that this is caused by increased surface roughness bringing the boundary layer separation point closer to the front of the tube, for the same Reynolds number, thus producing a larger wake. In the staggered array this leads to an increase in the pressure drop coefficient. However in the in-line array increasing the wake behind each tube reduces the expansion and contraction of the flow between each tube row, as the tubes lie in the wake of the preceding row of tubes, thus reducing the pressure drop coefficient.

Zukauskas (1972) presented a graphical correlation of pressure drop data from several sources, including his own extensive research, which was particularly concerned with isothermal, high Reynolds number flows. Two graphs are given for

pressure drop coefficient, ξ_p, versus Reynolds number, Re_{max}, from 20 to 2 x 10^6, one graph for in-line and one for staggered tube bank arrays. Graphs are also given for a geometrical correction factor, defined in terms of the transverse and longitudinal tube pitch-diameter ratios of the bank, allowing the pressure drop coefficient to be estimated for a wide range of tube arrays. His own data suggest that as Reynolds number increases above Re_{max} = 2 x 10^5, and the flow becomes increasingly turbulent, the pressure drop coefficients for both staggered and in-line banks become similar and constant.

Batham (1973) measured the mean and fluctuating pressure distributions around tubes in an in-line square tube bank, for tube pitch-diameter ratios of 1.25 and 2. Tests were performed for Reynolds numbers, Re_{max}, of 2.8 x 10^4 to 10^5. The tubes had a 50.8mm outside diameter. The closely pitched tube bank consisted of ten rows with seven tubes per row and the widely pitched bank nine rows with five tubes per row.

The level of turbulence in the incident flow was found to have a large effect on the pressure distributions measured in the widely pitched array. The pressure distribution around a tube in the $P_x/D = P_y/D = 1.25$ array was found to be highly sensitive to upstream tube movement of the order of 0.005 tube diameters. The author suggested that this phenomenon was caused by a Coanda switching effect. Measurements with surface roughened tubes confirmed the results of Achenbach, there being no effect on the overall pressure drop coefficient at Re_{max} below 10^5.

Pearce (1973) undertook an investigation of flow through tube banks. Although primarily interested in tube vibration, he also produced data on pressure drops through square in-line and equilateral-triangular banks; having one, two, four and ten rows in the flow direction. Pressure drop data were compared with the correlations of Grimison, Jakob and Zukauskas (1972). For in-line square tube banks Grimison was found to predict best the data for Re_{max} up to 40 000; Zukauskas predicted better at higher Re_{max}. Overall the measured pressure drops were within 15% of both correlations over the range of Reynolds numbers tested, viz. Re_{max} from 1.2 x 10^4 to 10^5. For equilateral-triangular arrays the measured values were

significantly lower than for any given by previous prediction methods; Zukauskas was the least inaccurate. Because of this lack of agreement Pearce presented his own correlation of his data for this array,

$$\xi_p = 112.4 \left[\frac{P_y}{D}\right]^{-6.8} (Re_{max})^b \qquad (2.22)$$

where $b = [\ln(P_y/D) - 0.92] / 1.61$

This was found to fit the data to within 6%. For all arrays tested it was found that the pressure drop coefficient, ξ_p, increased with a reduction in the number of tube rows, N, and that this increase became larger as the Reynolds number increased. The pressure drop coefficient was found to fall as the tube pitch-diameter ratio increased, and this was more marked for the in-line case than for the staggered tube configuration.

Butterworth (1978) showed how pressure drop data for one-dimensional flow in tube bundles can be used in the analysis of real multi-dimensional flow problems. The pressure drop for one-dimensional flow over a bank of depth L, in the flow direction, is given as

$$\Delta p = \frac{\mu u L}{k} \qquad (2.23)$$

where k is the flow conductivity and u is the approach velocity. He assumed that the tube bank could be treated as an isotropic porous medium. From this assumption it follows that k will be the same for all tube bank orientations to the flow direction, i.e. for square in-line and rotated square arrays, and similarly for equilateral-triangle and rotated equilateral-triangle arrays. He showed that this assumption is reasonably consistent with data obtained for some of the most commonly used arrays. Equilateral-triangle arrays, with pitch-diameter ratios of 1.25 and 1.33, correlated

well on this basis. There was some scatter between the square in-line and rotated square data but this was of a scale comparable to that of the variations between data for similar arrays obtained by different investigators.

Butterworth (1979) presented correlations of pressure drop data based on his isotropic flow model. For square in-line and rotated square arrays,

$$f = 0.061 \frac{D^2 D_v}{(P_t - D)^3} Re^{-0.088} \qquad (2.24)$$

and for equilateral-triangle and rotated equilateral-triangle arrays,

$$f = 0.45 \frac{D^2 D_v}{(P_t - D)^3} Re^{-0.267} \qquad (2.25)$$

where

$$f = \frac{\Delta p}{2\rho u^2 (L/D)}$$

These equations apply to turbulent, isothermal flows.

ESDU (1979) also presents correlations based on an isotropic model. The data are given as pressure loss coefficients, C', defined as

$$\frac{dp}{dx} = -\tfrac{1}{2} C' \rho \frac{u^2}{D} \qquad (2.26)$$

The correlations apply only to banks of six or more rows, when entry and exit effects are small in comparison to the overall pressure loss and only to isothermal flow without bypassing. It is shown that for a fixed pitch-diameter ratio the pressure loss is independent of the bank rotation for both equilateral-triangle and square arrays for $Re_D < 10\ 000$. This flow isotropy considerably simplifies the modelling of flow

through a complex heat exchanger as C' will be independent of the local flow direction. Pressure loss coefficients are given for equilateral-triangle arrays as :-

$$C' = WY^{\frac{1}{3}}(P_y/D - 1)^{-3} \qquad (2.27)$$

where $Y = f(Re_D)$

and $W = f(Re_D, P_y/D)$ for $Re_D < 10^6$.

For square arrays :-

$$C' = WY^{\frac{1}{3}}F(P_y/D - 1)^{-3} \qquad (2.28)$$

when $Re_D < 10\,000$ F is unity for both in-line and rotated square arrays,

when $10{,}000 < Re_D < 10^6$ $F = 1$ for square in-line arrays but $F = f(Re_D, P_y/D)$ for rotated square arrays.

The values of Y, W and F are given as complicated functions of bank geometry and Reynolds number.

Zukauskas et al. (1979) published details of an experimental study of flow resistance over tube banks for Reynolds number, Re_{max}, from 4×10^4 to 2×10^6. They gave two expressions for the pressure drop coefficient over this flow range, which were found to correlate accurately (±7%) all the data obtained from the eight different tube bank arrays they tested.

For staggered bundles:

$$\xi_p = 0.078(P_y/D - 1)^{-0.3}N \qquad (2.29)$$

and for in-line bundles

$$\xi_p = 0.08(P_y/D - 1)^{-0.4}N \qquad (2.30)$$

From this it can be seen that the transverse tube spacing has more effect on the flow resistance of in-line bundles than of staggered ones. The drag coefficient of tubes deep inside the banks was also measured. In a staggered bank, for Re_{max} from 4 x 10^4 to 10^5, the drag coefficient of an individual tube drops as the flow separation point shifts towards the rear of the tube. Within an in-line array, over the same Re_{max} range, the drag coefficient reflects the shift of both the separation point and the point where the flow over the previous row impinges on the tube. For Re_{max} > 10^5 the drag coefficient for a single tube within the bank remains constant as both the flow separation and impingement points are unchanged by increasing Re_{max}.

Lee (1981), in an investigation primarily concerned with simulating condensing flow over ideal tube banks, produced some pressure drop data for equilateral-triangle and in-line square arrays for Re_{max} from 28 x 10^3 to 100 x 10^3. Data obtained with more than five rows in the flow direction was predicted to within ±5% by the correlations of Butterworth and of Zukauskas. However, ESDU (1979) overpredicted the equilateral-triangle data by up to 10%, while matching the accuracy of the other two methods for the in-line square array.

Zukauskas (1983) summarises his extensive research programme in the Heat Exchanger Design Handbook. Correlations based on a large data set are given graphically in the form of a pressure drop coefficient, ξ_p, plotted against Reynolds number, $4 < Re_{max} < 10^6$. Inverse power series equations are given which fit these curves over small ranges of Re_{max}. Two sets of graphs and equations are given, one for in-line and the other for staggered arrays.

For in-line arrays, for $P_y/D = P_x/D = 1.25$ and $2 \times 10^3 < Re_{max} < 2 \times 10^6$,

$$\xi_p = 0.267 + \frac{0.249 \times 10^4}{Re_{max}} - \frac{0.927 \times 10^7}{Re_{max}^2} + \frac{0.10 \times 10^{11}}{Re_{max}^3} \qquad (2.31)$$

and for $P_y/D = P_x/D = 1.50$ for the same Re_{max} range,

$$\xi_p = 0.235 + \frac{0.197\times10^4}{Re_{max}} - \frac{0.124\times10^8}{Re_{max}^2} + \frac{0.312\times10^{11}}{Re_{max}^3} - \frac{0.274\times10^{14}}{Re_{max}^4} \qquad (2.32)$$

For equilateral-triangle arrays with $P_t/D = 1.25$ and $10^3 < Re_{max} < 2 \times 10^6$,

$$\xi_p = 0.245 + \frac{0.339\times10^4}{Re_{max}} - \frac{0.984\times10^7}{Re_{max}^2} + \frac{0.132\times10^{11}}{Re_{max}^3} - \frac{0.599\times10^{13}}{Re_{max}^4} \qquad (2.33)$$

and for $P_t/D = 1.5$ for the same array type and Re_{max} range,

$$\xi_p = 0.203 + \frac{0.248\times10^4}{Re_{max}} - \frac{0.758\times10^7}{Re_{max}^2} + \frac{0.104\times10^{11}}{Re_{max}^3} - \frac{0.482\times10^{13}}{Re_{max}^4} \qquad (2.34)$$

The above equations apply to banks with a large number of tubes in both the transverse and longitudinal directions. For banks with fewer tubes in the flow direction correction factors are given. Corrections factors are also given to enable the equations to be used for other geometries than those mentioned above, i.e.,for when P_x/D and P_y/D are not equal, for heating and cooling effects on fluid properties, and for finned or surface roughened tubes.

Although many investigations of ideal bank pressure loss have been undertaken, none of the ensuing reports are regarded as definitive. As will be seen in the next section, it is common practice to use a range of data and correlations when deriving loss coefficients for the crossflow stream. The most highly regarded of the unrestricted publications is the Heat Exchanger Design Handbook, of which Zukauskas (1983) forms a part. This publication attempts to bring together information from many open sources, and as much as possible from proprietary sources, and to recommend correlations based on these data for all aspects of heat exchanger design.

2.2 Pressure Losses of Flow Over Non-homogeneous Tube Banks and Through Real Exchangers

The pressure drop correlations derived from results for ideal tube bundles are the basis for predictions for geometrically complex equipment. Methods for calculating the pressure drop in real exchangers are based on assumptions which reduce the complex flow patterns to a simple model.

Tinker (1948) analysed the complex flow pattern in shell-and-tube heat exchangers. He identified the various flow streams, Fig. 1.6, and noted their effects upon the overall heat transfer and pressure loss. He gave equations by which friction factors can be found for all the flow streams and showed how the effective crossflow area and crossflow mass rate can be calculated, by balancing the mass flows and associated pressure drop across the alternative flow paths. This requires an iterative solution because the flow path friction factors are dependent on the Reynolds number. He suggests, however, that this can be avoided by choosing constant friction factors based on the anticipated Reynolds number and relative stream velocities for each of the flow paths; this requires design experience.

Tinker suggested that more flow resistance data on the leakage paths are needed if this method of design analysis is to be fully validated, because many of the flow resistances he quoted had been approximated from the previous limited data and from design experience. The friction factor for flow in the bypass lane, in particular, is based on the friction factor for flow through an in-line array with a transverse tube spacing equal to the bypass clearance width; this is then factored to account for Reynolds number in the bypass and multiplied by a factor of 0.75 to account for the smooth bypass wall. This method of predicting shell-side heat transfer and pressure drop was not widely used at the time, due to the complex solution required, but with the advent of computers it has been 'rediscovered' and is now the basis of several computer-based design programs.

Tinker also examined the effects of the various leakage paths on the overall pressure drop. A measure of the pressure drop was taken as the relative pumping

power loss for a fixed amount of heat transfer surface operating at a constant heat transfer coefficient. For the particular exchanger used in the tests, for which the internal shell diameter was 0.391m and the tube bundle outside diameter was 0.374m, an increase in the shell-to-bundle clearance of 12.7mm increased the shell-side relative pumping loss by 25%. In some cases the total elimination of any clearance between the tube bundle and the shell reduced the relative pumping loss by over 50%. It is suggested that the use of sealing-strips in most common types of exchanger would reduce the relative pumping loss by over 25%. Other methods for improving the heat transfer and pressure loss characteristics were suggested. These include designing floating head type closures to allow the outside of the tube bundle to extend to within 5mm of the shell, and to make the outer tubes lie on a circle as close as possible to the shell, so as to give a uniformly small bypass clearance. These methods reduce the leakage area and result in the bulk of the shell-side flow passing over the heat transfer surface so that a high ratio of overall heat transfer to relative pumping power can be obtained.

Kern (1951) produced a simple pressure drop correlation by modelling the shell-side flow as a single flow stream, which does not differentiate between crossflow and window-flow. Data from real exchangers are correlated in a Fanning type-equation, in which the pressure drop is taken to be proportional to the number of times the flow crosses the bundle and to the shell inside diameter, viz.,

$$\Delta p_s = \frac{f G_s^2 D_{sh}(N_B+1)}{2\rho D_v(\mu/\mu_w)^{0.14}} \qquad (2.35)$$

where D_{sh} = inside diameter of shell.

Overall shell-side friction factors, f, are given for a 25% cut segmental baffle exchanger over a range of Re_k from 10 to 10^6. The use of equivalent volumetric diameter, the author claims, allows f to be plotted on one curve for all tube configurations with relatively little scatter. This method takes no account of

bypassing or other internal leakages, but despite this became an industrial standard because of its simplicity.

Fritzsche (1951), in a discussion of Tinker's paper, gave some results of his investigation into the effects of bypassing. Initially using an ideal tube bank, he carried out a series of tests in which the total mass flow rate was measured for a constant pressure drop when first the outer half row of tubes was removed and then the bypass wall moved in successive steps outwards. The tests were for water flow over equilateral-triangle tube banks with a range of tube pitch-diameter ratios, and over a range of Re_D from 200 to 8 000. The results were presented as the ratio of Reynolds number in the ideal bundle to Reynolds number in the arrangement with a bypass, for the same pressure drop. These ratios were plotted against the ratio of ideal flow area to the effective flow area with the bypass. Graphs showing the relation between these ratios were given for a range of Reynolds numbers. It was found that the Reynolds number only influenced the relation for the smallest pitch-diameter ratio tested, $P_y/D = 1.2$, in which an increasing proportion of fluid flowed through the tube bundle as the Reynolds number increased; no influence could be detected for the other ratios, $P_y/D = 1.35$ and $P_y/D = 1.5$.

Tinker (1958) developed a system for rating the shell-side performance of commercial exchangers, based on the flow model proposed in Tinker (1948) and new research data. Using resistance factor approximations, the author derived simple formulae for evaluating the fluid flow fraction through the crossflow area of the bundle. Tabulations of heat transfer and pressure drop characteristics may be derived from these formulae for a series of heat exchangers having consistent design proportions. This allows many of the parameters used in his design method to be determined more accurately than previously, when such parameters had to be estimated from design experience. This leads to a simpler, non-iterative solution of his flow model which, he claims, produces results accurate enough for most practical requirements.

Tinker suggests modifying the bypass friction factor, by using a correction factor, to account for the use of sealing-strips. The correction factor takes account

of the fact that bypassing still occurs between the sealing-strip positions. He found that this approach produces results consistent with the performance of commercial exchangers provided that two or more sealing-strips are used on each side of the bundle and are spaced less than 300mm apart. The bypass friction factors given by him in this paper are two-thirds of the values proposed in his previous paper.

Tinker suggests that further accuracy can be obtained from this method by modifying the resistance factors when more experimental data on the leakage streams become available.

The results of investigations by Cernik, Destremps and Bryce were presented by Bergelin et al. (1958); they comprised part of an extensive experimental programme into shell-and-tube heat exchangers undertaken at the University of Delaware.

Cernik (1955) carried out flow visualisation studies of bypassing. In-line square, rotated square and equilateral-triangle arrays were tested, with 19.1mm diameter tubes spaced at 23mm pitches, and bypass clearances from 1.6mm to 9.5mm. Both rectangular and cylindrical tubes bundles were examined. Water was used as the test fluid over a range of Reynolds numbers in the turbulent flow regime. Flow patterns were visualised by photographing plastic particles introduced into the flow. This investigation showed that there is a substantial interchange of fluid between the bypass and crossflow streams; in particular that there is a large fluid transfer from the crossflow stream to the bypass in the first two or three tube rows.

Destremps (1956) and Bryce (1957) studied rectangular tubes bundles with bypassing. Two test models were examined, both having an equilateral-triangle array but one having a tube pitch-diameter ratio of 1.25 and the other of 1.5. In each model the distance between the outer row of tubes and the shell wall could be varied. Tests were carried out in the laminar and turbulent flow regimes with bypass flow area to total flow area ratios of 21% and 30%. The bypass flow area is based on the minimum gap between the shell wall and the outermost tube. Experiments were also carried out with one or two sealing-strips blocking the bypass stream. Runs were

made for the isothermal flow of oil on the shell-side and also with heating and cooling by water flowing on the tube-side.

Bergelin et al. (1959) discuss the Delaware reports on bypass flows and give a method for separating the total flow measured by Destremps and Bryce into effective bypass and effective crossflow components. By assuming that the flow through the bundle is unaffected by the presence of the bypass stream, it follows that the pressure drop measured across the bundle with a bypass is the same as that across an ideal bundle having the same crossflow velocity. Therefore the effective crossflow can be calculated, for a bundle with bypass, from the measured pressure drop, the tube bundle dimensions and pressure drop - flow rate data from ideal tube banks. By eliminating the effective crossflow rate from the total measured flow rate the effective bypass flow rate can be found. The authors state that the assumption on which this method is founded is not generally true, due to flow interaction, and that the actual bypass flow varies from row to row. However they justify the use of the effective bypass flow because it gives them a basis upon which to predict exchanger performance when bypassing is present. Bergelin et al. plot the data of Destremps and Bryce as the effective bypass ratio,

$$R_{eff} = \frac{\dot{V}_{Beff}}{\dot{V}_{Ceff}} \tag{2.40}$$

against total flow rate, where $\dot{V}_{Beff}$ and $\dot{V}_{Ceff}$ are the effective volume flow rates of the bypass and crossflow streams respectively. This shows that R_{eff} increases as the relative amount of bypass area increases and R_{eff} decreases with increasing Reynolds number. From their analysis of the sealing-strip data they found that using one strip reduced R_{eff} to 40% of its original unblocked bypass value and two strips reduced R_{eff} to about 30% of its original value. They also found that the effectiveness of a sealing-strip in reducing the bypass flow decreases as the depth of the tube bank increases, indicating that more strips need to be used with increasing bank depth.

The authors suggested that uniform spacing of the sealing-strips is likely to produce the maximum reduction in R_{eff}.

Bergelin et al. proposed two different models of the flow through tube bundles with bypassing. For the laminar flow regime the assumption was made that there is little mass transfer between the bypass and crossflow streams. A model of the flow was proposed which consisted of two channels, one being an ideal tube bank and the other formed between the centre-line of the outermost row of tubes and the shell wall. Pressure drop data for an ideal bundle had been obtained before and an expression for the pressure loss in the bypass channel was derived which accounted for losses due to the contractions created between the tubes and the shell and the frictional loss. This did not take into account any frictional losses due to the transverse interaction between the crossflow and bypass streams, as the model assumes that they are separated by a solid boundary. Since the pressure drop along the length of each stream has to be the same, the mass flow in each can be found for a given total flow rate and then the cross flow rate can be used to give the exchanger performance.

In the turbulent flow regime Cernik found that there is a considerable interaction between the crossflow and bypass flow streams, thus the simplifying assumptions made for the laminar regime do not hold in this case. It was suggested that the pressure drop in the bypass channel can be found from analysis of the data produced by Destremps and Bryce. Friction factors were derived from these data and plotted against Reynolds number but only for a limited flow range. These friction factors strictly apply only to the bypass area ratios and tube configurations used in those tests.

The application of these results to practical exchangers was also discussed, as most commercial exchangers have cylindrical shells and the Delaware results are for rectangular tube bundles. It was suggested that the method could be applied rigorously row by row, balancing the pressure drop through the bundle and the bypass for each row, to take account of the fact that in a cylindrical exchanger the bypass area ratio changes for each row. However, in most cases the accuracy of the

method does not warrant such a complex approach and they suggested that an average bypass area ratio could be used.

Bell (1960) in a further article on the Delaware programme gave a simple empirical equation representing the results obtained for the effects of bypassing on the pressure drop through an exchanger

$$\frac{\Delta p_{BP}}{\Delta p_I} = e^{-\alpha F(1-\sqrt[3]{(2N_s/N_x)})} \qquad (2.41)$$

where the constant α is 4.5 for laminar flow and 3.8 for turbulent flow. He presented an exchanger design method based on the Delaware research. This method recognises all the flow streams of Tinker's flow model but, in order to avoid an iterative calculation procedure, uses correction factors applied to the principal crossflow stream to account for them. He also gave some general design guidelines. He cited the bypass around the tube bundle as the cause of the most serious loss of heat exchangers operational efficiency and suggested that the bypass clearance should be minimised. Where this is not possible, such as in floating head designs, two or more pairs of sealing-strips should be used and for these to be most effective they should completely block the bypass channel.

Whitely (1961) compared data from nine operating shell-and-tube heat exchangers with several pressure drop correlations including those of Kern and Bell. Kern was found to overpredict the pressure drop by up to tenfold. Bell's method was found to be the most accurate, as it was the only one examined which took account of internal leakage effects and the author recommended its use for design calculations.

In 1963 Bell presented the final report of the Delaware research programme. He noted that bypassing accounts for a significant part of the total flow and that typically up to 75% of the total flow passes through the bypass in the laminar case and up to 50% in the turbulent case, and that such flow avoids the heat transfer surface. He redefined the bypass flow area. Previously it had been based on the

bypass clearance width but he suggested that it should be based on the bypass clearance less half of a transverse intertube space; as a tube bundle with half of the intertube clearance between the shell walls and its outermost rows of tubes corresponds to an ideal bundle. This redefinition causes the constant, α, in equation (2.41) to change; the new values being $\alpha = 5.0$ in the laminar regime and $\alpha = 4.0$ in the turbulent regime. Bell also suggested that the tubes which are closest to the wall govern the bypass behaviour and so the characteristic bypass flow area should be taken at the row with the minimum clearance.

Bell concluded that knowledge of the nature of bypassing remained unsatisfactory but suggested that bypass channels should be avoided where possible. On the effects of sealing-strips he noted that the data were limited and the only conclusion reached was that the use of sealing-strips leads to a performance closer to that of an ideal bank.

Palen and Taborek (1969) reintroduce a design method based on an iterative solution of Tinker's flow model. This method is known as the "stream analysis method". Resistance characteristics of the five flow streams, Fig. 1.6, were determined from semi-theoretical models and extensive experimental results. They introduced an additional flowstream F to Tinker's model to account for tube bundles with a tube pass partition in the direction of the flow. Resistance coefficients for the tube-baffle leakage and baffle-shell leakage were derived from the Delaware data. The bundle bypass and tube pass partition bypass stream resistance coefficients were correlated from the data of Heat Transfer Research Inc. (HTRI) on commercial-size exchangers; these had a range of bypass clearances representative of those found in industrial applications. It was noted that the bypass resistance is very sensitive to bypass channel width because the nature of the losses depends on the size of the clearance. For small clearances the acceleration losses are dominant while for larger clearances the flat plate resistance of the shell wall is dominant. The correlation produced is based on a model of the flow consisting of two parallel channels, one with tubes and one without. The method is proprietary to HTRI and therefore only

the qualitative form of the correlations is included in the paper. The pressure losses for each stream are presented as flow resistance coefficients, for example

$$\Delta P_B = kK_B G_B^2 \tag{2.42}$$

where

$$K_B = 4f_B N \phi_B \tag{2.43}$$

ϕ_B is an empirical correction factor accounting for fluid viscosity differences between the bypass flow and the crossflow; because the bypass stream avoids the heat transfer surface it will have a different temperature, and therefore viscosity, than the crossflow stream. The bypass channel friction factor is given as

$$f_B = \frac{k_1}{Re_B}\left[\frac{1}{1 + k_2(D_B N/L_B)^{0.5}}\right]^2 \tag{2.44}$$

for laminar flow, and

$$f_B = k_3 \frac{D}{D_B}\left[\frac{1}{Re_B}\right]^{k_4} \tag{2.45}$$

for turbulent flow, where Re_B is the bypass channel Reynolds number and k, k_1, k_2, k_3 and k_4 are constants derived from HTRI data. The relationship between f_B and Re_B was presented graphically.

The flow resistance caused by the presence of sealing-strips was also considered. The resistance consists of two terms: a momentum change coefficient, due to velocity changes as the bypass stream is turned and accelerated into the bundle then decelerated back into the bypass channel, and a friction loss term, as the bypass stream penetrates the bundle. The total sealing-strip resistance coefficient was given

as

$$K_{ss} = K_{vs} + 4f_C N_C \tag{2.46}$$

where

$$K_{vs} = \frac{k_5}{Re_B^{k_6}} \left[\frac{1}{R^{k_7}} - 1 \right] \tag{2.47}$$

K_{vs} being the flow resistance coefficient of the momentum change. k_5, k_6, k_7 are constants, N_C is the effective number of tube rows which are in pure crossflow as a result of the presence of the sealing-strip and R is the ratio of bundle penetration area, of the diverted flow, to the bypass flow area. All these constants were calculated from HTRI data.

By using computers the mass flow and pressure drop across the various flow streams can be solved simultaneously and the balance found by iteration because the pressure drop between any two points in the exchanger is the same regardless of the route the flow takes between them.

This method was compared with the Tinker and the Delaware methods for a data set containing more than a thousand experimental operating points for various sizes and types of exchanger. The authors claim that their stream analysis method gave a considerable improvement over the other two methods, particularly in the laminar range.

It was also discovered in this study that it is possible to use too many sealing-strips; if the bypass channel is severely blocked, flow is forced into the baffle-shell leakage stream which is even less heat transfer effective than the bypass stream. The authors noted that the bypass flow was one of the most significant flowstreams but that its friction factor relations are not known; the correlations they used in their method were deduced from theoretical considerations and information reduced from data obtained from investigations of complex geometries. They suggest that basic

studies into bypass flow and flow obstruction devices such as sealing-strips are needed.

ESDU (1974) presents a method for calculating the pressure drop for single-phase flow over a plain tube bank. The pressure drop is given by

$$\Delta p = N_x K \rho \frac{u_{max}^2}{2} + \left[\frac{A_{min} u_{max} \rho}{A_T \sin\gamma}\right]^2 \left[\frac{1}{\rho_N} - \frac{1}{\rho_1}\right] \qquad (2.48)$$

The first term deals with the irrecoverable component of static pressure loss and depends on K, the overall pressure loss coefficient. K is found from a set of curves of ideal pressure loss coefficient, K, against Re_{max} for staggered and in-line arrays, to which a set of correction factors are applied which take account of the variation of fluid properties, due to heating or cooling, bypass effects, tube inclination to the flow direction and the tube surface roughness.

The second term in the pressure loss equation deals with momentum considerations allowing for density changes between inlet and outlet of the bank; these, it is suggested, are significant only if the density changes are greater than 15%.

The method covers Re_{max} from 1 to 10^6 and applies to flows of gases or liquids which are isothermal or are being heated or cooled. Because of the complexity of the method a full calculation procedure was given.

The bypass correction factor, by which the ideal tube bundle pressure loss coefficient is multiplied to give an overall loss coefficient for the exchanger, is calculated differently depending on the flow regime. For the laminar regime the effects of bypassing are treated as being due to the effective porosity change in the bank caused by the presence of the bypass channel. Bypass correction factors are given graphically as a function of the effective porosity increase. For the turbulent flow regime it is assumed that the two flow paths, through the ideal bank and the bypass channel, may be treated independently provided that the pressure drop across each is the same; hence it is assumed that flow interaction between the paths does not significantly change the pressure loss coefficients for each channel due to a change in

the effective Reynolds number. The bypass loss coefficients were derived by comparing the bypass lane geometry with that of an ideal tube bank, see Fig. 2.3. However, the bypass loss coefficients produced in this way were found to be too low and therefore they were increased by a "factor" so that they became consistent with unspecified experimental data. The resulting bypass loss coefficients were presented graphically and are dependent on the transverse pitch-diameter ratio and the bypass width-tube diameter ratio. The bypass loss coefficient is then used in conjunction with the ideal tube bundle loss coefficient and the tube bank geometry, with bypass, to give a bypass correction factor for the overall loss coefficient; using an equation based on a simple parallel flow model.

Grant et al. (1974) investigated the pressure drop and phase distribution of air and water mixtures flowing vertically upward through a tube bank with and without bypassing. They also carried out tests with single-phase fluids; air and water. Their ideal bundle consisted of twenty tube rows, N, with nine tubes in each row. The tubes had an outside diameter of 19mm and were 232mm in length. The tubes were arranged in an equilateral-triangle array with a tube pitch-diameter ratio of 1.5. The ideal bundle had half-tubes attached to the duct walls either side of the tube bundle to eliminate bypass flow. These half tubes were removed to create a bypass lane on each side of the bundle, the bypass flow area thus produced amounted to 22% of the minimum crossflow area. They found that their friction data could be represented by a Blasius-type equation,

$$f = a_1 Re_g^{a_2} \tag{2.49}$$

where

$$f = \frac{\rho_m \Delta p}{2 G_S^2 N}$$

For the ideal bundle: $a_1 = 0.63$ and $a_2 = 0.22$,

for the bundle with bypass: $a_1 = 0.52$ and $a_2 = 0.21$,

and for the bypass channel alone: $a_1 = 0.34$ and $a_2 = 0.18$.

When a bypass lane is present the friction factor is based on the velocity through the mean minimum flow area of the bundle and bypass. The friction factors for the bypass channel alone were estimated from the effective bypass flow rate, as calculated by Bergelin et al. (1959), through the minimum bypass clearance.

Bell (1980) presented a revised form of the Bell-Delaware method. A full method for the thermal-hydraulic design of shell-side flow through shell-and-tube heat exchangers is described and tables and graphs are given to enable the calculations to be carried out. Pressure drops for the ideal crossflow and ideal window flow are calculated, as the principal flow stream, to which are applied correction factors to account for leakage, bypassing and entry/exit effects. Typically the total correction to the ideal value is from 0.5 to 0.8; the lower figure being representative of floating-head types, although the use of sealing-strips would increase this, and the higher value being representative of well designed, fixed tube-sheet types. The author claimed that the Bell-Delaware method was the most accurate one published in the open literature, although when examined against a large data set it gave predictions of overall exchanger pressure drop which ranged from 50% low to 200% high. On average it was found to predict 100% high at low Reynolds numbers, which is conservative, to 5% low at high Reynolds numbers, which is unsafe.

Lee et al. (1983) published some data on the effects of bypass lanes on pressure loss in tube banks. Measurements were carried out for three configurations, in-line square, equilateral-triangle and triangular constant gate, each with seven rows of tubes with seven tubes per row and with a transverse pitch-diameter ratio of 1.25. The various bypass lane widths were created by removing successive rows of tubes. The overall pressure loss and the flow fraction in the bypass on exit from the bank were measured. Results are presented graphically as a pressure drop coefficient plotted against Re_D and bypass mass flow fraction plotted against Re_D for a range of $7 \times 10^3 < Re_D < 27 \times 10^3$. It is noted that the bypass flow fraction measured

contained flow diverted ahead of, as well as inside, the bundle. The bypass flow fraction was shown to be highly dependent upon the ratio of bypass lane width to the transverse width of the bank, but largely independent of the Reynolds number. The authors suggested that, from the limited data gathered, it would appear that predictions based on Bell-Delaware substantially underestimate the pressure drop coefficient.

Taborek (1983), after reviewing previous pressure drop prediction methods, recommends a method based on the Bell-Delaware approach although he says that this method cannot match the accuracy of Tinker's method in its full iterative form with flow resistance correlations for all the flow streams. However, these correlations either do not exist or are not publicly available and the Bell-Delaware method is accurate enough for use with "well-designed" exchangers.

A series of graphs of friction factor are given for each tube array type. They are also presented as an equation

$$f_c = b_1\left[\frac{1.33}{P_t/D}\right]^b (Re_S)^{b_2} \qquad (2.50)$$

where $b = b_3 / (1 + 0.14(Re_S)^{b_4})$

and

$$f_c = \frac{\Delta p \rho}{2G_s^2 N}$$

f_c is the crossflow friction factor and Re_S is the Reynolds number based on the total free flow area at the exchanger's centre-line, including crossflow and bypass. Different parameters b_1, b_2, b_3 and b_4 are given depending on the tube geometry and flow conditions. For example, for an equilateral-triangle array for Re_S from 10^4 to 10^5, $b_1 = 0.372$, $b_2 = -0.123$, $b_3 = 7.0$ and $b_4 = 0.5$. The pressure drop calculated from this crossflow friction factor is then subject to a correction factor for bypassing. This is the same as Bell's equation (2.41) except that $\alpha = 3.7$ for turbulent flow ($Re_S > 100$).

The published pressure drop data and correlations for flow through shell-and-tube heat exchangers are very limited regarding the effects of bypassing and the use of sealing-strips. When methods are proposed which take account of these factors they are based upon a very limited amount of data. The authors of prediction methods based on Tinker's flow model usually recommend that more data are needed on the flow streams before the method can be used effectively.

The present work seeks to provide more data and produce correlations for the bypass flow and the effects of sealing-strips to meet the requirements of computer-based stream analysis methods for more reliable information and also provide data against which empirical prediction methods can be checked.

3. EXPERIMENTAL APPARATUS

The general layout of the rig is shown in Fig. 3.1 and Fig. 3.2. The rig consists of three basic components: the air supply, the test section, in which tube banks with various geometries can be mounted, and the measuring tubes.

3.1 PRELIMINARY DESIGN CONSIDERATIONS

3.1.1 THE TEST SECTION

A number of points had to be considered in the design of the test section. The most important aim was to make the model tube bank with bypass lane as similar as possible geometrically to that which exists inside a real shell-and-tube exchanger but to allow the effect of different bypass widths to be examined in isolation from other geometric factors; hence the use of a rectangular tube bank with a straight bypass wall was adopted. The main factors considered were :-

(a) The range of tube pitch-diameter ratios tested should be that commonly used in industry, i.e. $P_t/D = 1.25$ and $P_t/D = 1.375$ but the rig should be adaptable enough to allow other ratios, such as $P_t/D = 1.5$, to be investigated.

(b) The test section needed to be sufficiently flexible to allow a range of tube configurations to be used. Square in-line and equilateral-triangle arrangements, for both of the pitch-diameter ratios chosen, were decided upon for the tests but allowance was made for rotated square and rotated equilateral-triangle to be used in the future.

(c) In order to make the ratios of bypass width to tube bank width as geometrically realistic as possible a large number of tubes, n, are

required per row. However, the width and height of the tube bank used were restricted by the cross-section of the available contraction; as it had been decided that the diffuser, settling length and contraction built for the rig described in Lee (1981) should be used to reduce the time and expense needed to build the rig. Therefore the smallest tube diameter commonly met in practice was chosen, viz. 12.7mm, to enable n to be as large as possible.

(d) The pressure drop over the first and last few rows of tubes in a bank is different from that over the rest of the rows. Therefore it is important to have as large a number of tube rows, N, in the flow direction as possible in order to make these entry/exit effects small in comparison with the total bank pressure drop. However, the number of tube rows is limited by the pressure rise from the fan available. N was chosen to be the maximum that would allow a sufficient range of turbulent Reynolds number to be investigated to enable comparison with other available data.

(e) The bypass width should be adjustable in steps of less than half a tube pitch to allow a closer examination of the dependence of the pressure drop on the bypass width than was obtained in Lee et al. (1983).

(f) While the majority of this investigation concerns rectangular tube banks, the test section and exit duct should be capable of being adapted to allow the effect of a curved wall to be examined, to simulate the real situation existing in the shell-and-tube exchangers where the bypass width and tube bank width are not uniform in the flow direction.

(g) It should be possible to fit sealing-strips to block the bypass channel in various positions along the bypass wall.

To meet the requirements of adaptability the test sections were designed to be removeable so that test sections having different tube bank configurations could be interchanged. The bypass wall was designed so that it could be moved in a direction transverse to the flow, giving an infinitely variable bypass ratio.

3.1.2 THE EXPERIMENTAL RIG

The main requirements of the rig, before and after the test section, were as follows:-

(a) A filter should be used to remove particles from the flow, to prevent damage to the hot-wire anemometer probes used in measuring the velocity distribution on entry to the bundle.

(b) The boundary layer formed on the bypass wall after exit from the contraction section should be removed to eliminate the effect it would otherwise have on the relatively narrow bypass channel.

(c) The entry and exit sections should be long enough to allow the flow to be fully developed on entry to the bundle and allow a complete pressure recovery after the bundle. The entry duct should be long enough to allow a linear pressure gradient to be established when the bundle is not present in the duct. This empty duct drop can be accounted for, when the bundle is present, to provide the pressure loss contribution of the tube bank alone.

(d) The bypass and crossflow outlets should be separate to allow the mass flow split between the two to be determined.

(e) It should be possible to divide the inlet flow into bypass and crossflow streams and allow their flow rates to be controlled to permit a thorough investigation of the mass flow distribution between the bypass and crossflow streams.

Air flow is supplied by a fan which is connected to a wide angle diffuser by a length of flexible tubing. The expanded flow then enters a filter; the air velocity here is low and therefore the pressure drop across the filter is relatively small. After a settling length the flow passes through a contraction which reduces the cross-sectional area of the duct to that of the inlet to the test section. The air then flows through the entry duct where the boundary layer on the bypass wall is bled off. Provision is made to divide the flow here using a splitter plate and control its

distribution by use of an adjustable, slatted restrictor placed across the crossflow channel. The flow then passes through the test section into the exit duct where the flow channels are separated by a splitter plate. The location of the whole bypass wall, from the boundary layer bleed to the end of the exit duct, is adjustable to allow various bypass clearance widths to be created. The flow is channelled at the end of the exit duct into two measuring tubes with orifice plates mounted in them, where the flow rates of the bypass and crossflow streams on exit can be separately measured. At the end of these tubes are mounted slide valves used to control the flow rates of the two streams.

3.2 Description of the Individual Rig Components

3.2.1 Fan

The air flow is supplied by a two-stage fan, manufactured by the Midland Fan Co. Ltd., which is powered by a 15kW electric motor. The maximum volumetric free air delivery is 0.65 m^3/s with a pressure rise of 13,500Pa. The maximum head produced is 17,000Pa in the range of 0.2 m^3/s and 0.4 m^3/s of air supply. The flow rate may be controlled by a hand-operated slide valve positioned across the outlet of the fan.

3.2.2 Wide Angle Diffuser

The diffuser used has an outlet-to-inlet ratio of 6.5 and included angle of 28°, this was used instead of the more conventional 5° of a small angle diffuser because of the limitations on the total length of the rig.

3.2.3 Filter and Settling Length

A filter from Vokes Ltd. is used, which has a 96% efficiency for particles down to 5μm diameter. This is followed by a 1m long constant cross-section settling duct.

3.2.4 Contraction

The contraction has an inlet-to-outlet area ratio of 12.4 and reduces the cross-section from that of the settling duct down to 0.2m x 0.15m i.e. to that of the entry duct. It was designed to produce a flat velocity profile at exit using the method of Cheers (1945).

3.2.5 Entry and Exit Ducts

The entry and exit ducts are made of 10mm thick plexiglass sheet and form a rectangular three-sided duct of internal dimensions 0.2m x 0.15m, each of 1m length, At a position 0.25m along the entry duct a pair of sliding plates with parallel slots cut in them can be mounted to act as a restrictor to control the crossflow stream, Fig. 3.3.

3.2.6 Test Section

A number of interchangeable test sections were produced, one for each tube bank configuration; Fig. 3.4 shows an example.

The test sections are made from 15mm thick plexiglass and consist of ducts 0.15m wide and 0.25m long with adjustable heights created by sliding bypass walls. Four test sections have been built suitable for tube pitch-diameter ratios of 1.25 and

1.375 for square in-line and equilateral-triangle arrays. Holes 13.1mm in diameter were drilled through at the tube positions and the "tubes" held in place and sealed by O-rings mounted in grooves at each end of the tubes. The tubes are represented by 12.7mm diameter aluminium rods, which are 190mm long with one shaped end to assist their removal from the test section. On the crossflow wall of the duct are mounted half-tubes to eliminate any bypass gap.

3.2.7 Moveable Bypass Wall

The fourth side wall in the test section and entry/exit ducts, the bypass wall, is formed by a sliding wall which is made airtight by rubber seals along its length. The bypass wall is built in three lengths spanning each part of the duct. The entry duct section is shaped at its front end to form the boundary layer bleed. Three test section bypass walls were built: a plain one, one on which half-tubes can be mounted, to eliminate the bypass lane and allow ideal bundle tests to be carried out, and one with slots in which sealing-strips can be fixed to block the bypass lane at the tube positions.

3.2.8 Boundary Layer Bleed and Yaw Meter

The boundary layer bleed is shown in Fig. 3.5. It consists of a wedge-shaped plate, the front of the moveable bypass wall, which channels the flow next to the wall from the main duct. This flow then passes to atmosphere via a hand operated slide valve. A yaw meter, a hot-wire anemometer X-probe, is mounted in a slide tube so it can be positioned level with where the flow divides. Thus the yaw valve, in combination with the yaw meter, can be adjusted to ensure that the main flow remains parallel to the bypass wall.

3.2.9 Splitter Plates

In both entry and exit ducts adjustable splitter plates can be used to divide the bypass and crossflow streams. These are made of sheet metal and are located at one end in either the crossflow control valve plate or the front of the end flange, and at the other in a slot in a modified tube. The plates have rubber seals along their length where they butt against the duct side walls.

3.2.10 End Flange, Transition Piece and Measuring Tubes

At the rear of the exit duct the flow passes through the end flange plate. This has two holes in it to allow the flow to divide into an ensuing transition piece which channels the flow into the two measuring tubes.

3.3 Instrumentation

The methods of measuring the air flow rates, velocity distributions, temperatures and static pressures are detailed below. A diagram showing the layout of the instrumentation is given in Fig. 3.6.

3.3.1 Air Flow Rates

The air flow velocity at the beginning of the entry duct can be determined from measurement of the pressure drop over the contraction using a calibration. Flow rates in the separate entry flow channels are found by traversing a hot-wire anemometer probe across them and measuring the velocity distribution; from this the volume flow rates can be estimated. Flow rates for the flow streams on exit from the

tube bank can be found from the pressure drop across calibrated orifice plates in the final measuring tubes; these orifices were manufactured to BS1042. These pressure drops were measured using a U-tube manometer with a resolution of ±0.5mm H_2O.

3.3.2 Velocity Distribution

From the uniform velocity profile at the inlet to the entry duct, the velocity profile will alter along the ducts length as flow distributes itself ahead of the tube bundle and the low resistance bypass channel. This distribution is determined by traversing across the duct at various upstream positions a 55P63 2-channel probe using a Dantec 56C00 constant temperature anemometer system. Traverses close to the inlet of the bypass lane were also performed in order to estimate the bypass inlet flow fractions.

3.3.3 Temperature

The air temperature upstream of the test section was measured using a 0.2mm diameter Chromel-Alumel thermocouple.

3.3.4 Static Pressures

Static pressures were measured at various positions along the entry, test and exit sections using pressure tappings in the duct walls. All the tappings were 1.6mm in diameter and were checked after drilling to ensure they were free of burrs. The tappings were connected to a transducer by PVC tubing via a Scanivalve incorporating wafer switches, which enabled many static pressures to be measured using only one pressure transducer. A Setra model 271 high accuracy differential

pressure transducer is used having a range of ±17 500Pa with an output of ±2.5V. It has an accuracy of ±0.05% of full scale output. A calibration of the transducer was carried out using a U-tube manometer, the result being given in Fig. 3.7. Provision is made to check the calibration whilst running tests by making some of the measurements with both transducer and U-tube manometer. The signal from the pressure transducer passes, via an amplifier and analogue-to-digital converter, to a BBC microcomputer. The Scanivalve is driven by an output from the computer, allowing the pressures to be recorded automatically from the various tappings.

4. PRESENTATION OF RESULTS

4.1 NORMALISATION OF THE DATA

Data are presented in the form of a pressure drop coefficient, ξ_p, and a bypass exit mass flow ratio plotted against Reynolds number, Re_{max}. The bank pressure drop was expressed as a pressure drop coefficient per row by dividing the corrected drop, Δp, by the dynamic head and the number of tube rows, to give

$$\xi_p = \frac{\Delta p}{\frac{1}{2}\rho_m u_{max}^2 N} \tag{4.1}$$

The dynamic head is based on a nominal maximum velocity, u_{max}, through the bank which is derived from the ratio for the tube bundle of total flow area to minimum flow area, A_C/A_{Cmin}, and the mean approach velocity, u, such that

$$u_{max} = u \frac{A_C}{A_{Cmin}} \tag{4.2}$$

and

$$u = \frac{\dot{m}_B + \dot{m}_C}{\rho_m A_T} \tag{4.3}$$

See Fig. 3.4 for definitions of A_C, A_{Cmin} and A_T. Pressure drop coefficients with and without bypassing are compared on the basis of a common value for u_{max}.

The bypass exit mass flow ratio is expressed as

$$\phi = \frac{\dot{m}_{Bexit}}{\dot{m}_T} \tag{4.4}$$

where

$$\dot{m}_T = \dot{m}_{Bexit} + \dot{m}_{Cexit} \tag{4.5}$$

The bypass effective mass flow ratio is expressed as

$$\phi_{eff} = \dot{m}_{Beff} / \dot{m}_T \tag{4.6}$$

The bypass inlet mass flow ratio is expressed as

$$\phi_{in} = \dot{m}_{Bin} / \dot{m}_T \tag{4.7}$$

The Reynolds number is based on the nominal maximum velocity and the tube diameter,

$$Re_{max} = \frac{u_{max} D \rho_m}{\mu} \tag{4.8}$$

4.2 Notation for Bypass Lanes

The width of the bypass lane was altered in a series of fixed steps by removing first the half-tubes from the wall and subsequently one, two or more complete longitudinal rows of tubes. The nomenclature $\frac{1}{2}T$ denotes a bypass lane formed by the removal of the half-tubes from an ideal bundle with a triangular array and $1\frac{1}{2}T$, $2\frac{1}{2}T$ and $3\frac{1}{2}T$ denote bypass lanes in which one, two and three rows of tubes, in addition to the row of half-tubes, have been removed from an ideal triangular array, see Fig. 3.4. An equivalent notation is used for square arrays with S replacing T.

4.3 Correlation of Experimental Data

The experimental data obtained from each test geometry were correlated in the form

$$\xi_p = a_1(Re_{max})^{a_2} \tag{4.9}$$

This allowed easier manipulation of the data. The parameters for this equation are tabulated in Appendix A.

5. EXPERIMENTAL PROGRAMME AND PROCEDURE

5.1 PRELIMINARY CONSIDERATIONS

The results from the present experimental investigation are intended to be applied to computer-based exchanger design models. These describe the flow through a shell-and-tube heat exchanger as a network of flow streams; such a model is shown in Fig. 1.7. It is assumed that there are no transverse pressure gradients across any of these streams, and they can be considered one-dimensional, the pressure drop along each stream being dependent on the flow resistance and flow rate of that stream. The network is solved by balancing the pressure drop across each parallel stream.

At the nodes, where the flow divides and recombines, the pressures of all the streams are considered equal. Thus, when experimentally modelling bypassing flow, the pressure tappings need to be located in regions of negligible transverse pressure gradient and the pressure drops across the bypass and crossflow streams need to be the same. This latter factor is especially important if the bypass and crossflow streams are divided downstream of the test section to allow their exit mass flow rates to be measured.

In the rig used in the tests, the upstream pressure tapping was located ten tube diameters ahead of the bank, where there is an essentially uniform velocity profile, see Section 7.3.3.

Ideally, in a bank which is infinitely long in the flow direction, the flow will become fully developed. Far downstream there will be no flow transfer across the bypass-tube bundle boundary. This will come about by the mass flow ultimately dividing between bypass and bundle so that the longitudinal pressure gradients are equal and a constant static pressure will exist across each transverse section. When a downstream splitter plate is being used, this situation can be approached by equalising the static pressures between bypass and crossflow exit ducts; this also satisfies the conditions of the network flow model. The downstream tappings need to be located

sufficiently far from the exit of the bank for the pressure in each duct to have recovered to its maximum extent and a linear pressure gradient become re-established.

With a splitter plate, the flowstreams pass through exit ducts having different cross-sectional areas and hence different flow resistances. This results in each flow having a different exit duct pressure gradient, the bypass exit duct gradient always being higher than that of the crossflow exit duct, because it has a smaller cross-sectional area and a greater flow velocity. Examples of the errors that may result from equalising the static pressures at a point ten tube diameters downstream, the chosen tapping location, are given in Appendix B. In the worst case the difference between the pressure drop of the two alternative flowstreams was only 5.3% of the crossflow stream pressure drop; in all other cases examined the difference was lower.

Before a comprehensive series of tests was undertaken, it was necessary to establish whether the presence of the splitter plate, and balancing the downstream pressures, significantly affected the flow behaviour. Therefore, a series of preliminary tests was carried out. The pressure drop over the equilateral-triangle bank, with a pitch-diameter ratio of 1.25, was measured with the exit flow undivided and then with the splitter plate present. This was performed for four bypass widths, namely $\frac{1}{2}$T, $1\frac{1}{2}$T, $2\frac{1}{2}$T and $3\frac{1}{2}$T. The pressure drop coefficients obtained are plotted against Re_{max} in Figs. 5.1 to 5.4. These figures show that there is little difference between the two sets of measurements. This was also observed by Lee (1983) in a similar experiment. There is more scatter in the data at lower Reynolds numbers, due probably to measuring errors; the uncertainty in measuring the pressure drop across the orifices becoming more significant when small flow rates, and hence small pressure drops, are being recorded.

It has thus been shown that the presence of a splitter plate has a negligible overall effect on the bank pressure drop and that the exit duct pressure drops are insignificant relative to the total bank pressure drop. For these reasons, effects of the splitter plate on the flow behaviour were considered to be negligible and in all

further tests where bypassing was present the flow was divided by a splitter plate to allow the bypass exit mass flow rate to be found.

5.2 EXPERIMENTAL PROGRAMME

5.2.1 IDEAL TUBE BANKS

Measurements of the pressure drop over ideal rectangular tube banks were performed for a range of flow rates. These results form the basis with which data from banks with bypassing can be compared. Ideal bank data can also be checked against the extensive range of published pressure loss data and correlations. Tests were also carried out to examine the effect of changing the number of tube rows, N, in the flow direction.

5.2.2 TUBE BANKS WITH BYPASSING

A comprehensive series of tests was undertaken to study the effect of creating and varying the bypass clearance in rectangular tube banks. For each array type tested a range of bypass widths was examined; the total pressure drop, crossflow and bypass exit flow rates were measured, over a range of Reynolds numbers. For the equilateral-triangle array with a pitch-diameter ratio of 1.25, a hot-wire probe was traversed across the inlet of the bypass in order to obtain an estimate of the bypass inlet flow.

5.2.3 Flow Distribution

Between the exit of the contraction, where the velocity distribution across the duct is intended to be uniform, and the entry to the bank, the flow distributes itself preparatory to entering the low resistance bypass channel and the tube bundle. Velocity measurements were taken at various positions along the duct, and as close to the tube bundle as possible, by traversing a hot-wire anemometer probe across the duct. Therefore this changing flow pattern was determined and, in particular, the angle and velocity at which the fluid enters the bypass. Hence the approximate distribution of mass flow between the bundle and the bypass at entry could be established.

5.2.4 Bypass Channel

Pressure drop measurements were taken over the bypass channel alone. Tests were performed with a number of ducts having the same widths as the bypass lanes tested in Sec. 5.2.2. The ducts had half-tubes fixed to one wall which were placed at a variety of spacings corresponding to the outermost row of tubes in the tube banks tested previously. This modelled a bypass lane without flow transfer from the tube bundle, i.e.,with constant mass flow along its entire length.

5.2.5 Tube Banks with Bypass Lanes Blocked by Sealing-Strips

Tests were carried out on equilateral-triangle and in-line square arrays, both with a tube pitch-diameter ratio of 1.25, which had the same bypass widths as examined in Sec. 5.2.2 but with the bypass lane blocked by one or more sealing-strips. With a single sealing-strip blocking the bypass at the first tube row,

measurements were taken of the bypass exit flow to determine how the bypass flow re-establishes after a sealing-strip.

5.2.6 Tube Banks with a Cylindrical Shell Wall

The 1.25 equilateral-triangle array test section used in Sec. 5.2.2 was adapted so that it modelled the situation in a real heat exchanger, where the shell wall is cylindrical and hence the tube bank width and bypass clearance are not constant in the flow direction. Pressure drop measurements were taken for a variety of bypass lane widths.

5.3 Experimental Procedure

5.3.1 Pressure Measurements

Initial measurements were undertaken to establish the empty duct pressure drop so that this could be allowed for when pressure drops were measured with the tube bank in position. The empty duct loss, between the tappings and the entry/exit of the bank, was found to be negligible in comparison with the total bank pressure drop. A series of tests was then carried out to find the downstream position, in both the bypass and crossflow exit ducts, where a constant pressure gradient became established after the tube bank, corresponding to the point where the pressure had fully recovered following its flow through the bundle or bypass. The downstream pressure tappings were located accordingly, approximately ten tube diameters downstream from the exit of the bank.

The experimental procedure for tests on banks with separated bypass and

crossflow exit streams was as follows :-

(a) The slide valve at the exit of the air supply fan was adjusted to give the approximate flow rate required.

(b) The final exit valves, at the ends of the pipes carrying the measuring orifices, were adjusted to equalise the pressure of the crossflow and bypass flow at the downstream pressure tappings.

(c) The yaw valve at the boundary layer bleed was then adjusted to give parallel flow at the yaw meter.

(d) After the flow rates and temperature had become steady, the downstream pressures were checked to ensure that they remained equal and the yaw meter reading was checked again. If no readjustment was needed, the overall pressure drop across the bank, the air temperature in the inlet duct and the pressure drops across the orifice plates were recorded. The overall bank pressure drop was frequently measured using both a U-tube manometer and the pressure transducer to check that the transducer calibration had not changed.

This procedure was then repeated for a range of total flow rates.

5.3.2 Velocity Measurements

Longitudinal and transverse velocity components of the flow were found across transverse sections 15mm, 30mm and 103mm upstream of the tube bank using a constant temperature hot-wire anemometer. Starting at the crossflow wall, measurements were made at intervals of half a transverse tube pitch for the first five transverse tube rows and subsequently every quarter of a transverse tube pitch. Using the longitudinal flow velocities, a total mass flow rate was calculated, as described in Section 7.3.3, which could be compared with the total mass flow rate measured on exit from the bank. This procedure was carried out for one flow rate for each of the bypass widths examined. For a range of flow rates, traverses were

performed across the inlet to the bypass lane alone at the closest position. From these results, inlet bypass flow rates could be estimated; see Appendix C.

6. IDEAL TUBE BUNDLES

6.1 INTRODUCTION

Four ideal tube bank arrays were investigated, viz., equilateral-triangle and in-line square, both with tube pitch-diameter ratios of 1.25 and 1.375. These results form the basis with which results for more complex, non-homogeneous tube geometries can be compared.

The effect of varying the number of tube rows in the direction of the flow was also examined.

6.2 EQUILATERAL-TRIANGLE ARRAYS

The pressure drop coefficient, ξ_p, for a bank with a tube pitch-diameter ratio of 1.25 is shown in Fig. 6.1, together with four appropriate correlations by other authors and the data of Lee (1981). For the range of Reynolds number examined, Re_{max} from 15 000 to 60 000, ξ_p falls with increasing Re_{max}, the rate of fall decreasing with increasing Re_{max}. This trend is also observed in all the correlations. The correlations of Zukauskas (1983) and Butterworth (1979) fit the data well, as do the experimental results of Lee. ESDU (1979) overpredicts the data by an average of approximately 20% and Pearce (1973) considerably underpredicts.

Fig. 6.2 shows the pressure coefficient, ξ_p, obtained for the tube pitch-diameter ratio of 1.375. Over the same Re_{max} range the relationship has the same form as for the 1.25 pitch-diameter ratio but is approximately 15% lower. The experimental data are well predicted by the correlations of Pearce and Butterworth and are in good agreement with Lee's results. ESDU, as before, considerably overpredicts, especially at higher Re_{max}. The Zukauskas correlation was not used for

this pitch-diameter ratio as it does not give direct results for this array but requires interpolation between results for pitch-diameter ratios of 1.25 and 1.5.

6.3 In-Line Square Arrays

Experimental results for ξ_p are shown in Fig. 6.3 for an in-line square array with a tube pitch-diameter ratio of 1.25. They are approximately 25% higher than ξ_p for the triangular array with the same pitch-diameter ratio and exhibit a similar fall with Re_{max}, though to a lesser extent. The correlations all underestimate the measured ξ_p; ESDU by only about 7% but Zukauskas and Butterworth are worse, especially at low Re_{max}.

Finally, pressure drop coefficients for the 1.375 pitch-diameter ratio are given in Fig. 6.4. These show the same trend as the more closely pitched bank but are approximately 15% lower. As with the other pitch-diameter ratio, all the correlations fall below the experimental data, with ESDU being the closest.

The most interesting feature of the in-line square arrays, particularly that with the larger pitch-diameter ratio, is the reduced dependence upon Reynolds number compared with the triangular arrays. At the highest Re_{max} attained, viz.,60 000, ξ_p for the 1.375 pitch-diameter in-line array is some 30% higher than that for the 1.375 triangular array.

6.4 Effect of Bank Length

Fig. 6.5 shows ξ_p for three equilateral-triangle banks of tubes with a pitch-diameter ratio of 1.375. The difference between the banks was the number of tube rows, N, in the flow direction (N = 7, 10 and 13). As can be seen, entry and exit effects are still in evidence, ξ_p for N = 10 being higher, at all Re_{max}, than for N = 13. However, the differences in the measured data for all three bank lengths are

generally no greater than the differences between the author's data and those of other investigators and of the corresponding correlations obtained from those data. Hence, it may be assumed that the error arising from applying data from measurements from banks with 10 rows to banks with a larger number of rows is not significant, bearing in mind the difficulty of establishing precise data for this type of flow.

6.5 Discussion

One interesting feature of the results is the difference between the pressure coefficients for the in-line and the staggered arrays. The measured data show that the in-line pressure drop coefficients are generally higher than those of the triangular array having the same pitch-diameter ratio, for the Reynolds number range investigated. This is in agreement with the results of Lee and of Pearce but not with the correlations of ESDU (1979), Zukauskas (1983) or Butterworth (1979). ESDU gives slightly higher pressure drop coefficients for the triangular array than for the in-line array, for both pitch-diameter ratios tested. Zukauskas's correlation produces higher ξ_p for the triangular than for the in-line arrays at low Reynolds number but as Re_{max} increases the difference becomes less until, at the highest Re_{max} achieved experimentally, ξ_p is approximately the same for both arrays. Butterworth's correlation, for both pitch-diameter ratios, has ξ_p for the triangular array higher at low Reynolds numbers, as has that of Zukauskas, but lower than the in-line array at higher Reynolds numbers. All these correlations show that ξ_p for in-line arrays is less dependent on Reynolds number, particularly at the higher values of Re_{max}, than the staggered arrays, as was observed by the present author. It should be noted that, for a particular flow Reynolds number, the actual pressure loss over an in-line bank may be lower than that over a triangular bank of the same length in the flow direction, despite the in-line array having a higher ξ_p. This is because ξ_p is defined as the number of velocity heads lost per tube row crossed and equilateral-triangle arrays have more tube rows for a given length in the flow direction.

The nature of flow through a tube bundle is complex, depending upon the geometry of the bank and the flow conditions. The difference in geometry between in-line and staggered arrays leads to a fundamental difference in the way fluid flows over them. In an in-line bank, flow can pass through the longitudinal channels between each layer of tubes. Large recirculating regions may exist which can completely fill the space between longitudinally neighbouring tubes. Thus, the principal flow is essentially one-dimensional, although contracting at each tube row and expanding in between. This is not the case in a staggered bank, providing it has a transverse pitch-diameter ratio of less than two, as it provides no direct longitudinal passage for the flow. In an equilateral-triangle bank the flow will reach a maximum velocity at the minimum flow area between the tubes in one transverse row and then it will expand and divide around the tubes in the next before accelerating into the restricted flow area created in the diagonal space between tubes in neighbouring rows (this is double the minimum flow area). The flow will then expand and recombine before accelerating into the next minimum transverse flow area. Thus, the flow area is continuously changing, varying between two minima. With both array types the degree of expansion and contraction of the flow depends on the size of the wake created behind each tube. On first examination it would appear that the smaller flow volume of the staggered array, for the same total bank volume, would lead to this array having a greater resistance than the in-line array. However, the volume occupied by recirculating flow is probably higher in the in-line case than in the staggered, where the flow is forced over the rear of the tubes by the presence of neighbouring tubes. The resistance of both arrays is dependent on the Reynolds number of the flow and the wakes created behind the tubes in the bank. Without further, more detailed study, reasons for the differences in flow pattern and the relative resistance of each array cannot be firmly established.

Despite there being a long history of research into pressure loss over ideal tube bundles, there is considerable variation between the values predicted by even the most up-to-date correlations. As well as the differences between the relative flow resistances of in-line and staggered arrays, the correlations predict a wide range of

values for similar tube arrays; including equilateral-triangle and in-line square arrays having a pitch-diameter ratio of 1.25, the most commonly used in practice. ESDU and Zukauskas differ markedly. One possible explanation for this is the location of the pressure tappings used in the investigations. When supplying the data on which the correlations were based, very few of the published reports detail exactly where the pressure tappings were positioned and those that do, put them in different locations. For example, in the Delaware research the tappings were located two tube diameters upstream and downstream of the bank, whilst Pearce (1973) located his downstream tapping at a position where a uniform velocity gradient had been re-established.

When measuring the static pressure drop over any resistance in a duct, the tappings should be located at positions with equal flow areas, so that the velocity heads at both tappings are the same. Therefore, in the case of flow over tube bundles in a duct, the tappings could be located either both in the minimum inter-tube space or in the inlet/exit ducts. The first option gives data more representative of flow inside a shell-and-tube heat exchanger, where there is little pressure recovery after leaving the tube bank, due to the tube bundle filling the shell and the flow passing through nozzles when entering and leaving the shell. However, in this location the pressure recorded is very sensitive to the exact tapping position and alignment, as the pressure and velocity distribution around a tube is highly non-uniform. For this reason most investigators have used tappings located in the free duct ahead of and behind the bundle. In this case the downstream tapping position is critical. If too close to the bundle the tapping will measure pressures which are still recovering after exit from the bundle and so the measured pressure drop will show a large dependence on tapping location.

Pressure tapping location may account for many of the discrepancies between the data of different investigators. In order to produce consistent data, it is important to position the downstream tapping where the pressure has recovered to its maximum extent. This occurs where the pressure gradient becomes constant. The

tappings must also be clear of wakes downstream of the bank and positioned away from any upstream disturbance.

6.6 Conclusions

In order to compare the data obtained accurately when bypassing is present with those for an ideal bundle, the experimental conditions need to be consistent with regard to pressure tapping location; and this may be the cause of discrepancies between the results of different investigators for similar ideal banks. Zukauskas (1983) and Butterworth (1979) predict the equilateral-triangle data extremely well but ESDU predicts the in-line square data better.

The pressure coefficient for banks of thirteen rows is somewhat lower than that for banks of ten rows, indicating that even with this large number of rows the "end effects" are still noticeable. This difference is small, however, suggesting that little would be gained by extending the work to investigate banks with yet more longitudinal rows.

7. RECTANGULAR TUBE BANKS WITH BYPASSING

7.1 INTRODUCTION

A range of bypass widths was investigated, for each of the arrays tested in Chapter Six. The overall pressure drop and the crossflow and bypass flows on exit were measured. Effective flow rates for the crossflow and bypass flow streams were calculated, using the method of Bergelin (1959) based on the ideal bundle pressure drops obtained in the previous chapter, and these were compared with the measured flow rates.

For the equilateral-triangle array with a pitch-diameter ratio of 1.25, bypass entry flows were estimated by traversing a hot-wire anemometer probe across the inlet duct just upstream of the bypass; this was undertaken for various flow rates.

7.2 PRESSURE DROP MEASUREMENTS

7.2.1 EQUILATERAL-TRIANGLE ARRAYS WITH BYPASSING

The pressure drop coefficients, ξ_p, for a bank with a pitch-diameter ratio of 1.25 and having various bypass widths are shown in Figs. 7.1, 7.2 and 7.3.

In Fig. 7.1, ξ_p is shown compared with the predictions of ESDU (1974) for ideal banks and for banks with ½T, 1½T, 2½T and 3½T bypasses. ESDU overpredicts the ideal bank pressure drop, as mentioned previously, and also overpredicts the pressure drop when bypassing is present; this is not surprising as the drop with bypassing is found by applying a correction factor to the ideal bank drop. However, the relative effect of different bypass widths as predicted by ESDU is not always the same as was observed experimentally. For the smallest bypass width, ½T, ESDU predicts that the pressure drop is almost identical to that of the ideal bank, and this is

borne out by the experimental results. ESDU predicts an almost equal reduction in ξ_p with each subsequent increase in bypass width but this is not confirmed by the experimental data. In the experimental data for bypasses greater than ½T the drop in ξ_p, with each increase in bypass width, decreases substantially, the difference between ξ_p for 2½T and 3½T bypasses being very much smaller than that between ½T and 1½T bypasses. On the other hand, ESDU's values for ξ_p do exhibit the reduced effect that Reynolds number has with increasing bypass width, which is confirmed by the author's data.

Fig. 7.2 shows the results of applying Bell's bypass correction factor, given in Equation (2.41), to the ideal bundle pressure drops obtained by the author for the 1.25 equilateral-triangle bank (the correction factor is used in conjunction with the correlation for the ideal bundle pressure coefficient given in Appendix A). The use of Bell's equation is recommended by the Heat Exchanger Design Handbook (1983), although it is seen to underestimate ξ_p for all the bypass widths tested. Bell predicts a much greater difference in ξ_p between the ½T bypass and the ideal bank than ESDU or than found by the author. Nevertheless, Bell's correction factor does produce the experimentally established trend regarding the decreasing difference of ξ_p with each increase in bypass, after ½T.

Fig. 7.3 compares the author's pressure drop data with those of Lee et al. (1983). The bypass-bundle configurations are compared on the basis of F, the ratio of minimum bypass flow area to the total minimum flow area, the bypass parameter used by Bell. It was not possible to compare exactly the same bypass area ratios but there is close agreement of ξ_p for the ideal bundle, the smallest bypass (F = 5% and 7.1%) and the largest comparable bypass (F = 45.7% and 50%). Between the two extremes, however, the data disagree; Lee's pressure drop coefficients being approximately 30% higher for the one other comparable bypass (F = 36.7% and 33.3%).

The pressure drop coefficients for the 1.375 equilateral-triangle array with bypassing are shown in Figs. 7.4 and 7.5. These show the same trends as for the closer pitched array. ESDU overestimates ξ_p for all the bypass-bundle configurations

and Bell underestimates. The experimental data show little difference in ξ_p between the two largest bypass widths examined for this array, 2½T and 3½T.

7.2.2 In-Line Square Arrays With Bypassing

The pressure drop coefficients for a 1.25 in-line square array with ½S and 1½S bypasses are given in Fig. 7.6. ESDU (1974) underpredicts the ideal bundle pressure losses but, as with the staggered arrays, overpredicts ξ_p when bypassing is present; although to a lesser degree at low Reynolds numbers in the large bypass case. Fig. 7.7 shows Bell's correction factor applied to the author's ideal bundle pressure drops. Bell, as before, underpredicts ξ_p for bypassing and, as with ESDU, estimates the larger bypass values best. A comparison with the data of Lee et al. is shown in Fig. 7.8. The bypass widths he examined are not the same as those in the present investigation. By comparing on a basis of F, however, it can be seen that Lee's pressure drop data are higher than those found by the author; Lee's plots of ξ_p for values of F of 33% and 61.5% being approximately the same as the author's bypass layouts having F equal to 23.1% and 47.1% respectively.

Figs. 7.9 and 7.10 show ξ_p for the 1.375 in-line square array with bypassing. These show the same trends as for the closer pitched in-line array except that ESDU predicts ξ_p for the large bypass extremely well and Bell considerably underpredicts ξ_p for both bypasses.

7.3 Flow Distribution

7.3.1 Equilateral-Triangle Arrays With Bypassing

The bypass mass flow ratios for the 1.25 equilateral-triangle array with bypassing are given in Figs. 7.11 to 7.15. These flow ratios are of bypass mass flow to total mass flow.

The bypass exit mass flow ratio is found from the mass flow rates measured at exit from the bank when using the splitter plate. The bypass entry mass flow ratio is based on the entry mass flow rate found by hot-wire anemometer traverses across the bypass lane inlet, close to the tube bank; its estimation is described in Appendix C. The effective bypass mass flow ratio is calculated using Bergelin's method, as described in Section 2.2.

Figs. 7.11 to 7.14 give the bypass mass flow ratios for the ½T, 1½T, 2½T and 3½T bypasses respectively. Fig. 7.15 shows the exit bypass mass flow ratios for all four bypass widths compared with the values found by Lee et al. (1983). The bypass mass flow ratios for all four bypass widths show the same trends. The exit bypass mass flow is the highest, as would be expected, the entry is the lowest and the effective bypass flow ratio is between these two.

To the best of the author's knowledge, this has been the first investigation of the bypass entry mass flow rate. This, in combination, with the exit bypass mass flow rate, gives a measure of the proportion of flow transferring into the bypass ahead of the bank and the amount transferring along the length of the bypass. Section 7.3.3 presents measurements of the upstream duct velocity profiles, where a progressive division of the upstream flow into the two alternative flow routes can be seen. The bypass entry mass flow rates were obtained only for the 1.25 equilateral-triangle bank with bypassing, as their measurement was complex and time-consuming.

For the smallest bypass, ESDU (1974) underestimates the bypass flow ratio, it being even lower than that found experimentally for the entry bypass flow ratio. ESDU's predicted bypass flow ratios should be directly comparable with the values

determined using Bergelin's method as they are both based on an independent, parallel-flow model of the tube bundle and bypass. With increasing bypass width, ESDU's predictions shift from being just higher than the effective flow ratio, in the 1½T case, to being much closer to the exit bypass flow ratio in the 3½T case. In the widest bypass configuration, up to 75% of the flow leaves the bank in the bypass stream and approximately 30% of the total flow transfers from the crossflow to the bypass stream along the length of the bank. For the 1½T bypass, up to 45% of the flow leaves the bank in the bypass stream and approximately 10% transfers to the bypass within the bank.

The effective bypass flow ratios calculated from Bergelin's method are surprisingly good, always falling between the entry and exit values determined experimentally. For the two widest bypass widths, the effective bypass flow ratios fall approximately on the arithmetic mean of the entry and exit values.

In Fig. 7.15 it can be seen that for the smallest bypass the exit bypass mass flow ratios are similar to those found by Lee et al. but for larger bypasses they found relatively lower bypass flows on exit.

Figs. 7.16 to 7.19 show the exit and effective bypass mass flow ratios for the 1.375 equilateral-triangle array. These results show similar trends to those for the closer pitch and ESDU predicts them as before; underpredicting for the small bypass and increasingly overpredicting for larger bypasses. For the largest bypass examined, up to 67% of the flow leaves the bank in the bypass stream, compared with 75% for the 1.25 pitch-diameter ratio, reflecting the effect of the decreased resistance of the greater pitched array.

7.3.2 In-Line Square Arrays With Bypassing

Bypass mass flow ratios for the 1.25 in-line square array are shown in Figs. 7.20, 7.21 and 7.22. The first two show the exit and effective bypass mass flow ratios compared with the predictions of ESDU and the last shows the exit bypass mass

flow ratios compared with the data obtained by Lee et al. The results are similar to those for the staggered array

The bypass area ratios, F, that Lee et al. examined are substantially different from the ones in this investigation but it can be seen from Fig. 7.22 that Lee et al. generally found lower exit bypass mass flow ratios than were found by the author.

Figs. 7.23 and 7.24 show the exit and effective bypass mass flow ratios for the 1.375 in-line square array and the ESDU predictions for these geometries. These results are similar to those of the staggered arrays; for the smaller bypass, ESDU's estimate is similar to the effective bypass mass flow ratio and for the larger bypass it is closer to the higher exit bypass mass flow ratio.

The bypass mass flow ratios for all the bypasses and arrays examined, both in-line and staggered, show only a slight dependence on Reynolds number; the bypass mass flow ratios dropping slowly with increasing Re_{max}.

7.3.3 Upstream Flow Distribution

Upstream velocity profiles for the 1.25 equilateral-triangle bank having ½T, 1½T, 2½T and 3½T bypass widths are given in Figs. 7.25 to 7.28 respectively. For all four bypass widths, the flow is seen to have started to diverge before the 103mm traversing position but the distortion in the velocity profile is still small. Hence, the upstream pressure tapping, located 135mm from the bank, should lie in an almost flat velocity profile. At the 30mm position there is a significant increase in the velocities closest to the bypass wall for all but the smallest bypass widths and at 15mm upstream of the bank these flow velocities are greater still. As it approaches the tube bank, the flow near the bypass to bundle boundary becomes increasingly angled towards the bypass. The angle at which the flow enters the bypass varies with bypass width. Where the flow divides on entry, into either the bypass or bundle, the angle of the flow to the main flow direction is approximately 14°, 29°, 25° and 21° for the ½T, 1½T, 2½T and 3½T bypasses respectively.

As the bypass width increases the flow close to the bypass wall on entry to the bypass lane becomes more uniform; in the 3½T case, the flow is almost parallel to the main flow direction and, for a distance of 15mm from the bypass wall, it is approximately uniform. Also from the crossflow wall there extends a region of uniform flow on entry to the tube bundle; this region covers approximately 70%, 60%, 55% and 55% of the crossflow area for the ½T, 1½T, 2½T and 3½T bypasses respectively. The ratio of maximum longitudinal velocity of the bypass entry flow to the velocity within the uniform part of the crossflow entry are approximately 1.2, 2.0, 2.2 and 2.7 for the ½T, 1½T, 2½T and 3½T bypasses respectively.

The total mass flow rate was found from the orifice plates placed after the exit duct. This value was compared with the total mass flow rate found from longitudinal components of the upstream velocity measurements. The mass flow rates derived in this way generally fell within 6% of those measured on exit. This good agreement shows that the upstream velocity measurements form a sound basis from which to derive inlet bypass mass flow ratios, shown in Figs. 7.11 to 7.14.

The inlet flow distributions observed are not unexpected. The smallest bypass shows least effect because it has a resistance comparable with that of the bank. For the larger bypasses, the flow begins to distribute itself prior to entering the alternative flow paths from approximately 100mm upstream and becomes increasingly non-uniform as it approaches the tube bank. With the larger bypasses, the two alternative flow areas are large enough for approximately uniform velocities to exist in the regions near the walls, one extending (from the crossflow wall) over half-way across the tube bundle and one extending partly across the bypass lane (from the bypass wall). Between these two fairly uniform regions there is a region of transition from one to the other.

7.4 Discussion

7.4.1 Comparison with ESDU (1974) Correlation

For the staggered arrays, ESDU overestimates the ideal bundle pressure drop coefficient, ξ_p, and when ESDU's ideal bank resistance is used in conjunction with ESDU's bypass resistance factors, in a simple parallel flow model, the predicted pressure drop coefficient for the bypass-bundle combination is also too high.

ESDU predicts the bypass flow ratios best for smaller bypasses, where ESDU's estimates are close to the effective bypass flow ratios derived from the author's data; the author's values are calculated using the same basic assumption as ESDU, that the two flow streams are independent except for having the same overall pressure drop. With larger bypass widths, ESDU overestimates the bypass flow ratio, suggesting that the relative resistance of the bypass is too low in comparison with the resistance of the crossflow.

In the 1.25 equilateral-triangle tests the relative difference between the inlet and exit bypass flow ratios generally increases with increasing bypass width (the inlet bypass flow ratios for the ½T bypass should be treated with caution as they were estimated using different assumptions than those used for the other bypass widths, see Appendix C). Thus, an increasing proportion of the flow transfers from the crossflow to the bypass flow over the length of the bundle, with increasing bypass width. The flow that passes from the crossflow to the bypass is subjected to losses associated with passing through the transverse contractions and expansions created by the tubes, and from jetting into the high velocity bypass flow at the bypass-bundle boundary. Thus, as the bypass width increases, the flow pattern becomes increasingly different from the two independent flow streams model; this probably explains the larger discrepancy between the experimental data and ESDU's predictions for larger bypass widths.

It is not surprising that ESDU's method does not predict the experimental data well. The bypass resistance factors used in it were derived from a geometrical

comparison with ideal bundles, in which there is a uniform flow resistance and no nett mass transfer between flow streams. The resistance factors so produced then had to be "factored" to make them give results consistent with unspecified data. The modified resistance factors were then applied to a simple parallel flow model with no stream interaction.

For in-line square arrays, ESDU underestimates the ideal bundle pressure drop coefficient. But, as with the staggered arrays, with larger bypasses ESDU overestimates the effective bypass mass flow ratio and hence underestimates relative flow resistance of the bypass lane. For the smaller bypass, for both pitch-diameter ratios, ESDU predicts the effective bypass flow ratio well. This is similar to the trend noted in the triangular arrays. For the in-line arrays, ESDU generally predicts ξ_p better than for staggered arrays when bypassing is present; this may be connected with the lower ξ_p predicted by ESDU for the ideal in-line crossflow bundle.

7.4.2 Comparison With Bell's (1960) Correlation

In both staggered and in-line banks with bypassing, Bell's correction factor generally underestimates ξ_p. It predicts best for closely pitched banks with large bypasses. The range of geometries tested in the Delaware investigation, and on which the method of prediction is based, was limited to equilateral-triangle arrays with two pitch-diameter ratios, 1.25 and 1.5, and only two different bypass widths, equivalent to F = 0.21 and 0.3. The range of flow conditions covered was also restricted. In the laminar range, Re_{max} from approximately 1 to 90 was examined. In the turbulent range, for the 1.25 equilateral-triangle bank, Re_{max} varied from 2 000 to 16 000 and for the 1.5 equilateral-triangle bank it varied from 2 000 to 8 000. From the data obtained in the current investigation, it can be observed that variations of resistance with Re_{max} are different in the bundle and in the bypass. ξ_p for the crossflow falls with Re_{max} but ξ_p for the bypass stays approximately constant, being far less

dependent on Re_{max}; this can be seen by comparing ξ_p for the widest bypass, where the majority of the flow is in the bypass, with that of the ideal bundle, see Fig. 7.1. The result of this difference in Re_{max} dependency leads to the relative resistance of the crossflow falling with increasing Re_{max}. This explains the fall in bypass exit mass flow ratio with increasing Re_{max}, observed for all the bypass widths tested. Because of this effect, the validity of extrapolating Bell's correction factor to the higher Re_{max} of the present investigation must be questioned, although this is commonly done in practice.

The reason for the relatively better performance of Bell's method at larger bypass widths can be explained by the fact that the correlation is based only on data for two large bypass widths, no data being available for $F < 0.21$, and therefore the correlation was not influenced by data covering a large range of bypass widths; although Bell's correlation does converge to the correct limiting cases, when $F = 0$ it gives the ideal bank pressure drop and when $F = 1$ it gives the empty duct pressure drop.

There may be some uncertainty in the precise pressure drop measured by Destremps (1956) and Bryce (1957), as part of the Delaware investigation from which Bell's bypass correlation was produced. The pressure tappings they used were located only two tube diameters upstream and downstream of the tube bank, and half-way between the bypass and crossflow walls. In these positions there must be some inconsistency in the pressure drops measured for different bypass widths. Upstream the tapping will lie in a position where the flow has partially distributed itself between the two flowstreams and downstream it will have only partially recombined. From Figs. 7.25 to 7.28 it can be seen that there is a considerable transverse velocity at the duct centre line two tube diameters upstream, indicating the presence of a transverse pressure gradient, and the ratio of transverse to longitudinal velocity varies with bypass width.

7.4.3 Comparison With the Data of Lee et al. (1983)

The values of ξ_p found by Lee et al. for the ideal bundle and the smallest bypass width agree well with the author's data. But, when compared on a basis of F, the fraction of the total flow area that is in the bypass lane, their values of ξ_p are generally higher than the author's and as would be expected their values of bypass exit mass flow ratio are lower. This is true for all bypass widths in the 1.25 in-line and 1.25 equilateral-triangle arrays except for the largest bypass examined in the triangular array, 3½T, where there is good agreement between the author's values of ξ_p (for F = 45.7%) and the values of Lee et al. (for F = 50%). The experimental rigs used in this and in Lee's investigations are very similar in design; the main differences between them are in tube diameter, Lee used 19mm diameter tubes, and n, the number of tubes across the flow direction. In the current investigation, for the 1.25 equilateral-triangle bank n = 19.5, for the in-line square bank n = 10.5 with the ½S bypass and n = 9.5 with the 1½S bypass. In experiments of Lee et al., n varied from 10.5 to 13.5 in the triangular bank and from 6.5 to 7 in the in-line square bank. Therefore, it is possible to have two bundle-bypass geometries with the same value of F, the only parameter in Bell's correction factor, Equation (2.41), needed to define the bypass geometry, but to have a very different number of transverse tube rows, n. Fig. 7.29 shows an example of this, two tube banks having the same value of F but one having twice the value of n as the other. However, from a comparison of the experimental data with those of Lee et al., it has been seen that two banks, with bypassing, having a common value of F do not necessarily have the same flow resistance which is almost certainly due to a difference in the value of n. The number of transverse rows crossed by flow transferring from the tube bundle to the bypass affects the resistance to this flow transfer, in the same way as the pressure drop in the main flow direction depends on the number of tube rows crossed.

From the inlet velocity profiles, Figs. 7.25 to 7.28, it can be seen that flow entering the crossflow is approximately uniform over much of its width; varying substantially only in the region of the bypass-bundle interface. Thus, the influence

of the bypass on the transverse flow decreases with distance from the bypass lane. Within the bank there will be a region where the bypass affects the flow only by virtue of the decrease in the effective crossflow velocity and not significantly by transverse flow transfer. In the tests of Lee et al. with narrower banks this effect may not have become established and the whole width of the crossflow has been influenced by transverse flow, leading to his pressure drop coefficients being higher than the author's, except for the small and ideal bypass case where there is less or no transfer between flowstreams.

One interesting feature of the flow distribution data is that for similar bank widths, across the flow direction, two different array types, staggered and in-line, having the same pitch-diameter ratio and F produce similar bypass mass flow ratios, both based on the exit and effective flow rates; compare Fig. 7.12 with 7.20, Fig. 7.15 with 7.23 and Fig. 7.19 with 7.24. The only exception is the 1.25 staggered and 1.25 in-line banks with the largest bypass, Figs. 7.14 and 7.21 respectively, in which the in-line array has a generally higher bypass exit flow ratio.

7.5 Conclusions

ESDU (1974) generally overestimates the pressure drop coefficients. Bell's (1960) correction factor overestimates the influence of the bypass lane, underpredicting the bank pressure drop coefficients.

The proportion of the flow transferring from the bundle to the bypass increases with increasing bypass width. This may lead to independent, parallel flowstream models becoming less valid at these larger bypass widths. There is a considerable redistribution of flow ahead of the tube bank when a bypass lane is present. It would, therefore, be inaccurate to base the inlet flow distribution upon

the relative areas alone, except possibly for very small bypass widths. The flow redistribution occurs mostly within ten tube diameters upstream of the bank.

The pressure drop over a tube bank with a bypass lane is dependent on the number of tube rows across the flow as well as the ratio of bypass flow area to total flow area.

8. BYPASS LANE, WITH NO FLOW TRANSFER FROM BUNDLE

8.1 INTRODUCTION

In exchanger flow models the bypass lane is commonly defined as being between the centreline of the outermost row of tubes and the shell wall; hence a duct with one plain wall (the shell-side) and one wall having half-tubes (the bundle-side) was used to model a bypass lane in which there was no transfer from the adjacent bundle. In simple parallel-flow models the boundary between the bypass lane and the bundle is considered solid, with no flow transfer between the two.

A long splitter plate was positioned between the inlet control valve and the exit flow dividing plate, see Fig. 3.1; this represented the shell wall. The bundle-side was created by using the bypass walls built for the ideal bundle tests; these had half-tubes attached to them at the correct transverse pitch.

The bypass lane for the triangular array had N/2 half-tubes (for even N), one for every other row in the flow direction, whereas the square array bypass had N half-tubes, one every row. The pressure drop and flow rate were measured over a range of duct widths, corresponding to the bypass widths 1½T, 2½T and 3½T for the 1.25 equilateral-triangle array and ½S and 1½S for the 1.25 in-line square array. The same number of tubes along the duct was used as in Chapter 7. Fig. 8.1 is a diagram of typical geometries tested. No tests were performed using the ½T triangular array as previous tests on tube banks with these narrow bypass lanes had shown that the pressure drop was found to differ little from the ideal bundle case, see Fig. 7.1. Measurements were also taken of empty duct pressure drop, where the ducts had the same widths as the bypass lanes but no half-tubes.

Data for the crossflow section of the independent parallel-flow model could be obtained from the ideal bundle tests of Chapter 6.

8.2 PRESSURE DROP MEASUREMENTS

The results are presented as a bypass pressure drop coefficient, ξ_b, plotted against Reynolds number, Re_b.

$$\xi_b = \frac{\Delta p_B}{\frac{1}{2}\rho_m u_b^2 (L/D_e)} \tag{8.1}$$

where D_e = hydraulic diameter of the duct,

$$= \frac{4bl}{2(b+l)} \tag{8.2}$$

and

$$Re_b = \frac{u_b \rho_m D_e}{\mu} \tag{8.3}$$

where u_b = mean velocity of flow in duct,

$$= \frac{\dot{m}_B}{\rho_m bl} \tag{8.4}$$

Fig. 8.2 shows ξ_b plotted against Re_b for the 15.8mm bypass width, corresponding to the 1½T and ½S bypass. Values are given for the empty duct, for the equilateral-triangle array bypass and for the in-line square array bypass. In addition points are included for ξ_b from the data obtained with flow transfer into the bypass from the bundle, as described in Chapter 7. For the latter, two values of ξ_b are given:

(i) based on the measured bypass exit mass flow;

(ii) based on the effective bypass mass flow.

This figure shows that the pressure drop with half-tubes present is considerably higher than for the empty duct. The values of ξ_b for the bypass lane alone and those based on the bypass exit mass flow rates for the bundle-bypass configuration are similar, both for the triangular and the in-line geometries. However, the values of ξ_b based on the effective bypass mass flow rates are higher than those found for the other two cases, based on exit flow rates and for the bypass lane alone.

Fig. 8.3 shows the values of ξ_b, based on the same bypass flow rates as Fig. 8.2, for the 1.25 equilateral-triangle array having a 2½T bypass; there is no equivalent bypass width for the in-line square array corresponding to a bypass width of 23.8mm. ξ_b for the bypass lane alone, with no flow transfer, is approximately half that for the smaller bypass. The values of ξ_b based on the exit bypass flow rates are approximately 80% of those for the smaller bypass. The main difference between these data and those of Fig. 8.2 is that the ξ_b based on the exit bypass flows are higher than those for the bypass lane alone, as before, the values of ξ_b based on the effective flow are higher than the other two.

Fig. 8.4 shows the values of ξ_b for a 31.8mm bypass width, corresponding to a 3½T bypass in the 1.25 equilateral-triangle array and a 1½S bypass in the 1.25 in-line square array. It can be seen that, for the bypass lane alone, ξ_b for the triangular array bypass is higher than that for the square array. Values of ξ_b based on the exit bypass mass flow rates are higher for the in-line square array bypass than for the triangular array. For the staggered array, ξ_b based on the bypass exit mass flow is approximately 70% of that for the 23.8mm bypass.

ξ_b for all bypass widths and array types, whatever bypass flow rate it is based upon, is generally independent of Reynolds number. The main exception is for the 1½S bypass,and based on the effective bypass flow rate; this shows a dramatic fall with Reynolds number at low Re_b before reaching a steady value.

8.3 Discussion

For all the bypass widths examined it can be seen that there is considerable scatter in the pressure coefficient based on the effective bypass mass flow rates found by Bergelin's method. This is due to the fact that they are derived from both the ideal bundle data and data for bundles where bypassing is present and are thus susceptible to the errors in both data sets. At low Reynolds number the measuring errors in both sets of data become more significant.

For the smallest bypass width, viz. 15.9mm, ξ_b for both the in-line and staggered banks are similar. ξ_b is based on the length of the bypass, not on the number of flow constrictions, to allow comparison with the empty duct pressure drop. The number of flow constrictions is different in the two array types for banks of approximately equal length. The triangular array has seven half-tubes in the bypass lane and the in-line array has twelve. This suggests that, for this bypass width, the pressure drop is not dependent on the number of flow constrictions, unlike flow in the bundle. Thus, flow in this bypass probably does not significantly recover between each tube, the number of flow contractions and expansions being the only factor dependent on N.

Values of ξ_b based on the flow through the bypass lane alone and those based on the exit bypass flow rate, which includes a flow transfer from the bundle component, are similar. This indicates that flow transfer between the flowstreams does not significantly alter the pressure drop. Note, however, that in Chapter 7 it was seen that the ratio of flow transfer to total flow becomes less as the bypass width becomes smaller. ξ_b based on the effective bypass flow rates are seen to be higher than those based on the other bypass flow rates. The only difference in the values between those based on the exit and on the effective bypass flow rates is in u_b. The bypass stream velocity, u_b, at the exit of the bypass is always higher than the effective bypass stream velocity, resulting in a higher ξ_b for the effective bypass stream.

The values of ξ_b based on exit bypass flow rate and on the flow through the bypass lane alone are directly comparable. Both are based on a flow rate at the "exit" of the bypass. Any difference in ξ_b will be due to the formation of the exit bypass flow upstream. For the bypass lane with no flow transfer, the pressure drop associated with the approaching flow accelerating into the minimum bypass clearance is approximately half of the total pressure drop, for both array types.

Turning now to the 23.8mm bypass, ξ_b based on the exit bypass flow that includes transferred flow is approximately double the value based on the flow through the bypass lane alone with no flow transfer. This indicates that the increased proportion of flow transferring between the streams leads to an increase in the bypass pressure drop, as seen in Chapter 7. For the bypass lane alone (no flow transfer) the pressure drop associated with the approaching flow accelerating into the minimum bypass clearance is now approximately 90% of the total bypass pressure drop.

For the 31.8mm bypass, with a triangular array, ξ_b based on the exit bypass flow including transferred flow is approximately double that of the value for the bypass lane alone, similar to the 23.8mm bypass. But for the in-line square array this ξ_b, the pressure coefficient described above, is over four times higher than ξ_b for the bypass lane alone and 60% higher than the equivalent ξ_b for the triangular array. This would indicate that there is more resistance to flow transfer in the square array than for the staggered. This is as would be expected. In an ideal in-line bundle the flow is essentially in the main flow direction, in the longitudinal channels between the tube rows. However, in an equilateral-triangle array flow between tubes in neighbouring rows is at an angle of ±30° to the main flow direction. Therefore, at the boundary of the bypass lane and tube bundle flow transferring from an in-line bundle must turn through 90° and jet at this angle into the bypass, whereas in the staggered array, flow entering the bypass from the bundle will have a longitudinal velocity component and thus experience less associated pressure loss. For this larger bypass width ξ_b for the triangular array is higher than that for the in-line array, for the bypass lane alone, i.e.,with no flow transfer. This is despite the fact that there are more flow constrictions in the in-line bypass. The closer tube pitch of the in-line

bypass means that there is probably less flow expansion between the tubes and consequently less associated pressure loss. This effect is in contrast to the smallest bypass width where there was little difference in ξ_b between array types. The pressure coefficient based on the effective bypass flow rates are inconsistent with values calculated by the other means. At low Re_b, ξ_b is higher for the square array than for the staggered, but at higher Re_b the opposite is true. Also ξ_b found for all other bypass widths and array types are approximately independent of Reynolds number. ξ_b based on the effective flow for the square array having the largest bypass falls dramatically with Re_b. This effect could be due to the compounded error in these effective values mentioned earlier, which are especially significant at low Reynolds number. If the ξ_b found for the lowest four values of Re_b were neglected, the Reynolds number dependency would be less pronounced and the ξ_b for the staggered array would generally be higher than for the in-line array.

For the bypass lane alone (no flow transfer) the pressure drop associated with the approaching flow accelerating into the minimum bypass clearance is approximately equal to the total bypass pressure drop for the triangular array, and approximately double the total bypass pressure drop for the square array, the irrecoverable pressure drop over the triangular bypass being much higher than over the in-line bypass.

8.4 Conclusions

The pressure drop coefficients for the bypass lane are generally independent of Reynolds number.

Bypass pressure drop coefficients for the bypass-bundle combination become increasingly higher, in relation to those for the bypass lane alone, with increasing bypass width, confirming the effect seen in Chapter 7 that there is an increasing contribution to the bypass pressure drop from the flow transfer with increasing

bypass width. At the smallest bypass width the effect of flow transfer was seen to be negligible. Bypass pressure drop coefficients fall with increasing bypass width.

For large bypasses there is more resistance to flow transferred from bundle to bypass in the in-line square array than in the triangular array but less resistance to flow in the in-line bypass than in the triangular one.

9. RECTANGULAR TUBE BANKS WITH BYPASS LANES BLOCKED BY SEALING-STRIPS

9.1 INTRODUCTION

Two tube arrays were investigated, 1.25 equilateral-triangle and 1.25 in-line square, having bypass lanes blocked by sealing-strips. The ½T, 1½T, 2½T and 3½T bypasses investigated in Chapter 7 were re-examined for the situation where one, two and four sealing-strips were present. The ½S and 1½S bypasses were investigated with one, two and five sealing-strips. When only one sealing-strip was used it was always placed at the most upstream minimum bypass wall-to-tube clearance and completely blocked the gap between the wall and the nearest longitudinal row of tubes. When a second sealing-strip was used it was placed to block the similar clearance furthest downstream, see Fig. 9.1. Further sealing-strips were placed equidistantly along the bank.

When only one sealing-strip was present the splitter plate was used to measure the bypass exit mass flow; when more than one sealing-strip was present the bypass exit was always blocked, making the splitter plate redundant.

9.2 PRESSURE DROP MEASUREMENTS

The pressure drop coefficient, ξ_p, for a 1.25 equilateral-triangle bank having ½T, 1½T, 2½T and 3½T bypasses, each blocked in turn by one, two and four sealing-strips, is shown in Figs. 9.2 to 9.5 respectively. It is compared with the coefficients predicted by Bell's bypass and sealing-strip correction factor, Equation (2.41), applied to the ideal bundle pressure drop obtained in Chapter 6. Also shown is the pressure coefficient that would be obtained if the bypass were completely filled in and all the flow passed through the now restricted tube bundle.

Fig. 9.2 shows ξ_p for the ½T bypass. Experimentally there is very little difference in ξ_p for any number of sealing-strips, although generally the ideal bundle and the bypass with four sealing-strips result in a slightly higher value than that for the plain bypass and the bypass with one sealing-strip. As seen before, Bell underestimates ξ_p for the bypass without sealing-strips but when sealing-strips are present it predicts ξ_p very well.

Fig. 9.3 shows ξ_p for the 1½T bypass. The experimental data show that the use of two sealing-strips results in ξ_p increasing approximately to that obtained from the ideal bundle. The use of four sealing-strips produces a value higher than that of the ideal bundle. Bell once again underpredicts ξ_p for the plain bypass and also underpredicts the effects of using sealing-strips; when $N_s = 4$ Bell estimates ξ_p to be lower than for the ideal bundle.

Fig. 9.4 shows ξ_p for the 2½T bypass with sealing-strips, which follows the same pattern as for the 1½T bypass. Bell also predicts these data with much the same discrepancy as for the 1½T bypass.

Fig. 9.5 shows the pressure drop coefficients for the 3½T bypass. The experimental data and Bell's predictions are similar to those for the 2½T bypass except that when two sealing-strips are present the resulting ξ_p are slightly higher than for the ideal bundle.

The pressure drop coefficients, ξ_p, for a 1.25 in-line square bank having ½S and 1½S bypasses, each blocked in turn by one, two and five sealing-strips, are shown in Figs. 9.6 and 9.7 respectively. These are also compared with values using Bell's correction factor applied to the ideal bundle pressure drop data found in Chapter 6.

Fig. 9.6 shows ξ_p for the ½S bypass. The experimental data show that the use of sealing-strips has less effect when used to block bypasses in the in-line square array than in the equilateral-triangle array. The presence of one strip has almost no impact, ξ_p being the same as for the plain bypass, and when $N_s = 5$ it is still less than for the ideal bundle. Bell underpredicts for the plain bypass but predicts ξ_p for the cases when sealing-strips are present much better, in general over-predicting them by less than 10%, compared with underpredicting for the plain bypass by around 25%.

Fig. 9.7 shows the pressure drop coefficient for the 1½S bypass. The experimental data, as before, show the sealing-strips having a reduced effect in comparison with that of the staggered array. The use of two sealing-strips produces a ξ_p just less than that for the ideal bundle but when $N_s = 5$ it is much higher than for the ideal bundle. Bell predicts ξ_p for the 1½S plain bypass better than for the ½S and also well predicts ξ_p resulting from the use of one sealing-strip. However, Bell considerably underpredicts ξ_p when two or five sealing-strips are used.

9.3 Flow Distribution

The exit bypass mass flow ratios, when only one sealing-strip was present, are given in Figs. 9.8 and 9.9. They are compared with the exit bypass mass flow ratios obtained for the bypass without sealing-strips.

Fig. 9.8 shows the exit bypass mass flow ratios, ϕ_s, for the ½T, 1½T, 2½T and 3½T bypasses in a 1.25 equilateral-triangle array. The exit bypass mass flow ratios obtained with a sealing-strip, ϕ_s, are compared with those found for the plain bypass, ϕ , where $N_s = 0$. There is little difference between the values obtained for the smallest, ½T, bypass. For all the larger bypass widths, the exit bypass mass flow ratios found when one strip is present are lower than those found for the plain bypass. For the 1½T, ϕ_s is approximately 15% lower than ϕ and for the 2½T and 3½T approximately 20% lower.

Fig. 9.9 shows ϕ_s and ϕ for the ½S and 1½S bypasses in a 1.25 in-line square array. As with the triangular array, there is little difference between them for the smallest bypass width. For the larger bypass, 1½S, ϕ_s is approximately 12% lower than ϕ.

9.4 DISCUSSION

In order that these experimental data can be applied to flow network models, it is necessary to know the longitudinal distance over which a sealing-strip is effective; over how many tube rows can the flow (diverted by the sealing-strip) be considered to remain within the tube bundle as pure crossflow ? A simple measure of this can be obtained by considering the flow over the tube bank, with bypass and sealing-strips, in two parts: one consisting of "pure crossflow" for $N_s.N_c$ rows (N_c is the number of rows of pure crossflow equivalent to one sealing-strip) and the other consisting of the remainder of the tube bank subject to crossflow with bypassing (having the same pressure drop characteristics as found in Chapter 7), see Fig. 9.10.

Appropriate values for N_c are found by equating the predicted pressure drop across these two "model" banks with the measured pressure drop across the bank with sealing-strips. For details of the calculation method, see Appendix D. In some cases N_c is negative; this occurs when the pressure drop over a bank with bypass and sealing-strips is less than that of the same bank and bypass with no strips. In this situation, N_c represents the number of tube rows of pure crossflow per sealing-strip that would need to be added to the "model" bank to make the pressure drop over it equal to that measured over the bank with sealing strips.

Figs. 9.11 to 9.16 show N_c plotted against Reynolds number for all the bypass and sealing-strip combinations mentioned in Section 9.1.

Fig. 9.11 shows N_c for the ¼T bypass, in a 1.25 equilateral-triangle array, with sealing-strips. For one sealing-strip N_c is just negative. The N_c found when two and four sealing-strips are used falls with Reynolds number until attaining a steady value above Re_{max} = 40 000. When two strips are present N_c reaches a steady value of zero and when four strips are present the value of N_c becomes approximately one.

The graphs of N_c show much more scatter in the values for the smallest bypass width than for the wider ones. The effect of N_c in these narrow lanes is, however, very much smaller because the pressure drops of pure crossflow and of flow with bypassing are almost the same, so whether N_c is 0 or +3 makes little difference

to the overall pressure drop. The negative values of N_c are so small, never greater in magnitude than -0.12, that they can be accounted for by experimental errors, such as unavoidable measurement uncertainties.

Fig. 9.12 shows N_c for the 1½T bypass with sealing-strips. The values of N_c obtained for one and two sealing-strips are approximately equal; when four strips are present N_c is approximately 30% lower. For all numbers of strips, N_c increases slightly with Re_{max}. In Fig. 9.3 it was seen that the overall effect of using four sealing-strips in this bypass, 1½T, was to increase the pressure drop coefficient above that of the ideal bundle. With this number of strips N_c is approximately three, hence for around twelve rows out of a total of fourteen, the flow can be treated as pure crossflow. This crossflow occurs in a diminished flow area, due to the presence of the strips, compared with the area that would exist if the tube bundle extended into the bypass and was thus an ideal bundle. This creates a higher flow velocity in the crossflow than in the ideal bundle, resulting in a greater pressure drop.

Fig. 9.13 shows N_c for the 2½T bypass with sealing-strips. When one or two sealing-strips are used N_c is higher than that for the 1½T bypass. When four strips are used N_c, as with the 1½T case, is approximately three. All values of N_c for this bypass show a different Reynolds number dependency that that seen in the 1½T bypass, but the variation is slight. From Fig. 9.4 it can be observed that when $N_s = 2$ the pressure coefficient of the resulting bank is approximately the same as for the ideal bundle; this occurs when approximately two-thirds of the tube rows in the bank are behaving as if they were experiencing pure crossflow.

Fig. 9.14 shows N_c for the 3½T bypass with sealing-strips; it exhibits the same trends seen with the 2½T bypass. As more sealing-strips are added the pressure drop coefficient approaches the value that would exist if the flow passed just through the tube bundle and avoided the bypass altogether due to the presence of the strips, i.e., the pure crossflow case. When four sealing-strips are used N_c is approximately three for all bypasses, i.e., around twelve of the fourteen tube rows are experiencing pure crossflow. In this situation flow in the bypass is almost stagnant. The addition of

more strips, in this case, would have little effect as the flow is already constrained within the tube bundle.

Fig. 9.15 shows N_c for the ½S bypass, in a 1.25 in-line square array, with sealing-strips. As with the smallest triangular bypass, the use of one sealing-strip has little effect, N_c being approximately zero. When two and five sealing-strips are used N_c is similar, around unity, which is considerably less than found for the equivalent bypass width in the staggered bank.

Fig. 9.16 shows N_c for the 1½S bypass with sealing-strips. For five sealing-strips N_c is approximately constant at two, equivalent to ten rows out of twelve behaving as if in pure crossflow; this is similar to the situation seen in the staggered array where the flow in the bypass lane becomes almost stagnant.

From the data, it would appear that the addition of each sealing-strip has a similar effect for each separate array type, until the situation is reached where flow in the bypass lane becomes stagnant, after which the addition of more strips has a considerably reduced effect. As seen in the 2½T bypass, the addition of one strip is equivalent to approximately 35% of the tube rows experiencing pure crossflow, two strips 70% and four strips 85%.

The Reynolds number dependencies of N_c are small and probably not significant. Therefore, the error in the overall pressure drop introduced by assuming a constant value of N_c with respect to Re_{max} will be small. An average value of N_c from the data for one and two sealing-strips is given in Table 9.19 for each bypass and array type investigated.

The effectiveness of sealing-strips in producing pure crossflow, a measure of their ability in eliminating bypassing flow, is less in in-line arrays compared with staggered arrays. This is probably due to the different Reynolds number dependency of the pressure drop coefficients of the ideal bundle between in-line and staggered arrays. In in-line arrays ξ_p is far less dependent on Re_{max} than in staggered arrays where ξ_p falls with Re_{max}. When a sealing-strip is introduced all the flow is diverted into the bundle. This results in the Reynolds number in the reduced pure crossflow area, see Fig. 9.10, increasing. In the staggered array this causes the pressure drop

coefficient to fall more than it does with the in-line array; thus the relative flow resistance between the bundle and bypass lane is less in the staggered array. This leads to relatively less flow transferring back into the bypass after a sealing-strip in the staggered array. Hence, in a staggered array relatively more flow remains pure crossflow, resulting in higher values of N_c in these arrays.

9.5 Conclusions

It was found that sealing-strips are more effective in keeping the diverted bypass flow within the tube bundle in staggered arrays than in in-line ones. For the tube bank depths examined, it was found that one sealing-strip produced an overall pressure drop equivalent to having approximately five rows of pure crossflow in a triangular array and approximately three tube rows in an in-line array. The addition of a large number of sealing-strips caused the flow in the bypass to become almost stagnant.

For small bypass widths the use of only one sealing-strip was found to have little or no effect.

In the triangular array the effectiveness of each sealing-strip was found to increase slightly with increasing bypass width.

Tabulated average values of N_c are given in Table 9.19.

10. BYPASS FLOWS IN CYLINDRICAL EXCHANGERS

10.1 INTRODUCTION

Up to this point the current study has been solely concerned with flow through rectangular tube banks, in which the duct has constant dimensions in the flow direction. However, the vast majority of shell-and-tube heat exchangers have cylindrical shells. This leads to the bundle width and the bypass width changing row by row. In order to investigate the effects of a cylindrical shell on bypassing flow, a series of tests was performed using a curved bypass wall in a modified test section of the earlier, rectangular bank rig. The bypass and bundle geometry were designed to model the section of the exchanger shown in Fig. 10.1. The curved bypass wall represents the shell wall of an exchanger with approximately four times the diameter of the tube bank width studied in chapters 6, 7 and 9. The tube bank model extends in the main flow direction from the transverse shell diameter to the position of a 25% baffle cut. Transverse to the flow, the tube bank model extends from the shell wall one quarter of the way across the shell diameter. Therefore the model will differ from the region it represents in the real exchanger, see Fig. 10.1, in that no flow can enter the model tube bank through its crossflow wall, see Fig. 10.2. Any flow that might have occurred in this region is likely to be small. Figs. 7.25 to 7.28 have shown that the magnitude of transverse flow decreases with distance from the bypass and, therefore, the assumption that no transverse flow occurs at the point halfway between the shell and the longitudinal diameter of the exchanger should not result in a significant error. If the rectangular tube bank described in previous chapters had been adapted to model half of the exchangers transverse width, it would have had only half the number of longitudinal tube rows, N, and entry/exit effects would have been more significant.

The test section used is shown in Fig. 10.2. On exit from the tube bank the flow passes into a duct where pressure recovery occurs before its flow rate is

measured using orifice plates, as for the rectangular bank tests. The exit duct has its bypass wall extending from the curved bypass wall at the point where the baffle edge would be for a 25% baffle cut. Thus the bypass wall of the exit duct, and the whole of the exit duct, is at an angle of 30° to the bypass wall of the inlet duct, and the exit bypass flow is channelled into the duct at the same angle that it has when it emerges from the bank.

Several bypass widths were tested. The first included a shell-tube bundle clearance which, at one transverse row, was zero; i.e. the tube touched the bypass wall. Tubes were removed to create three successively wider bypass lanes; the tubes removed are marked on Fig. 10.2.

Pressure drop coefficients are calculated taking account of the static pressure drop associated with the velocity increase due to the contraction of the flow area over the bank length.

10.2 Pressure Drop Measurements

The pressure drop coefficients of these cylindrical tube bundles with bypassing are shown in Fig. 10.3. They are similar in form to those found for the rectangular tube bundle with bypassing. With large bypass widths, ξ_p is almost constant and as bypass width decreases ξ_p becomes more dependent on Reynolds number, ξ_p falling with Re_{max}. Also given in Fig. 10.3 is the calculated pressure coefficient of an "ideal" cylindrical bank. This ideal ξ_p is calculated on a row-by-row basis using the ideal bundle pressure drop data found in Chapter 6; it takes into account both the increase in Reynolds number, as the bank width decreases, and the pressure drop associated with the velocity increase between the bank inlet and exit. It can be seen that this calculated ideal bundle pressure drop coefficient is slightly higher than that found experimentally for the smallest bypass width.

10.3 Discussion

The addition of a cylindrical shell wall considerably increases the complexity of the geometry. It creates the need for four more parameters to describe the geometry;

i) D/D_{sh}, the ratio of tube diameter to shell diameter,

ii) P_t/D_{sh}, the ratio of tube pitch to shell diameter,

iii) B_c/D_{sh}, the ratio of baffle cut to shell diameter,

iv) a parameter to account for the ratio of bypass width to shell diameter.

The last of these variables is particularly complicated because the bypass width is not generally constant with a cylindrical shell, but changes from row to row. In the absence of other leakage flows, the method given by ESDU (1974) and network flow models simplify the flow into two parallel independent flow streams. This requires the determination of an effective crossflow width and an effective bypass width, in order that the different flow areas and resistances of the two streams can be calculated. Semi-analytical methods, such as in Bell (1960) and the Heat Exchanger Design Handbook (1983), also require effective values of crossflow and bypass widths to calculate F, the ratio of bypass flow area to total flow area, the parameter used to account for bypassing.

ESDU (1974) does not give details of how its method can be applied to cylindrical shells and HEDH (1983) just recommends that the outermost row of tubes of a bundle are placed on a constant diameter, thus giving a constant bypass width. The methods used in commercial network flow models to determine effective flow areas are not available in the open literature. Tinker (1948), presenting the first network flow model, gives the effective bypass width as being equivalent to the smallest gap, and the effective crossflow width as the mean crossflow width between the two baffle cuts. Emerson (1962) suggests using the inverse root mean square of the crossflow areas, which are different for each tube row in a cylindrical heat exchanger, as the effective crossflow area. If A_{Ceff} is the effective crossflow area then the effective velocity is proportional to $(1/A_{Ceff})$ and the mean pressure drop

proportional to $(1/A_{Ceff})^2$, assuming a constant friction factor in the tube bundle; this is not strictly true but the difference in Reynolds number, between inlet and exit of the bundle, will generally not be large enough to cause a significant variation of ξ_p through the bank. Hence

$$N(1/A_{Ceff})^2 = \sum_{i=1}^{N} (1/A_{Cmin})^2$$

and

$$A_{Ceff} = \frac{N}{\sum_{i=1}^{N} (A_{Cmin})^{-2}}$$

The same principle could equally well be applied to the effective bypass width.

The values of ξ_p, Fig. 10.3, show a very similar pattern to that of rectangular banks with bypassing. With a small, or no, bypass, ξ_p falls with Reynolds number. As the bypass width is increased a greater proportion of the flow is in the bypass stream, the pressure drop coefficient of which is lower and less Reynolds number dependent than that of the crossflow stream. The "effective" width of a bypass in a cylindrical exchanger should be equal to the bypass width in a rectangular exchanger having the same effective crossflow width and pressure drop characteristics. By comparing the results shown in Fig. 10.3 with the pressure drop coefficients obtained for rectangular tube banks with bypassing, given in Chapter 7, it can be seen that the "effective" bypass width has a greater dependency on the smaller bypass clearances than the larger ones. The pressure drop coefficients of bypass width number 1 are just lower than the calculated values for the ideal bundle, despite the fact that for some of the tube rows there are relatively large bypass clearances, see Table 10.1. The mean bypass clearance for this geometry is 6.9mm. In the rectangular bundle such a bypass would have led to a much greater fall in ξ_p, a bypass clearance of

6.9mm is equivalent to a 13.3mm bypass width in the rectangular bank. The inverse root mean square of the bypass clearances, for this geometry, would give a mean bypass clearance of zero, which is more characteristic of the effective bypass clearance than the arithmetic mean. The weighting that the inverse root mean square gives to small values over large values of the bypass clearance makes it more characteristic of the effective bypass clearance than the arithmetic mean. The inverse root mean square method of defining the effective bypass clearance gives a better representation of the varying bypass width than the smallest clearance methods because it includes all the clearances in its calculation. In a tube bank with a large number of tube rows in the flow direction, N, the smallest bypass clearance is unlikely to be characteristic of the effective bypass width, as a significant amount of bypassing may take place upstream and downstream of the tube row where the smallest clearance occurs. This is similar to the situation seen in Chapter 9, where a sealing-strip, which totally eliminates bypassing at one row, only influences the flow over a finite portion of the tube bank.

10.4 Conclusions

Although the data are limited,a number of general conclusions can be drawn.

The general pressure drop characteristics of bypassing flow with a cylindrical shell wall are similar to those seen in rectangular tube banks with bypassing.

The inverse root mean square of the bypass clearance characterises the effective bypass clearance better than either the arithmetic mean or the smallest clearance.

11. SHELL-SIDE FLOW VISUALISATION RIG

11.1 INTRODUCTION

This investigation using flow visualisation forms part of the current research programme of the Heat Transfer and Fluid Flow Service (HTFS) into the shell-side flow structure and pressure drop in cylindrical shell-and-tube heat exchangers. The shell-side flow visualisation rig used in the HTFS study consists of a glass shell-and-tube heat exchanger model, which is installed at AERE Harwell. To date this rig has principally been used in an investigation of the effects of baffle spacing and baffle-shell leakage, see Murray (1988). The tube bundle used in that study extended close to the shell wall. However, as part of the current investigation, tests were performed by the author in which the effects of enlarging the bypass clearance, and then blocking the bypass with sealing-strips, were studied.

11.2 EXPERIMENTAL APPARATUS

The rig consisted of a glass cylindrical shell, a tube bundle framework (consisting of baffles and tie rods) into which a number of 12mm diameter glass rods could be fitted, a water circulation system and instrumentation. A full description can be found in Murray (1988).

In this investigation the baffle-shell and tube-baffle clearances were eliminated by the use of neoprene sheeting attached to the baffles.

Fig. 11.1 shows the tube bundle investigated. Three arrangements were tested: one by Murray (1988) with all the tubes present and only a very small bypass and two in this study, one with tubes removed to form an enlarged bypass and one with this bypass blocked by sealing-strips. The tube array investigated was rotated square (or 45°) with a pitch-diameter ratio of 1.25. The baffle spacing for all three tests was

112mm. The large bypass lane examined was not as large as is often found in commercial shell-and-tube heat exchangers, but the maximum bypass lane available in the test model was limited by the presence of the tie rods. The sealing-strips were made of PTFE and located in longitudinal slots in modified tubes. The sealing-strips were positioned close to the baffle cut and completely blocked the tube-to-shell clearance between each baffle spacing.

11.3 Pressure Drop Measurements

Pressure measurements, using several pressure tapping locations in the exchanger, were made for six different total flow rates of water through the exchanger. The pressure at each tapping was found relative to a common reference tapping. From these measurements, pressure drops over certain sections of the exchanger could be derived. The pressure tappings were located in modified tubes, and were always positioned at 135° from the main flow direction, see Fig. 11.2. The locations of the tappings are shown in Fig. 11.3; they cover pressure drops over the crossflow section of the bank, both at the shell centreline and near to the shell wall, and also pressure drops over the window region. The exact details of the measurements are proprietary to HTFS and only a limited number can be presented here. These cover the crossflow pressure drop, from baffle cut to baffle cut, between tappings positioned mid-way between baffles at the shell centreline.

The results are presented as a pressure drop coefficient, ξ_p', plotted against the Reynolds number of the flow Re', see Fig. 11.4. The exact definitions of ξ_p' and Re' are proprietary to HTFS and cannot be published here, but nevertheless the results are worth including here since they show the relative effects of bypassing and sealing-strips on the pressure drops. The results show a similar trend to that for the rectangular bundle with bypassing and sealing-strips, see Chapter 9. Increasing the bypass width reduces the pressure drop coefficient and the addition of sealing-strips increases it; this is observed for both flow in the crossflow region and for flow

through the window. Further details of the experimental data obtained are given in Murray, Martin and Haseler (1988).

11.4 Flow Visualisation

For each of the two tube bundle geometries investigated by the author, one with a large bypass and the other with a large bypass lane blocked by sealing-strips, see Fig. 11.1, flow visualisation studies were performed. Dye was injected into the shell-side flow at various points using a modified tube. The dye used was red food dye. The resulting dye trace was photographed using a filter to enhance the contrast. The modified tube consisted of a stainless steel tube through which a 1mm diameter plastic capillary tube could be fed. A hypodermic syringe was used to inject a fixed volume of dye into the flow via the capillary tube. For flow visualisation within the bypass lane, the plastic tube was extended from the modified tube into the clearance between the shell wall and the tube bundle. In both tube bank geometries examined the dye was injected at the shell centreline, at the outer edge of the tube bundle (close to the boundary of bundle and bypass) and within the bypass lane, and in all cases level with the baffle tips; the position of the modified tube can be seen in Fig. 11.5, in contrast to the glass rods. For each of these locations dye was released at points 0.1 B_s, 0.5 B_s and 0.9 B_s across the baffle spacing, where B_s is the baffle spacing, i.e.,at points close to the upstream baffle, midway between baffles and close to the downstream baffle respectively. All the flow visualisation studies were carried out at the same shell-side flow rate. The results are shown in Figs. 11.5 to 11.17.

11.4.1 Results with the Large Bypass

Figs. 11.5 to 11.7 show the flow pattern revealed by dye released at the shell centreline. Fig. 11.18 gives a diagrammatic view of these dye traces.

Dye released close to the upstream baffle, Fig. 11.5, is seen to flow along the baffle face before entering the window. It then turns at the top of the window region before entering the next compartment as crossflow. Asymmetry between crossflow in neighbouring compartments can be clearly seen, the dyed flow in the second compartment being separated from the downstream baffle by an undyed region. Dye can be seen upstream of the release point indicating the presence of a recirculating flow region behind the baffle tip.

Dye released midway between the baffles, Fig. 11.6, shows that the crossflow is parallel to the baffles.

Dye released near the downstream baffle, Fig. 11.7, is seen to flow close to the baffle face before turning asymmetrically around the baffle tip, indicating the presence of a large recirculating region behind the baffle, seen, in part, in Fig. 11.5. The recirculating region can also be distinguished in Fig. 11.6 from the shape of the dye trace in the second compartment.

Figs. 11.8 to 11.10 show the flow pattern revealed by dye released at the outer edge of the tube bundle, close to the bypass. Fig. 11.19 gives a diagrammatic representation of these dye traces.

The flow of dye released close to the upstream baffle at the outer edge of the bundle, Fig. 11.8, differs in two main ways from that at the shell centreline. Firstly, it detaches from the baffle showing that there is a larger separated region behind the baffle near the shell than at the centreline. After the flow has entered the window, away from the separated region, it behaves in a similar way to that seen at the shell centreline except that the dye trace extends all the way to the downstream baffle in the second compartment, there is no undyed region as seen at the centreline.

From midway across the baffle the dye trace is drawn back towards the upstream baffle, Fig. 11.9, where it merges with the flow originating from closer to the upstream baffle.

Dye released from close to the downstream baffle is also drawn across the compartment, Fig. 11.10. The dye trace spreads across the compartment before being swept around the baffle tip.

Figs. 11.11 to 11.13 show the flow pattern revealed by dye released in the bypass lane. Fig. 11.20 gives a diagrammatic representation of these dye traces.

The trace produced from the dye released in the bypass lane close to the upstream baffle is very similar to that just within the bundle, indicating that the recirculating zone behind the baffle extends into the bypass. However, dye released midway across the compartment flows normal to the tubes, similar to the crossflow, and is not drawn back towards the upstream baffle, as seen in the flow just inside the bundle. The would indicate that the recirculating region is much smaller within the bypass lane than just within the tube bundle. Before reaching the window, the dye trace remains narrower than seen at the centreline, Fig. 11.6, and is also less intense. This probably indicates that the flow in the bypass lane is at a higher velocity than that in the bundle. The nature of the dye trace, for this particular geometry, suggests that there is no significant interchange of flow between bypass and tube bundle in the crossflow region. After the crossflow region the dye trace, from midway across the bypass, turns at the top of the window, in contrast to flow at the centreline. The dye traces in Figs. 11.11 and 11.12 (and part of the trace in Fig. 11.13) appear to merge at the top of the window before entering the second compartment close to the downstream baffle. The dye traces in the second compartment have dispersed far less than those seen at the outer edge of the bundle, and appear more characteristic of crossflow. It is probable that dye released in the bypass lane in one compartment transfers into the bundle and becomes crossflow in the next compartment, the transfer occurring as the flow is turned within the window. Thus the undyed region adjacent to the face of the downstream baffle in the second compartment, Fig. 11.5, would appear to be occupied by flow transferring from the bypass lane.

Dye released close to the downstream baffle, Fig. 11.13, remains close to the baffle face, unlike flow just within the bundle. While turning around the baffle tip, the flow divides. One part flows towards the top of the window and merges with the bypass flow transferring into the bundle, which can be seen from the dye trace close to the downstream baffle face. The remainder of the flow turns sharply around the baffle tip and appears to remain in the bypass lane in the next compartment.

11.4.2 Results with the Large Bypass Blocked by Sealing-Strips

The traces produced by dye released at the shell centreline, Fig. 11.14, are very similar to those without sealing-strips, except that the dye traces are slightly narrower and less intense when sealing-strips are present. This is probably due to higher crossflow velocities.

Figs. 11.15 to 11.17 show the flow pattern revealed by dye released at the outer edge of the tube bundle. Dye injected into the bypass lane, at the same locations, resulted in very similar traces. In each of Figs. 11.15 to 11.17, showing dye released near the upstream baffle, midway between baffles and near the downstream baffle respectively, the dye traces are very intense close to the release point, indicating a low velocity in the bypass lane and in the part of the tube bundle close to it. After passing a sealing-strip position the dye trace spreads across the whole width of the next compartment, the bypassing flow being forced into the tube bundle, by the sealing-strip, and then dispersing.

The presence of sealing-strips appears to push the crossflow at the centreline higher into the window before being turned into the next compartment, compare Fig. 11.6 with Fig. 11.14.

11.5 Discussion

The relative pressure drop results obtained from the three geometries (small bypass, large bypass and large bypass blocked by sealing-strips)are not unexpected. The pressure drop coefficients found for the large bypass are the lowest, consistent with it having the greatest free flow area.

An interesting feature of the pressure drop results, Fig. 11.4, is the difference in Reynolds number dependency. As with the pressure drop coefficients in the rectangular bundle with bypassing, the larger the bypass width the less the Reynolds number dependency of the pressure drop coefficient, ξ_p', which falls with increasing

Re' for the small bypass geometry but is almost constant for the large bypass. This indicates, as in Chapter 7, that the Reynolds number dependency of the bypass flow in a cylindrical exchanger is less than that of the flow within the tube bundle. With increasing bypass width a greater proportion of the flow is in the bypass lane and hence the overall Reynolds number dependency of the tube bundle and bypass lane combination decreases. The tube bank with a large bypass blocked by sealing-strips has a Reynolds number dependency between the two cases, ξ_p' falling only slightly with Re'. This would suggest that there is still a significant proportion of flow in the bypass lane. Although the flow velocity in the bypass when blocked is lower than in the bundle, as is suggested by flow visualisation, because there is still a relatively large proportion of free flow area in the bypass lane a significant proportion of flow will still occur there. Another factor which may affect the Reynolds number dependency of the whole bank, making it similar in nature to that with an unblocked bypass, is that a significant amount of bypassing of the tube bundle may occur in the window region, flow parallel to the tubes not being restricted by sealing-strips.

It should be noted that the two tube bank geometries examined did not have tube-baffle leakage or baffle-shell leakage. These two leakage streams, which are present in reality, would distort the flow patterns observed in this study. In particular the shell-baffle leakage will distort the bypass flow; in practice, the bypass flow would not be normal to the tubes, Fig. 11.12, and in a similar way the tube-baffle leakage will affect the crossflow, Fig. 11.6. Despite these effects, the dye traces observed show some very interesting features of the interaction between the crossflow and bypass flow streams. The transfer of most of the bypass flow into the crossflow at each window results in the two streams mixing. Therefore even if a large proportion of the flow bypasses the tube bundle, it only does so in one compartment before mixing with the crossflow in the next. Hence, for this geometry at least, the presence of a bypass lane does not cause a large portion of the flow to completely avoid the heat transfer surface in total isolation from the crossflow.

Bypassing, though, does lead to a fall in hear transfer effectiveness of an exchanger as part of the flow avoids the tube bundles in each compartment.

The use of sealing-strips to block the tube bundle to shell clearance is seen to considerably reduce the bypass flow velocity, and hence the proportion of flow avoiding the hear transfer surface. It also causes a thorough mixing of the bypass and crossflow streams, at each sealing-strip position, which is seen by the dye spreading across the whole compartment after each sealing-strip.

The interpretation of the dye trace photographs also relies on observations of the flow at the time of the experiment. The photographs are only a two-dimensional view of the highly complex three-dimensional shell-side flow. In order to get a clearer view of the dye traces the author recommends that the flow is simultaneously photographed at two positions, at 90° to each other, around the exchanger shell; giving a view along the main crossflow direction as well as normal to it.

11.6 Conclusions

Increasing the width of the bypass lanes in cylindrical exchangers and using sealing-strips to block them have similar effects on the pressure drop coefficient - Reynolds number relationship, as obtained for rectangular tube banks.

Bypassing flow in one compartment in an exchanger is seen to become crossflow in the next compartment. The bypass stream flows to the top of the window region before re-entering the next compartment, next to the face of the downstream baffle, as crossflow. Hence the bypass flow stream and crossflow stream do not remain isolated; no flow completely avoids the hear transfer surface. Over the crossflow region very little interaction of the bypass flow and crossflow streams was noted for this geometry.

The bypass flow velocity was observed to be higher than the crossflow velocity. This, in combination with the fact that there is a relatively large proportion of free flow area in the bypass lane, means that a significant part of the flow

bypasses the tube bundle in each compartment. The use of sealing-strips considerably slows the bypass flow and causes it to mix thoroughly with the crossflow at each sealing-strip position. The use of sealing-strips causes the crossflow to turn higher in the window region than otherwise.

12. CONCLUSIONS AND FURTHER WORK

12.1 CONCLUSIONS

ESDU (1974) generally overestimates the pressure drop coefficient of flow across a tube bank when a bypass lane is present. .

Bell's (1960) correction factor generally underestimates the pressure drop coefficient for tube banks with bypass lanes.

The pressure drop over a tube bank with a bypass lane is dependent on the number of tube rows across the flow as well as the ratio of bypass flow area to total flow area. The pressure drop coefficient for the bypass lane alone is generally independent of the Reynolds number of the flow. For the tube bundle the pressure drop coefficient generally falls with increasing Reynolds number, more markedly so with staggered arrays.

Bell's (1960) correction factor overestimates the effect of sealing-strips in increasing the pressure drop over a tube bank. Sealing-strips are more effective in producing regions of 'pure crossflow' in staggered arrays than in in-line ones, hence they are more effective in reducing the bypass flow and retaining the flow within the tube bundle.

In an exchanger with a cylindrical shell wall, in which the bypass width is not constant in the flow direction, the inverse root mean square of the bypass clearance appears to characterise the effective bypass clearance better than either the arithmetic mean or the smallest bypass clearance.

Similar trends of behaviour are seen in both rectangular and cylindrical exchangers in the relationship between pressure coefficient and bypass width.

For the cylindrical exchanger investigated, there was little interchange of flow between the bypass and crossflow streams over the crossflow region. Interchange between these two streams did occur in the window region, in which bypass flow becomes crossflow and crossflow transfers into the bypass lane.

Sealing-strips positioned at the baffle tips, at the boundary of the crossflow and window regions, caused thorough mixing of the bypass and crossflow streams.

In a cylindrical exchanger, even without the presence of tube-to-baffle and shell-to-baffle leakages, the shell-side flow is extremely complex, especially in the window region.

12.2 Suggestions for Further Work

Rotated square (45°) and rotated equilateral-triangle (60°) tube arrays should be investigated to determine whether their behaviour differs from the staggered array examined in this investigation.

Arrays having a tube pitch-diameter ratio of 1.5 should be examined, as such arrays are used commercially. The effect of a particular bypass width, in reducing the pressure drop coefficient, was seen to decrease with increasing tube pitch-diameter ratio; this would extend the data over a wider range of tube pitches.

A wider range of bypass width to tube bank width needs to be examined to fully determine the effect of n, the number of tube rows transverse to the flow, on a particular bypass width. Lee's (1983) study and the current investigation offer only two data sets between the two extreme cases of n = 0, an empty duct, and n = infinity, the ideal tube bundle.

The build-up of bypass flow within the bypass lane from tube bank inlet to exit could be investigated to fill in the data obtained so far, of inlet and exit bypass flow rates. This could be achieved for large bypasses by modifying the current rig to allow access for a HWA probe in the bypass wall of the test section.

Although the current study, and the further work suggested, on a rectangular tube bank will give a greater understanding of the pressure drop - flow rate relationship and flow interaction of the bypass and crossflow streams, in order to apply this information to network flow models of real exchangers more work needs to be carried out on flow visualisation in models of cylindrical exchangers; such as the

flow visualisation rig at Harwell. The shell-side flow structure needs to be investigated, and the effects on it of the various leakage paths known, before a representative network flow model can be produced, to which the pressure drop - flow rate relationships can be applied.

One of the areas where the flow in the model rectangular bundle lacks similarity with the flow through real exchangers is in the inlet flow distribution to the bank. The inlet flow to the crossflow region in a real exchanger is non-uniform, in both velocity and direction, due to its being turned previously through 180° in the window region. Further work could be carried out using the rectangular bundle, with bypassing, to examine the effect on the pressure drop and flow distribution over the bank of non-uniform inlet flows.

APPENDIX A

CORRELATION OF EXPERIMENTAL DATA

The experimental pressure drop data, represented by a pressure drop coefficient, can be correlated in the form,

$$\xi_p = a_1 Re_{max}^{a_2} \tag{4.9}$$

This allows simpler manipulation of the data, such as calculating the effective bypass mass flow ratio.

The results of this correlation are presented in Table A.1 and A.2 for ideal tube banks, tube banks with bypassing and tube banks with bypass lanes blocked by sealing-strips. The average and maximum errors at each correlation are also given.

APPENDIX B

ESTIMATION OF THE DISCREPANCY BETWEEN THE PRESSURE DROPS OVER THE CROSSFLOW AND THE BYPASS STREAMS CAUSED BY BALANCING THE DOWNSTREAM PRESSURES

As described in Sec. 5.1, when a downstream splitter plate is used to divide the exit flow from the tube bank with bypass and crossflow streams errors arise due to the different exit duct pressure gradients. The pressure drop in the bypass exit duct is greater than that in the crossflow exit duct, due to its higher pressure loss coefficient. The relative difference between the two downstream exit duct pressure drops will be greatest at the lowest Reynolds number flows, because the proportion of flow leaving via the bypass exit duct is greatest at the lowest flow rates. For this reason the errors that arise when the pressures are equalised some distance from the tube bank exit are presented for the lowest flow rate used in each bypass width investigated with the 1.25 equilateral-triangle tube bank.

For the ½T bypass in a 1.25 equilateral-triangle tube bank at the lowest total volume flow rate, from Table 7.1:

Temp / K	$\dot{V}_T$ / m^3/s	u_{max} / m/s	$\dot{m}_{Bexit}/\dot{m}_T$	$\Delta p_{measured}$ / Pa
322.9	0.123	25.6	0.097	1910

$\dot{V}_{Bexit} = 0.123 \times 0.097 = 0.012\ m^3/s.$

$\dot{V}_{Cexit} = 0.123 - 0.012 = 0.111\ m^3/s.$

Bypass exit duct area $= 0.079 \times 0.15 = 1.19 \times 10^{-3}\ m^2.$

Average bypass duct velocity, $u_b = 0.012 / (1.19 \times 10^{-3}) = 10.1$ m/s.

Equivalent diameter of bypass lane, $D_e = 15$mm.

$$Re_b = \frac{u_b D_e \rho_m}{\mu} = 8570.$$

Extrapolated from Table 8.1, the

pressure drop of flow through duct for Re_b = 8570, is 120 Pa/m, so that over a distance of 0.136m the pressure drop in the exit bypass duct, $\Delta p = 120 \times 0.136 =$ 16.3 Pa.

When the downstream pressures are equalised, crossflow pressure drop (= measured pressure drop) = bypass pressure drop + bypass exit duct pressure drop.

Now the crossflow exit duct pressure loss is negligible, see Sec. 5.3.1, as it is so small in comparison with the total measured pressure drop; in this case the crossflow exit pressure drop is only approximately 1 Pa.

Therefore,

crossflow pressure drop = 1910 Pa,

bypass pressure drop = 1910 - 16.3 = 1893.7 Pa.

Hence the difference in pressure drop over the two streams = (1910-1893.7)/1910 x 100% = 0.9%.

Similarly for the 1.25 equilateral-triangle tube bank at the lowest total volume flow rate and with the 1½T bypass the difference in pressure drop between the two streams = 5.5%, for the 2½T bypass it is 3.7%, and for the 3½T bypass it is 3.6%.

Generally the errors arising at higher volume flow rates were found to be lower than these values.

APPENDIX C

ESTIMATION OF INLET BYPASS FLOW RATES

The inlet bypass rates are estimated differently depending on the bypass width. Flow approaching the entry to the ½T bypass is almost parallel to the main flow direction, see Fig. 7.25, and a proportion of the flow entering the tube-bypass wall clearance at the first row will re-enter the bundle before the minimum tube-shell clearance, which occurs at the second tube row. This is in contrast to the flow approaching the 1½T, 2½T and 3½T bypasses, where the flow on entry, i.e. at the first tube row, is angled towards the bypass at approximately 30° from the main flow; at this angle the flow will pass into the minimum bypass clearance at the second row and will not be diverted into the bundle, see Figs. 7.26, 7.27 and 7.28. Thus, for the larger bypasses, it is unlikely that much flow re-enters the tube bundle after the first tube row, whereas this will occur with the smaller bypass.

C.1 ½T Bypass

The point where the flow divides between bypass and crossflow on entry is found graphically, see Fig. C.1.

The measured flow directions are drawn onto a scale drawing of the bypass entry, with the measuring positions and tube positions marked. The stagnation point on the uppermost tube in the first row is found, assuming that the flow direction at the measuring position is unchanged at the bank inlet. It is then assumed that the flow divides around this point. The flow entering the bypass inlet can then be found. Close to the dividing point the proportion of flow entering the bypass which originated from the closest measuring position may need to be estimated. The longitudinal velocity components and measurement positions are then used to calculate the bypass inlet flow rate.

C.1.1 Calculation Procedure

A typical set of velocity measurements for the ½T bypass is,

Temp / K	$\dot{V}_T$ / m^3/s	$\Delta p_{measured}$ / Pa
315.4	0.381	12030

Position No.	Transverse distance from bypass wall / m	Longitudinal velocity, u / m/s	Transverse velocity, v / m/s
1	0.004	18.8	0.4
2	0.0079	18.7	1.3
3	0.0119	18.4	3.6
4	0.0159	17.8	3.8
5	0.0198	17.1	4.1
6	0.0238	16.9	4.3
7	0.0278	16.4	4.5

The measured longitudinal flow velocity at position number 1 is taken as the average velocity from the bypass wall to the point equidistant from positions 1 and 2. The longitudinal velocities for the other positions are taken as the average over the area half way to the adjacent measuring positions; i.e. the velocity measured at position 2 is taken to be the average over the area between the points equidistant from positions 1 and 2 and from positions 2 and 3. From Fig. C.1 all the flow through position numbers 1 to 4 and an estimated three-quarters of the flow through position number 5 passes above the stagnation point of the uppermost tube in row one, and thus into the bypass at row one. The inlet bypass volume flow rate, $\dot{V}_{Bin}$, however is the flow rate through the minimum bypass clearance, which occurs at the

second row. The flow is assumed to divide on an area basis between the bundle and the minimum bypass clearance.

Volume flow rate through bypass at first row

$$= [5.95(18.8) + 3.97(18.7 + 18.4 + 17.8 + 3/4(17.1)] \times 0.15 \times 10^{-3}$$

$$= 0.0571 \text{ m}^3/\text{s}$$

$$\dot{V}_{Bin} = 1/3 \times 0.0571 \text{ m}^3/\text{s}$$

$$= 0.019 \text{ m}^3/\text{s}$$

Calculated as described in Appendix D,

$\frac{\rho_N}{kg/m^3}$	$\frac{\rho_1}{kg/m^3}$	$\frac{\rho_m}{kg/m^3}$	$\frac{\mu}{kg/m\,s}$
1.119	1.252	1.186	1.917×10^{-5}

$$\dot{V}_{Tin} = (\rho_N/\rho_1)\dot{V}_T$$

$$= 0.341 \text{ m}^3/\text{s}$$

$$\phi_{in} = \dot{V}_{Bin}/\dot{V}_{Tin} = 0.056$$

C.2 1¼T, 2¼T AND 3¼T BYPASSES

The calculation method is the same as for the ¼T bypass except that all the flow entering the bypass at the first row is assumed to enter the minimum bypass clearance, at the second row. See Fig. C.2 for graphical representation of the 1¼T bypass.

APPENDIX D

SPECIMEN CALCULATIONS

D.1 PRESSURE DROP COEFFICIENT FOR A RECTANGULAR TUBE BANK WITH BYPASSING

A typical data set, taken from Table 7.7, for a 1.25 equilateral-triangle bank with a 3½T bypass is,

$\frac{\text{Temp}}{\text{K}}$	$\frac{\dot{V}_T}{m^3/s}$	$\frac{u_{max}}{m/s}$	$\frac{\dot{m}_{Bexit}}{\dot{m}_T}$	$\frac{\Delta p_{measured}}{\text{Pa}}$
319.7	0.265	48.0	0.721	1580

Pitch/diameter ratio, $P_t/D = 1.25$.

Tube diameter, D = 12/7mm.

Number of tube rows in flow direction, N = 14.

Tube length = 150mm.

Bank width = 0.1508m.

Bypass width = 0.0318m.

Duct height = 0.1826m.

Air temperature is assumed constant throughout the rig as the flow is essentially adiabatic with very small density variations.

Dynamic viscosity, μ, does not vary greatly with pressure, therefore viscosity was found for each air temperature by interpolating between values given in Rogers and Mayhew (1981).

For T = 319.7 K

$\mu = 1.937 \times 10^{-5}$ kg/m s.

The air density used in the calculation of ξ_p and Re_{max} is the mean density within the tube bank, the mean is taken as the arithmetic mean of the air inlet and exit densities.

Mean air density within the bank, assumed constant throughout the bank,

$$\rho_m = \frac{\frac{1}{2}(1580) + 1.014 \quad x\ 10^5}{287 \times 319.7}$$

$$= 1.113 \text{ kg/m}^3$$

Air density at test section exit,

$$\rho_{out} = \frac{1.014 \quad x\ 10^5}{287 \times 319.7}$$

$$= 1.104 \text{ kg/m}^3$$

Total mass flow rate at exit of the tube bank,

$$\dot{m}_T = 1.104 \times 0.265$$

$$= 0.293 \text{ kg/s}$$

From continuity, superficial velocity within the test section,

$$u = \frac{0.293}{1.113 \times 0.150 \times 0.1826}$$

$$= 9.60 \text{ m/s}$$

From Equation 4.2,

$$u_{max} = u \frac{A_C}{A_{Cmin}}$$

$$\frac{A_C}{A_{Cmin}} = 5$$

$$\therefore \quad u_{max} = 48.0 \text{ m/s}$$

Hence,

$$Re_{max} = \frac{u_{max} D \rho_m}{\mu}$$

$$= \frac{48.0 \times 12.7 \times 10^{-3} \times 1.113}{1.937 \times 10^{-5}}$$

$$= 35030$$

and,

$$\xi_p = \frac{\Delta p_{measured}}{\frac{1}{2} \rho_m u_{max}^2 N}$$

$$= \frac{1580}{\frac{1}{2} \times 1.113 \times (48.0)^2 \times 14N}$$

$$= 0.088$$

The inlet and exit duct pressure losses, between pressure tappings and bank inlet/exit, are neglected, see Sec. 5.1.

D.2 Bypass Mass Flow Ratios for Rectangular Tube Banks with Bypassing

Three bypass mass flow ratios are calculated from the experimental data. The bypass exit mass flow ratio is found from the mass flow rates measured on exit from the bank, using the splitter plate. The bypass entry mass flow ratio, calculated only for the 1.25 equilateral-triangle bank with bypassing, is found by hot-wire anemometer traverses close to the tube bank. The effective bypass mass flow rate is calculated using the method of Bergelin et al. (1959).

For the same data set used in Sec. D.1.

Bypass exit mass flow ratio,

$$\phi = \frac{\dot{m}_{Bexit}}{\dot{m}_T}$$

$$= 0.721$$

Bypass inlet mass flow ratio found as described in Appendix C.

D.2.1 Bypass Effective Mass Flow Ratio

The pressure drop coefficient correlation for the 1.25 equilateral-triangle ideal bank, from Appendix A,

$$\xi_p = 6.269\ (Re_{max})^{-0.2797}$$

$$\frac{\Delta p}{\frac{1}{2}\rho_m u_{max}^2 N} = 6.269 \left[\frac{u_{max} D \rho_m}{\mu}\right]^{-0.2797}$$

$$u_{max}^{(2-0.2797)} = \frac{\Delta p}{(6.269/2)\rho_m N} \left[\frac{D\rho_m}{\mu}\right]^{-0.2797}$$

From the data set given in D.1, the maximum velocity through the ideal part of the tube bank having a 3¼T bypass, u_{max} = 22.04 m/s.

Hence,

$$\dot{m}_{Ceff} = 1/5 \times 0.1508 \times 0.150 \times 22.04 \times 1.113$$

$$= 0.111 \text{ kg/s}$$

$$\dot{m}_{Beff} = \dot{m}_T - \dot{m}_{Ceff}$$

$$= 0.182 \text{ kg/s}$$

$$\phi_{eff} = \frac{\dot{m}_{Beff}}{\dot{m}_T}$$

$$= 0.622$$

D.3 Calculation of N_c, the Number of Rows of Pure Crossflow Equivalent to One Sealing-Strip

N_c is a measure of how effective a sealing-strip is in forcing the flow into the tube bank. A tube bank with a bypass blocked by sealing-strips is considered in two parts; see Fig. 9.10,

i) $N - N_c.N_S$ rows of tube bank with a plain bypass,

ii) $N_c.N_S$ rows of pure crossflow through the tube bank with the bypass completely blocked.

The total pressure drop of the equivalent tube bank,

$$\Delta p_T = \Delta p_{PB} + \Delta p_{PC}$$

where Δp_{PB} = pressure drop over the tube bank with plain bypass,

and Δp_{PC} = pressure drop of bank having pure crossflow.

$$\Delta p_T = \tfrac{1}{2}\rho u_{max}^2 N \xi_{PS}$$

$$\Delta p_{PB} = \tfrac{1}{2}\rho u_{max}^2 (N - N_c N_S) \xi_{PB}$$

$$\Delta p_{PC} = \tfrac{1}{2}\rho u_{maxC}^2 N_c N_S \xi_{PC}$$

u_{maxC} is the maximum velocity through the restricted pure crossflow area.

ξ_{PS}, ξ_{PB} and ξ_{PC} are the pressure drop coefficients for the tube bank with bypass and sealing-strips, the tube bank with a plain bypass and the pure crossflow bank respectively.

Hence,

$$N_c = \frac{u_{max}^2 (\xi_{PS} - \xi_{PB}) N}{(\xi_{PC} u_{maxC}^2 - \xi_{PB} u_{max}^2) N_S} \qquad (D.1)$$

A typical data set, taken from Table 9.11, for a 1.25 equilateral-triangle bank with a 3½T bypass and two sealing-strips is,

Temp / K	$\dot{V}_T$ / m^3/s	u_{max} / m/s	$\Delta p_{measured}$ / Pa
315.2	0.224	40.0	4790

Pitch / diameter ratio, P_t/D = 1.25.

Tube diameter, D = 12.7mm.

Number of tube rows in flow direction, N = 14.

Tube length = 150mm.

Bank width = 0.1508m.

Bypass width = 0.0318m.

Duct height = 0.1826m.

From Appendix A,

$$\xi_{PC} = 6.269(Re_{max})^{-0.2797} \qquad (D.2)$$

$$\xi_{PB} = 0.161(Re_{max})^{-0.0596} \qquad (D.3)$$

The Reynolds number of the flow through the tube bank with plain bypass,

$$Re_{max} = \frac{u_{max} D \rho}{\mu}$$

$$= 30370$$

(calculate as in Sec. D.1)

Hence,

$$\xi_{PB} = 0.087$$

$$u_{maxC} = \frac{\text{total bankwidth}}{\text{pure crossflow bankwidth}} \times u_{max}$$

$$= \frac{0.1826}{0.1506} \times 40.0$$

$$= 48.50 \text{ m/s}$$

The Reynolds number of the flow through the pure crossflow part of the tube bank,

$$Re_{maxC} = 36820$$

Hence,

$$\xi_{PC} = 0.331$$

$\xi_{PS} = 0.374$ as calculated using the same procedure given in Sec. D.1.

$\therefore \quad N_c = 5.03$ from Equation D.1.

In some cases, with very small bypass lanes, the pressure drop of a particular bank with a plain bypass was found to be just greater than that of the same tube bank with the bypass blocked by sealing-strips. In this case, N_c becomes negative, resulting in the equivalent tube bank consisting of $(N - N_cN_s)$ tube rows (where $(N - N_cN_s)$ is greater than N) of pure crossflow less N_cN_s tube rows having plain bypass flow. N_c no longer represents the number of tube rows of pure crossflow equivalent to one sealing-strip, and its physical meaning becomes unclear. In these situations N_c is defined differently, the equivalent tube bank consisting of N rows of plain bypass flow less N_cN_s rows of pure crossflow.

Hence $-N_c$ is the number of tube rows of pure crossflow per sealing-strip that need to be added to the actual bank with bypass and sealing-strips to make it equivalent to a bank with a plain bypass of the same length.

$$\Delta p_T + \Delta p_{PB} = \Delta p_{PC}$$

$$\tfrac{1}{2}\rho u_{max}^2 N\xi_{PS} - \tfrac{1}{2}\rho u_{maxC}^2 \xi_{PC} N_c N_S = \tfrac{1}{2}\rho u_{max}^2 N\xi_{PB}$$

$$N_c = \frac{u_{max}^2 N(\xi_{PS}-\xi_{PB})}{N_S u_{maxC}^2 \xi_{PC}} \qquad (D.4)$$

In all cases when N_c is negative it is defined in this way; there are not many and in each, N_c is always very small, never greater in magnitude than -0.12.

A typical data set, taken from Table 9.2, for a 1.25 equilateral-triangle bank with a ¼T bypass and two sealing-strips is,

Temp / K	$\dot{V}_T$ / m^3/s	u_{max} / m/s	$\Delta p_{measured}$ / Pa
313.9	0.369	72.9	12640

Pitch / diameter ratio, $P_t/D = 1.25$.

Tube diameter, $D = 12.7$mm.

Number of tube rows in flow direction, $N = 14$.

Tube length = 150mm.

Bank width = 0.1508m.

Bypass width = 0.0079m.

Duct height = 0.1588m.

From Appendix A,

$$\xi_{PB} = 2.959(Re_{max})^{-0.2134} \qquad (D.5)$$

$$u_{maxC} = \frac{0.1588}{0.1508} \times 72.9$$

$$= 76.8 \text{ m/s}$$

The Reynolds number of the flow through the tube bank consisting of pure crossflow = 61000.

Hence,

$\xi_{PC} = 0.288$ from Equation (D.2).

The Reynolds number of the flow through the tube bank with plain bypass,

$$Re_{max} = 57930.$$

Hence,

$$\xi_{PS} = 0.284 \quad \text{calculated as in Sec. D.1.}$$

$$\therefore \quad N_c = -0.022 \quad \text{from Equation (D.4).}$$

APPENDIX E

THE EFFECT OF BYPASS WIDTH / BUNDLE WIDTH RATIO

A particular bypass lane width will have different effects on the pressure drop over a bank for different bundle transverse widths, n. At one extreme a bank may contain no tube rows, n = 0; this corresponds to an empty duct. The other extreme is a bank having an infinite number of tube rows in the transverse direction; in this case the effect of the bypass lane will be negligible and the bank will have the same pressure drop characteristics as an ideal bundle. Between these extreme cases there exists, for each bypass width, banks having n varying from one to infinity.

Data exist from this investigation and from that of Lee (1983) for banks having bypasses having similar bypass widths. The main differences between Lee's bypass tests and those of the author are the number of longitudinal rows, n (the effect of which is being investigated here), the ratio of tube length to tube diameter, ℓ/D, and the ratio of the length to intertube spacing, $\ell/(P_t-D)$. However, Huge (1937) found that the effects of differences between banks caused by these last two factors could be neglected. It can be seen from the similarity of Lee's and the author's ideal bundle data that this is so. It is equally clear that bank entry and exit effects, due to differences in the number of transverse tube rows, N, are negligible.

Data have been obtained from four geometries having four different ratios of bypass width to bank width;

i) n = 0 (empty duct),

ii) n = infinity (ideal bundle),

plus sets of data from two intermediate geometries between n = 0 and infinity,

iii) from Lee,

and

iv) from the current study.

Using these data it is possible to establish the relationship between pressure drop coefficient and n for each fixed bypass width and tube array type. Although data are

limited, a method of predicting pressure losses for a range of bypass to bundle transverse widths is proposed.

For each array type and bypass width, and for the limited range of Reynolds number where the data sets overlap, the ratios are found of the pressure drop coefficients for the plain bypass (n = 0), Lee's bank and for the author's bank to the pressure drop coefficient for the ideal tube bank (n = infinity). From these results an approximate, linear relationship between pressure drop coefficient and the transverse bank width is derived.

The ratio of the pressure coefficient of a bypass to the pressure coefficient of the ideal bank, for the same Reynolds number, is plotted against n, and the relationship between these found graphically. From these results the width of the tube bank for which a particular bypass lane would have no effect (i.e. it would have the same pressure drop coefficient as the ideal bundle) was found. The results of this analysis are presented in Table E.1 . It can be seen from this table that there is a similar relationship for staggered and in-line square arrays. It can be seen that the relationship between bypass width and the width of the bank which would make the effect of that bypass negligible, is linear. After removing ½ a tube row, in the staggered array, the removal of two extra tube rows has twice the effect of removing one tube row. From the relationship found between the ratio of bypass width to bundle width and the pressure drop coefficient, it is possible to derive pressure drop coefficients, for each of the bypass widths tested (½T, 1½T, 2½T, 3½T, ½S and 1½S), for various ratios of bypass to bundle width.

TABLE 6.1

COMMON DIMENSIONS OF ALL TEST SECTION USED

Tube diameter = 12.7mm.

Tube length = 0.15m.

Distance from upstream pressure tapping to tube bank inlet:

for all geometries = 0.135m.

Distance from downstream pressure tapping to tube bank exit:

for 1.25 equilateral-triangle bank = 0.136m;

for 1.375 equilateral-triangle bank = 0.134m;

for 1.25 in-line square bank = 0.140m;

for 1.375 in-line square bank = 0.140m.

CALCULATION OF ξ_p AND Re_{max}

Inlet and exit duct pressure losses are neglected, see Appendix B.

Air density and dynamic viscosity are calculated using the equation of state and by linear interpolation between values in Rogers and Mayhew (1980).

TABLE 6.2

DATA FOR 1.25 EQUILATERAL-TRIANGLE BANK, NO BYPASSING

Ideal bundle.

Pitch / diameter ratio, $P_t/D = 1.25$.

No. of tube rows in flow direction, $N = 14$.

No. of tube rows across flow, $n = 20.5$.

Bank width = 0.1667m.

Atmospheric pressure, p_{atm}=1002.0 mbar.

Temp / K	$\dot{V}_T$ / m^3/s	u_{max} / m/s	$\Delta p_{measured}$ / Pa
314.7	0.096	19.1	1282
313.9	0.120	23.8	1780
312.7	0.147	29.0	2570
311.4	0.176	34.6	3500
310.9	0.207	40.5	4490
309.2	0.231	45.0	5520
308.4	0.254	49.1	6560
310.2	0.278	53.3	7660
310.7	0.308	59.1	8860
310.9	0.329	62.8	9840
312.7	0.358	67.7	11550
312.9	0.390	73.3	13100
313.7	0.423	78.8	15100

TABLE 6.3

DATA FOR 1.375 EQUILATERAL-TRIANGLE BANK, NO BYPASSING

Ideal bundle.

Pitch / diameter ratio, $P_t/D = 1.375$.

No. of tube rows in flow direction, $N = 13$.

No. of tube rows across flow, $n = 18.5$.

Bank width = 0.1659m.

Atmospheric pressure, p_{atm}=1015.5 mbar.

Temp / K	$\dot{V}_T$ / m^3/s	u_{max} / m/s	$\Delta p_{measured}$ / Pa
318.9	0.121	17.8	930
317.7	0.148	21.7	1270
319.4	0.220	32.1	2190
318.7	0.283	41.0	3530
317.9	0.319	46.0	4520
318.9	0.408	58.1	6890
316.2	0.450	63.9	7700
315.7	0.519	73.0	9640
314.7	0.552	77.3	10620
314.4	0.569	79.2	11280

TABLE 6.4

DATA FOR 1.375 EQUILATERAL-TRIANGLE BANK, NO BYPASSING

Ideal bundle.

Pitch / diameter ratio, $P_t/D = 1.375$.

No. of tube rows in flow direction, $N = 10$.

No. of tube rows across flow, $n = 18.5$.

Bank width = 0.1659m.

Distance from downstream pressure tapping to tube bank exit = 0.179m.

Atmospheric pressure, p_{atm}=1020.0 mbar.

Temp / K	$\dot{V}_T$ / m^3/s	u_{max} / m/s	$\Delta p_{measured}$ / Pa
314.9	0.130	19.1	810
321.4	0.160	23.4	1100
316.7	0.241	35.1	2260
319.4	0.320	46.3	3630
320.9	0.391	56.2	5060
320.2	0.465	66.6	6990
320.7	0.555	78.2	9350
320.7	0.590	82.6	10580

TABLE 6.5

DATA FOR 1.375 EQUILATERAL-TRIANGLE BANK, NO BYPASSING

Ideal bundle.

Pitch / diameter ratio, P_t/D = 1.375.

No. of tube rows in flow direction, N = 7.

No. of tube rows across flow, n = 18.5.

Bank width = 0.1659m.

Distance from downstream pressure tapping to tube bank exit = 0.225m.

Atmospheric pressure, p_{atm}=1022.0 mbar.

Temp / K	$\dot{V}_T$ / m^3/s	u_{max} / m/s	$\Delta p_{measured}$ / Pa
318.4	0.142	20.9	700
318.7	0.214	31.3	1400
318.4	0.252	36.8	1760
320.4	0.334	48.5	2860
318.9	0.389	56.3	3690
317.7	0.419	60.5	4290
319.9	0.509	72.9	5990
318.2	0.576	81.9	7450

TABLE 6.6

DATA FOR 1.25 IN-LINE SQUARE BANK, NO BYPASSING

Ideal bundle.

Pitch / diameter ratio, $P_t/D = 1.25$.

No. of tube rows in flow direction, $N = 12$

No. of tube rows across flow, $n = 10$.

Bank width = 0.1588m.

Atmospheric pressure, p_{atm}=1015.0 mbar.

Temp / K	$\dot{V}_T$ / m^3/s	u_{max} / m/s	$\Delta p_{measured}$ / Pa
315.2	0.112	23.5	1790
312.9	0.117	24.5	2000
313.7	0.145	30.3	2790
316.4	0.165	34.3	3570
316.9	0.185	38.3	4420
316.4	0.211	43.5	5530
316.2	0.225	46.2	6240
316.4	0.242	49.5	7120
313.2	0.267	54.2	8490
316.2	0.299	60.2	10330
313.2	0.325	64.9	12060
312.7	0.353	69.9	13990
312.4	0.366	72.2	14800
312.4	0.381	74.3	15360

TABLE 6.7

DATA FOR 1.375 IN-LINE SQUARE BANK, NO BYPASSING

Ideal bundle.

Pitch / diameter ratio, $P_t/D = 1.375$.

No. of tube rows in flow direction, $N = 11$.

No. of tube rows across flow, $n = 10$.

Bank width = 0.1746m.

Atmospheric pressure, p_{atm}=1010.0 mbar.

Temp / K	$\dot{V}_T$ / m^3/s	u_{max} / m/s	$\Delta p_{measured}$ / Pa
314.2	0.152	21.2	1130
313.2	0.184	25.6	1570
316.2	0.206	28.6	1911
314.7	0.237	32.8	2530
315.2	0.284	39.1	3510
313.4	0.341	46.6	4950
315.2	0.384	52.2	6070
315.4	0.414	56.0	7110
313.4	0.456	61.3	8420
314.7	0.489	65.4	9450
313.2	0.519	69.0	10710
312.4	0.547	71.3	11810
312.4	0.565	73.4	12500

TABLE 7.1

DATA FOR 1.25 EQUILATERAL-TRIANGLE BANK, WITH 'T' BYPASS

Bypass and crossflow streams separated on exit from bank by splitter plate.

Pitch / diameter ratio, P_t/D = 1.25.

No. of tube rows in flow direction, N = 14.

No. of tube rows across flow, n = 19.5.

Bank width = 0.1508m.

Bypass width = 0.0079m.

Ratio of bypass flow area to total flow area, F = 0.05.

Atmospheric pressure, p_{atm}=1004.5 mbar.

Temp / K	$\dot{V}_T$ / m^3/s	u_{max} / m/s	$\dot{m}_{Bexit}/\dot{m}_T$	$\Delta p_{measured}$ / Pa
322.9	0.123	25.6	0.097	1910
321.9	0.177	36.6	0.068	3310
321.9	0.214	43.9	0.089	4940
320.2	0.263	53.4	0.088	6940
321.2	0.288	58.1	0.087	8120
319.9	0.323	64.6	0.087	10150
319.2	0.353	70.0	0.088	11860
317.9	0.368	72.7	0.082	12710
315.9	0.378	74.6	0.079	12960

TABLE 7.2

DATA FOR 1.25 EQUILATERAL-TRIANGLE BANK, WITH ½T BYPASS

Bypass and crossflow undivided on exit from bank.

Pitch / diameter ratio, P_t/D = 1.25.

No. of tube rows in flow direction, N = 14.

No. of tube rows across flow, n = 19.5.

Bank width = 0.1508m.

Bypass width = 0.0079m.

Ratio of bypass flow area to total flow area, F = 0.05.

Atmospheric pressure, p_{atm}=1019.5 mbar.

Temp / K	$\dot{V}_T$ / m^3/s	u_{max} / m/s	$\Delta p_{measured}$ / Pa
311.4	0.084	17.6	920
310.9	0.099	20.7	1230
309.7	0.126	26.2	1900
311.4	0.148	30.7	2430
309.9	0.173	35.7	3350
310.7	0.205	42.1	4480
310.7	0.235	48.0	5880
310.4	0.262	53.2	6870
309.9	0.292	58.8	8630
309.9	0.314	63.1	9210
309.7	0.345	68.6	11290
309.7	0.364	72.2	11890

TABLE 7.3

DATA FOR 1.25 EQUILATERAL-TRIANGLE BANK, WITH 1½T BYPASS

Bypass and crossflow streams separated on exit from bank by splitter plate.

Pitch / diameter ratio, P_t/D = 1.25.

No. of tube rows in flow direction, N = 14.

No. of tube rows across flow, n = 19.5.

Bank width = 0.1508m.

Bypass width = 0.0159m.

Ratio of bypass flow area to total flow area, F = 0.24.

Atmospheric pressure, p_{atm}=1004.0 mbar.

Temp / K	$\dot{V}_T$ / m^3/s	u_{max} / m/s	$\dot{m}_{Bexit}/\dot{m}_T$	$\Delta p_{measured}$ / Pa
324.2	0.102	20.3	0.451	570
323.9	0.117	23.3	0.462	830
322.9	0.157	31.2	0.439	1370
323.2	0.231	45.5	0.441	3000
322.9	0.266	52.2	0.436	4030
322.9	0.313	61.0	0.422	5220
323.2	0.352	68.3	0.426	6350
323.2	0.387	74.6	0.419	7680
322.4	0.410	78.7	0.454	8490
323.2	0.435	83.1	0.457	9390
322.4	0.464	88.2	0.412	10450
320.9	0.498	94.1	0.410	11810

TABLE 7.4

DATA FOR 1.25 EQUILATERAL-TRIANGLE BANK, WITH 1½T BYPASS

Bypass and crossflow undivided on exit.

Pitch / diameter ratio, P_t/D = 1.25.

No. of tube rows in flow direction, N = 14.

No. of tube rows across flow, n = 19.5.

Bank width = 0.1508m.

Bypass width = 0.0159m.

Ratio of bypass flow area to total flow area, F = 0.24.

Atmospheric pressure, p_{atm}=1013.0 mbar.

Temp / K	$\dot{V}_T$ / m^3/s	u_{max} / m/s	$\Delta p_{measured}$ / Pa
314.7	0.154	30.6	1540
314.4	0.175	34.7	1930
313.9	0.231	45.5	3200
313.9	0.271	53.1	4190
312.9	0.308	60.0	5270
312.7	0.342	66.3	6270
312.7	0.368	71.1	7080
312.4	0.406	78.0	8380
312.2	0.422	80.8	9040
311.9	0.457	87.0	10300
311.9	0.499	94.2	12020
311.9	0.538	100.8	13690

TABLE 7.5

DATA FOR 1.25 EQUILATERAL-TRIANGLE BANK, WITH 2½T BYPASS

Bypass and crossflow streams separated on exit from bank by splitter plate.

Pitch / diameter ratio, P_t/D = 1.25.

No. of tube rows in flow direction, N = 14.

No. of tube rows across flow, n = 19.5.

Bank width = 0.1508m.

Bypass width = 0.0238m.

Ratio of bypass flow area to total flow area, F = 0.367.

Atmospheric pressure, p_{atm}=1013.0 mbar.

Temp / K	$\dot{V}_T$ / m^3/s	u_{max} / m/s	$\dot{m}_{Bexit}/\dot{m}_T$	$\Delta p_{measured}$ / Pa
321.2	0.137	26.1	0.649	690
320.2	0.159	30.2	0.623	820
322.2	0.195	37.0	0.626	1130
321.7	0.240	45.4	0.633	1920
319.9	0.295	55.6	0.614	2760
320.9	0.349	65.4	0.616	3860
319.7	0.371	69.4	0.612	4280
320.9	0.384	71.7	0.614	4610
320.4	0.399	74.4	0.614	4910
319.7	0.413	76.9	0.610	5180
319.4	0.428	79.5	0.608	5510
319.2	0.435	80.8	0.607	5630

TABLE 7.6

DATA FOR 1.25 EQUILATERAL-TRIANGLE BANK, WITH 2½T BYPASS

Bypass and crossflow undivided on exit.

Pitch / diameter ratio, P_t/D = 1.25.

No. of tube rows in flow direction, N = 14.

No. of tube rows across flow, n = 19.5.

Bank width = 0.1508m.

Bypass width = 0.0238m.

Ratio of bypass flow area to total flow area, F = 0.367.

Atmospheric pressure, p_{atm}=1014.0 mbar.

Temp / K	$\dot{V}_T$ / m^3/s	u_{max} / m/s	$\Delta p_{measured}$ / Pa
315.6	0.169	32.1	1080
315.7	0.214	40.5	1650
315.4	0.250	47.0	2190
315.4	0.277	52.2	2530
315.2	0.328	61.5	3570
315.2	0.347	65.0	3890
314.9	0.377	70.4	4510
314.9	0.413	76.8	5330
315.4	0.460	85.0	6710
315.4	0.500	92.2	7230
315.2	0.534	98.0	8200
315.2	0.575	104.7	9850

TABLE 7.7

DATA FOR 1.25 EQUILATERAL-TRIANGLE BANK, WITH 3½T BYPASS

Bypass and crossflow streams separated on exit from bank by splitter plate.

Pitch / diameter ratio, P_t/D = 1.25.

No. of tube rows in flow direction, N = 14.

No. of tube rows across flow, n = 19.5.

Bank width = 0.1508m.

Bypass width = 0.0318m.

Ratio of bypass flow area to total flow area, F = 0.457.

Atmospheric pressure, p_{atm}=1014.0 mbar.

Temp / K	$\dot{V}_T$ / m^3/s	u_{max} / m/s	$\dot{m}_{Bexit}/\dot{m}_T$	$\Delta p_{measured}$ / Pa
323.7	0.107	19.5	0.765	260
319.7	0.154	28.1	0.714	520
320.7	0.206	37.4	0.733	1000
320.2	0.236	42.8	0.729	1280
319.7	0.265	48.0	0.721	1580
320.2	0.282	51.0	0.724	1780
319.9	0.309	55.8	0.719	2100
319.7	0.323	58.3	0.718	2270
320.2	0.336	60.6	0.723	2470
319.4	0.351	63.3	0.715	2630
319.2	0.359	64.7	0.719	2760
319.2	0.367	66.1	0.717	2780

TABLE 7.8

DATA FOR 1.25 EQUILATERAL-TRIANGLE BANK, WITH $3\frac{1}{2}$T BYPASS

Bypass and crossflow undivided on exit.

Pitch / diameter ratio, P_t/D = 1.25.

No. of tube rows in flow direction, N = 14.

No. of tube rows across flow, n = 19.5.

Bank width = 0.1508m.

Bypass width = 0.0318m.

Ratio of bypass flow area to total flow area, F = 0.457.

Atmospheric pressure, p_{atm}=1024.0 mbar.

Temp / K	$\dot{V}_T$ / m^3/s	u_{max} / m/s	$\Delta p_{measured}$ / Pa
315.7	0.093	17.0	200
315.4	0.114	20.8	300
315.2	0.146	26.6	500
315.2	0.170	30.9	670
314.4	0.184	33.5	800
313.7	0.217	39.4	1030
313.7	0.253	45.9	1400
313.2	0.279	50.5	1810
312.9	0.301	54.4	2050
312.7	0.320	57.8	2350
311.9	0.357	64.3	2810

TABLE 7.9

DATA FOR 1.375 EQUILATERAL-TRIANGLE BANK, WITH ½T BYPASS

Bypass and crossflow streams separated on exit from bank by splitter plate.

Pitch / diameter ratio, P_t/D = 1.375.

No. of tube rows in flow direction, N = 13.

No. of tube rows across flow, n = 17.5.

Bank width = 0.1397m.

Bypass width = 0.0087m.

Ratio of bypass flow area to total flow area, F = 0.056.

Atmospheric pressure, p_{atm}=1017.0 mbar.

Temp / K	$\dot{V}_T$ / m^3/s	u_{max} / m/s	$\dot{m}_{Bexit}/\dot{m}_T$	$\Delta p_{measured}$ / Pa
315.7	0.097	15.1	0.175	530
316.2	0.213	32.8	0.193	2180
315.7	0.262	40.1	0.199	3120
315.9	0.296	45.2	0.196	3830
315.9	0.343	52.1	0.198	4950
317.9	0.386	58.3	0.194	6050
317.4	0.414	62.3	0.196	6950
317.2	0.449	67.2	0.192	8050
316.9	0.477	71.1	0.195	8830
316.7	0.514	76.2	0.195	9990

TABLE 7.10

DATA FOR 1.375 EQUILATERAL-TRIANGLE BANK, WITH 1½T BYPASS

Bypass and crossflow streams separated on exit from bank by splitter plate.

Pitch / diameter ratio, P_t/D = 1.375.

No. of tube rows in flow direction, N = 13.

No. of tube rows across flow, n = 17.5.

Bank width = 0.1397m.

Bypass width = 0.0175m.

Ratio of bypass flow area to total flow area, F = 0.215.

Atmospheric pressure, p_{atm}=1017.0 mbar.

Temp / K	$\dot{V}_T$ / m^3/s	u_{max} / m/s	$\dot{m}_{Bexit}/\dot{m}_T$	$\Delta p_{measured}$ / Pa
318.9	0.147	21.6	0.428	730
317.7	0.175	25.7	0.440	1000
317.9	0.266	38.8	0.432	2080
317.9	0.301	43.8	0.429	2510
317.2	0.346	50.2	0.431	3310
318.9	0.399	57.6	0.431	4320
318.9	0.436	62.7	0.424	5150
316.9	0.477	68.3	0.428	6000
319.7	0.515	73.4	0.427	6800
316.7	0.560	79.4	0.423	8000
315.9	0.600	84.6	0.422	9090
315.7	0.625	87.9	0.421	9770

TABLE 7.11

DATA FOR 1.375 EQUILATERAL-TRIANGLE BANK, WITH 2½T BYPASS

Bypass and crossflow streams separated on exit from bank by splitter plate.

Pitch / diameter ratio, P_t/D = 1.375.

No. of tube rows in flow direction, N = 13.

No. of tube rows across flow, n = 17.5.

Bank width = 0.1397m.

Bypass width = 0.0262m.

Ratio of bypass flow area to total flow area, F = 0.329.

Atmospheric pressure, p_{atm}=1016.0 mbar.

Temp / K	$\dot{V}_T$ / m^3/s	u_{max} / m/s	$\dot{m}_{Bexit}/\dot{m}_T$	$\Delta p_{measured}$ / Pa
322.4	0.159	22.2	0.566	470
323.2	0.203	28.3	0.581	730
323.2	0.294	40.9	0.575	1380
322.4	0.344	47.7	0.550	1770
322.4	0.360	49.9	0.567	2010
323.2	0.421	58.2	0.572	2740
322.2	0.469	64.6	0.569	3350
322.7	0.497	68.3	0.559	3690
318.7	0.530	72.7	0.557	4090
319.9	0.576	78.7	0.554	4860
317.7	0.633	86.2	0.550	5720

TABLE 7.12

DATA FOR 1.375 EQUILATERAL-TRIANGLE BANK, WITH 3½T BYPASS

Bypass and crossflow streams separated on exit from bank by splitter plate.

Pitch / diameter ratio, P_t/D = 1.375.

No. of tube rows in flow direction, N = 13.

No. of tube rows across flow, n = 17.5.

Bank width = 0.1397m.

Bypass width = 0.0349m.

Ratio of bypass flow area to total flow area, F = 0.414.

Atmospheric pressure, p_{atm}=1016.0 mbar.

$\frac{\text{Temp}}{\text{K}}$	$\frac{\dot{V}_T}{m^3/s}$	$\frac{u_{max}}{m/s}$	$\frac{\dot{m}_{Bexit}}{\dot{m}_T}$	$\frac{\Delta p_{measured}}{\text{Pa}}$
319.2	0.178	23.7	0.668	500
319.9	0.275	36.5	0.651	1070
320.2	0.321	42.5	0.651	1370
319.2	0.363	48.0	0.656	1720
320.4	0.384	50.7	0.659	1970
319.7	0.422	55.6	0.664	2410
320.4	0.450	59.2	0.658	2680
318.9	0.493	64.7	0.651	3190
321.2	0.560	73.3	0.652	3870

TABLE 7.13

DATA FOR 1.25 IN-LINE SQUARE BANK, WITH ½S BYPASS

Bypass and crossflow streams separated on exit from bank by splitter plate.

Pitch / diameter ratio, P_t/D = 1.25.

No. of tube rows in flow direction, N = 12.

No. of tube rows across flow, n = 10.5.

Bank width = 0.1588m.

Bypass width = 0.0159m.

Ratio of bypass flow area to total flow area, F = 0.231.

Atmospheric pressure, p_{atm}=1015.0 mbar.

Temp / K	$\dot{V}_T$ / m^3/s	u_{max} / m/s	$\dot{m}_{Bexit}/\dot{m}_T$	$\Delta p_{measured}$ / Pa
317.4	0.121	23.0	0.438	930
316.4	0.165	31.2	0.424	1770
319.4	0.201	37.9	0.443	2630
318.7	0.236	44.3	0.428	3330
318.4	0.275	51.3	0.418	4570
318.7	0.307	57.1	0.404	5380
316.4	0.319	59.2	0.401	5860
317.7	0.363	66.8	0.441	7550
316.2	0.404	73.8	0.391	9250
317.7	0.427	77.7	0.386	9950
315.9	0.452	81.7	0.387	11500
314.9	0.472	84.9	0.383	12740
314.7	0.482	86.3	0.390	13290

TABLE 7.14

DATA FOR 1.25 IN-LINE SQUARE BANK, WITH 1½S BYPASS

Bypass and crossflow streams separated on exit from bank by splitter plate.

Pitch / diameter ratio, P_t/D = 1.25.

No. of tube rows in flow direction, N = 12.

No. of tube rows across flow, n = 9.5.

Bank width = 0.1429m.

Bypass width = 0.0318m.

Ratio of bypass flow area to total flow area, F = 0.471.

Atmospheric pressure, p_{atm}=1010.0 mbar.

Temp / K	$\dot{V}_T$ / m^3/s	u_{max} / m/s	$\dot{m}_{Bexit}/\dot{m}_T$	$\Delta p_{measured}$ / Pa
317.7	0.126	24.0	0.770	500
318.9	0.135	25.7	0.785	570
320.4	0.148	28.2	0.777	670
318.2	0.152	28.9	0.776	700
317.9	0.184	35.0	0.767	940
318.2	0.206	39.1	0.762	1100
318.2	0.213	40.4	0.770	1110
318.9	0.248	47.0	0.774	1410
320.7	0.278	52.7	0.766	1680
318.4	0.294	55.6	0.772	1850
318.7	0.315	59.5	0.768	2130
317.9	0.327	61.7	0.771	2320
320.2	0.337	63.6	0.769	2420

TABLE 7.15

DATA FOR 1.375 IN-LINE SQUARE BANK, WITH ½S BYPASS

Bypass and crossflow streams separated on exit from bank by splitter plate.

Pitch / diameter ratio, P_t/D = 1.375.

No. of tube rows in flow direction, N = 11.

No. of tube rows across flow, n = 8.5.

Bank width = 0.1397m.

Bypass width = 0.0175m.

Ratio of bypass flow area to total flow area, F = 0.226.

Atmospheric pressure, p_{atm}=1017.0 mbar.

Temp / K	$\dot{V}_T$ / m^3/s	u_{max} / m/s	$\dot{m}_{Bexit}/\dot{m}_T$	$\Delta p_{measured}$ / Pa
319.2	0.155	24.0	0.406	900
319.9	0.217	33.5	0.410	1650
318.7	0.237	36.5	0.401	1920
317.9	0.277	42.5	0.394	2640
316.9	0.342	52.2	0.371	3670
317.7	0.357	54.4	0.392	4320
317.4	0.396	60.0	0.391	5230
316.9	0.457	68.9	0.407	6390
317.2	0.490	73.5	0.367	7450
316.7	0.518	77.5	0.363	8110
316.2	0.546	81.3	0.363	8980
315.7	0.563	83.7	0.362	9430

TABLE 7.16

DATA FOR 1.375 IN-LINE SQUARE BANK, WITH 1½S BYPASS

Bypass and crossflow streams separated on exit from bank by splitter plate.

Pitch / diameter ratio, P_t/D = 1.375.

No. of tube rows in flow direction, N = 11.

No. of tube rows across flow, n = 8.5.

Bank width = 0.1397m.

Bypass width = 0.0349m.

Ratio of bypass flow area to total flow area, F = 0.429.

Atmospheric pressure, p_{atm}=1017.5 mbar.

Temp / K	$\dot{V}_T$ / m^3/s	u_{max} / m/s	$\dot{m}_{Bexit}/\dot{m}_T$	$\Delta p_{measured}$ / Pa
316.4	0.127	17.8	0.622	270
317.2	0.210	29.3	0.662	730
315.4	0.244	34.0	0.656	930
316.4	0.267	37.2	0.663	1130
317.2	0.293	40.8	0.659	1250
317.7	0.300	41.7	0.660	1320
316.4	0.307	42.7	0.658	1410
315.7	0.335	46.5	0.654	1650
317.2	0.356	49.4	0.671	1870
315.7	0.379	52.5	0.652	2080
315.4	0.398	55.1	0.651	2270
314.9	0.408	56.5	0.652	2400

TABLE 7.17

INLET FLOW DATA FOR 1.25 EQUILATERAL-TRIANGLE BANK WITH BYPASSING

The same geometry and bank configuration was used as in Tables 7.1 to 7.4. Bypass inlet flow rates were calculated as described in Appendix C from HWA traverses.

Temp / K	$\dot{V}_T$ / m^3/s	u_{max} / m/s	$\dot{m}_{Bin}/\dot{m}_T$
For ½T bypass			
314.7	0.277	54.6	0.056
315.4	0.381	71.6	0.056
315.4	0.402	75.2	0.060
For 1½T bypass			
313.7	0.202	40.0	0.274
311.9	0.294	57.4	0.267
312.7	0.394	75.6	0.303
For 2½T bypass			
312.7	0.280	52.7	0.351
314.4	0.376	70.2	0.351
315.2	0.429	79.6	0.412
314.4	0.496	92.8	0.401
For 3½T bypass			
315.9	0.192	34.9	0.465
315.4	0.226	41.1	0.454
313.7	0.301	54.4	0.457
315.4	0.510	91.5	0.449

TABLE 8.1

DATA FOR BYPASS LANE ALONE, WITH NO FLOW TRANSFER

Tests on plain ducts having the same cross-sections as the bypass lanes of Chapter 7.

Empty bypass, no half-tubes.

Bypass width = 7.9mm.

Equivalent diameter, Equation 8.2, D_e = 15.0mm.

Length of duct, L = 1m.

Atmospheric pressure, p_{atm}=996.0 mbar.

Temp / K	$\dot{V}_B$ / m^3/s	u_b / m/s	$\Delta p_{measured}$ / Pa
312.2	0.016	13.5	170
312.2	0.020	16.9	260
313.7	0.029	24.4	530
314.2	0.034	28.6	720
312.7	0.038	31.4	910
314.2	0.040	33.6	980

TABLE 8.2

DATA FOR BYPASS LANE ALONE, WITH NO FLOW TRANSFER

Empty bypass, no half-tubes.

Bypass width = 15.9mm.

Equivalent diameter, Equation 8.2, D_e = 28.7mm.

Length of duct, L = 1m.

Atmospheric pressure, p_{atm}=1018.5 mbar.

Temp / K	$\dot{V}_B$ / m^3/s	u_b / m/s	$\Delta p_{measured}$ / Pa
311.4	0.053	22.2	440
314.2	0.065	27.2	350
314.4	0.098	41.0	830
314.2	0.135	56.2	1810
313.9	0.147	61.0	2390
313.7	0.168	69.2	3880
312.4	0.185	75.8	4940
313.2	0.219	89.4	5790

TABLE 8.3

DATA FOR BYPASS LANE ALONE, WITH NO FLOW TRANSFER

Empty bypass, no half-tubes.

Bypass width = 23.8mm.

Equivalent diameter, Equation 8.2, D_e = 41.1mm.

Length of duct, L = 1m.

Atmospheric pressure, p_{atm}=1008.5 mbar.

Temp / K	$\dot{V}_B$ / m^3/s	u_b / m/s	$\Delta p_{measured}$ / Pa
314.9	0.054	15.1	80
310.2	0.066	18.5	120
312.9	0.090	25.2	190
313.2	0.123	34.4	350
312.7	0.158	44.1	560
312.7	0.180	50.2	750
312.4	0.206	57.4	910
312.4	0.225	62.7	1100
311.9	0.257	71.4	1560

TABLE 8.4

DATA FOR BYPASS LANE ALONE, WITH NO FLOW TRANSFER

Empty bypass, no half-tubes.

Bypass width = 31.8mm.

Equivalent diameter, Equation 8.2, D_e = 52.4mm.

Length of duct, L = 1m.

Atmospheric pressure, p_{atm}=996.0 mbar.

Temp / K	$\dot{V}_B$ / m^3/s	u_b / m/s	$\Delta p_{measured}$ / Pa
314.7	0.057	12.0	40
310.2	0.067	14.1	40
314.7	0.095	19.9	100
314.9	0.129	27.1	170
314.7	0.165	34.6	250
314.2	0.199	41.7	410
311.7	0.222	46.5	540
313.9	0.256	53.5	950

TABLE 8.5

DATA FOR BYPASS LANE ALONE, WITH NO FLOW TRANSFER

Tests on ducts having the same cross-sections and tube arrangements of bypass lanes as those of Chapter 7.

1.25 equilateral-triangle 1½T bypass.

Bypass with half-tubes.

Bypass width = 15.9mm.

Equivalent diameter, Equation 8.2, D_e = 28.7mm.

Longitudinal tube pitch = 27.5mm.

Number of tubes along flow = 7.

Length of duct, L = 0.1777m.

Atmospheric pressure, p_{atm}=1018.5 mbar.

Temp / K	$\dot{V}_B$ / m^3/s	u_b / m/s	$\Delta p_{measured}$ / Pa	Δp_d / Pa
314.2	0.065	27.1	1570	110
313.9	0.101	41.7	3530	270
314.2	0.135	55.2	6000	520
313.9	0.147	59.7	7600	680
313.7	0.168	67.6	9870	1110

($\Delta p_{measured}$ includes the empty duct pressure loss between the pressure tappings and the first and last tube in the bypass lane. Δp_B, the pressure drop over the bypass lane, = $\Delta p_{measured} - \Delta p_d$, where Δp_d is the inlet and exit duct pressure drop.)

TABLE 8.6

DATA FOR BYPASS LANE ALONE, WITH NO FLOW TRANSFER

1.25 equilateral-triangle 2½T bypass.

Bypass with half-tubes.

Bypass width = 23.8mm.

Equivalent diameter, Equation 8.2, D_e = 41.1mm.

Tube pitch = 27.5mm.

Number of tubes along flow = 7.

Length of duct, L = 0.1777m.

Atmospheric pressure, p_{atm}=1008.5 mbar.

Temp / K	$\dot{V}_B$ / m^3/s	u_b / m/s	$\Delta p_{measured}$ / Pa	Δp_d / Pa
314.9	0.054	15.1	100	20
314.9	0.094	26.3	420	60
314.7	0.131	36.5	840	110
314.9	0.167	46.5	1340	190
314.9	0.193	53.6	1820	250
314.7	0.221	61.3	2350	330
314.4	0.241	66.7	2770	420

TABLE 8.7

DATA FOR BYPASS LANE ALONE, WITH NO FLOW TRANSFER

1.25 equilateral-triangle 3½T bypass.

Bypass with half-tubes.

Bypass width = 31.8mm.

Equivalent diameter, Equation 8.2, D_e = 52.4mm.

Tube pitch = 27.5mm.

Number of tubes along flow = 7.

Length of duct, L = 0.1777m.

Atmospheric pressure, p_{atm}=996.0 mbar.

Temp / K	$\dot{V}_B$ / m^3/s	u_b / m/s	$\Delta p_{measured}$ / Pa	Δp_d / Pa
310.2	0.067	14.1	30	10
309.9	0.104	21.8	150	20
310.4	0.136	28.5	320	50
310.4	0.175	36.7	480	90
310.7	0.200	41.9	660	120
310.4	0.253	52.9	970	240

TABLE 8.8

DATA FOR BYPASS LANE ALONE, WITH NO FLOW TRANSFER

1.25 in-line square ½S bypass.

Bypass with half-tubes.

Bypass width = 15.9mm.

Equivalent diameter, Equation 8.2, D_e = 28.7mm.

Tube pitch = 15.9mm.

Number of tubes along flow = 12.

Length of duct, L = 0.1873m.

Atmospheric pressure, p_{atm}=1008.5 mbar.

Temp / K	$\dot{V}_B$ / m^3/s	u_b / m/s	$\Delta p_{measured}$ / Pa	Δp_d / Pa
311.9	0.062	25.9	1470	90
311.9	0.108	44.3	4950	290
312.2	0.142	57.7	7400	620
312.2	0.158	63.7	9470	940
311.9	0.164	66.0	9930	1020

TABLE 8.9

DATA FOR BYPASS LANE ALONE, WITH NO FLOW TRANSFER

1.25 in-line square 1½S bypass.

Bypass with half-tubes.

Bypass width = 31.8mm.

Equivalent diameter, Equation 8.2, D_e = 52.4mm.

Tube pitch = 15.9mm.

Number of tubes along flow = 12.

Length of duct, L = 0.1873m.

Atmospheric pressure, p_{atm}=1014.0 mbar.

Temp / K	$\dot{V}_B$ / m^3/s	u_b / m/s	$\Delta p_{measured}$ / Pa	Δp_d / Pa
314.7	0.057	12.0	20	10
314.7	0.095	19.9	90	30
314.9	0.129	27.1	190	50
314.7	0.165	34.6	270	70
314.2	0.199	41.7	420	110
313.9	0.256	53.7	630	260

TABLE 9.1

DATA FOR 1.25 EQUILATERAL-TRIANGLE BANK, WITH ¼T BYPASS AND ONE SEALING-STRIP

Bypass and crossflow streams are separated on exit by a splitter plate.

Pitch / diameter ratio, P_t/D = 1.25.

Number of tube rows in flow direction, N = 14.

Number of tube rows across the flow, n = 19.5.

Bank width = 0.1508m.

Bypass width = 0.0079m.

Ratio of bypass flow area to total flow area, F = 0.05.

Number of sealing-strips, N_s = 1, placed at 2nd row.

Atmospheric pressure, p_{atm}=999.0 mbar.

$\frac{\text{Temp}}{\text{K}}$	$\frac{\dot{V}_T}{m^3/s}$	$\frac{u_{max}}{m/s}$	$\frac{\dot{m}_{Bexit}}{\dot{m}_T}$	$\frac{\Delta p_{measured}}{\text{Pa}}$
315.7	0.107	22.3	0.084	1375
313.7	0.125	26.0	0.080	1890
315.9	0.174	38.0	0.080	3250
315.4	0.203	41.7	0.084	4350
314.7	0.222	45.4	0.086	5240
313.4	0.245	49.9	0.082	6130
314.4	0.276	55.9	0.087	7610
313.4	0.317	63.6	0.082	9400
313.9	0.330	66.1	0.085	9950
313.7	0.349	69.5	0.083	11070
312.9	0.363	72.0	0.083	11890
312.9	0.372	73.6	0.083	12350

TABLE 9.2

DATA FOR 1.25 EQUILATERAL-TRIANGLE BANK, WITH ¼T BYPASS AND TWO SEALING-STRIPS

Pitch / diameter ratio, P_t/D = 1.25.

Number of tube rows in flow direction, N = 14.

Number of tube rows across the flow, n = 19.5.

Bank width = 0.1508m.

Bypass width = 0.0079m.

Ratio of bypass flow area to total flow area, F = 0.05.

Number of sealing-strips, N_s = 2, placed at 2nd and 14th rows.

Atmospheric pressure, p_{atm}=999.0 mbar.

Temp / K	$\dot{V}_T$ / m^3/s	u_{max} / m/s	$\Delta p_{measured}$ / Pa
315.7	0.098	20.4	1370
315.2	0.108	22.5	1580
315.4	0.124	25.8	2050
314.9	0.149	30.9	2740
314.9	0.180	37.1	3780
314.4	0.212	43.5	4940
314.7	0.239	48.7	6050
314.7	0.266	54.0	7160
314.4	0.287	57.9	8220
314.2	0.315	63.1	9670
314.2	0.343	68.3	11100
313.9	0.369	72.9	12640

TABLE 9.3

DATA FOR 1.25 EQUILATERAL-TRIANGLE BANK, WITH ¼T BYPASS AND FOUR SEALING-STRIPS

Pitch / diameter ratio, P_t/D = 1.25.

Number of tube rows in flow direction, N = 14.

Number of tube rows across the flow, n = 19.5.

Bank width = 0.1508m.

Bypass width = 0.0079m.

Ratio of bypass flow area to total flow area, F = 0.05.

Number of sealing-strips, N_s = 4, placed at 2nd, 6th, 10th and 14th rows.

Atmospheric pressure, p_{atm}=999.0 mbar.

Temp / K	$\dot{V}_T$ / m^3/s	u_{max} / m/s	$\Delta p_{measured}$ / Pa
313.4	0.093	19.4	1350
312.9	0.111	23.1	1770
312.9	0.123	25.6	2080
312.7	0.153	31.7	2960
312.2	0.170	35.1	3530
312.4	0.203	41.6	4830
312.2	0.233	47.5	6020
311.9	0.260	52.7	7190
311.4	0.289	58.2	8710
311.9	0.311	62.3	9870
311.7	0.336	66.9	11220
311.7	0.364	71.9	12720

TABLE 9.4

DATA FOR 1.25 EQUILATERAL-TRIANGLE BANK, WITH 1½T BYPASS AND ONE SEALING-STRIP

Bypass and crossflow streams are separated on exit by a splitter plate.

Pitch / diameter ratio, P_t/D = 1.25.

Number of tube rows in flow direction, N = 14.

Number of tube rows across the flow, n = 19.5.

Bank width = 0.1508m.

Bypass width = 0.0159m.

Ratio of bypass flow area to total flow area, F = 0.24.

Number of sealing-strips, N_s = 1, placed at 2nd row.

Atmospheric pressure, p_{atm}=997.5 mbar.

$\frac{\text{Temp}}{\text{K}}$	$\frac{\dot{V}_T}{m^3/s}$	$\frac{u_{max}}{m/s}$	$\frac{\dot{m}_{Bexit}}{\dot{m}_T}$	$\frac{\Delta p_{measured}}{\text{Pa}}$
315.7	0.126	25.0	0.381	1360
314.2	0.141	28.0	0.369	1650
316.4	0.186	36.7	0.382	2800
316.2	0.230	45.1	0.379	4050
313.7	0.268	52.2	0.358	5260
315.7	0.315	60.9	0.362	7090
314.9	0.343	65.9	0.361	8210
313.2	0.370	70.7	0.352	9360
314.7	0.398	75.6	0.349	10640
313.2	0.417	78.9	0.348	11610
312.7	0.436	82.1	0.346	12660
312.9	0.444	83.4	0.347	13170

TABLE 9.5

DATA FOR 1.25 EQUILATERAL-TRIANGLE BANK, WITH 1½T BYPASS AND TWO SEALING-STRIPS

Pitch / diameter ratio, P_t/D = 1.25.

Number of tube rows in flow direction, N = 14.

Number of tube rows across the flow, n = 19.5.

Bank width = 0.1508m.

Bypass width = 0.0159m.

Ratio of bypass flow area to total flow area, F = 0.24.

Number of sealing-strips, N_s = 2, placed at 2nd and 14th rows.

Atmospheric pressure, p_{atm}=998.0 mbar.

$\frac{\text{Temp}}{\text{K}}$	$\frac{\dot{V}_T}{m^3/s}$	$\frac{u_{max}}{m/s}$	$\frac{\Delta p_{measured}}{\text{Pa}}$
317.7	0.105	21.0	1230
317.4	0.131	26.0	1920
317.2	0.152	30.0	2470
317.4	0.182	35.8	3340
316.2	0.215	42.0	4620
315.7	0.250	48.6	5990
315.9	0.277	53.5	7140
315.7	0.302	58.0	8330
315.9	0.324	61.9	9390
315.7	0.344	65.4	10490
314.7	0.358	67.8	11200
314.7	0.377	71.1	12230

TABLE 9.6

DATA FOR 1.25 EQUILATERAL-TRIANGLE BANK, WITH 1½T BYPASS AND FOUR SEALING-STRIPS

Pitch / diameter ratio, P_t/D = 1.25.

Number of tube rows in flow direction, N = 14.

Number of tube rows across the flow, n = 19.5.

Bank width = 0.1508m.

Bypass width = 0.0159m.

Ratio of bypass flow area to total flow area, F = 0.24.

Number of sealing-strips, N_s = 4, placed at 2nd, 6th, 10th and 14th rows.

Atmospheric pressure, p_{atm}=998.0 mbar.

Temp / K	$\dot{V}_T$ / m^3/s	u_{max} / m/s	$\Delta p_{measured}$ / Pa
315.9	0.101	20.1	1390
316.2	0.114	22.6	1740
315.4	0.133	26.3	2360
315.4	0.159	31.3	3180
314.9	0.198	38.7	4640
314.9	0.234	45.4	6090
314.9	0.269	51.8	7740
314.2	0.286	54.9	8560
314.2	0.307	58.6	9830
313.9	0.325	61.7	10780
313.2	0.342	64.6	11800
313.2	0.355	66.8	12630

TABLE 9.7

DATA FOR 1.25 EQUILATERAL-TRIANGLE BANK, WITH 2½T BYPASS AND ONE SEALING-STRIP

Bypass and crossflow streams are separated on exit by a splitter plate.

Pitch / diameter ratio, P_t/D = 1.25.

Number of tube rows in flow direction, N = 14.

Number of tube rows across the flow, n = 19.5.

Bank width = 0.1508m.

Bypass width = 0.0238m.

Ratio of bypass flow area to total flow area, F = 0.3667.

Number of sealing-strips, N_s = 1, placed at 2nd row.

Atmospheric pressure, p_{atm}=994.0 mbar.

$\frac{Temp}{K}$	$\frac{\dot{V}_T}{m^3/s}$	$\frac{u_{max}}{m/s}$	$\frac{\dot{m}_{Bexit}}{\dot{m}_T}$	$\frac{\Delta p_{measured}}{Pa}$
316.4	0.125	23.7	0.504	1230
318.9	0.155	29.3	0.523	1700
318.9	0.175	33.0	0.520	2210
318.7	0.202	38.0	0.520	2790
318.2	0.217	40.8	0.507	3220
317.9	0.251	47.0	0.498	4100
317.2	0.268	50.1	0.497	4490
317.9	0.323	59.8	0.495	6350
316.9	0.349	64.3	0.493	7220
316.7	0.387	70.8	0.488	8870
316.7	0.404	73.7	0.490	9540
316.4	0.412	75.0	0.488	9920

TABLE 9.8

DATA FOR 1.25 EQUILATERAL-TRIANGLE BANK, WITH 2½T BYPASS AND TWO SEALING-STRIPS

Pitch / diameter ratio, P_t/D = 1.25.

Number of tube rows in flow direction, N = 14.

Number of tube rows across the flow, n = 19.5.

Bank width = 0.1508m.

Bypass width = 0.0238m.

Ratio of bypass flow area to total flow area, F = 0.3667.

Number of sealing-strips, N_s = 2, placed at 2nd and 14th rows.

Atmospheric pressure, p_{atm}=994.0 mbar.

Temp / K	$\dot{V}_T$ / m^3/s	u_{max} / m/s	$\Delta p_{measured}$ / Pa
315.7	0.103	19.5	1270
315.9	0.119	22.5	1650
315.4	0.126	23.8	1860
315.7	0.137	25.9	2210
314.9	0.175	32.9	3270
314.7	0.221	41.2	4710
313.7	0.250	46.4	5770
314.2	0.281	51.8	6890
314.2	0.309	56.7	8021
312.9	0.329	60.2	8940
313.2	0.358	65.1	10000
312.7	0.377	68.4	10560

TABLE 9.9

DATA FOR 1.25 EQUILATERAL-TRIANGLE BANK, WITH 2½T BYPASS AND FOUR SEALING-STRIPS

Pitch / diameter ratio, P_t/D = 1.25.

Number of tube rows in flow direction, N = 14.

Number of tube rows across the flow, n = 19.5.

Bank width = 0.1508m.

Bypass width = 0.0238m.

Ratio of bypass flow area to total flow area, F = 0.3667.

Number of sealing-strips, N_s = 4, placed at 2nd, 6th, 10th and 14th rows.

Atmospheric pressure, p_{atm}=994.0 mbar.

Temp / K	$\dot{V}_T$ / m^3/s	u_{max} / m/s	$\Delta p_{measured}$ / Pa
319.7	0.096	18.2	1380
319.7	0.110	20.8	1750
319.2	0.135	25.5	2470
319.2	0.163	30.6	3250
319.2	0.185	34.6	4030
318.9	0.220	40.9	5230
318.4	0.252	46.6	6460
318.7	0.275	50.6	7400
318.7	0.303	55.5	8530
319.4	0.326	59.4	9490
318.7	0.341	62.0	10170
318.4	0.354	64.1	10770

TABLE 9.10

DATA FOR 1.25 EQUILATERAL-TRIANGLE BANK, WITH 3¼T BYPASS AND ONE SEALING-STRIP

Bypass and crossflow streams are separated on exit by a splitter plate.

Pitch / diameter ratio, $P_t/D = 1.25$.

Number of tube rows in flow direction, $N = 14$.

Number of tube rows across the flow, $n = 19.5$.

Bank width = 0.1508m.

Bypass width = 0.0318m.

Ratio of bypass flow area to total flow area, $F = 0.4571$.

Number of sealing-strips, $N_s = 1$, placed at 2nd row.

Atmospheric pressure, p_{atm}=1005.5 mbar.

$\frac{\text{Temp}}{\text{K}}$	$\frac{\dot{V}_T}{m^3/s}$	$\frac{u_{max}}{m/s}$	$\frac{\dot{m}_{Bexit}}{\dot{m}_T}$	$\frac{\Delta p_{measured}}{\text{Pa}}$
313.2	0.143	25.9	0.594	1330
314.4	0.162	29.3	0.617	1650
314.4	0.182	32.9	0.599	2140
314.7	0.208	37.5	0.596	2710
313.7	0.235	42.2	0.592	3300
313.7	0.258	46.2	0.589	3870
313.4	0.285	50.9	0.593	4680
314.2	0.304	54.1	0.592	5250
313.2	0.325	57.6	0.588	5960
313.4	0.357	63.0	0.585	6910
313.4	0.370	65.2	0.587	7390
313.2	0.376	66.2	0.585	7650

TABLE 9.11

DATA FOR 1.25 EQUILATERAL-TRIANGLE BANK, WITH 3½T BYPASS AND TWO SEALING-STRIPS

Pitch / diameter ratio, P_t/D = 1.25.

Number of tube rows in flow direction, N = 14.

Number of tube rows across the flow, n = 19.5.

Bank width = 0.1508m.

Bypass width = 0.0318m.

Ratio of bypass flow area to total flow area, F = 0.4571.

Number of sealing-strips, N_s = 2, placed at 2nd and 14th rows.

Atmospheric pressure, p_{atm}=1005.5 mbar.

$\frac{Temp}{K}$	$\frac{\dot{V}_T}{m^3/s}$	$\frac{u_{max}}{m/s}$	$\frac{\Delta p_{measured}}{Pa}$
315.7	0.108	19.6	1260
315.4	0.120	21.7	1580
315.4	0.134	24.2	1930
315.7	0.155	28.0	2500
315.4	0.188	33.7	3530
315.2	0.224	40.0	4790
315.2	0.254	45.0	6010
315.2	0.284	50.0	7330
315.2	0.304	53.3	8360
315.4	0.329	57.4	9550
315.4	0.359	62.2	10920
315.2	0.379	65.4	11890

TABLE 9.12

DATA FOR 1.25 EQUILATERAL-TRIANGLE BANK, WITH 3½T BYPASS AND FOUR SEALING-STRIPS

Pitch / diameter ratio, P_t/D = 1.25.

Number of tube rows in flow direction, N = 14.

Number of tube rows across the flow, n = 19.5.

Bank width = 0.1508m.

Bypass width = 0.0318m.

Ratio of bypass flow area to total flow area, F = 0.4571.

Number of sealing-strips, N_s = 4, placed at 2nd, 6th, 10th and 14th rows.

Atmospheric pressure, p_{atm}=1005.5 mbar.

$\frac{Temp}{K}$	$\frac{\dot{V}_T}{m^3/s}$	$\frac{u_{max}}{m/s}$	$\frac{\Delta p_{measured}}{Pa}$
316.7	0.097	17.6	1370
316.4	0.115	20.8	1850
316.4	0.135	24.4	2410
316.2	0.160	28.8	3280
316.2	0.178	31.9	3860
315.9	0.204	36.4	4910
315.7	0.231	41.0	5990
315.9	0.262	46.1	7460
315.7	0.291	50.9	8810
315.4	0.309	53.8	9880
315.4	0.336	58.2	11160
315.2	0.357	61.6	11860

TABLE 9.13

DATA FOR 1.25 IN-LINE SQUARE BANK, WITH ½S BYPASS AND ONE SEALING-STRIP

Bypass and crossflow streams are separated on exit by a splitter plate.

Pitch / diameter ratio, P_t/D = 1.25.

Number of tube rows in flow direction, N = 12.

Number of tube rows across the flow, n = 10.5.

Bank width = 0.1568m.

Bypass width = 0.0159m.

Ratio of bypass flow area to total flow area, F = 0.2308.

Number of sealing-strips, N_s = 1, placed at 1st row.

Atmospheric pressure, p_{atm}=1017.0 mbar.

$\frac{\text{Temp}}{\text{K}}$	$\frac{\dot{V}_T}{m^3/s}$	$\frac{u_{max}}{m/s}$	$\frac{\dot{m}_{Bexit}}{\dot{m}_T}$	$\frac{\Delta p_{measured}}{\text{Pa}}$
321.2	0.144	27.3	0.417	1350
320.2	0.191	36.1	0.419	2270
319.7	0.225	42.3	0.418	3170
318.9	0.251	47.0	0.406	3770
318.2	0.284	53.0	0.398	4550
318.7	0.314	58.3	0.408	5700
318.7	0.347	64.1	0.398	6760
318.2	0.377	69.2	0.392	7970
318.4	0.404	73.8	0.396	9210
318.2	0.425	77.3	0.388	10020
316.7	0.443	80.2	0.386	10920
316.2	0.453	81.8	0.386	11480

TABLE 9.14

DATA FOR 1.25 IN-LINE SQUARE BANK, WITH ½S BYPASS AND TWO SEALING-STRIPS

Pitch / diameter ratio, P_t/D = 1.25.

Number of tube rows in flow direction, N = 12.

Number of tube rows across the flow, n = 10.5.

Bank width = 0.1568m.

Bypass width = 0.0159m.

Ratio of bypass flow area to total flow area, F = 0.2308.

Number of sealing-strips, N_s = 2, placed at 1st and 12th rows.

Atmospheric pressure, p_{atm}=1017.0 mbar.

Temp / K	$\dot{V}_T$ / m^3/s	u_{max} / m/s	$\Delta p_{measured}$ / Pa
319.4	0.122	23.2	1150
318.4	0.158	29.9	1900
319.9	0.175	33.0	2270
317.9	0.197	37.1	2890
318.2	0.232	43.5	3790
317.2	0.265	49.4	4800
318.9	0.291	54.0	5650
318.9	0.313	57.8	6670
316.7	0.334	61.4	7720
316.7	0.367	67.0	9230
316.2	0.382	69.5	10020
315.4	0.390	70.8	10570

TABLE 9.15

DATA FOR 1.25 IN-LINE SQUARE BANK, WITH ⅛S BYPASS AND FIVE SEALING-STRIPS

Pitch / diameter ratio, P_t/D = 1.25.

Number of tube rows in flow direction, N = 12.

Number of tube rows across the flow, n = 10.5.

Bank width = 0.1568m.

Bypass width = 0.0159m.

Ratio of bypass flow area to total flow area, F = 0.2308.

Number of sealing-strips, N_s = 5, placed at 1st, 4th, 7th, 10th and 12th rows.

Atmospheric pressure, p_{atm}=1017.0 mbar.

Temp / K	$\dot{V}_T$ / m^3/s	u_{max} / m/s	$\Delta p_{measured}$ / Pa
320.7	0.097	18.4	1170
320.2	0.137	25.9	1840
319.9	0.156	29.4	2310
320.2	0.172	32.4	2320
319.9	0.200	37.5	3540
319.2	0.222	41.5	4340
318.7	0.249	46.3	5280
320.7	0.270	50.1	6030
320.7	0.287	53.0	6940
318.4	0.307	56.4	8070
318.2	0.337	61.5	9500
316.9	0.349	63.4	10230
315.9	0.356	64.6	10640

TABLE 9.16

DATA FOR 1.25 IN-LINE SQUARE BANK, WITH 1½S BYPASS AND ONE SEALING-STRIP

Bypass and crossflow streams are separated on exit by a splitter plate.

Pitch / diameter ratio, P_t/D = 1.25.

Number of tube rows in flow direction, N = 12.

Number of tube rows across the flow, n = 10.5.

Bank width = 0.1568m.

Bypass width = 0.0318m.

Ratio of bypass flow area to total flow area, F = 0.4444.

Number of sealing-strips, N_s = 1, placed at 1st row.

Atmospheric pressure, p_{atm}=1016.0 mbar.

$\frac{\text{Temp}}{\text{K}}$	$\frac{\dot{V}_T}{m^3/s}$	$\frac{u_{max}}{m/s}$	$\frac{\dot{m}_{Bexit}}{\dot{m}_T}$	$\frac{\Delta p_{measured}}{\text{Pa}}$
312.9	0.122	21.3	0.696	830
315.2	0.148	25.8	0.648	1130
314.4	0.192	33.3	0.656	1840
313.9	0.214	37.0	0.678	2350
311.9	0.240	41.4	0.671	2770
313.9	0.271	46.6	0.675	3570
313.7	0.281	48.3	0.673	3790
311.7	0.304	52.1	0.671	4360
312.9	0.315	53.9	0.673	4640
311.9	0.328	56.0	0.674	4980
311.4	0.339	57.8	0.673	5350
311.2	0.352	60.0	0.662	5530

TABLE 9.17

DATA FOR 1.25 IN-LINE SQUARE BANK, WITH 1½S BYPASS AND TWO SEALING-STRIPS

Pitch / diameter ratio, P_t/D = 1.25.

Number of tube rows in flow direction, N = 12.

Number of tube rows across the flow, n = 10.5.

Bank width = 0.1568m.

Bypass width = 0.0318m.

Ratio of bypass flow area to total flow area, F = 0.4444.

Number of sealing-strips, N_s = 2, placed at 1st and 12th rows.

Atmospheric pressure, p_{atm}=1016.0 mbar.

Temp / K	$\dot{V}_T$ / m^3/s	u_{max} / m/s	$\Delta p_{measured}$ / Pa
314.9	0.130	22.6	1390
314.4	0.182	31.4	2650
313.2	0.199	34.3	3240
314.4	0.233	39.9	4260
314.2	0.267	45.5	5530
314.9	0.286	48.6	6210
312.7	0.308	52.1	7190
314.2	0.324	54.5	8010
314.4	0.349	58.5	9070
312.9	0.365	60.9	9920
312.4	0.393	65.1	11350
312.2	0.408	67.4	12170

TABLE 9.18

DATA FOR 1.25 IN-LINE SQUARE BANK, WITH 1½S BYPASS AND FIVE SEALING-STRIPS

Pitch / diameter ratio, P_t/D = 1.25.

Number of tube rows in flow direction, N = 12.

Number of tube rows across the flow, n = 10.5.

Bank width = 0.1568m.

Bypass width = 0.0318m.

Ratio of bypass flow area to total flow area, F = 0.4444.

Number of sealing-strips, N_s = 5, placed at 1st, 4th, 7th, 10th and 12th rows.

Atmospheric pressure, p_{atm}=1016.0 mbar.

Temp / K	$\dot{V}_T$ / m^3/s	u_{max} / m/s	$\Delta p_{measured}$ / Pa
316.2	0.101	17.6	1370
316.2	0.136	23.5	2320
315.9	0.169	29.1	3390
315.2	0.190	32.6	4300
315.9	0.219	37.3	5440
314.7	0.247	41.8	6700
316.4	0.271	45.7	7730
316.4	0.288	48.3	8790
314.4	0.308	51.3	10210
314.7	0.334	55.3	11510
313.9	0.345	57.0	12120
313.4	0.352	58.0	12580

TABLE 9.19

AVERAGE VALUES OF N_c, THE EFFECTIVE NUMBER OF ROWS BEHAVING AS IF THEY EXPERIENCED "PURE CROSSFLOW" PER SEALING-STRIP

	Bypass Width	N_c
1.25 Equilateral-triangle array	1T	*
"	3T	4.40
"	5T	5.03
"	7T	5.13
1.25 In-line square array	1S	*
"	3S	3.28

* There is more scatter and a significant Reynolds number dependency in the values of N_c for these small bypasses.

However, the differences between the flow resistances of the bundle and the bypass are less with these bypasses so the effect on the overall pressure drop of bypassing flow and sealing-strips is less; for the 1T bypass the differences are negligible, see Fig. 9.1.

TABLE 10.1

BYPASS CLEARANCE FOR TEST SECTION WITH CYLINDRICAL BYPASS WALL

No. of tubes rows in flow direction, N, from inlet	Bypass clearance, D_B / mm			
	Bypass No. 1	Bypass No. 2	Bypass No. 3	Bypass No. 4
1	1.0	16.9	16.9	16.9
2	8.7	8.7	8.7	24.6
3	0.0	15.8	15.8	15.8
4	6.6	6.6	22.3	22.3
5	12.6	12.6	12.6	28.2
6	2.4	17.9	17.9	17.9
7	7.2	7.2	22.6	22.6
8	11.4	11.4	11.4	26.7
9	15.0	15.0	15.0	15.0
10	3.0	17.8	17.8	17.8
11	5.3	5.3	20.0	20.0
12	7.1	7.1	21.4	21.4
13	8.1	8.1	22.0	22.0
14	8.4	8.4	22.0	22.0

TABLE 10.2

DATA FOR 1.25 EQUILATERAL-TRIANGLE BANK WITH A CYLINDRICAL BYPASS WALL AND BYPASSING (1)

Bypass and crossflow undivided on exit from bank.

Pitch / diameter ratio, P_t/D = 1.25.

Inlet duct height = 182mm.

Exit duct height = 110mm.

Distance from upstream pressure tapping to tube bank inlet = 135mm.

Distance from downstream pressure tapping to tube bank exit = 200mm.

Bypass lane No. 1, see Figure 10.1, all tubes present.

Atmospheric pressure, p_{atm}=1018.5 mbar.

$\frac{\text{Temp}}{\text{K}}$	$\frac{\dot{V}_T}{\text{m}^3/\text{s}}$	$\frac{u_{max}}{\text{m/s}}$	$\frac{\Delta p_{measured}}{\text{Pa}}$
314.4	0.104	26.1	1660
314.2	0.140	35.2	2380
314.4	0.163	41.0	3030
314.9	0.200	50.2	4420
314.2	0.230	57.6	5220
313.9	0.251	62.7	6370
314.2	0.273	68.1	7260
313.7	0.301	74.8	8350
313.4	0.341	84.8	10440
313.2	0.373	92.1	11890
313.4	0.424	104.2	14570

TABLE 10.3

DATA FOR 1.25 EQUILATERAL-TRIANGLE BANK WITH A CYLINDRICAL BYPASS WALL AND BYPASSING (2)

Bypass and crossflow undivided on exit from bank.

Pitch / diameter ratio, P_t/D = 1.25.

Inlet duct height = 182mm.

Exit duct height = 110mm.

Distance from upstream pressure tapping to tube bank inlet = 135mm.

Distance from downstream pressure tapping to tube bank exit = 200mm.

Bypass lane No. 2, see Figure 10.1.

Atmospheric pressure, p_{atm}=1017.0 mbar.

Temp / K	$\dot{V}_T$ / m^3/s	u_{max} / m/s	$\Delta p_{measured}$ / Pa
316.7	0.131	33.1	1390
316.4	0.190	47.9	2550
316.2	0.235	59.0	3860
316.4	0.280	70.1	5150
315.2	0.317	79.1	6360
315.7	0.342	85.2	7350
316.2	0.372	92.5	8380
315.2	0.398	98.7	9340
315.4	0.436	109.3	11030
314.7	0.358	112.9	12160

TABLE 10.4

DATA FOR 1.25 EQUILATERAL-TRIANGLE BANK WITH A CYLINDRICAL BYPASS WALL AND BYPASSING (3)

Bypass and crossflow undivided on exit from bank.

Pitch / diameter ratio, P_t/D = 1.25.

Inlet duct height = 182mm.

Exit duct height = 110mm.

Distance from upstream pressure tapping to tube bank inlet = 135mm.

Distance from downstream pressure tapping to tube bank exit = 200mm.

Bypass lane No. 3, see Figure 10.1.

Atmospheric pressure, p_{atm}=1017.0 mbar.

Temp / K	$\dot{V}_T$ / m^3/s	u_{max} / m/s	$\Delta p_{measured}$ / Pa
318.2	0.179	45.3	1330
318.4	0.198	49.9	1750
318.2	0.235	59.2	2410
317.4	0.264	66.4	3030
317.9	0.316	79.3	4190
317.9	0.390	97.5	5840
317.7	0.448	111.6	7360
317.7	0.474	117.8	8390
317.4	0.530	131.2	10090
316.9	0.551	136.2	11060

TABLE 10.5

DATA FOR 1.25 EQUILATERAL-TRIANGLE BANK WITH A CYLINDRICAL BYPASS WALL AND BYPASSING (4)

Bypass and crossflow undivided on exit from bank.

Pitch / diameter ratio, P_t/D = 1.25.

Inlet duct height = 182mm.

Exit duct height = 110mm.

Distance from upstream pressure tapping to tube bank inlet = 135mm.

Distance from downstream pressure tapping to tube bank exit = 200mm.

Bypass lane No. 4, see Figure 10.1.

Atmospheric pressure, p_{atm}=1014.0 mbar.

Temp / K	$\dot{V}_T$ / m^3/s	u_{max} / m/s	$\Delta p_{measured}$ / Pa
318.9	0.210	53.0	1640
318.7	0.247	62.3	2250
318.4	0.278	70.0	2710
318.9	0.334	83.9	3710
318.7	0.392	98.2	4930
318.7	0.459	114.5	6560
318.4	0.493	122.8	7400
318.7	0.555	137.6	9460
319.2	0.582	144.0	10360

TABLE A.1

CORRELATION OF EXPERIMENTAL DATA (TRIANGULAR ARRAYS)

Bypass width	No. of sealing-strips, N_s	a_1	a_2	Average error,%	Maximum error, %
		(1.25 equilateral-triangle array)			
Ideal	0	6.269	-0.2797	1.5	-3.1
½T	0	2.959	-0.2134	2.4	6.1
½T	1	2.821	-0.2125	1.5	-2.7
½T	2	6.665	-0.2892	1.0	-1.7
½T	4	7.879	-0.3015	1.4	-3.2
1½T	0	0.431	-0.8380	2.8	7.3
1½T	1	1.444	-0.1686	0.9	-1.8
1½T	2	2.040	-0.1778	1.0	2.9
1½T	4	3.898	-0.2256	1.1	-2.7
2½T	0	0.270	-0.0812	3.1	10.6
2½T	1	2.087	-0.2086	1.8	3.3
2½T	2	11.980	-0.3399	2.2	4.5
2½T	4	25.499	-0.4046	0.9	2.3
3½T	0	0.161	-0.0596	2.4	5.3
3½T	1	1.367	-0.1711	1.2	-2.9
3½T	2	2.364	-0.1784	1.0	-2.5
3½T	4	8.595	-0.2865	1.1	3.7
		(1.375 equilateral-triangle array)			
ideal	0	10.045	-0.3420	3.1	9.6
½	0	2.333	-0.2120	0.7	-1.3
1½	0	1.201	-0.1790	1.5	4.5
2½	0	0.667	-0.1686	2.1	6.0
3½	0	0.609	-0.1661	2.4	4.1

TABLE A.2

CORRELATION OF EXPERIMENTAL DATA (IN-LINE ARRAYS)

Bypass width	No. of sealing-strips, N_s	a_1	a_2	Average error,%	Maximum error, %
		(1.25 in-line square array)			
Ideal	0	2.620	-0.1741	0.9	-2.8
½S	0	0.609	-0.0836	2.3	-5.2
½S	1	0.789	-0.1087	1.7	5.1
½S	2	0.696	-0.0806	2.1	4.6
½S	5	3.566	-0.2153	4.4	-11.0
1½S	0	9.428	-0.4367	2.6	3.7
1½S	1	1.200	-0.1554	1.7	-2.9
1½S	2	0.808	-0.0708	0.6	-2.0
1½S	5	3.553	-0.1789	1.1	-2.7
		(1.375 in-line square array)			
Ideal	0	1.107	-0.1067	1.4	-2.7
½	0	0.999	-0.1405	2.1	4.9
1½	0	0.527	-0.1385	1.9	-4.8

TABLE E.1 ANALYSIS OF THE RELATIONSHIP BETWEEN THE RATIO OF BYPASS WIDTH TO TRANSVERSE BANK WIDTH AND THE PRESSURE DROP COEFFICIENT

Bypass Width	Pressure Drop Coefficient $\xi_{Pbypass}/\xi_{Pideal}$	Bypass Width, n, for which $(\xi_{Pbypass}/\xi_{Pideal} = 1)$
(1.25 equilateral-triangle array)		
* ½T	1	0
1½T	0.0355n	28.2
2½T	0.0205n	48.8
3½T	0.0140n	71.7
(1.25 in-line square array)		
½S	0.0385n	26.0
1½S	0.0133n	75.0

* There is little difference between the ½T bypass geometry and the ideal bank.

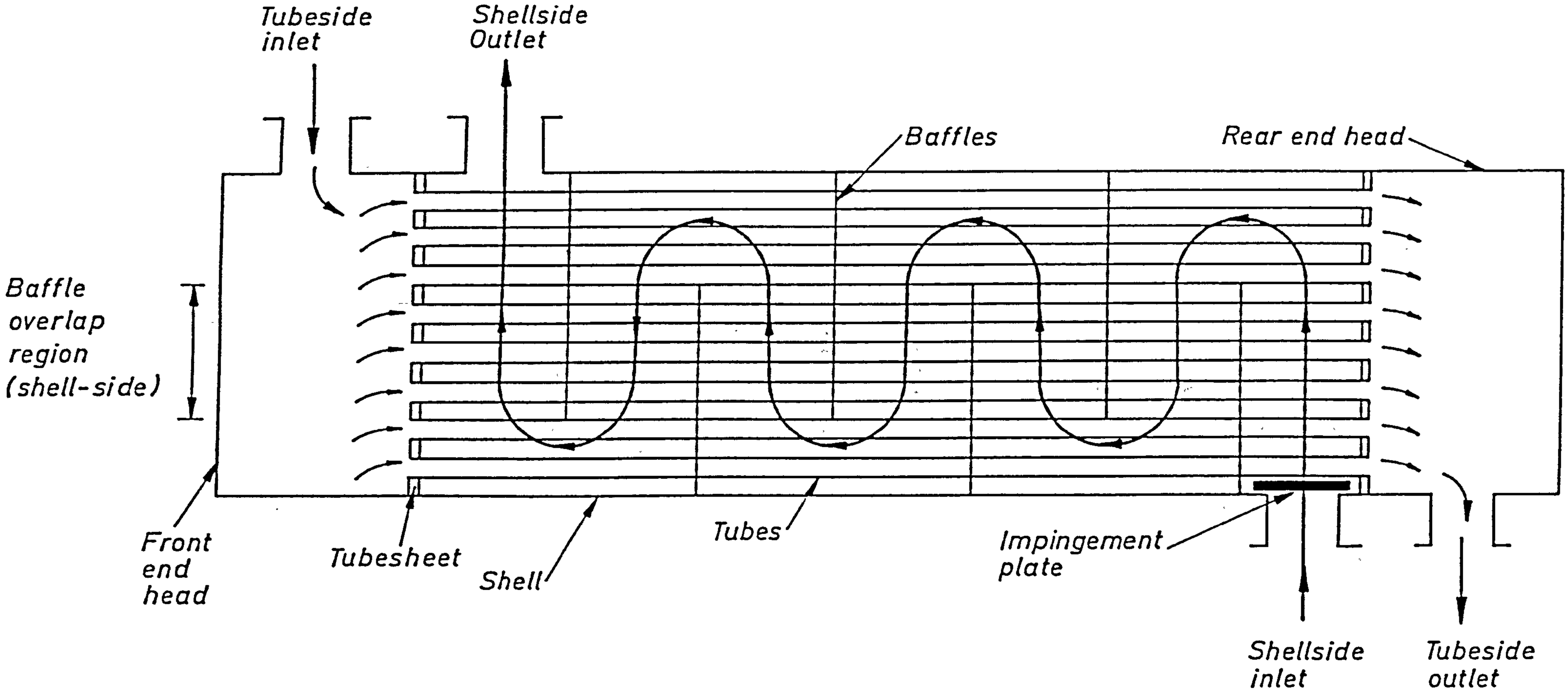

Figure 1.1 A typical shell-and-tube heat exchanger, with an E-type shell and one pass on both the shell-side and the tube-side.

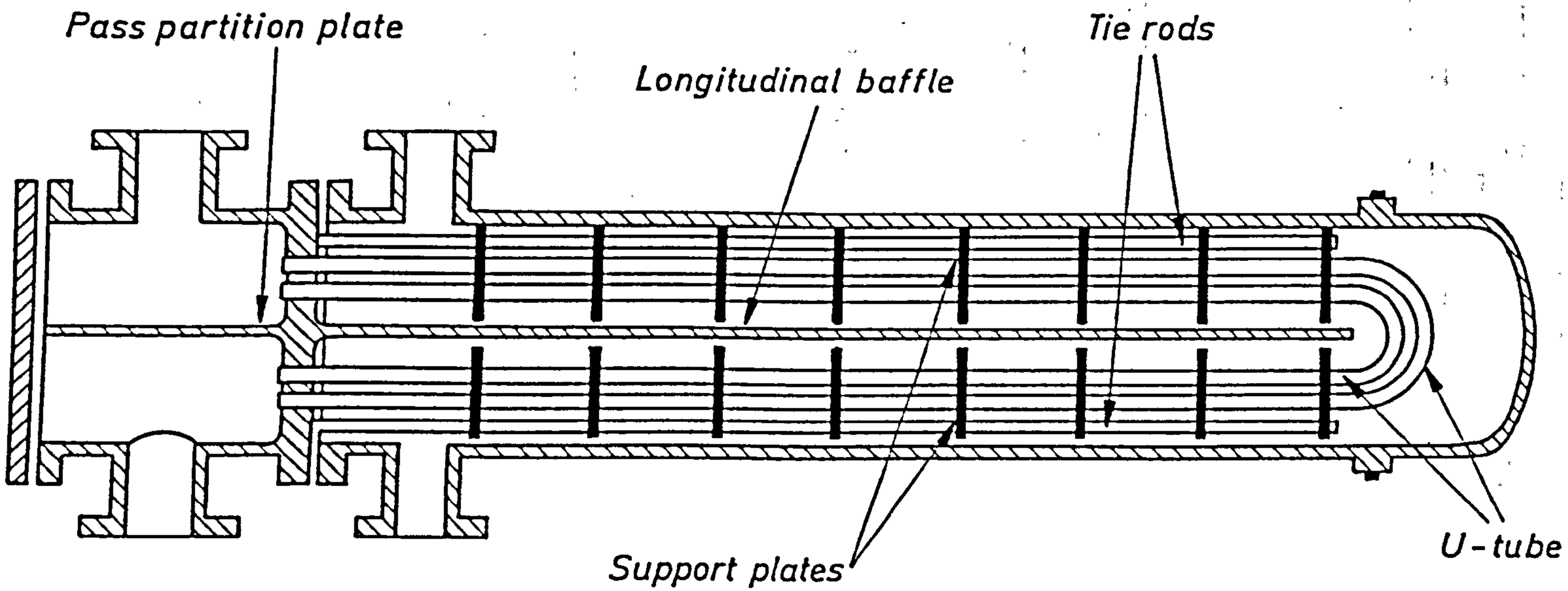

Figure 1.2 A shell-and-tube heat exchanger with a U-tube bundle.

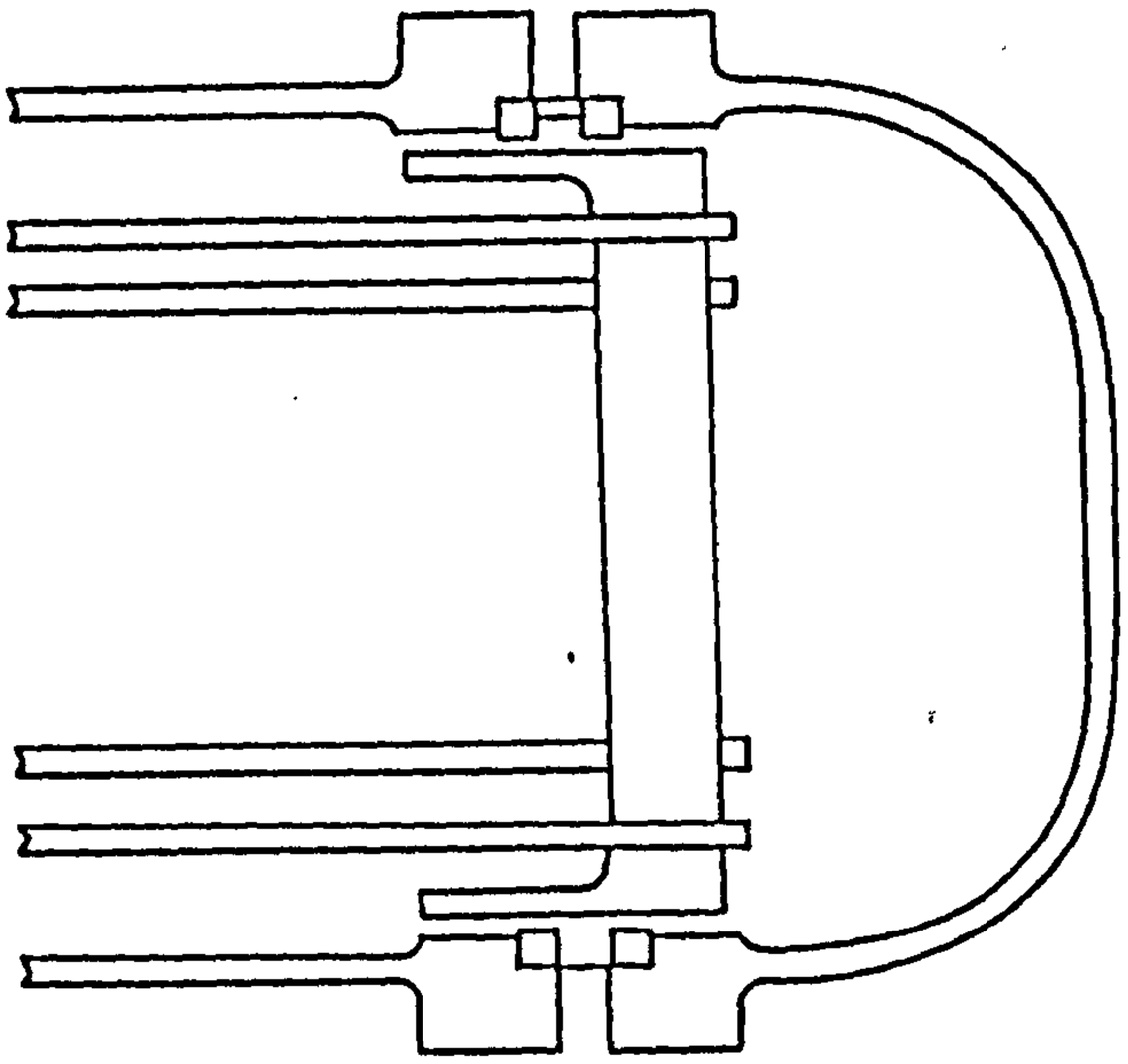

(a) Packed floating tubesheet

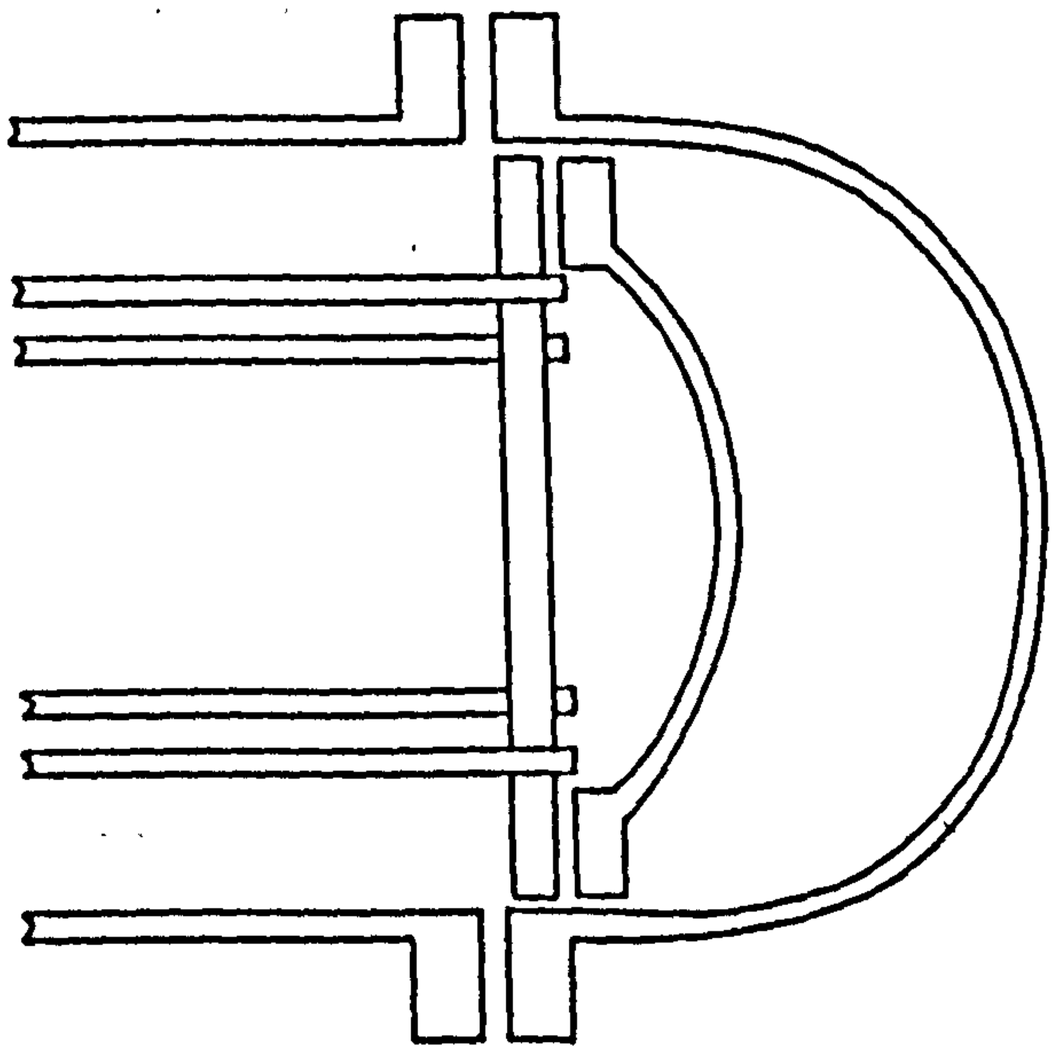

(b) Pull-through floating head

Figure 1.3 Floating head type closures.

Equilateral triangle (or 30°)

$P_x = 0.886\ P_t$

$P_y = P_t$

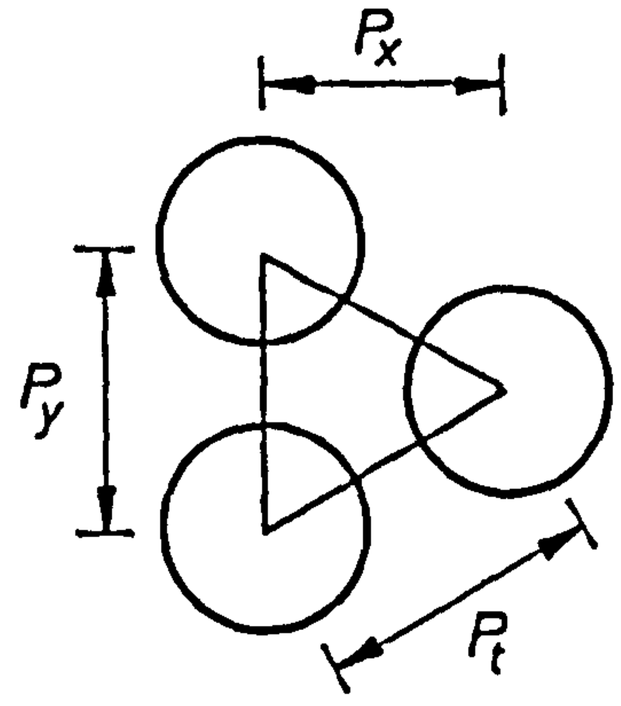

Rotated equilateral triangle (or 60°)

$P_x = 0.5\ P_t$

$P_y = 1.732\ P_t$

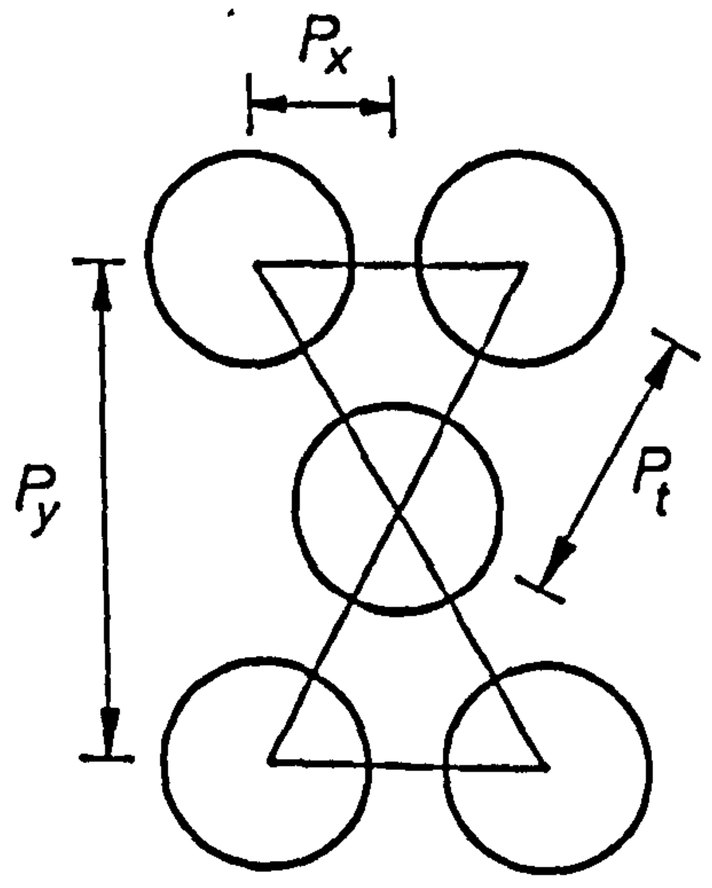

In-line square (or 90°)

$P_x = P_t$

$P_y = P_t$

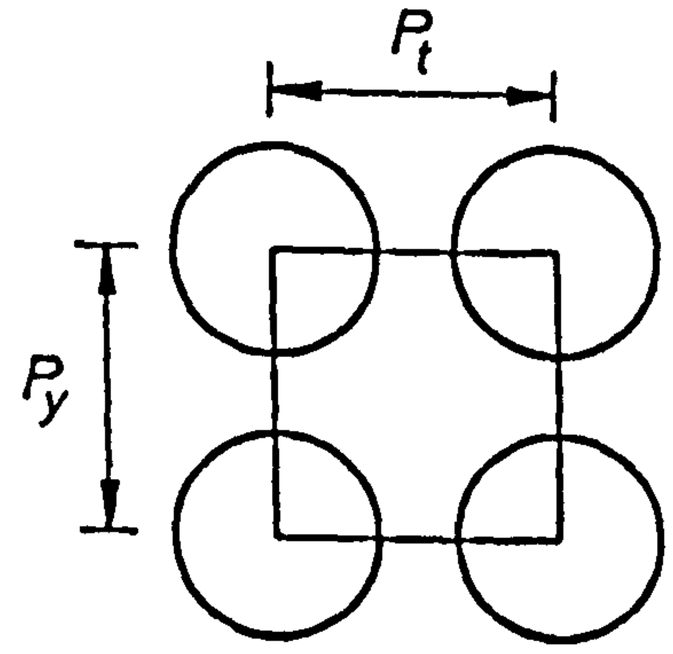

Rotated square (or 45°)

$P_y = \sqrt{2}\ P_t$

$P_x = \frac{\sqrt{2}}{2}\ P_t$

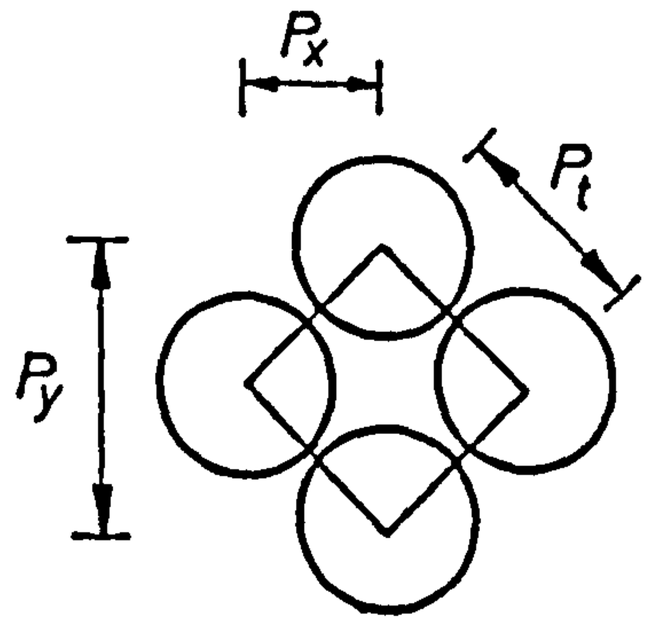

Figure 1.4 Tube array layouts, showing definition of tube pitches.

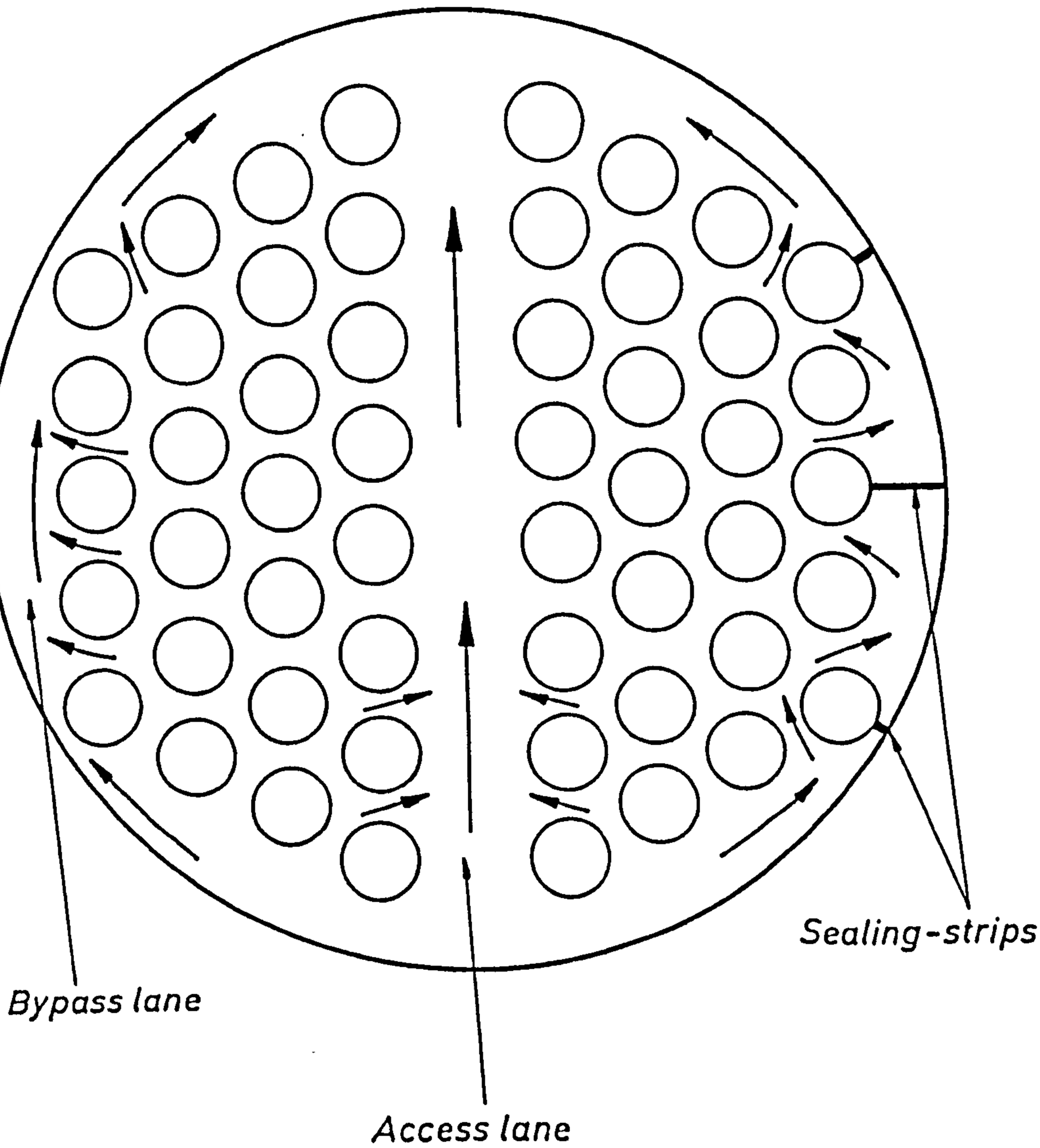

Figure 1.5 Bypass of the tube bundle, due to shell-tube bundle clearance and access lanes, and the use of sealing strips.

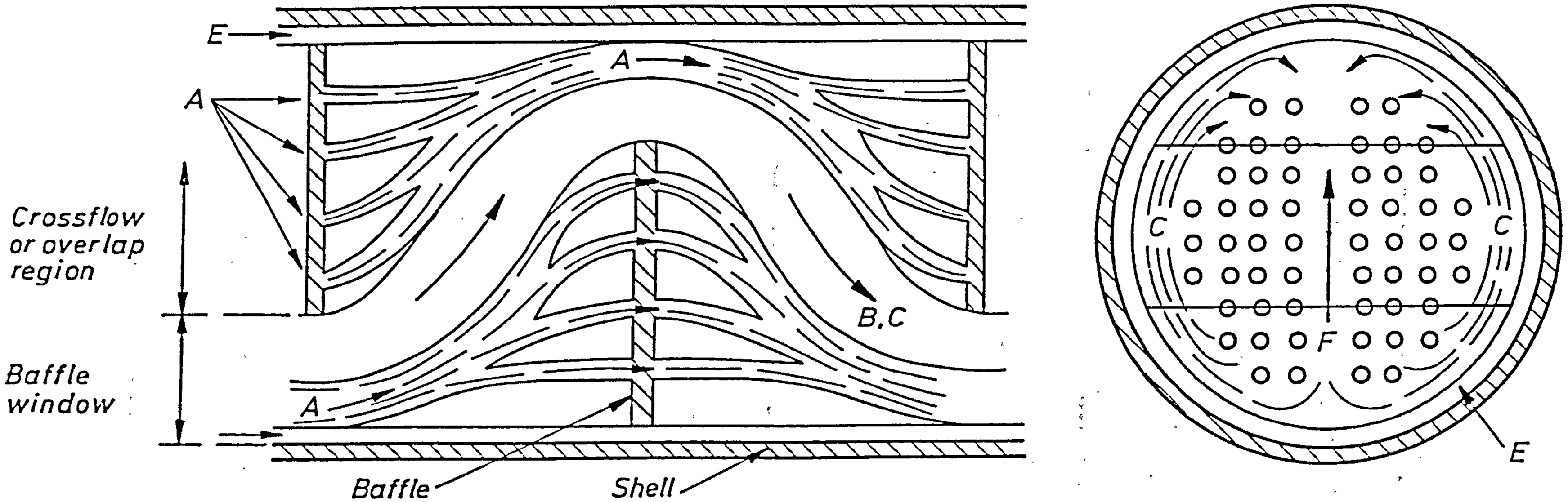

Flowstreams

A = Tube-baffle leakage
B = Crossflow
C = Crossflow bypass
E = Shell-baffle leakage
F = Tube pass partition bypass, added by Palen and Taborek (1969)

Figure 1.6 Tinker's (1968) flowstream model.

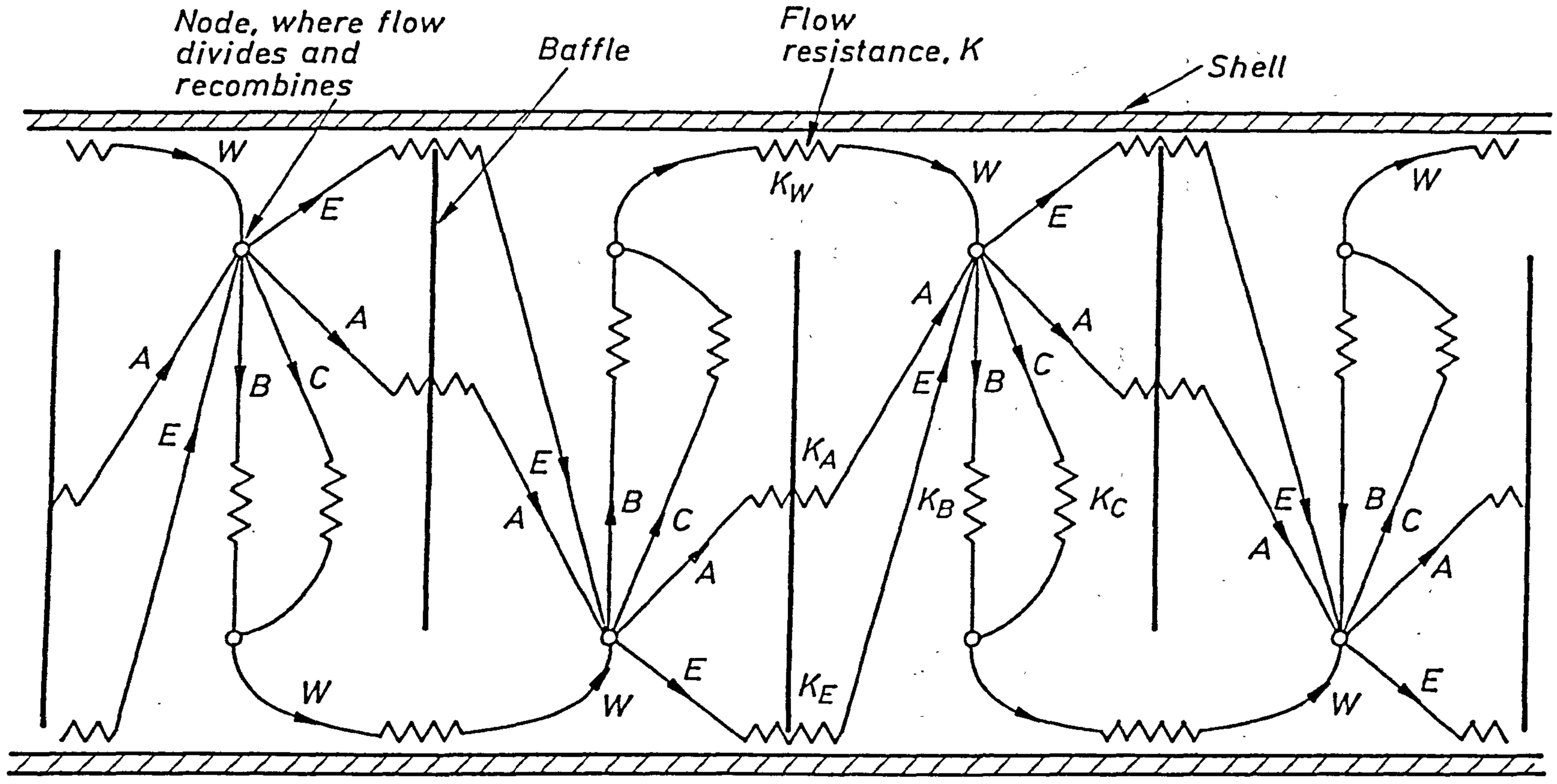

Flowstreams

A = Tube - baffle leakage, B = Crossflow, C = Crossflow bypass,
E = Shell - baffle leakage, W = Window flow

Figure 1.7 A network model of shell-side flow, from Palen and Taborek (1969).

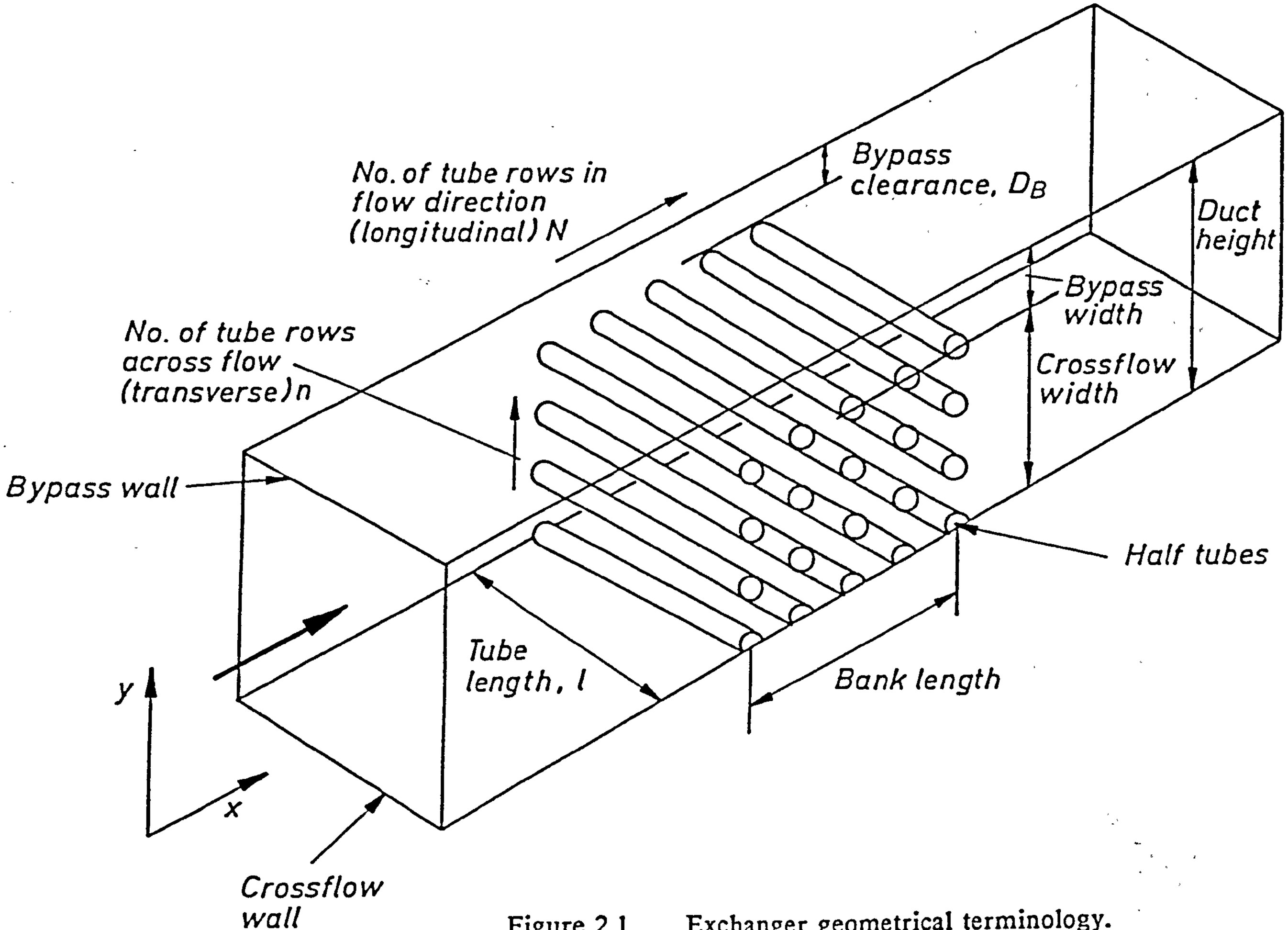

Figure 2.1 Exchanger geometrical terminology.

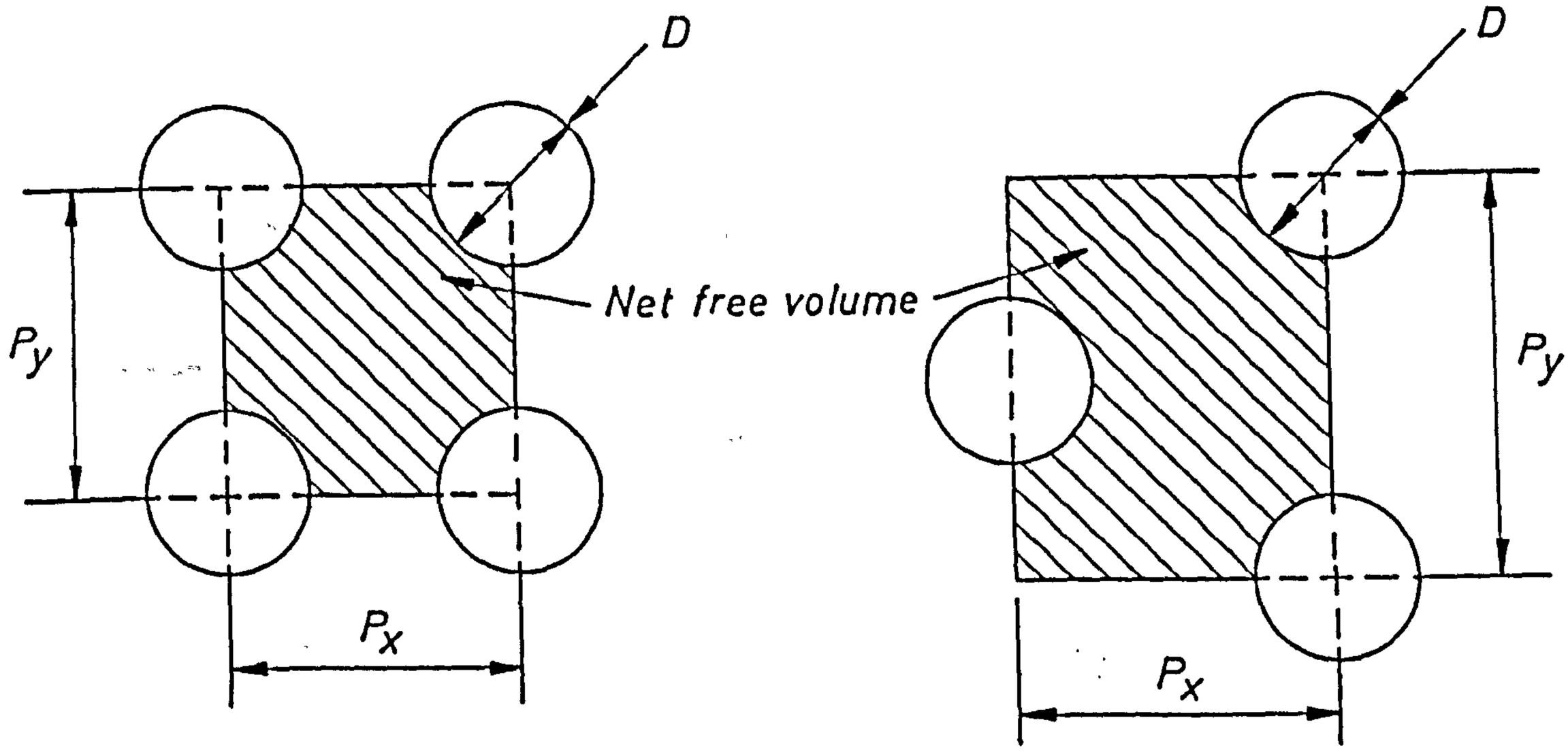

$$\text{EQUIVALENT VOLUMETRIC DIAMETER, } D_v = \frac{P_y P_x - \pi D^2}{\pi D}$$

Figure 2.2 Equivalent volumetric diameter, D_v.

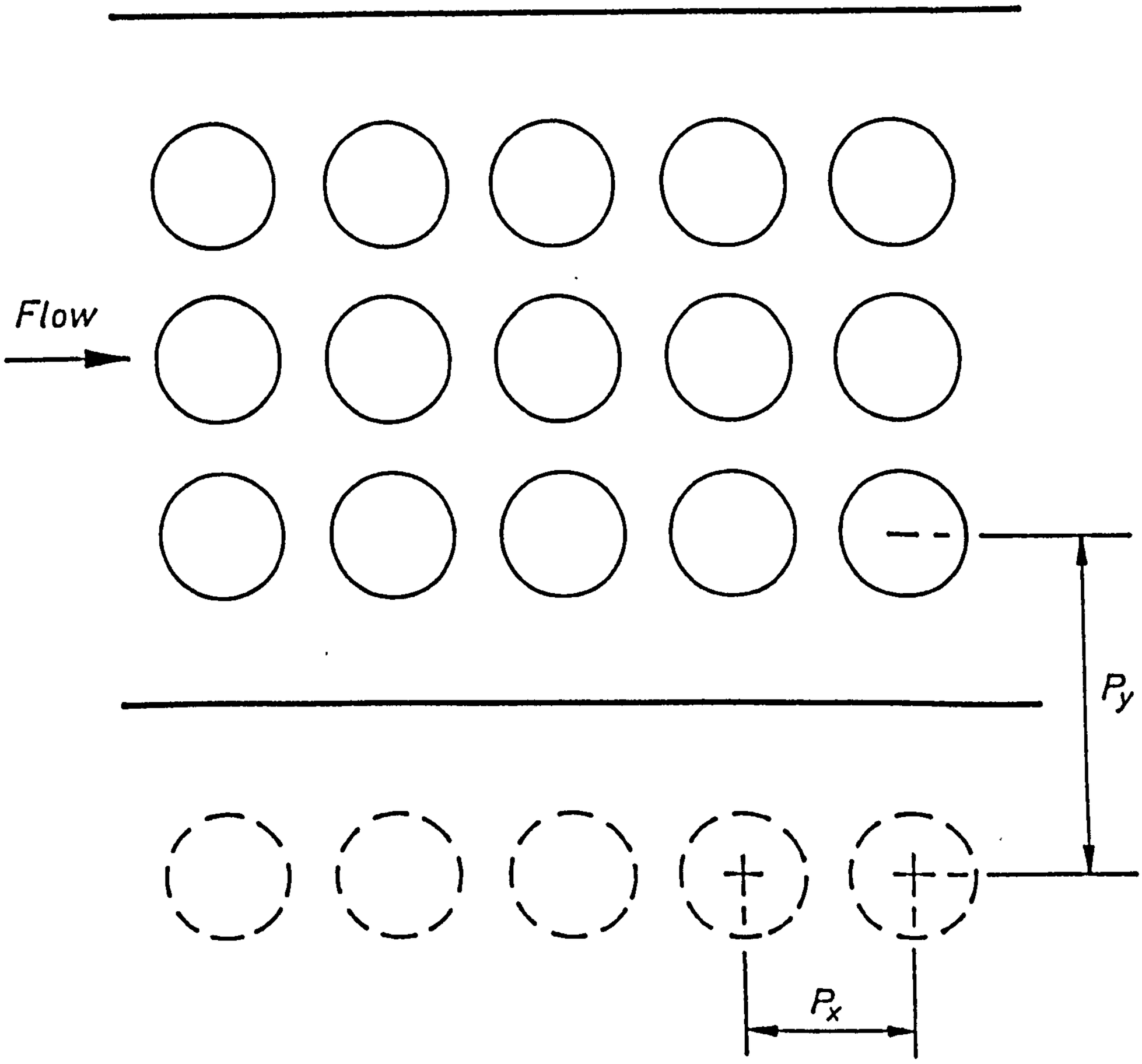

Bypass lane has pressure drop coefficient equal to ideal tube bank having :-

Longitudinal pitch = P_x

Transverse pitch = P_y

Figure 2.3 ESDU method of estimating bypass pressure drop coefficients.

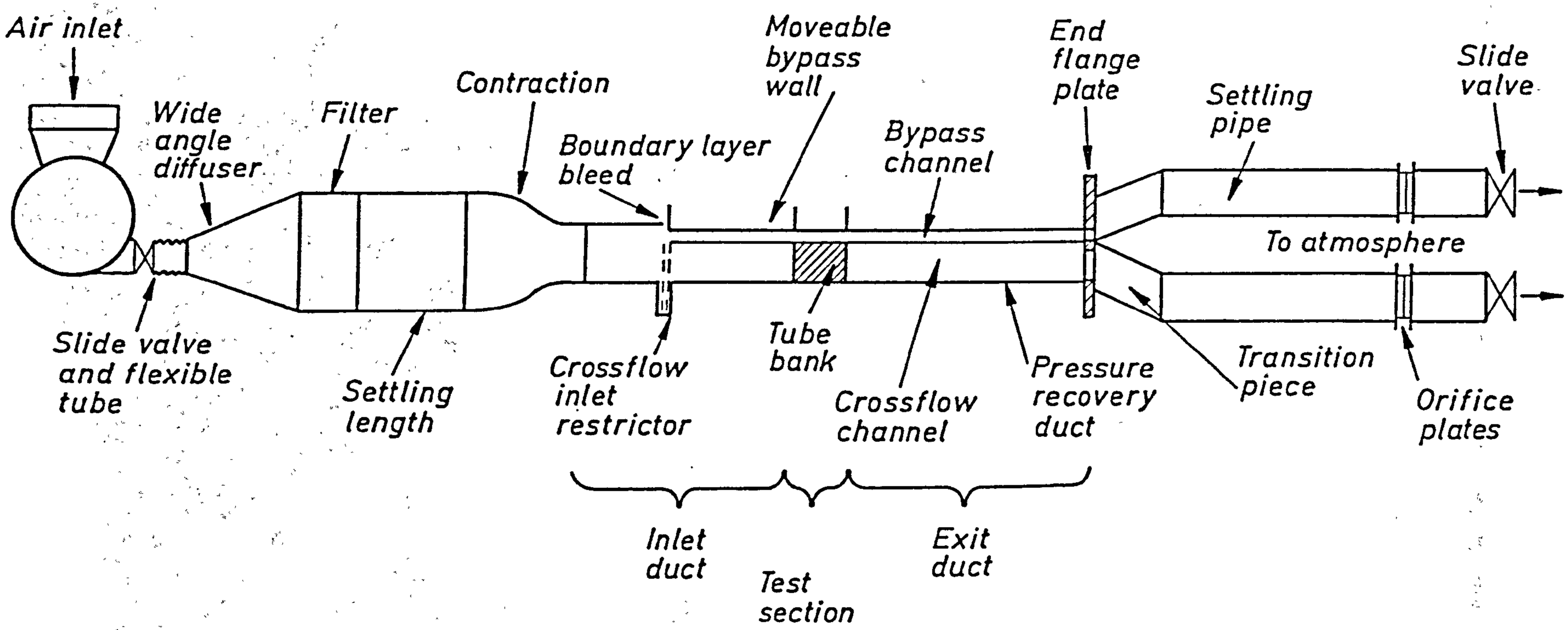

Figure 3.1 General layout of the experimental rig, with inlet and exit splitter plates and crossflow restrictor present.

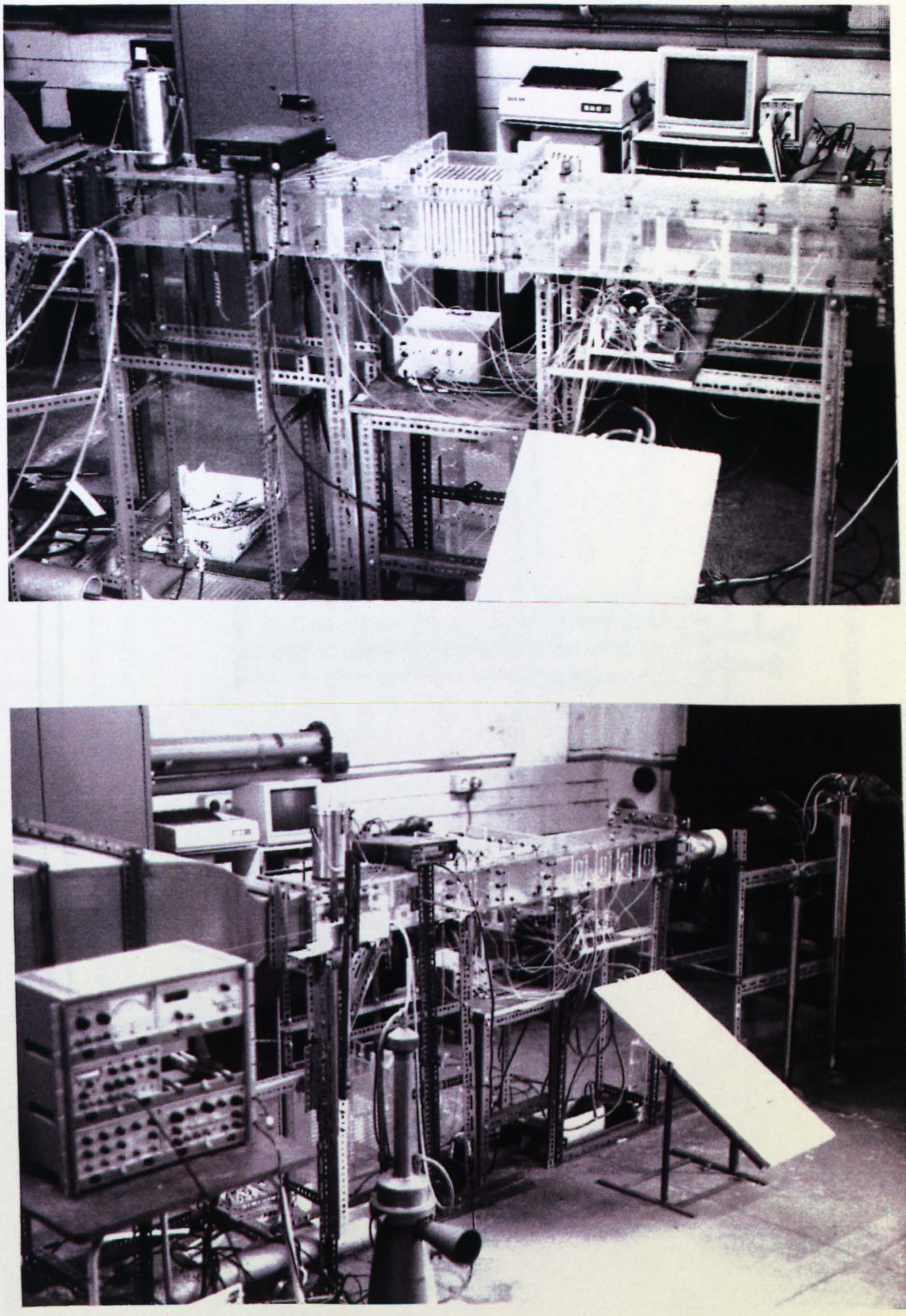

Figure 3.2 Experimental rig.

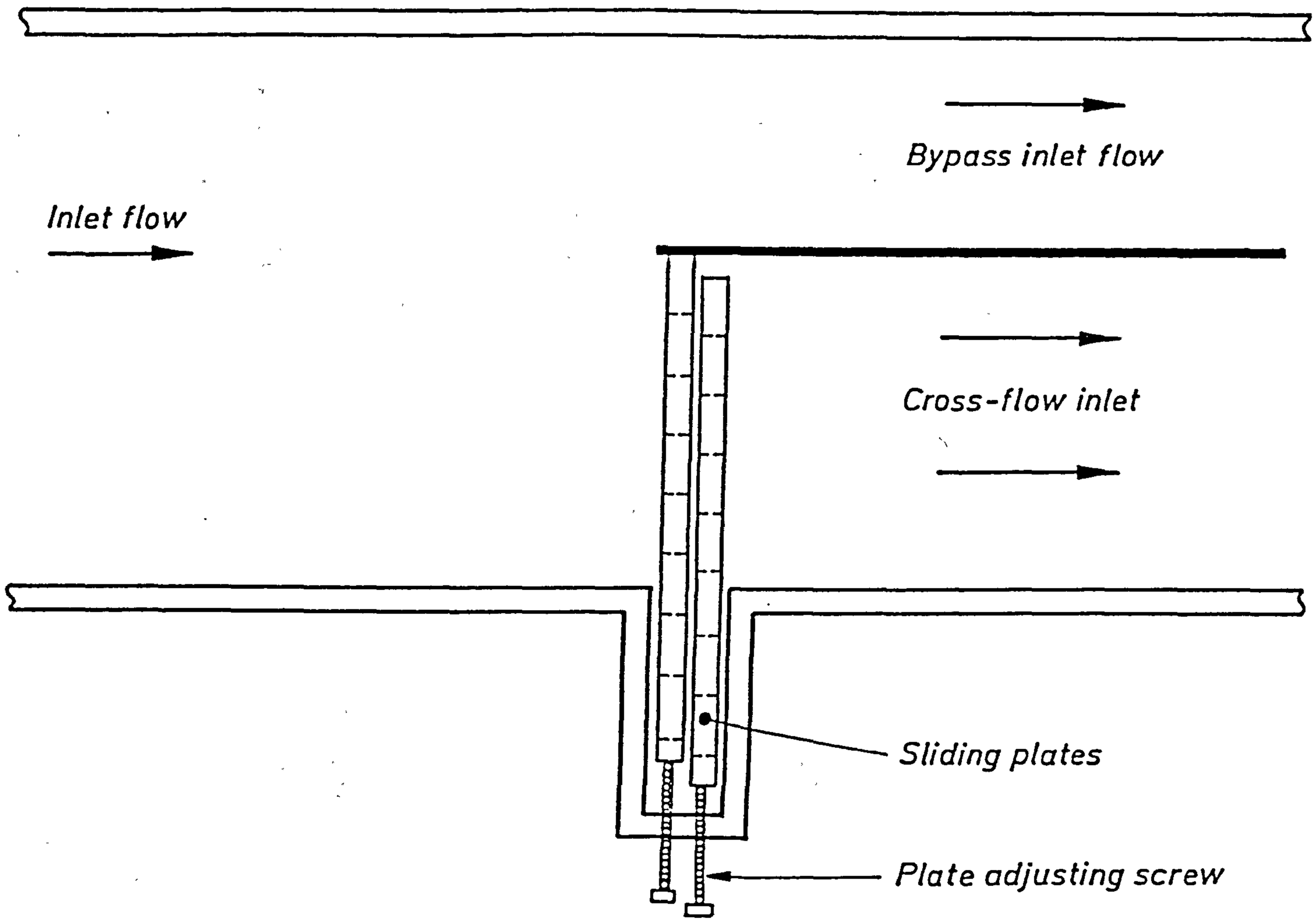

Figure 3.3 Crossflow restrictor.

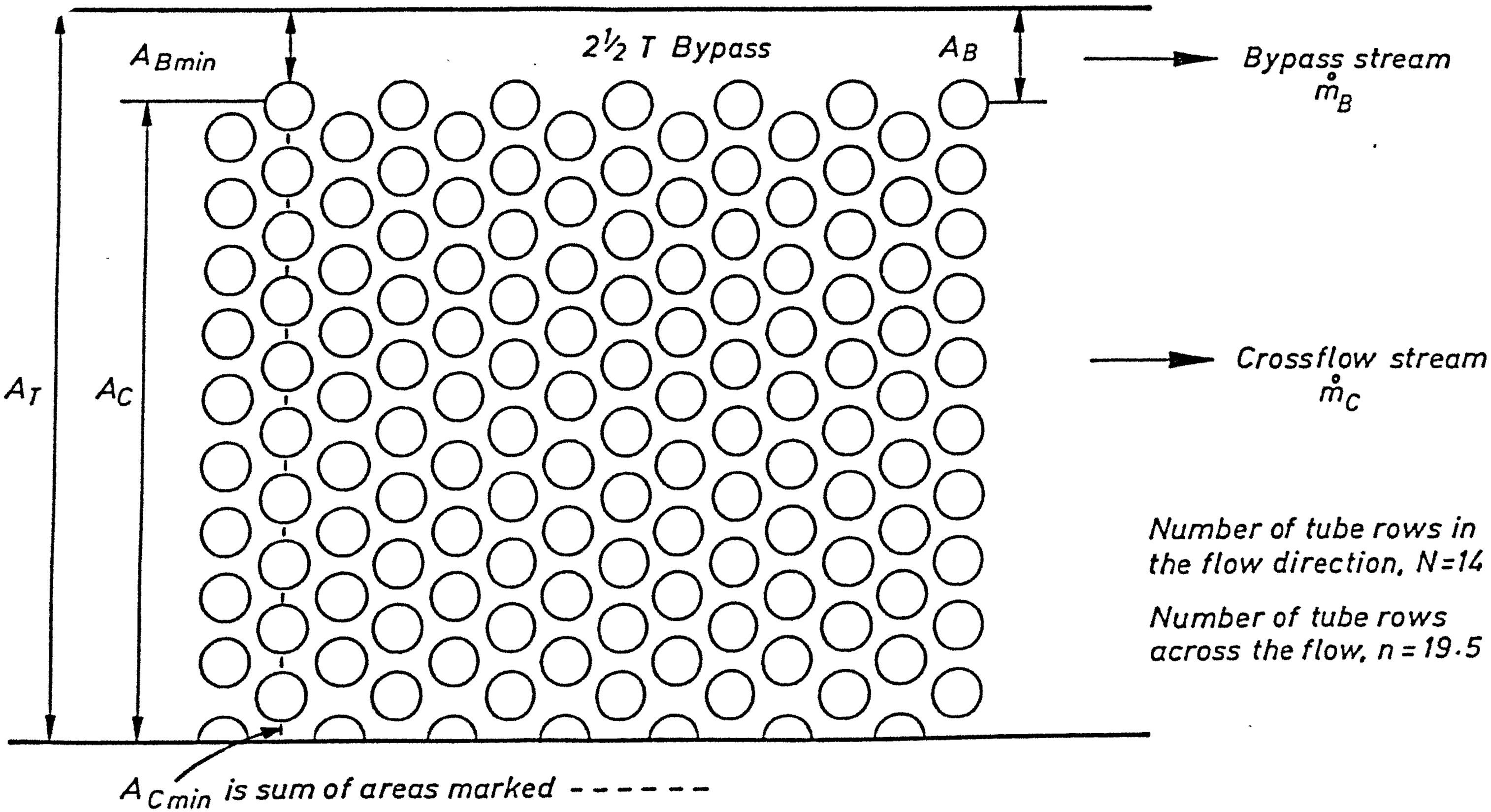

Figure 3.4 Test section.

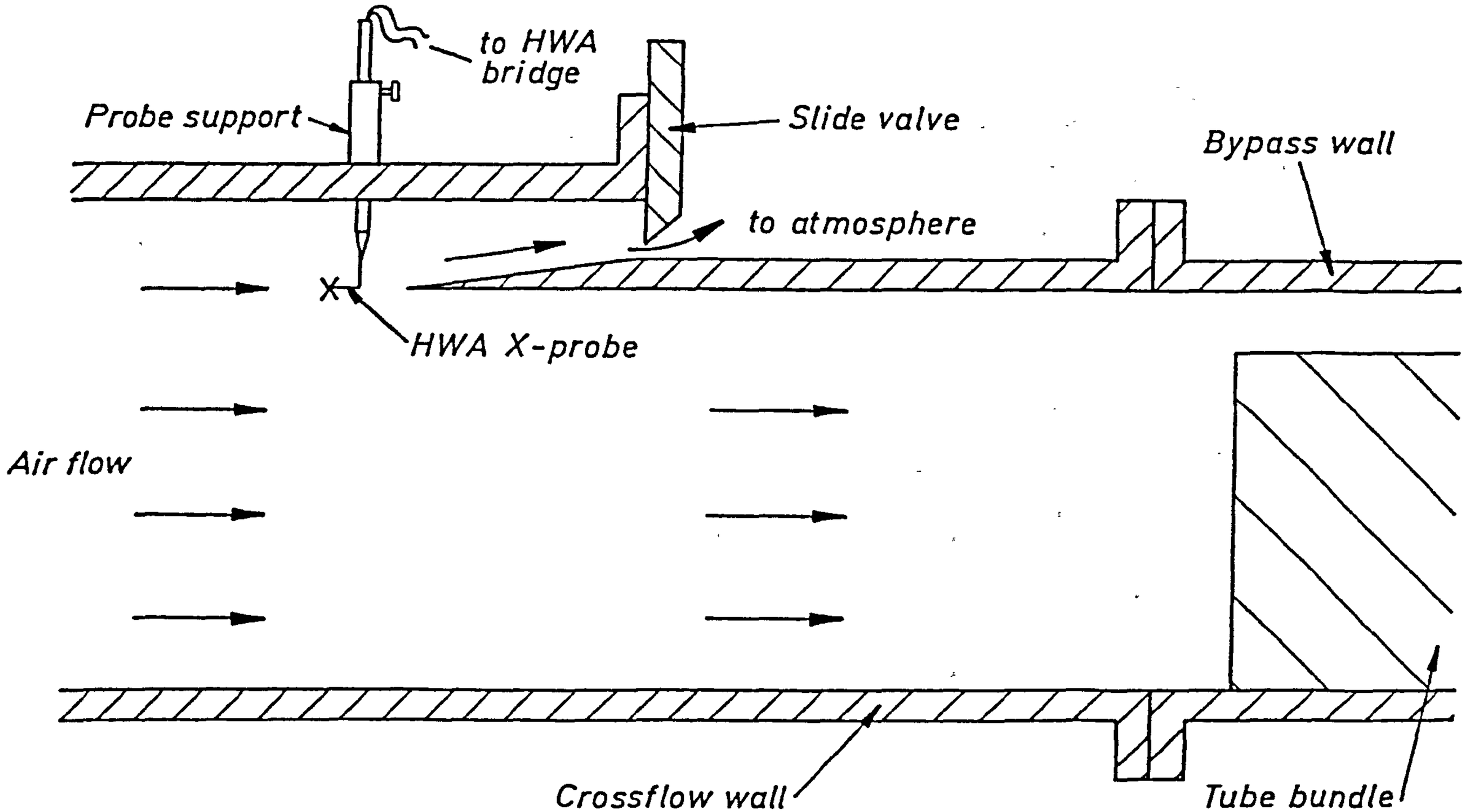

Figure 3.5 Boundary layer bleed.

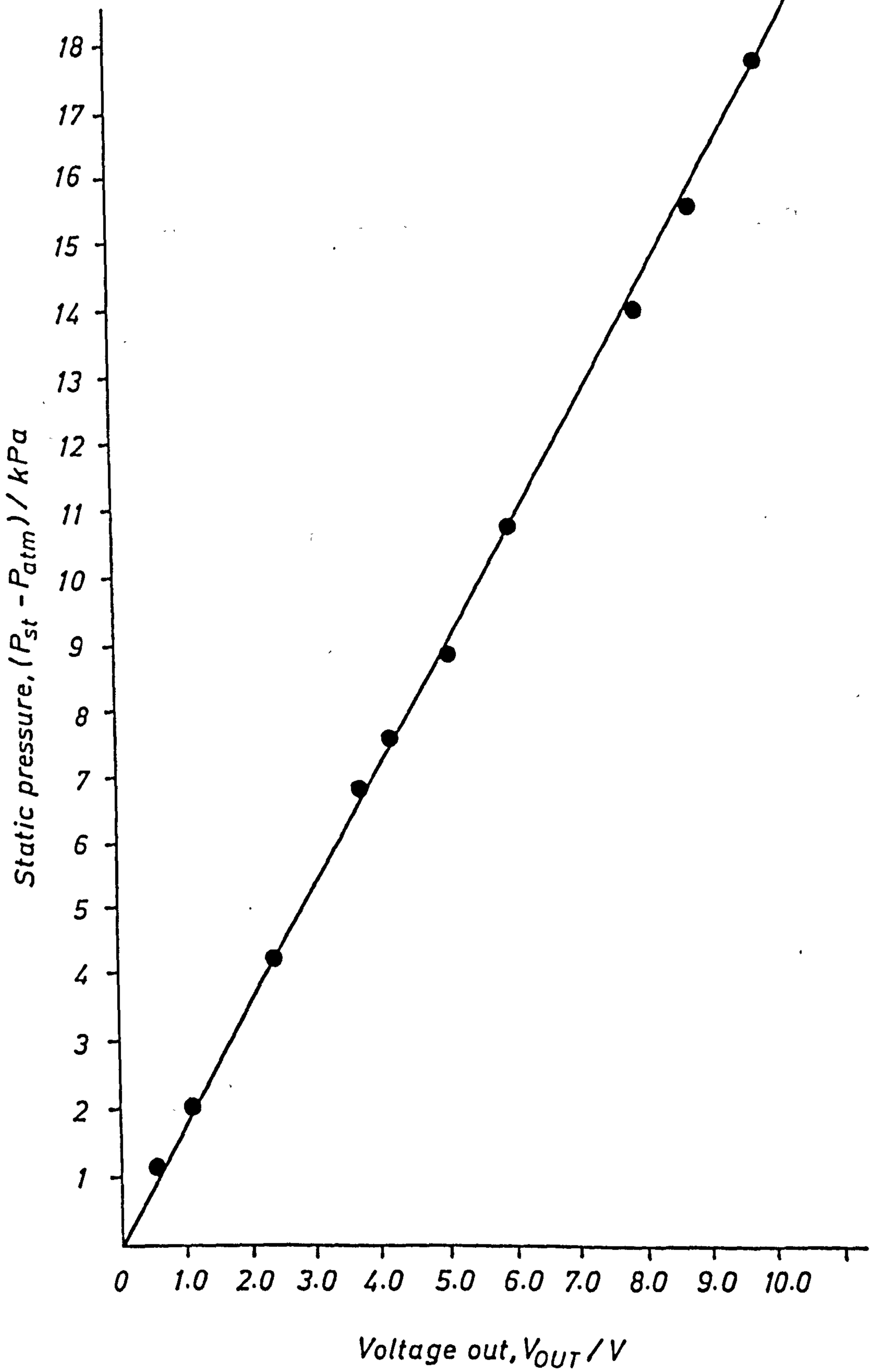

Figure 3.7 Pressure transducer calibration.

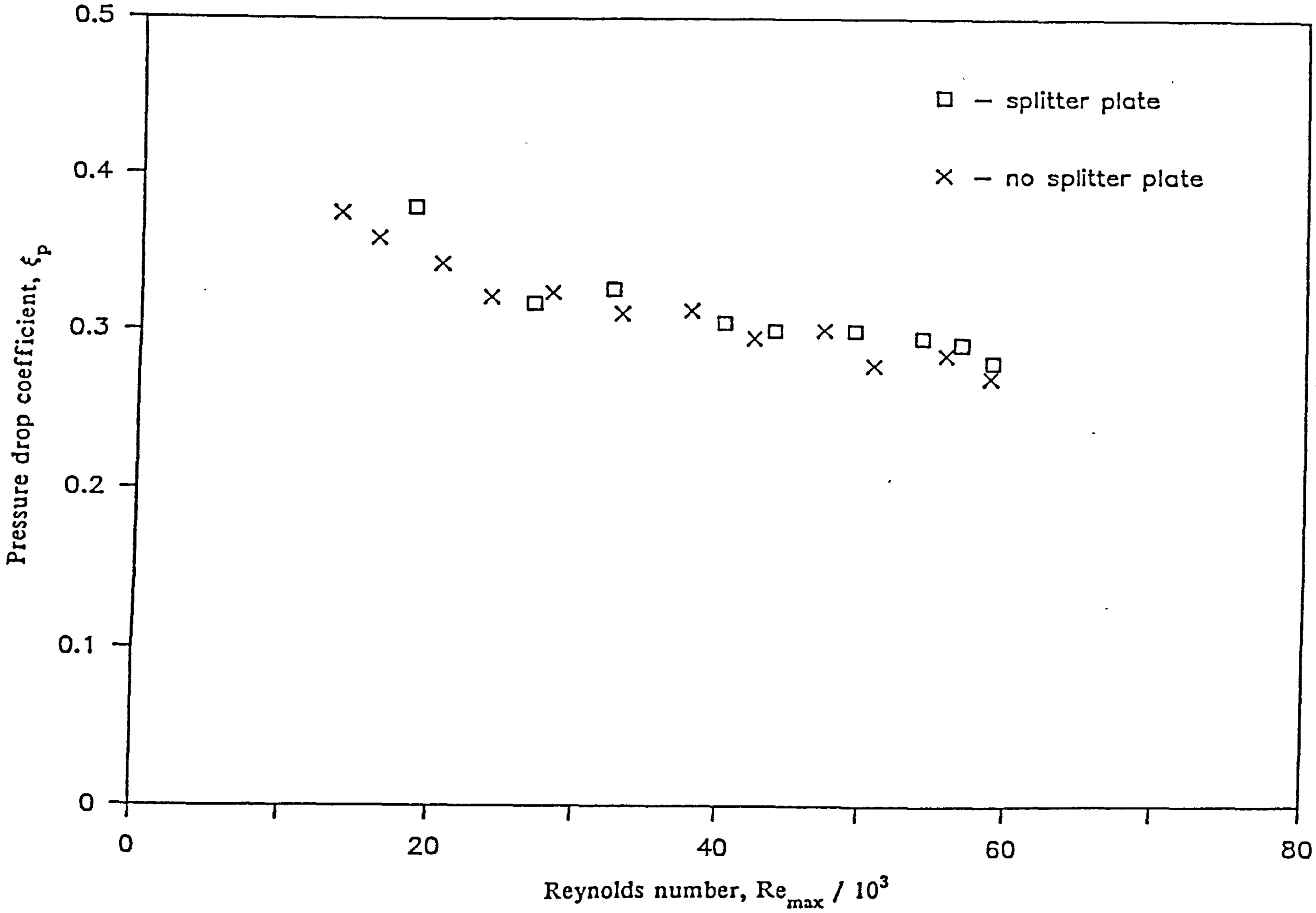

Figure 5.1 Pressure drop coefficients for 1.25 equilateral-triangle bank having a ½T bypass with and without the exit flow divided by a splitter plate.

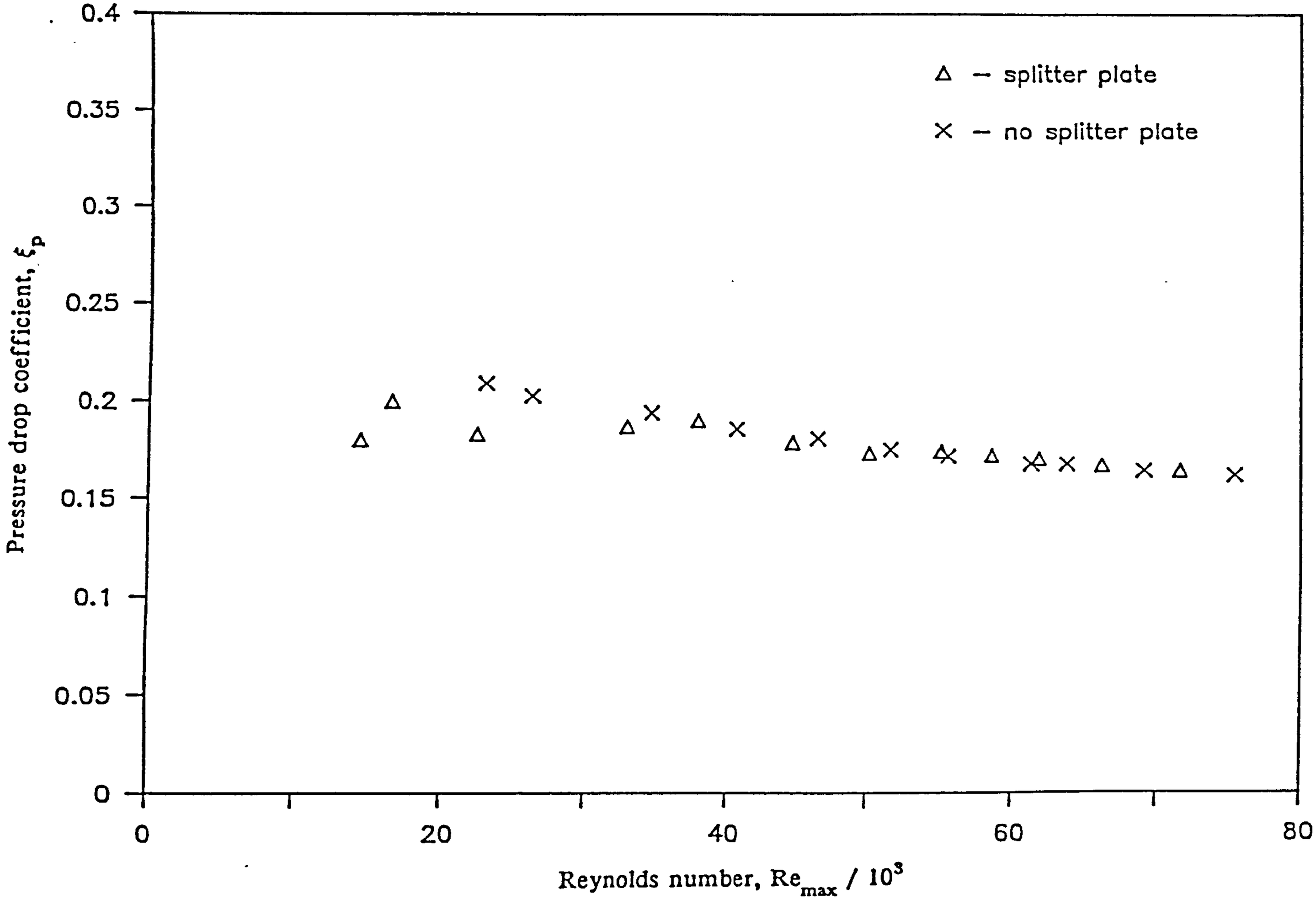

Figure 5.2 Pressure drop coefficients for 1.25 equilateral-triangle bank having a 1½T bypass with and without the exit flow divided by a splitter plate.

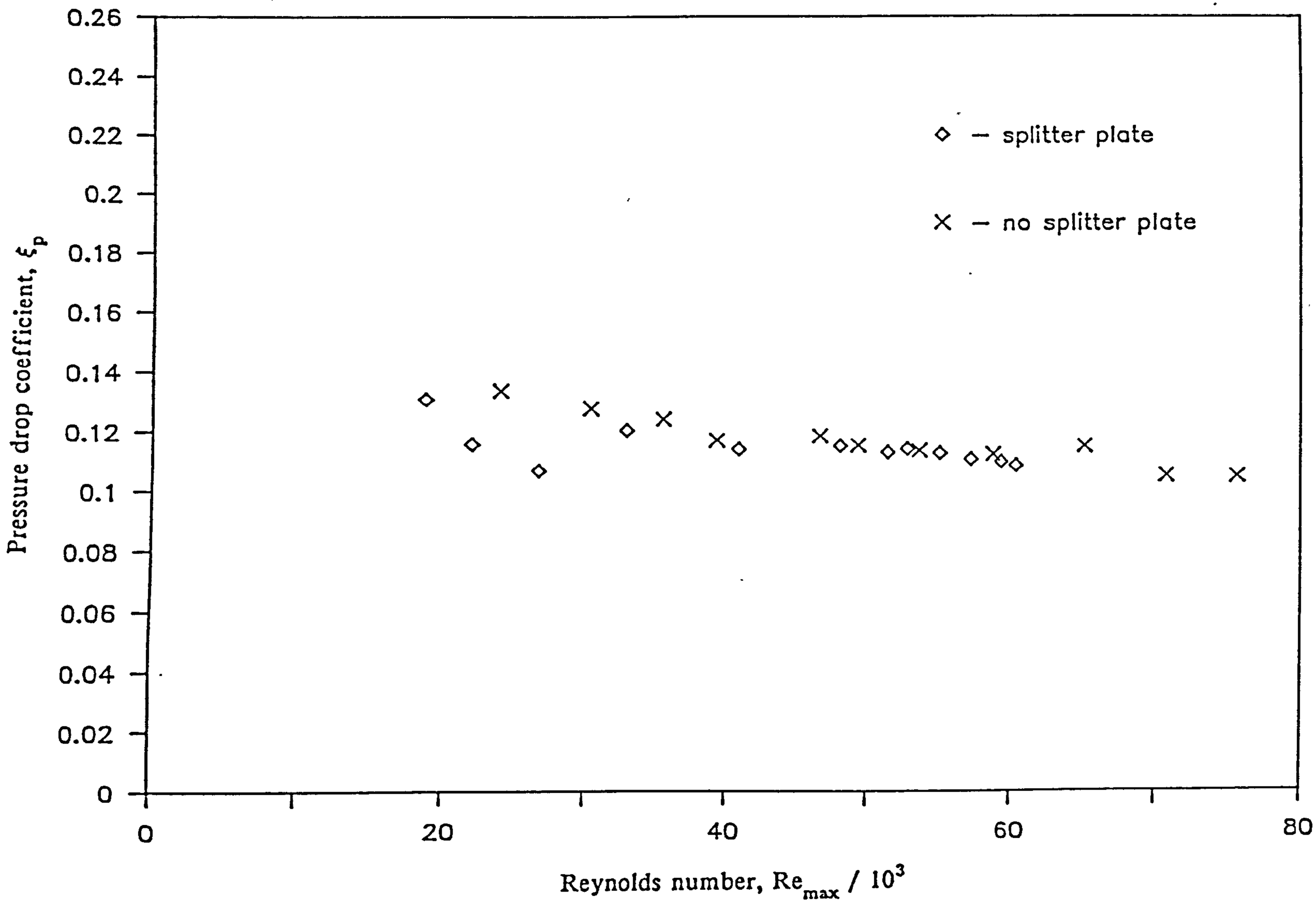

Figure 5.3 Pressure drop coefficients for 1.25 equilateral-triangle bank having a 2½T bypass with and without the exit flow divided by a splitter plate.

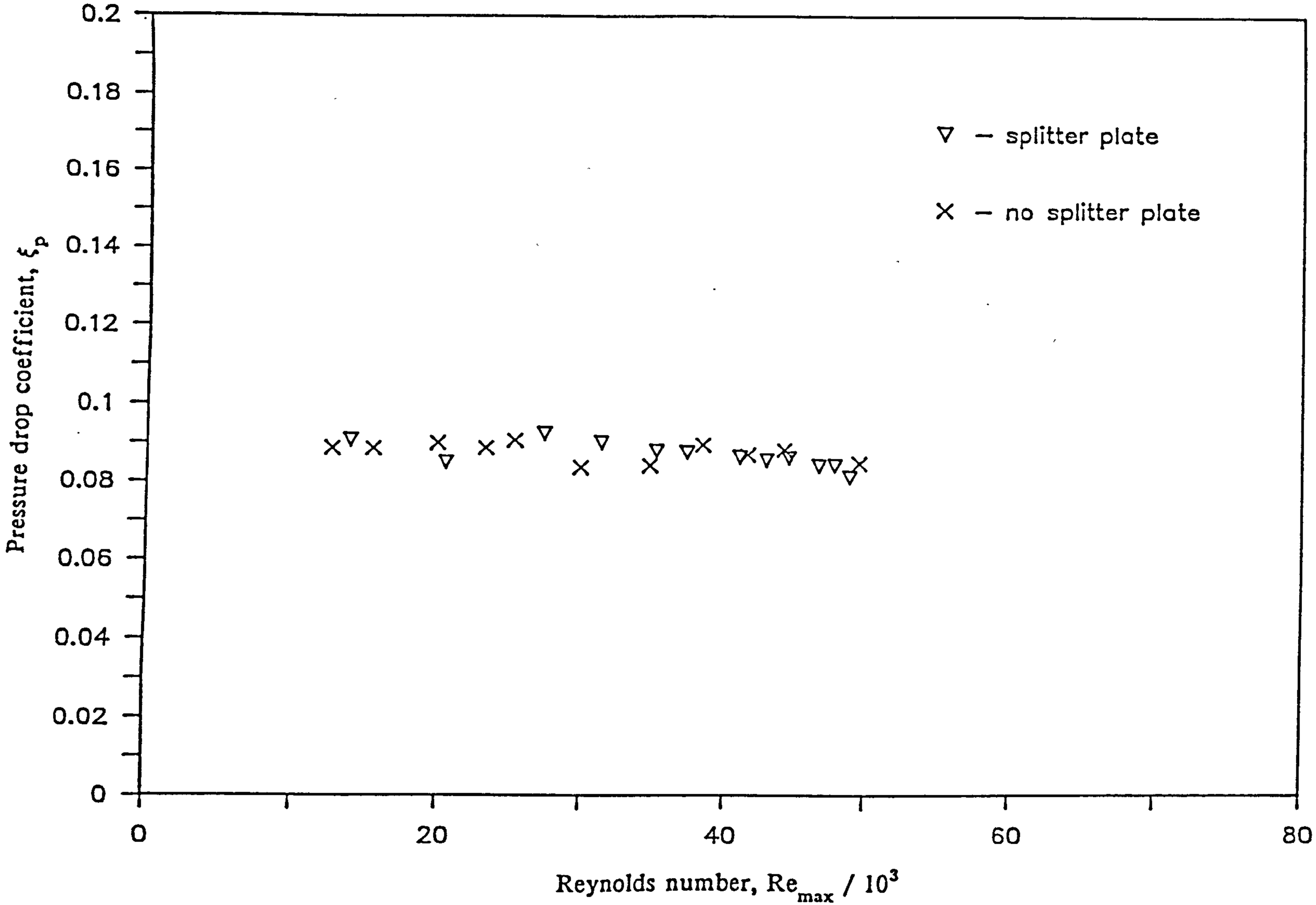

Figure 5.4 Pressure drop coefficients for 1.25 equilateral-triangle bank having a 3½T bypass with and without the exit flow divided by a splitter plate.

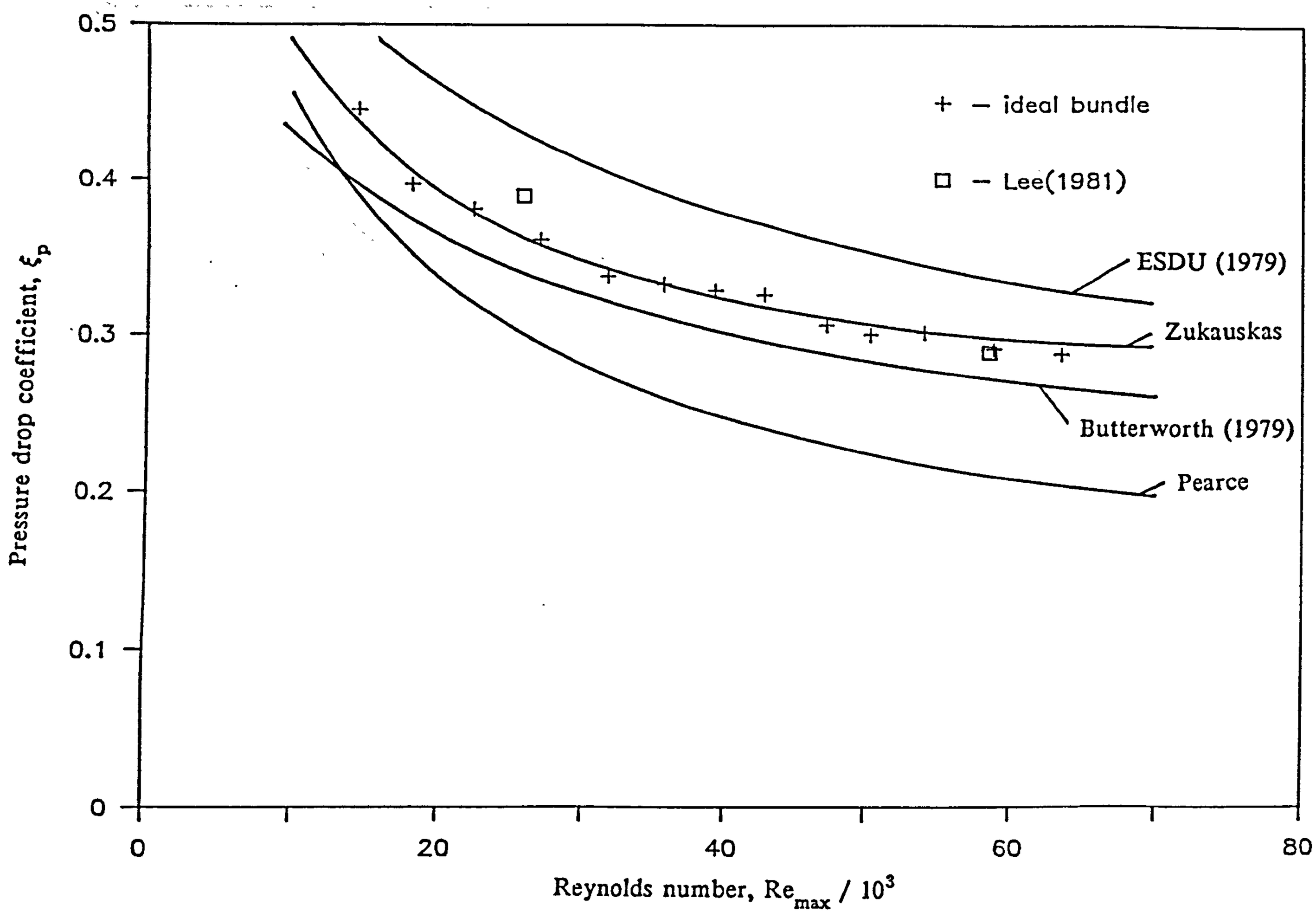

Figure 6.1 Pressure drop coefficient for an ideal equilateral-triangle bank with a pitch-diameter ratio of 1.25.

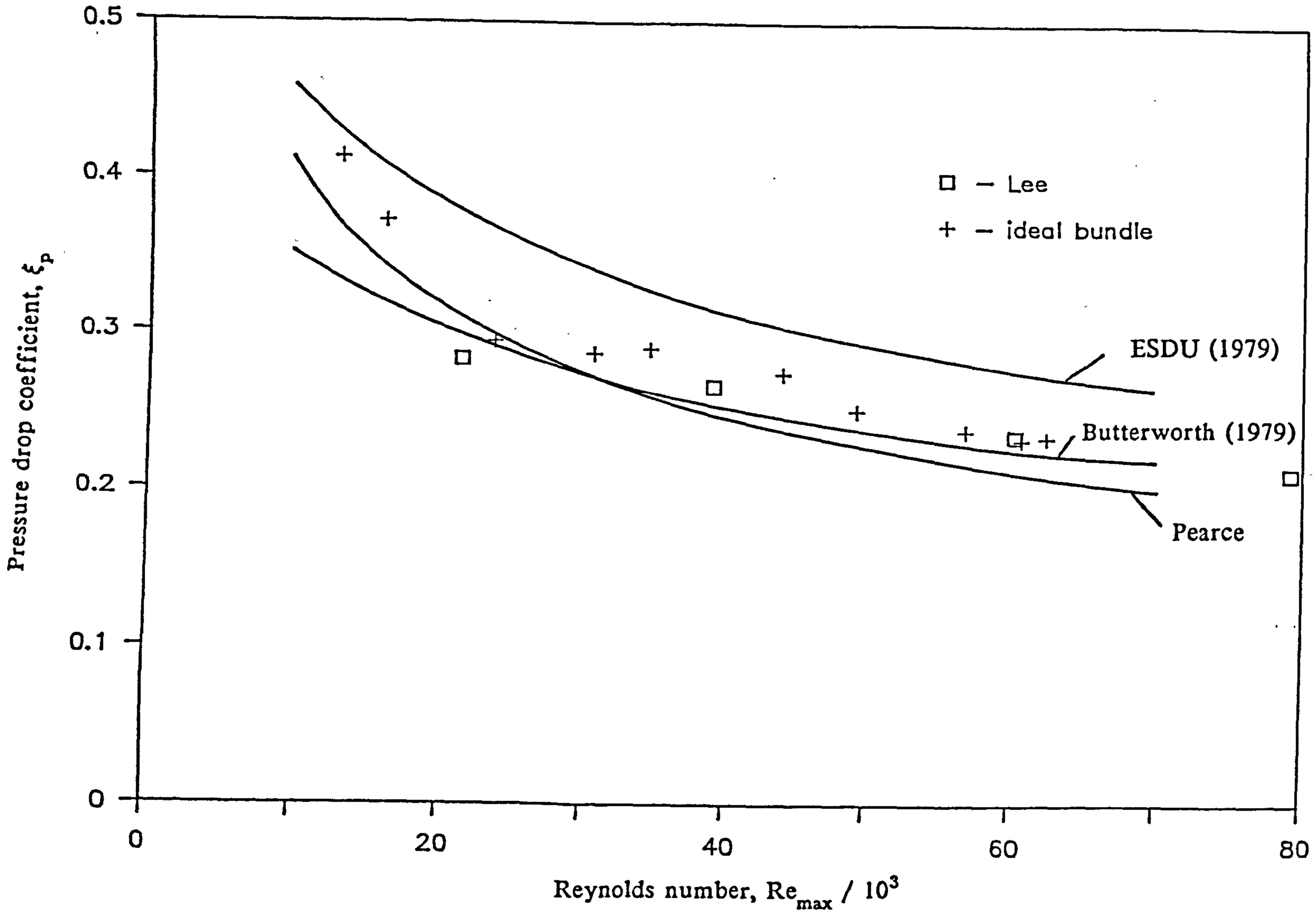

Figure 6.2 Pressure drop coefficient for an ideal equilateral-triangle bank with a pitch-diameter ratio of 1.375.

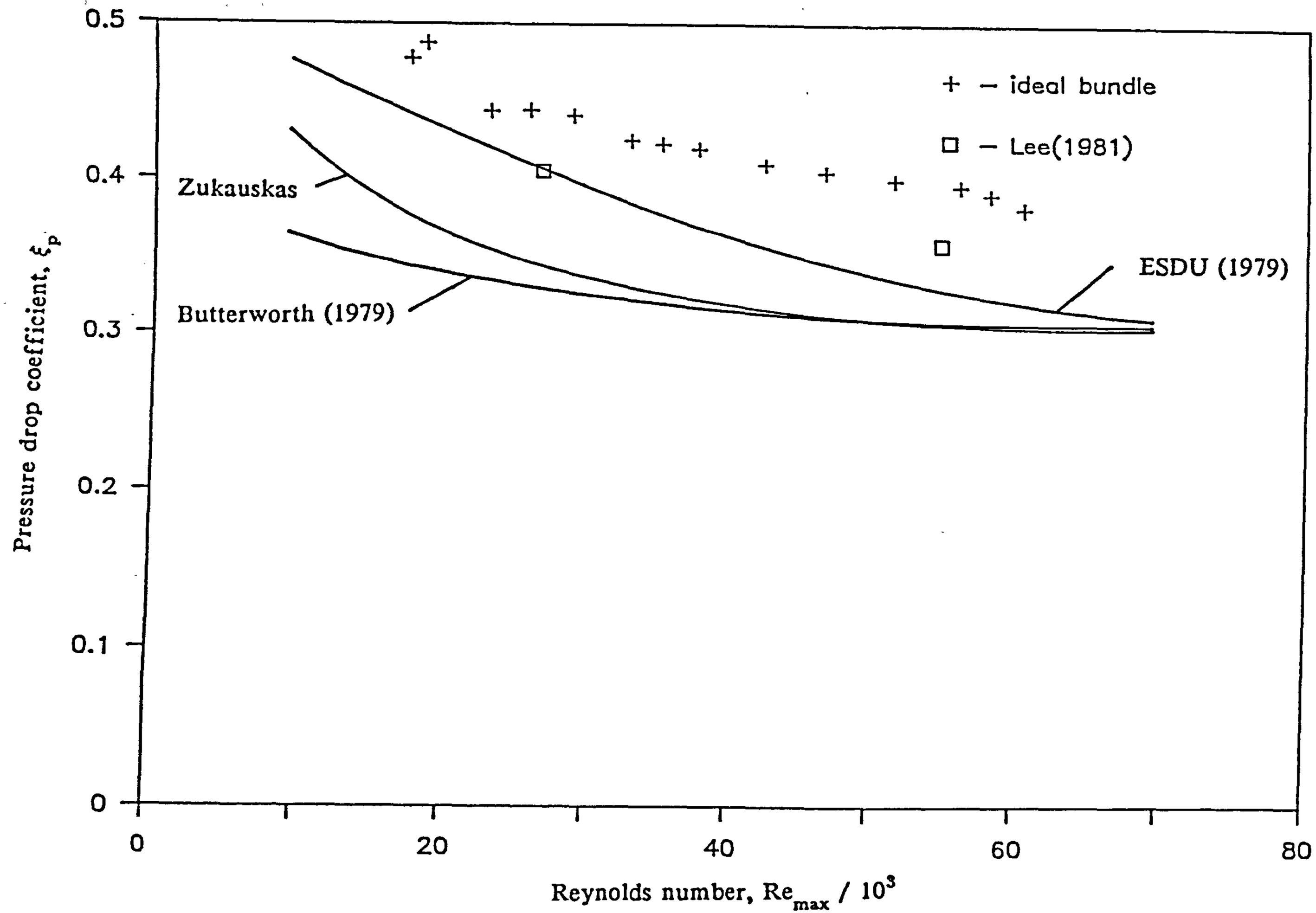

Figure 6.3 Pressure drop coefficient for an ideal in-line square bank with a pitch-diameter ratio of 1.25.

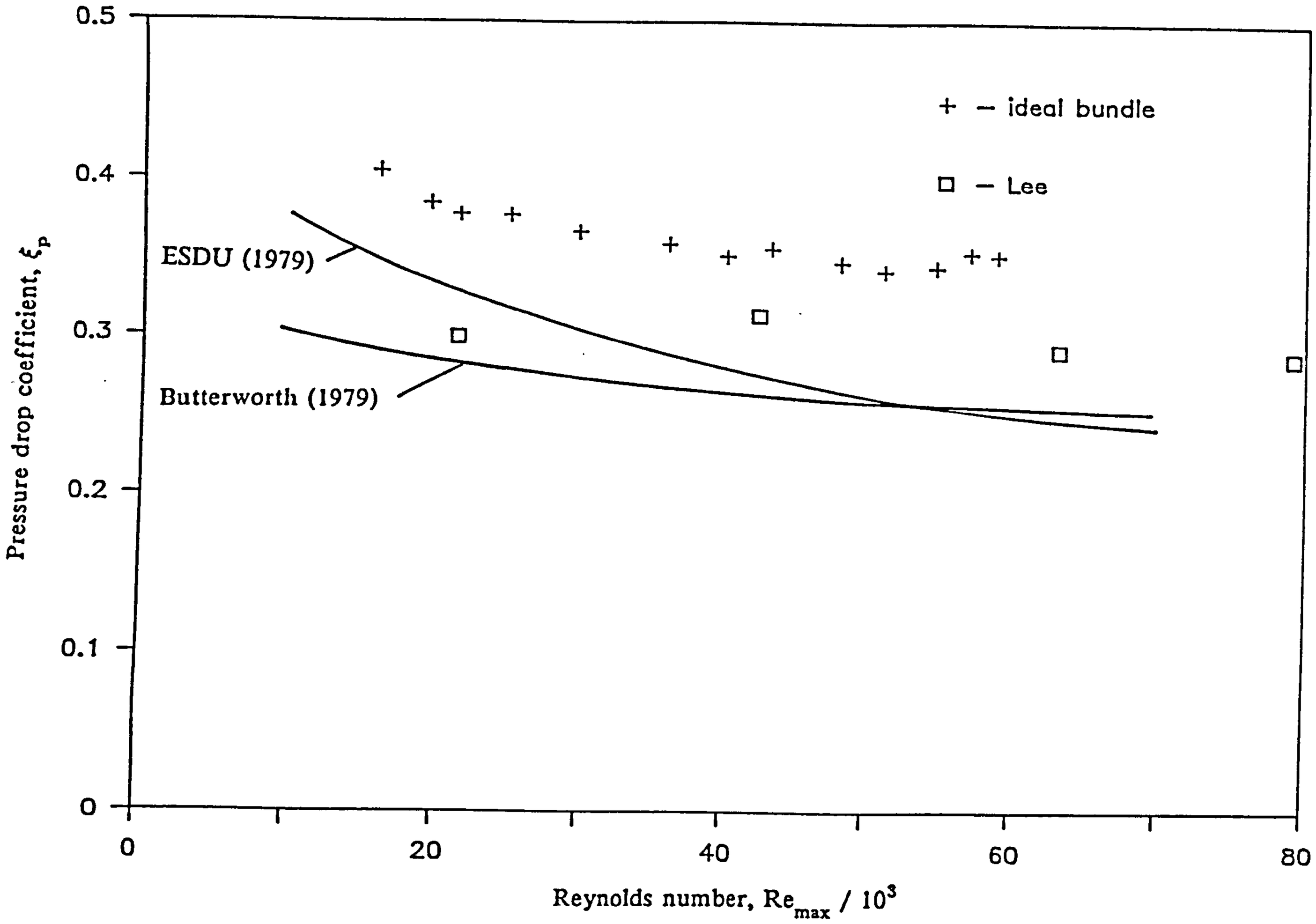

Figure 6.4 Pressure drop coefficient for an ideal in-line square bank with a pitch-diameter ratio of 1.375.

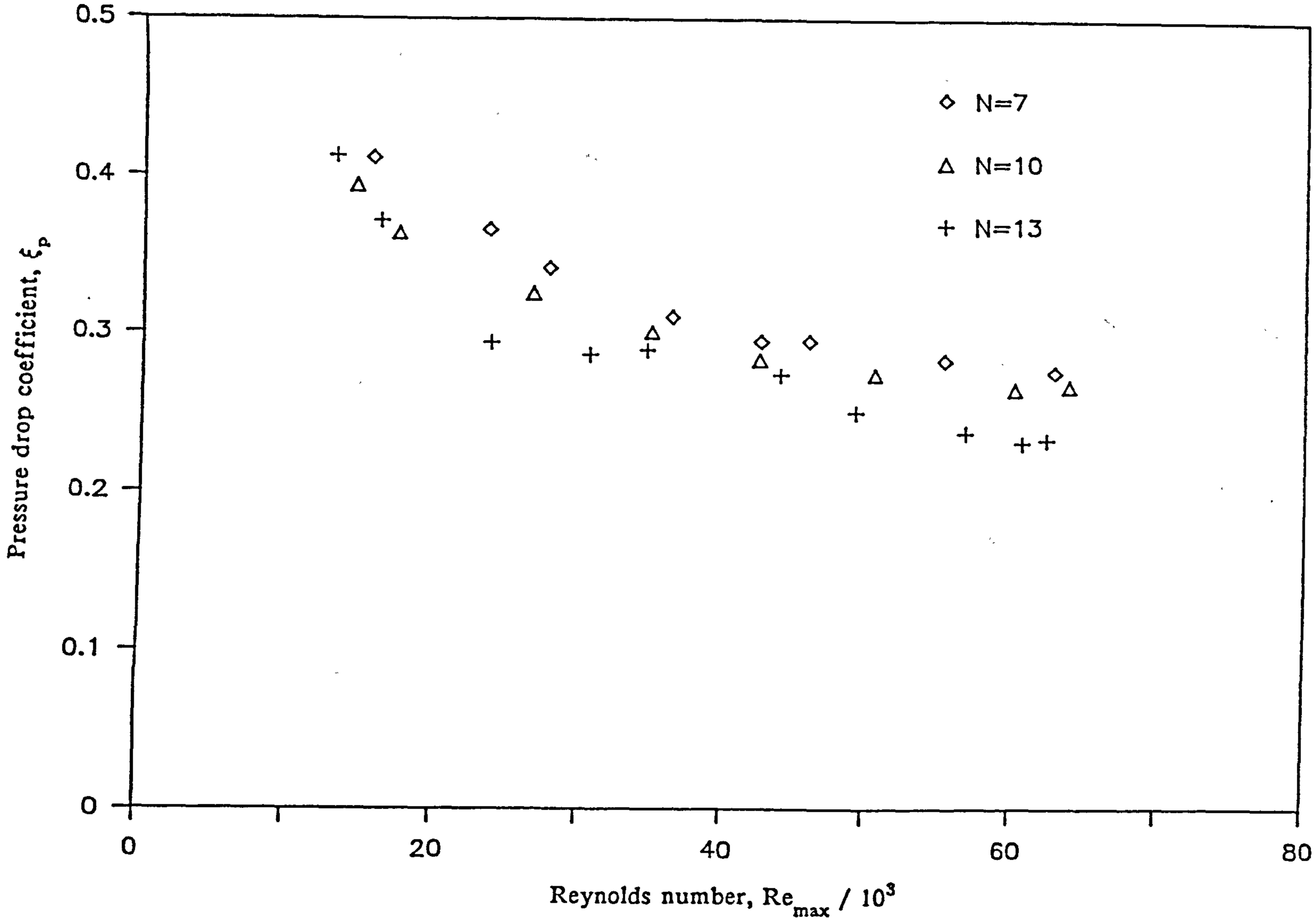

Figure 6.5 The effect of bank length. Pressure drop coefficients for an ideal in-line square bank, with a pitch-diameter ratio of 1.375, having N = 7, 10 and 13.

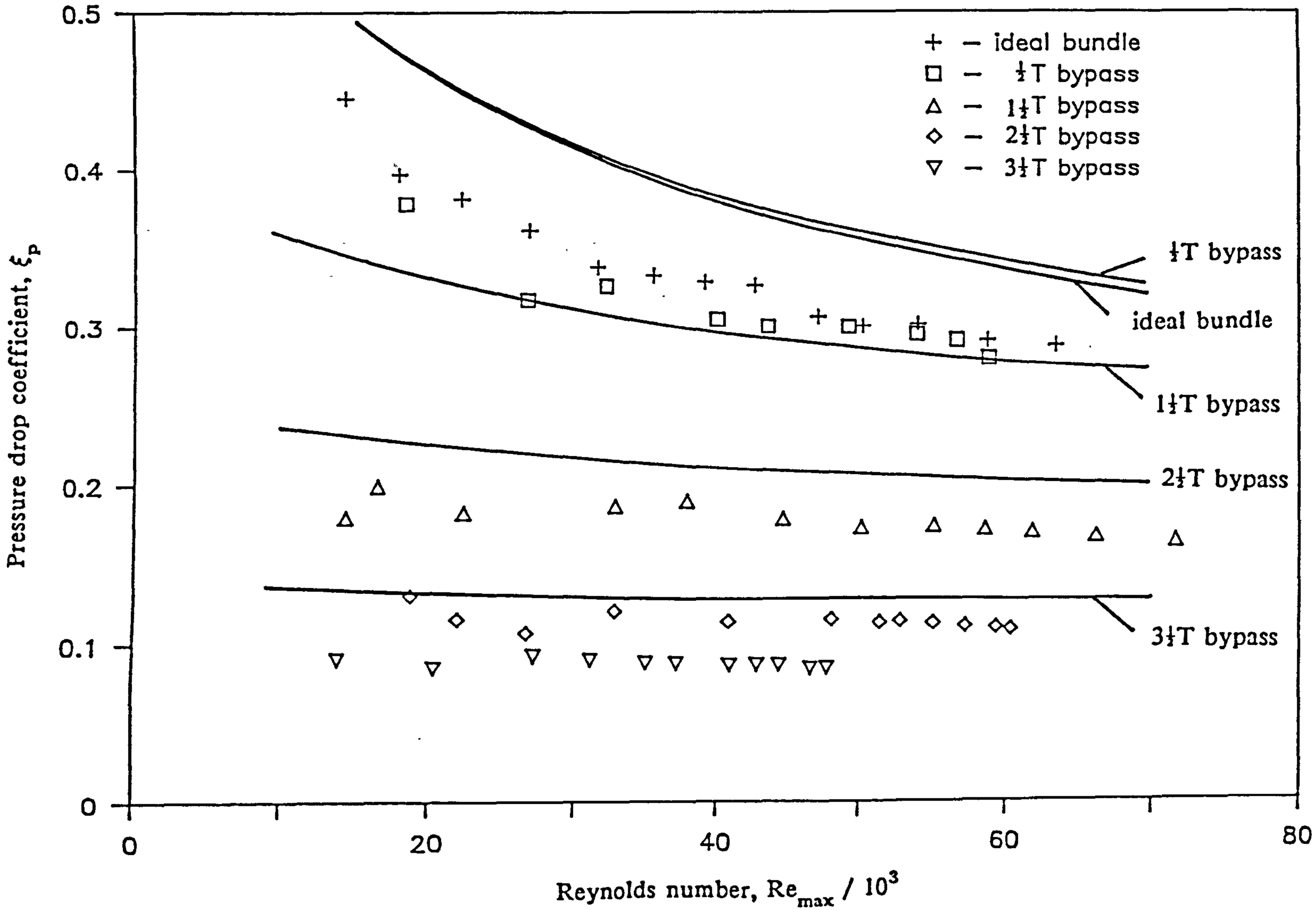

Figure 7.1 Pressure drop coefficient for a 1.25 equilateral-triangle bank with bypassing, compared with the predictions of ESDU (1974).

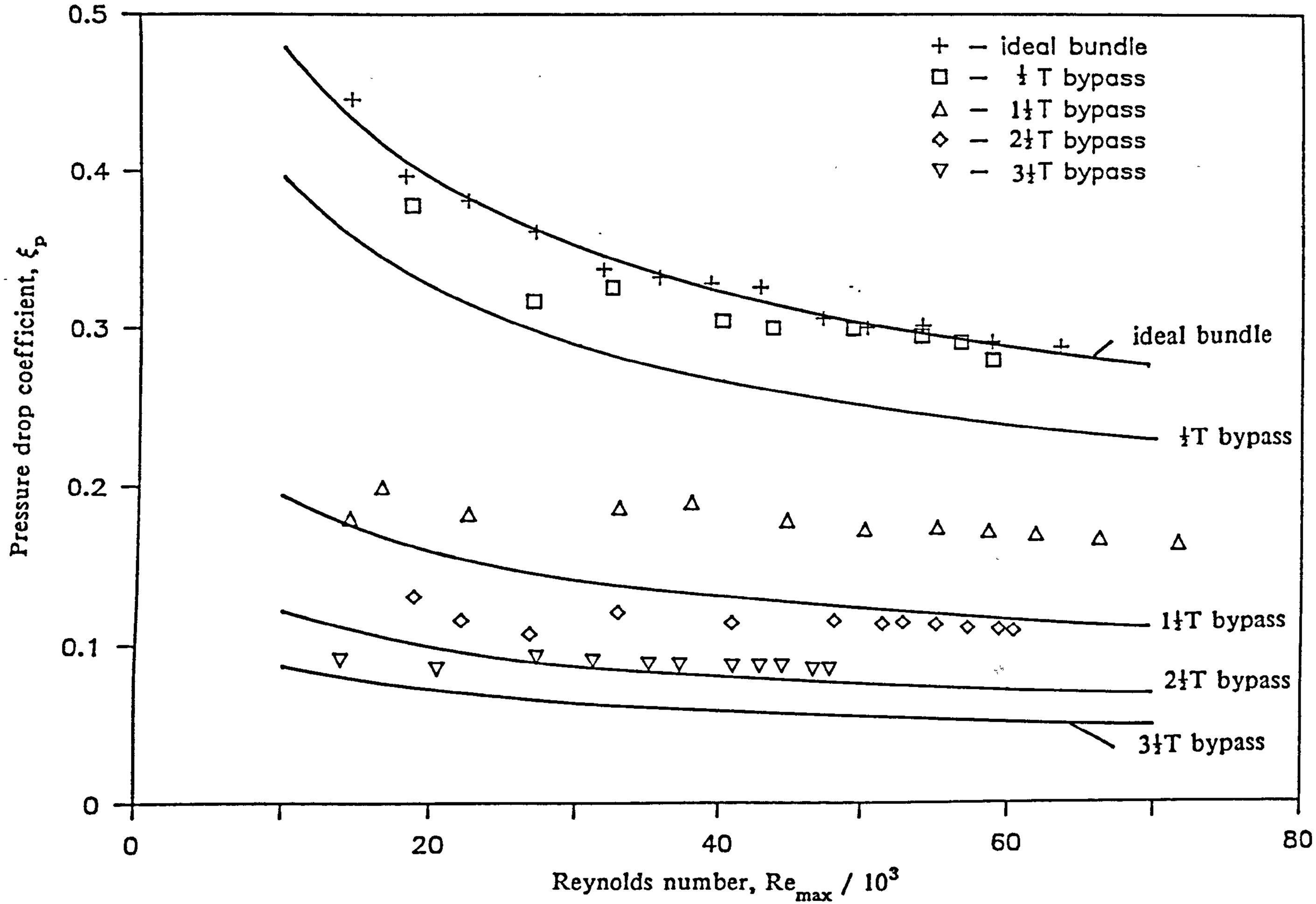

Figure 7.2 Pressure drop coefficient for a 1.25 equilateral-triangle bank with bypassing, compared with the results of Bell's (1960) bypassing correction factor.

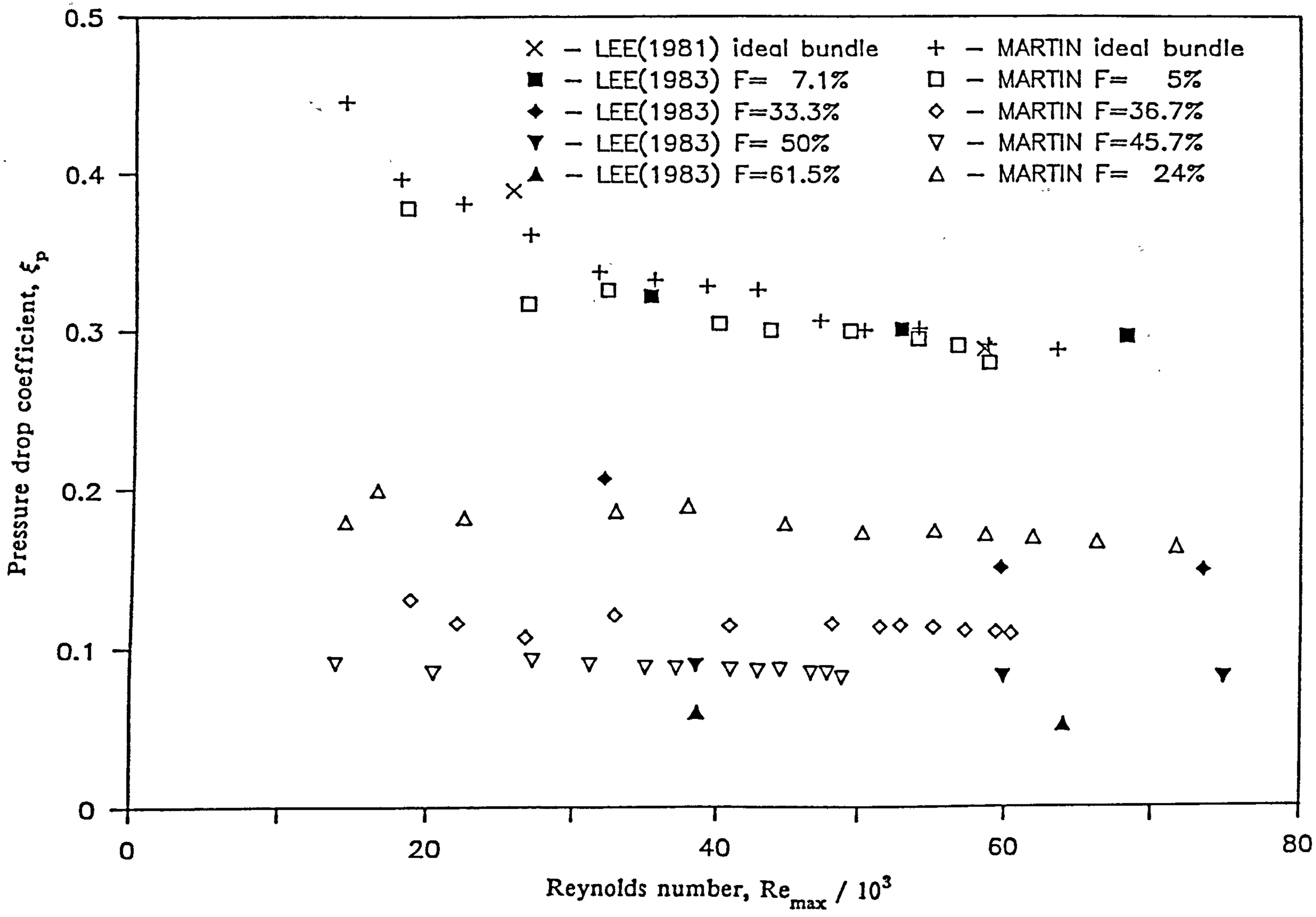

Figure 7.3 Pressure drop coefficient for a 1.25 equilateral-triangle bank with bypassing, compared with the data of Lee et al. (1983).

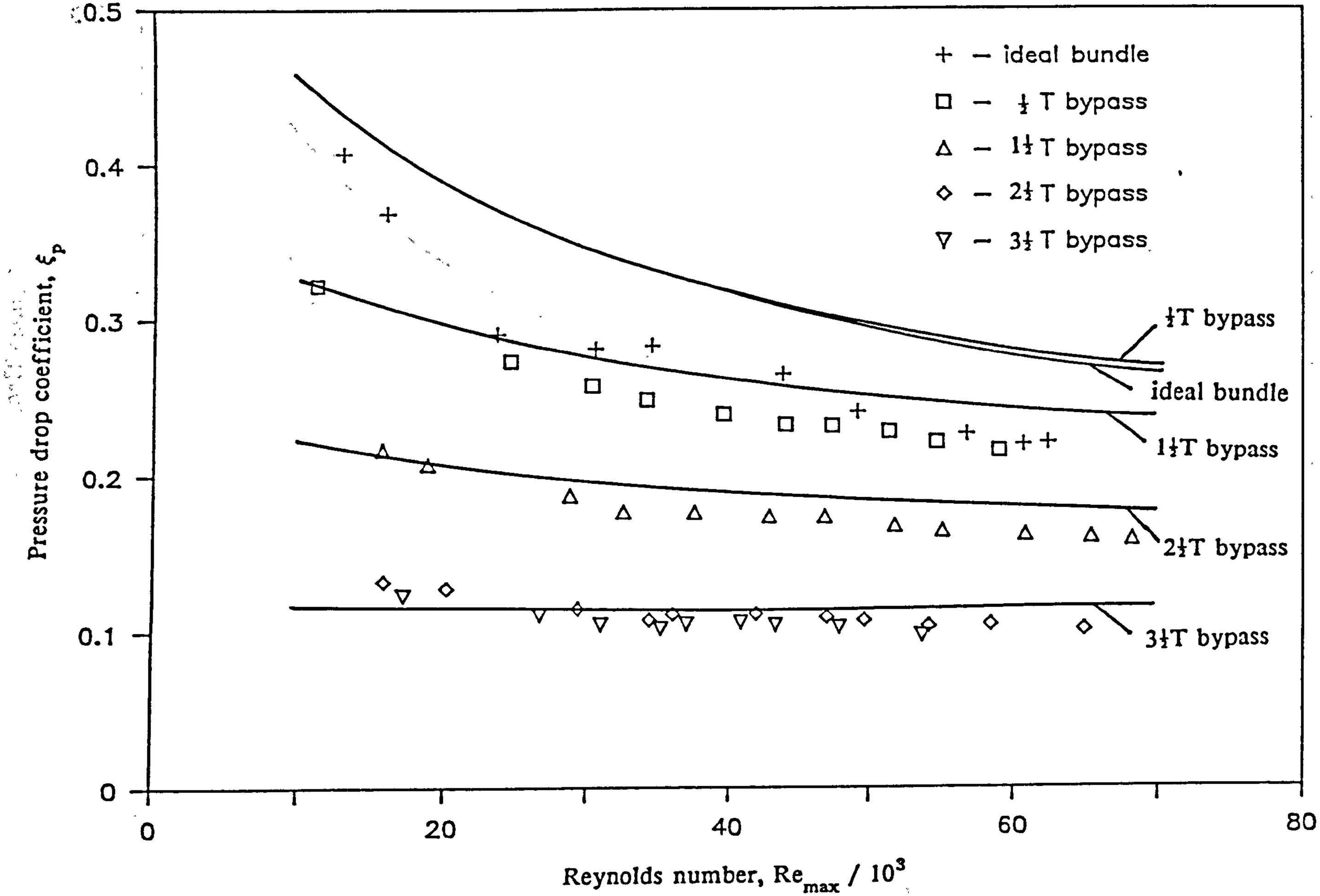

Figure 7.4 Pressure drop coefficient for a 1.375 equilateral-triangle bank with bypassing, compared with the predictions of ESDU (1974).

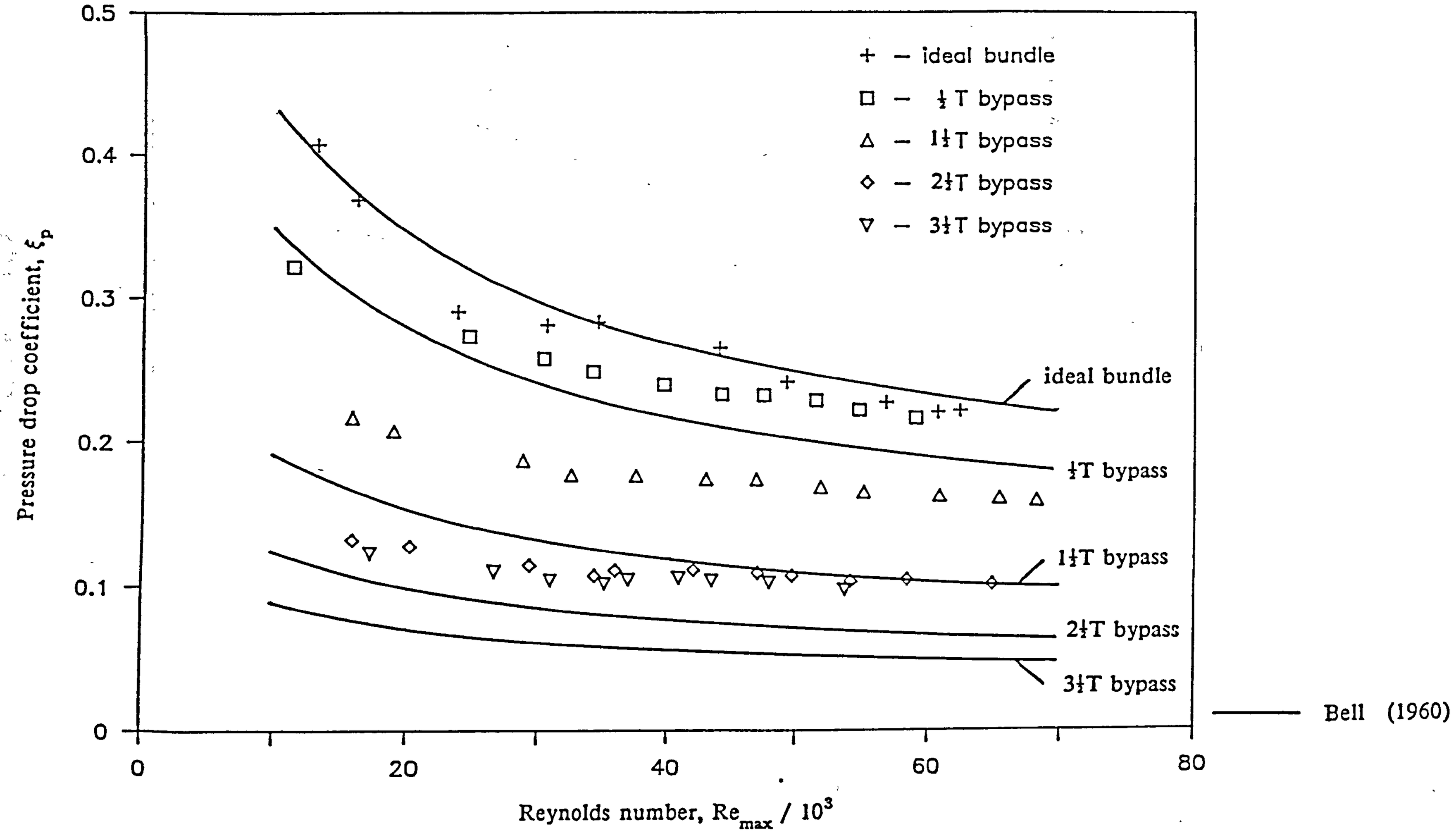

Figure 7.5 Pressure drop coefficient for a 1.375 equilateral-triangle bank with bypassing, compared with the results of Bell's (1960) bypassing correction factor.

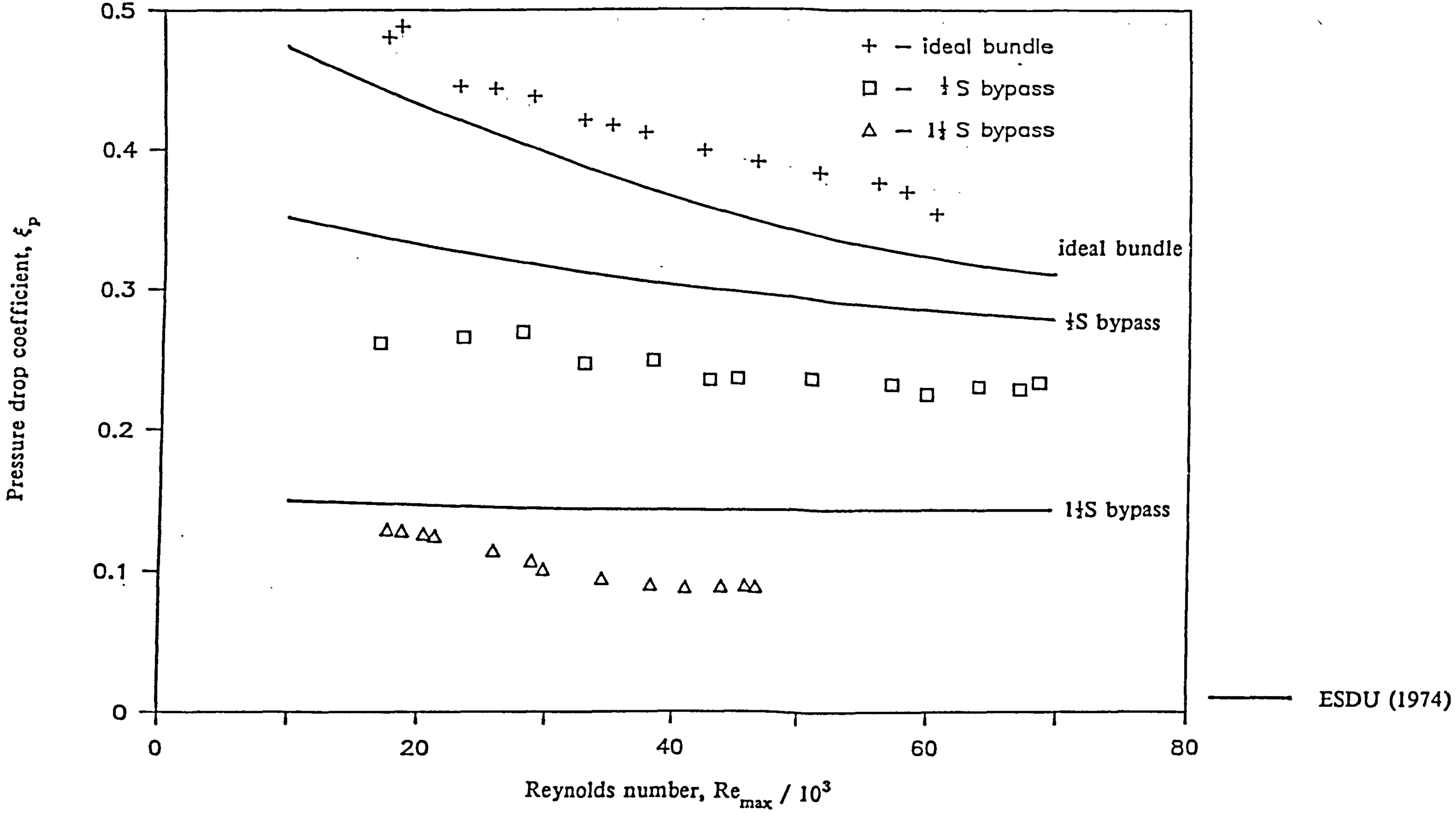

Figure 7.6 Pressure drop coefficient for a 1.25 in-line square bank with bypassing, compared with the predictions of ESDU (1974).

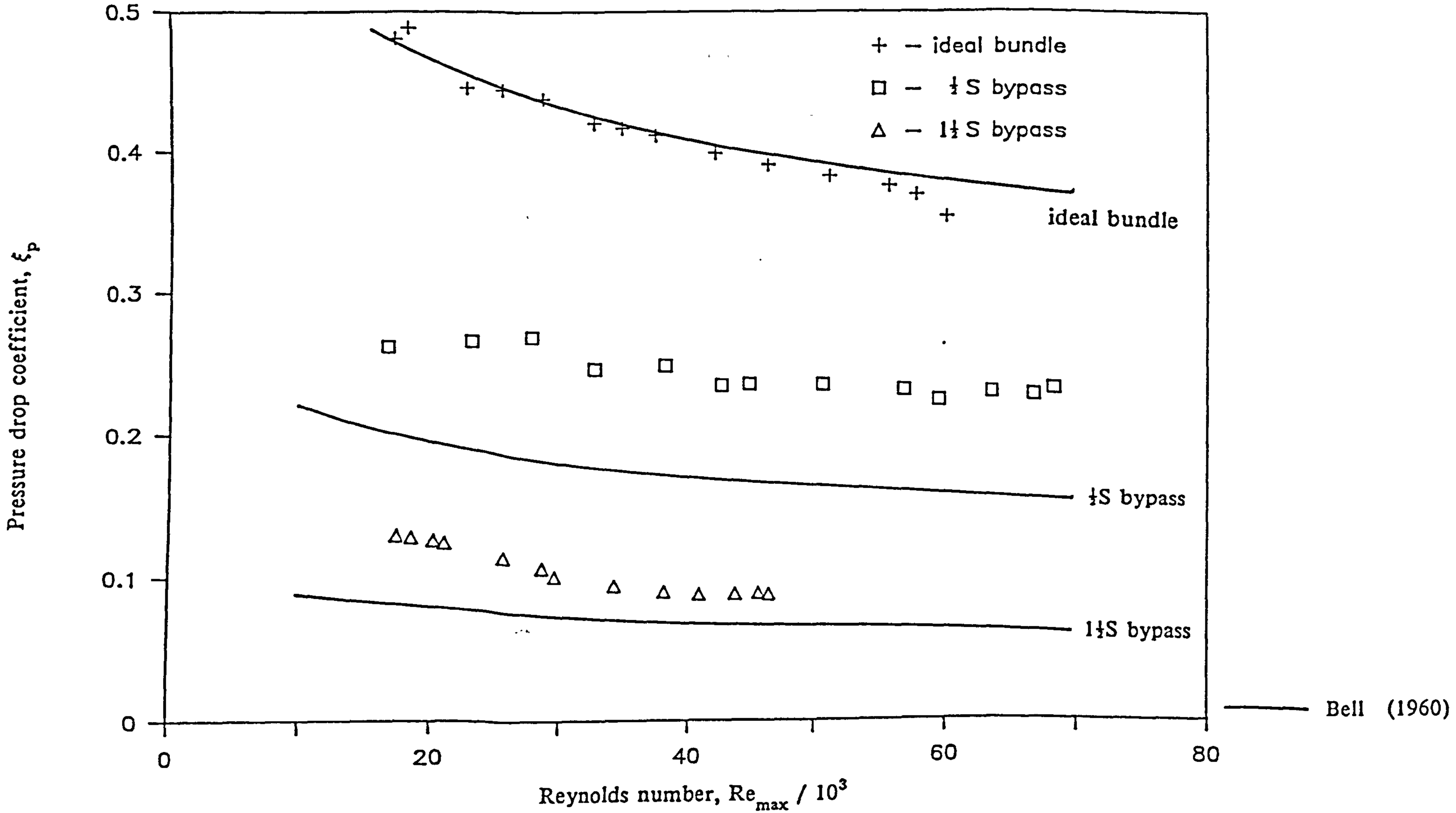

Figure 7.7 Pressure drop coefficient for a 1.25 in-line square bank with bypassing, compared with the results of Bell's (1960) bypassing correction factor.

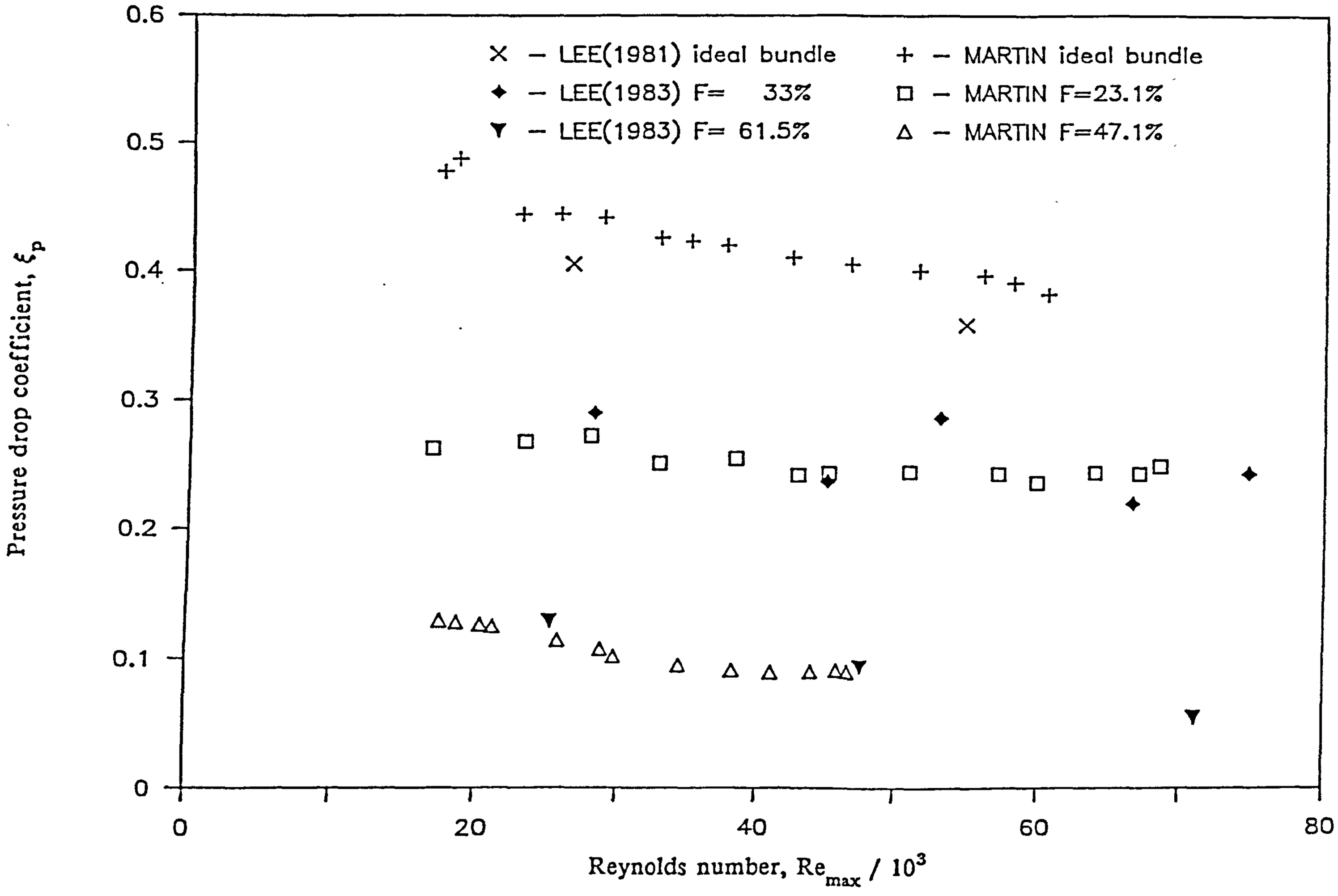

Figure 7.8 Pressure drop coefficient for a 1.25 in-line square bank with bypassing, compared with the data of Lee et al. (1983)

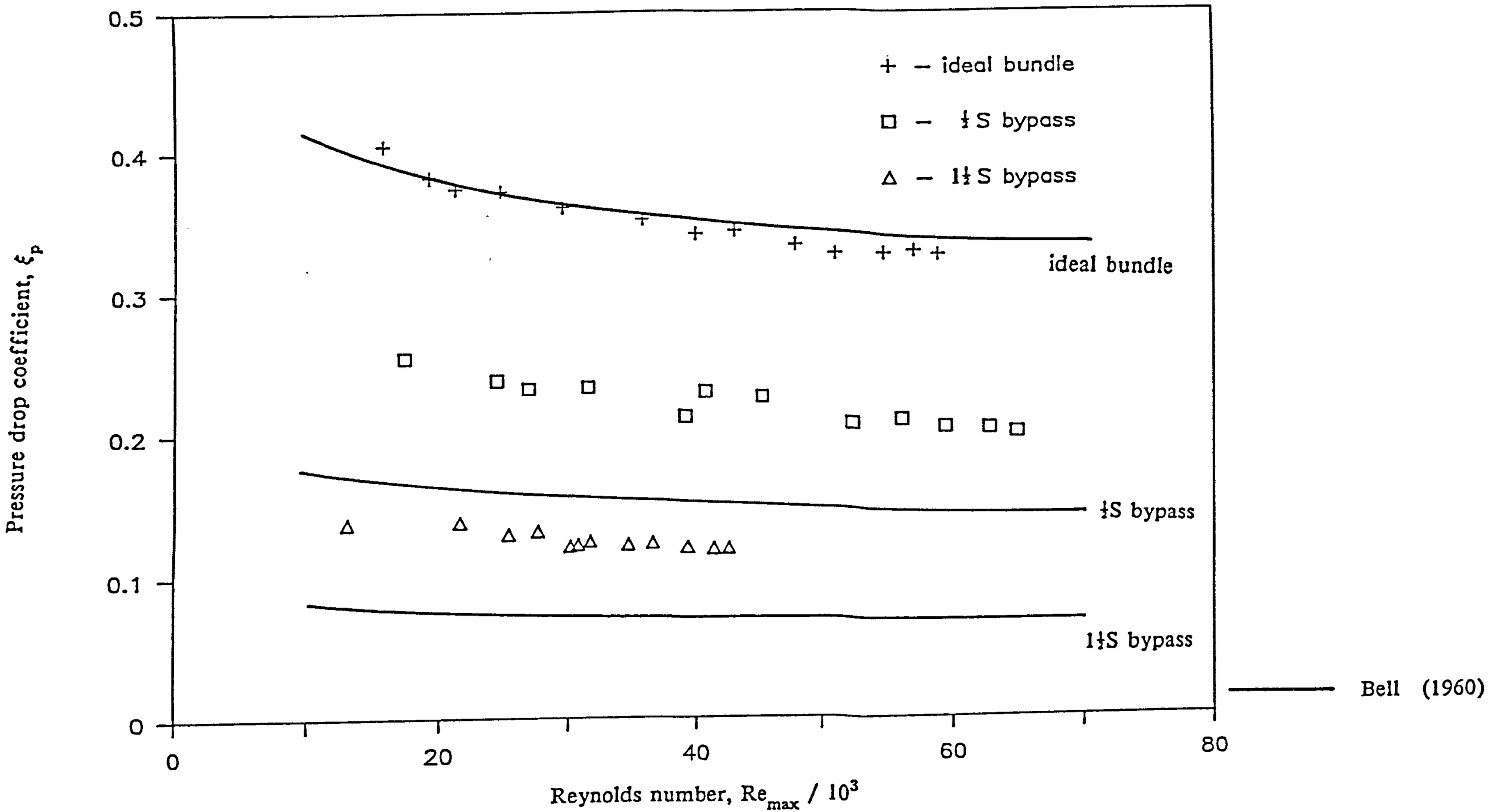

Figure 7.10 Pressure drop coefficient for a 1.375 in-line square bank with bypassing, compared with the results of Bell's (1960) bypassing correction factor.

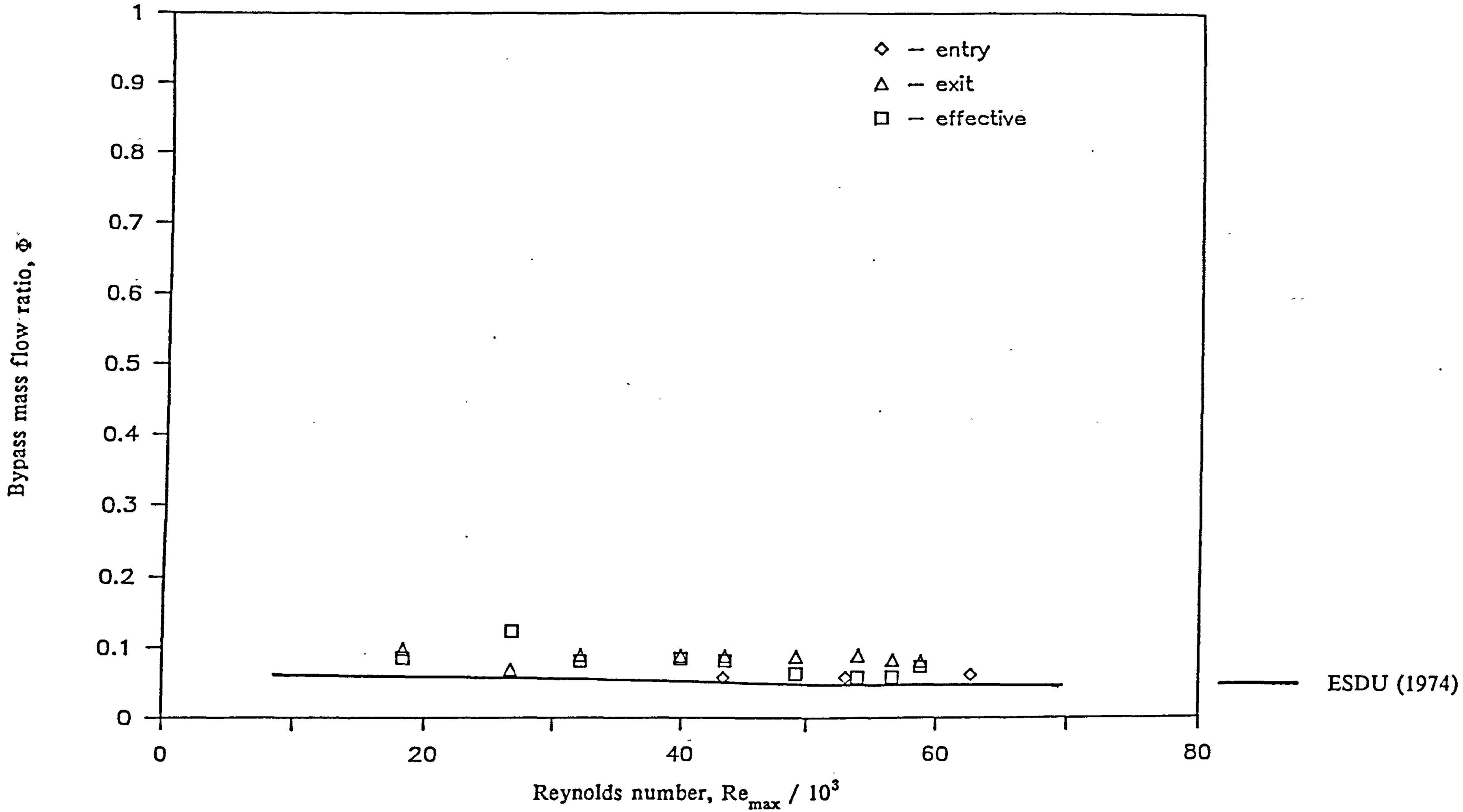

Figure 7.11 Bypass mass flow ratios for a 1.25 equilateral-triangle bank with a ½T bypass.

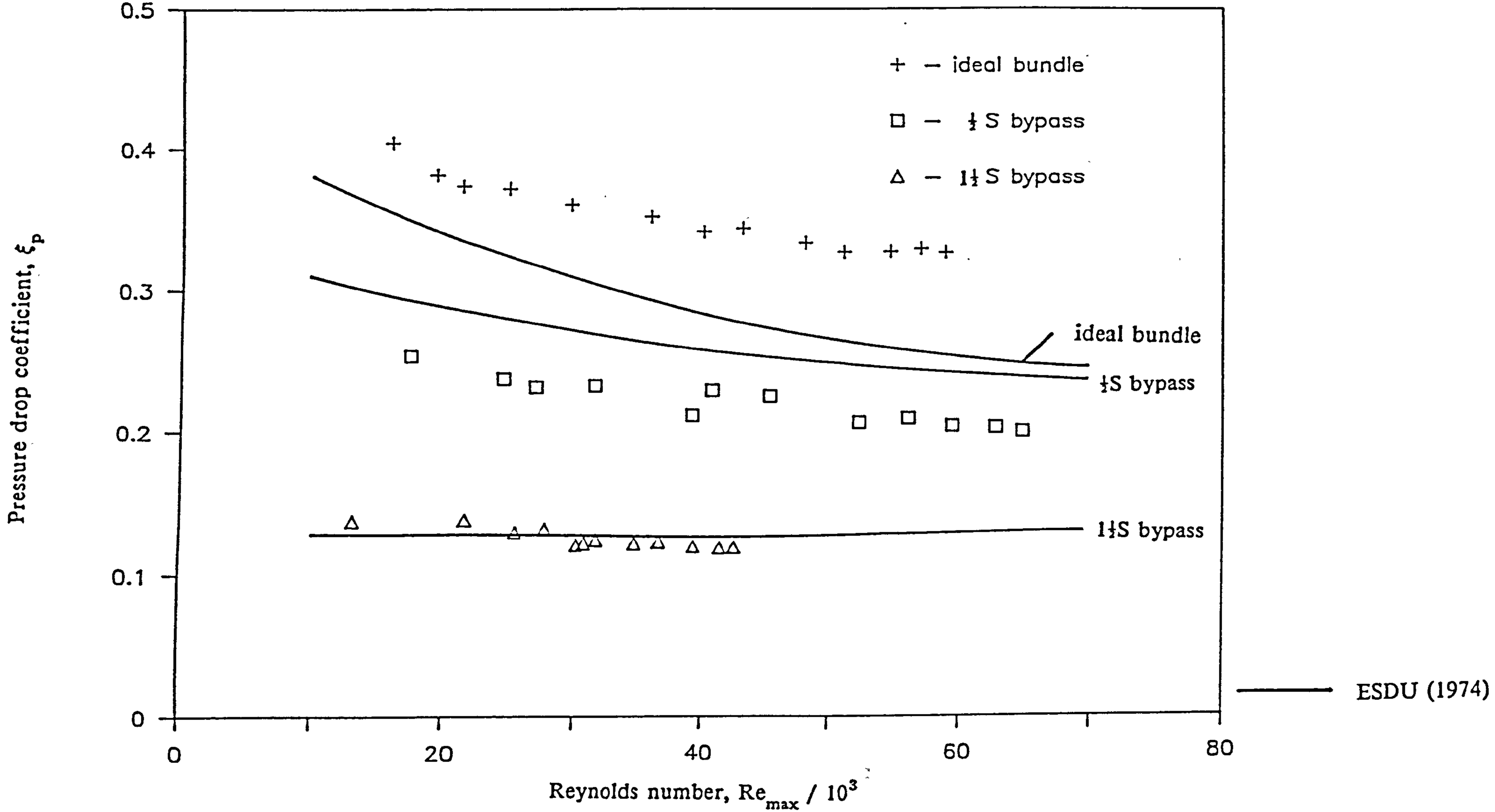

Figure 7.9 Pressure drop coefficient for a 1.375 in-line square bank, compared with the predictions of ESDU (1974).

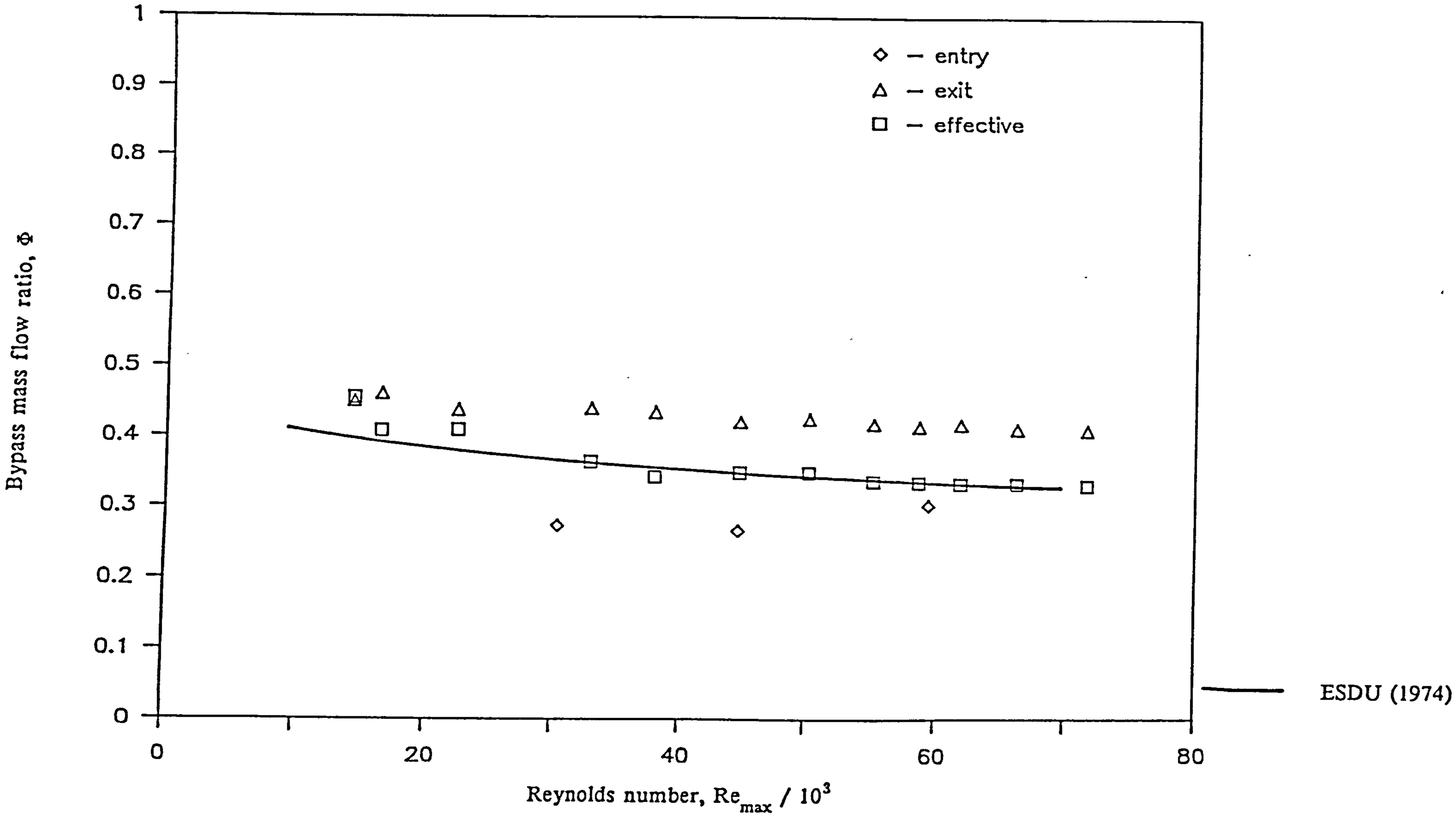

Figure 7.12 Bypass mass flow ratios for a 1.25 equilateral-triangle bank with a 1½T bypass.

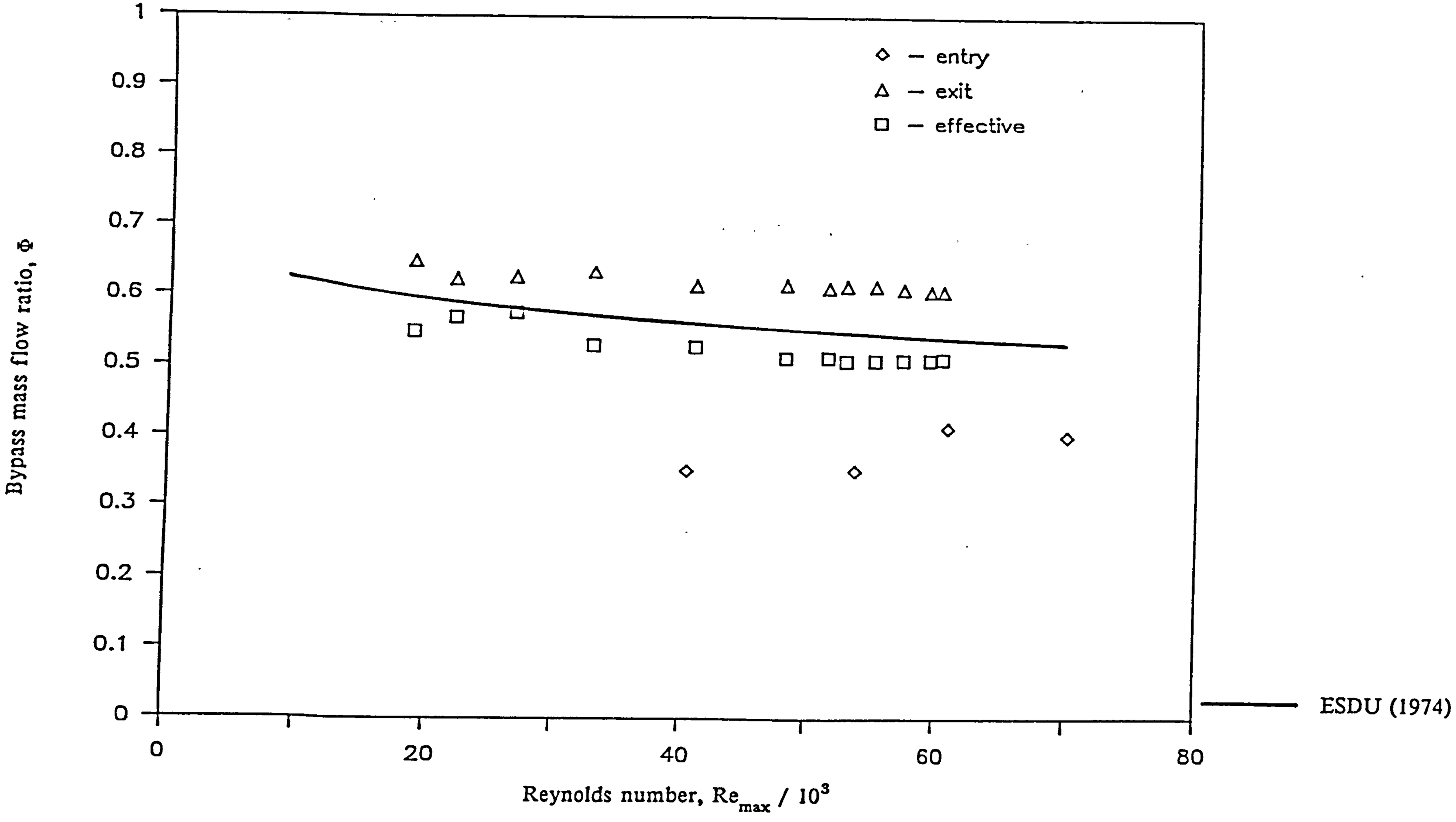

Figure 7.13 Bypass mass flow ratios for a 1.25 equilateral-triangle bank with a 2½T bypass.

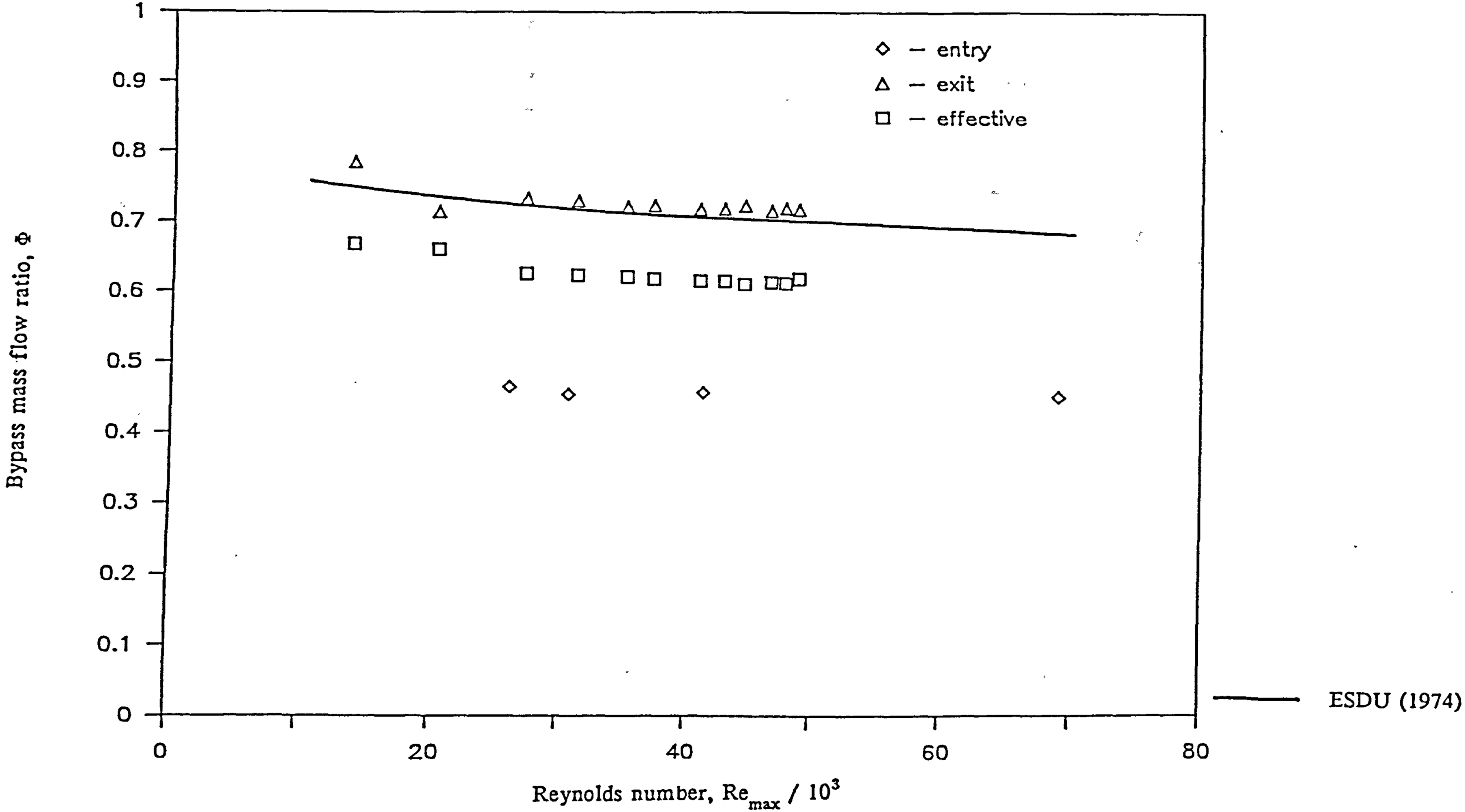

Figure 7.14 Bypass mass flow ratios for a 1.25 equilateral-triangle bank with a 3½T bypass.

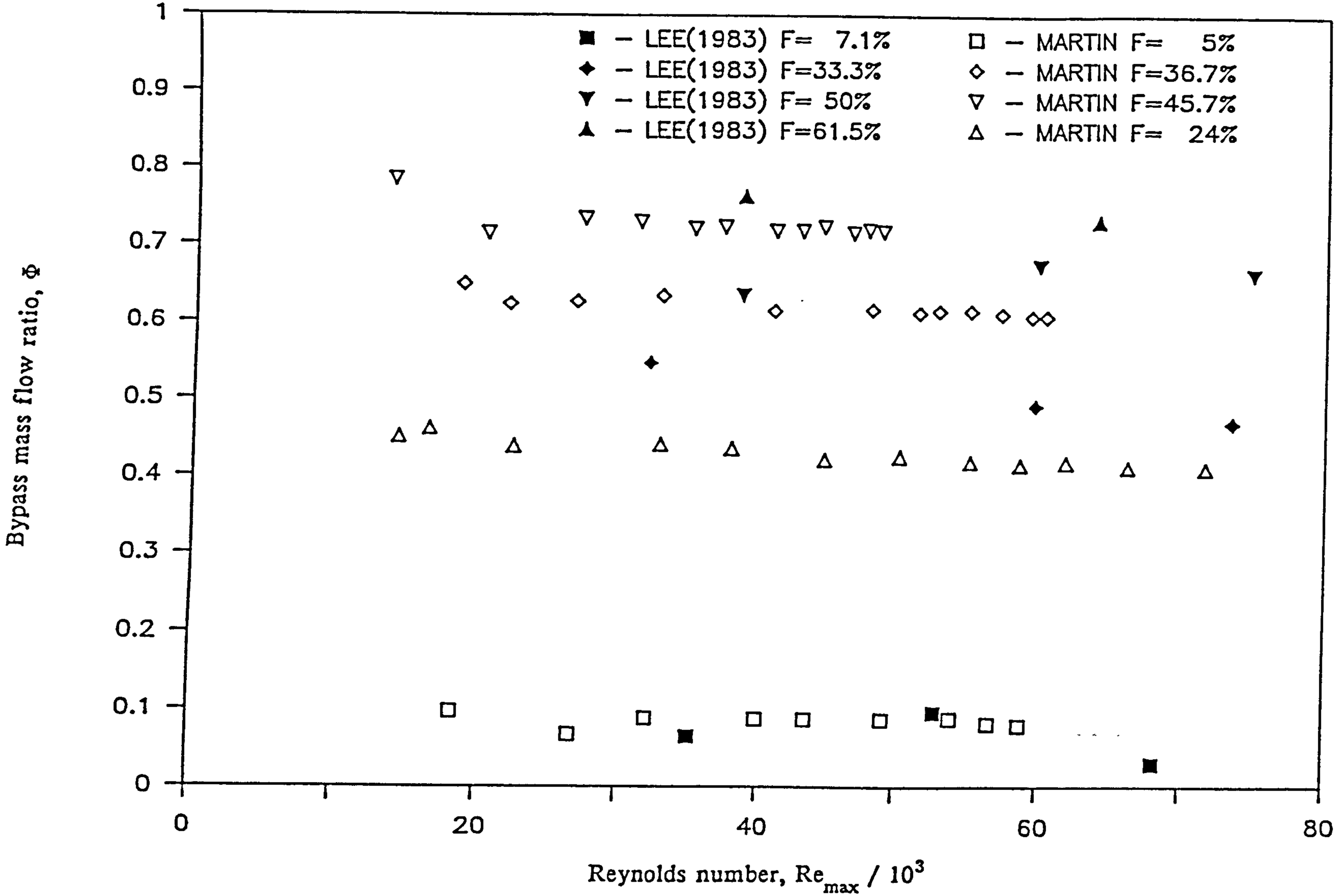

Figure 7.15 Bypass exit mass flow ratios for a 1.25 equilateral-triangle bank with bypassing, compared with the data of Lee et al. (1983).

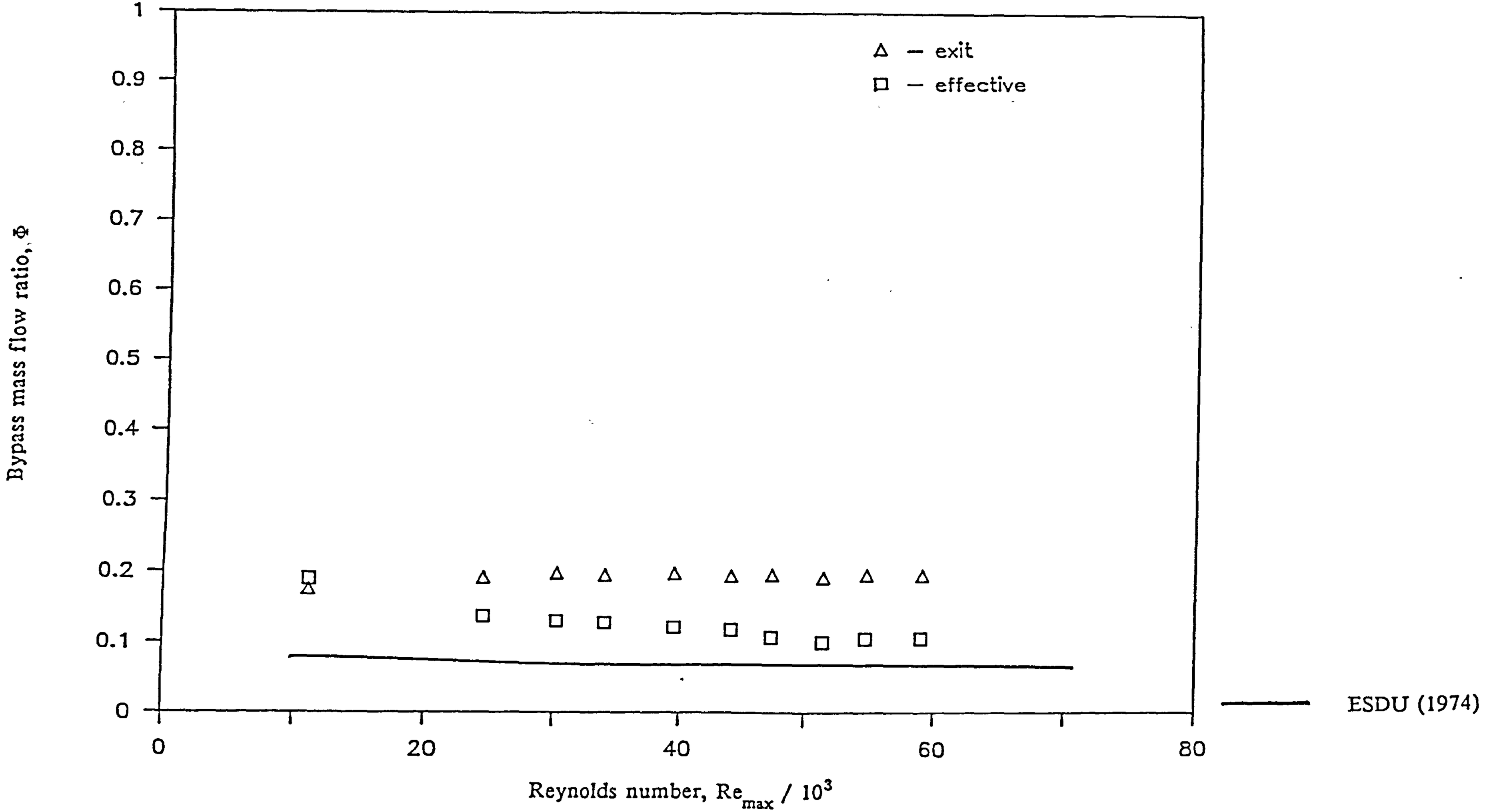

Figure 7.16 Bypass mass flow ratios for a 1.375 equilateral-triangle bank with a ½T bypass.

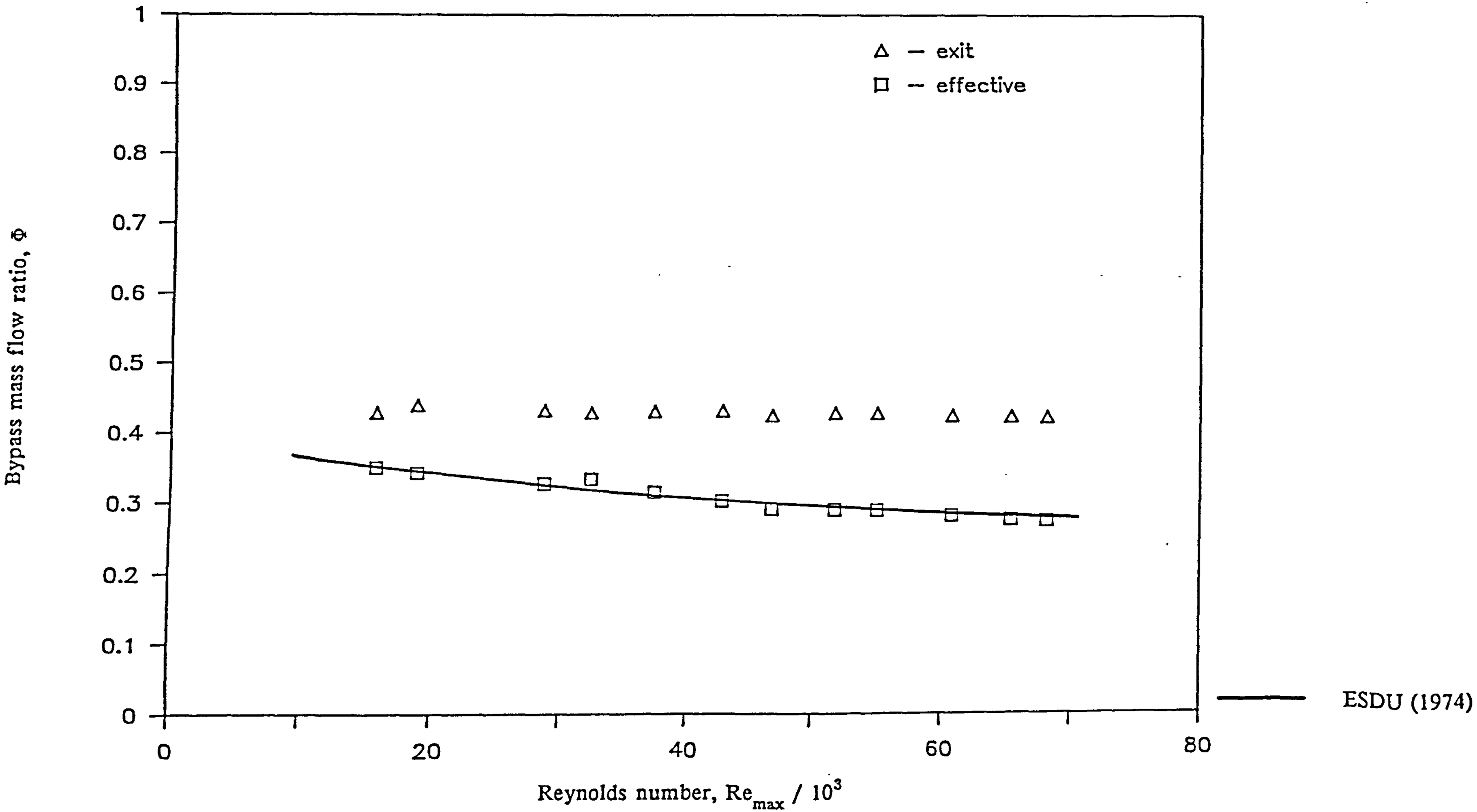

Figure 7.17 Bypass mass flow ratios for a 1.375 equilateral-triangle bank with a 1½T bypass.

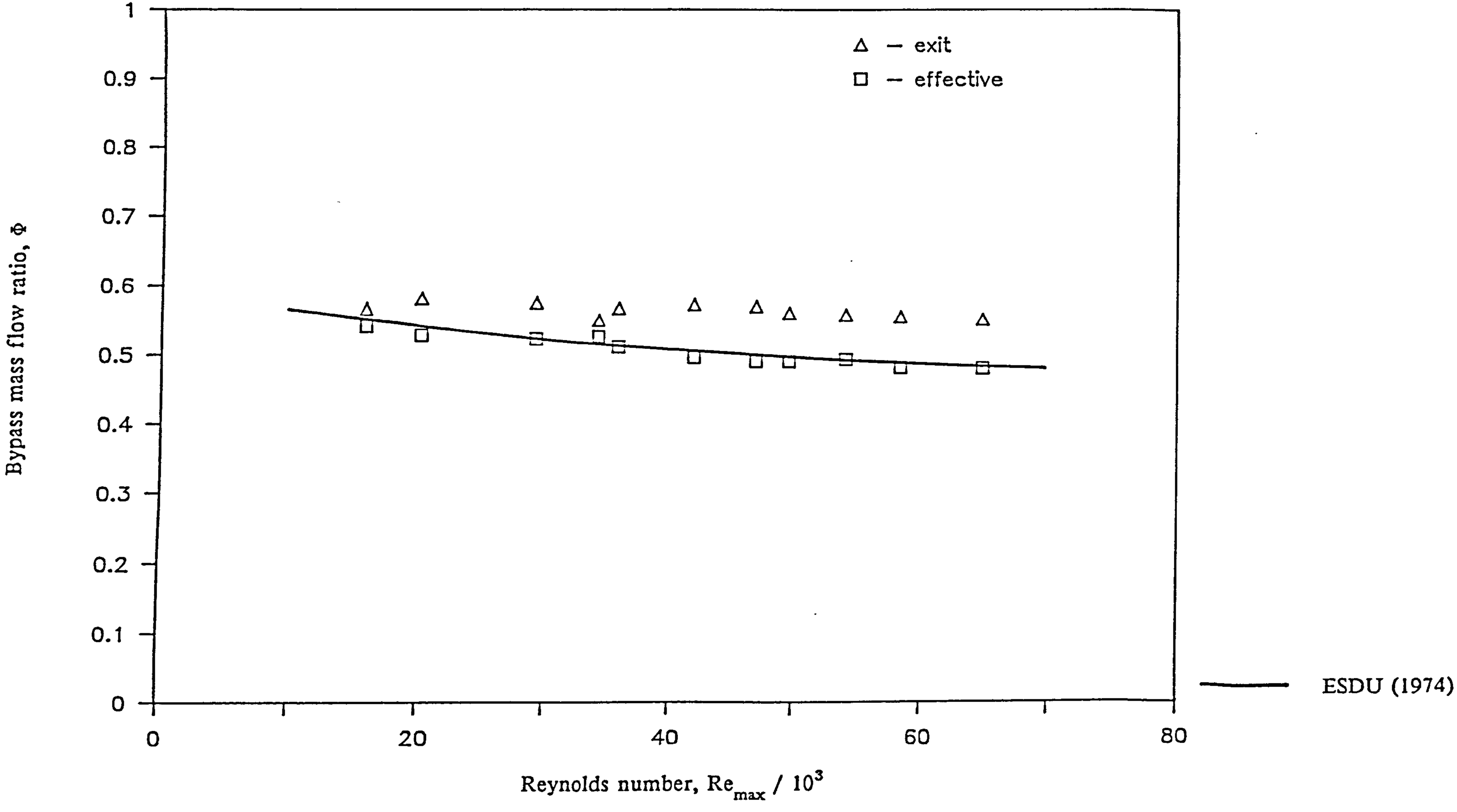

Figure 7.18 Bypass mass flow ratios for a 1.375 equilateral-triangle bank with a 2½T bypass.

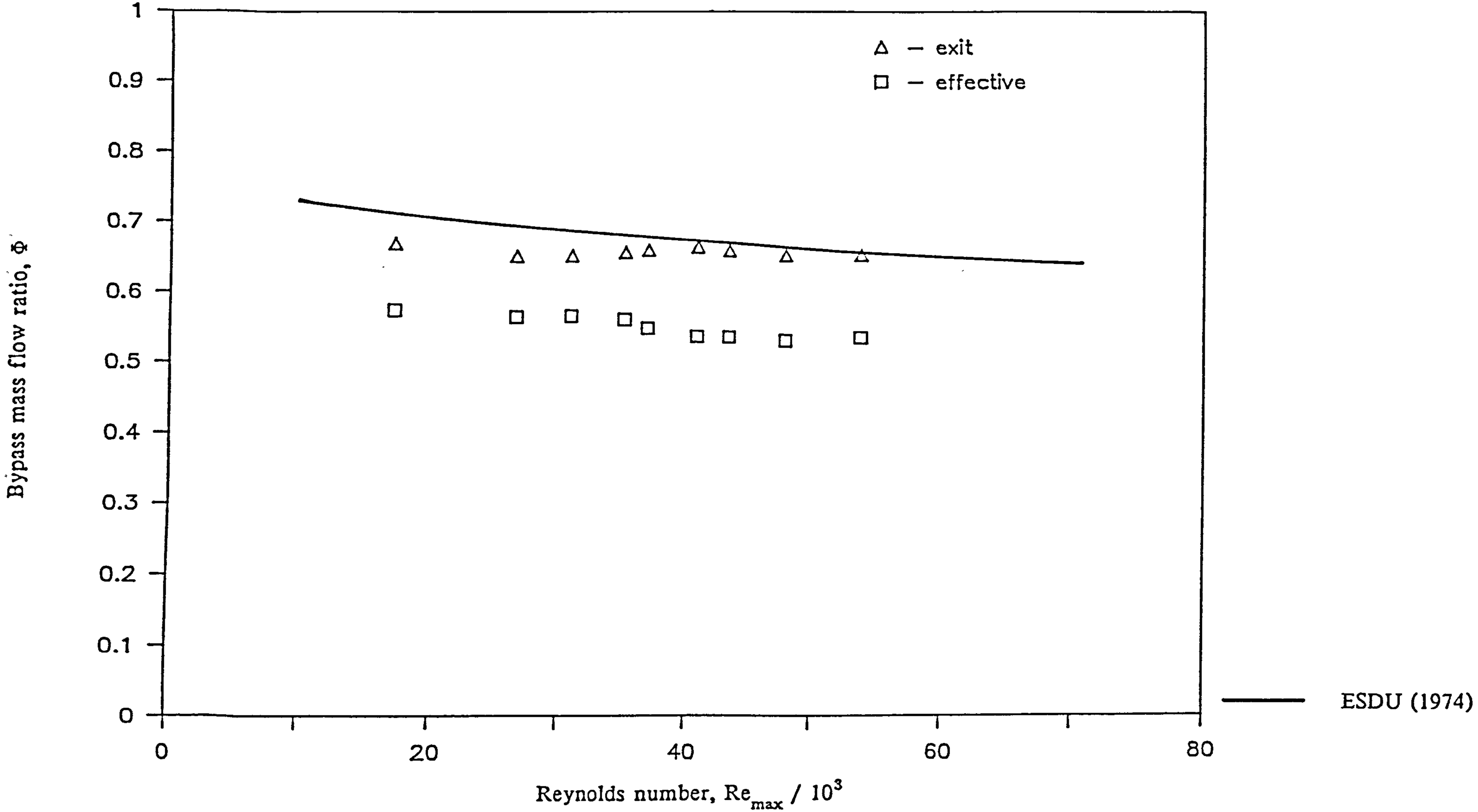

Figure 7.19 Bypass mass flow ratios for a 1.375 equilateral-triangle bank with a 3½T bypass.

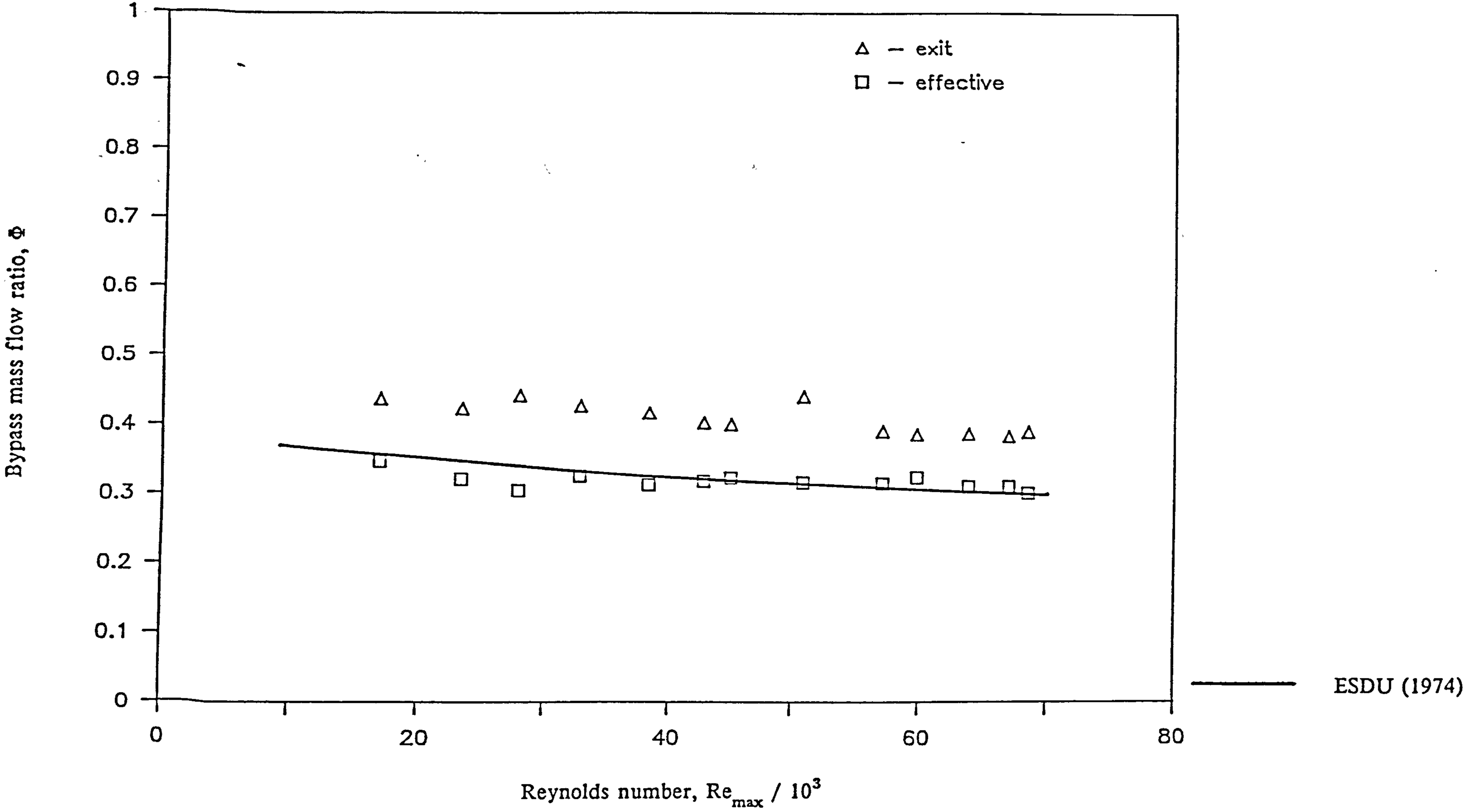

Figure 7.20 Bypass mass flow ratios for a 1.25 in-line square bank with a ½S bypass.

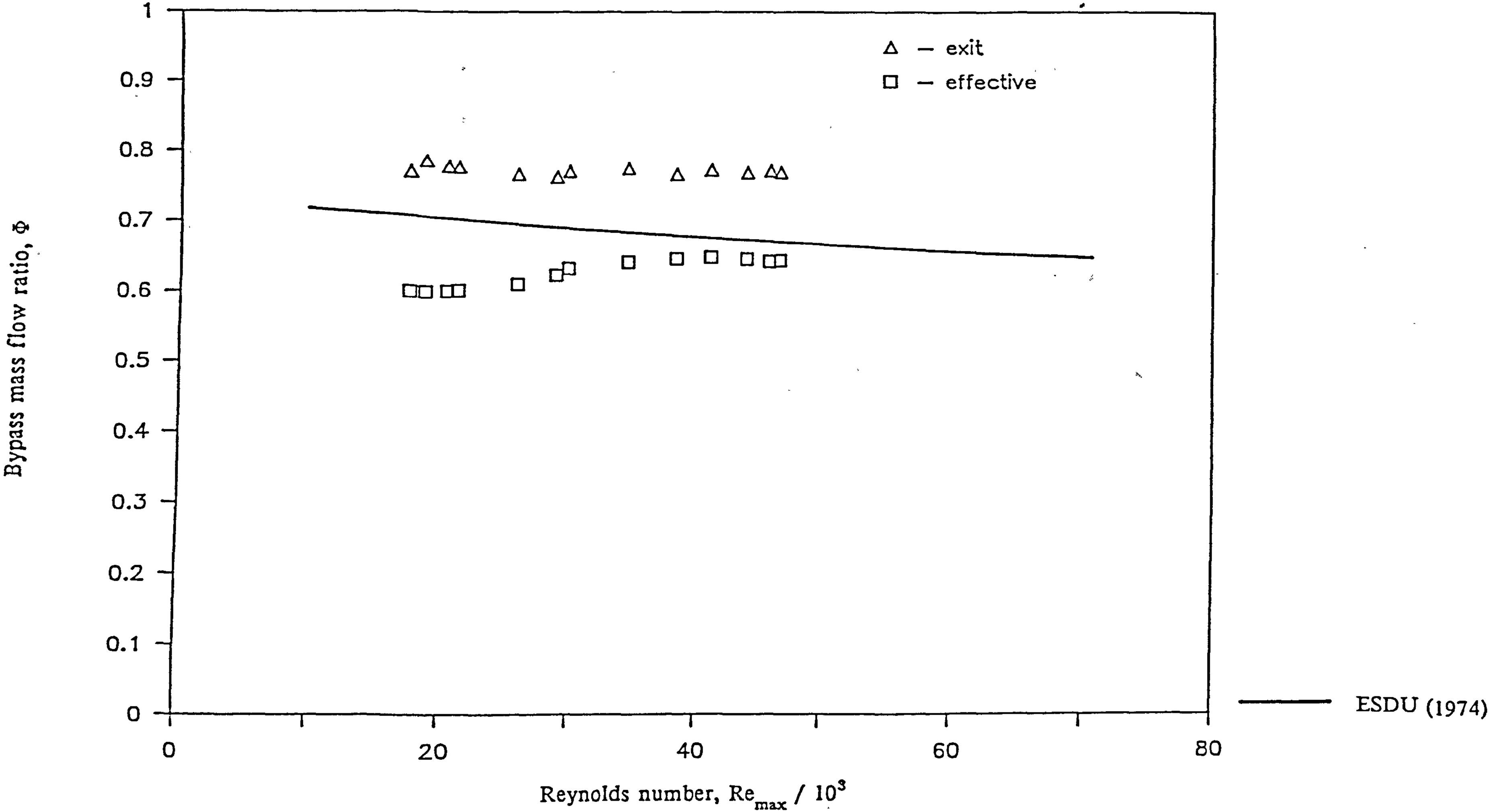

Figure 7.21 Bypass mass flow ratios for a 1.25 in-line square bank with a 1½S bypass.

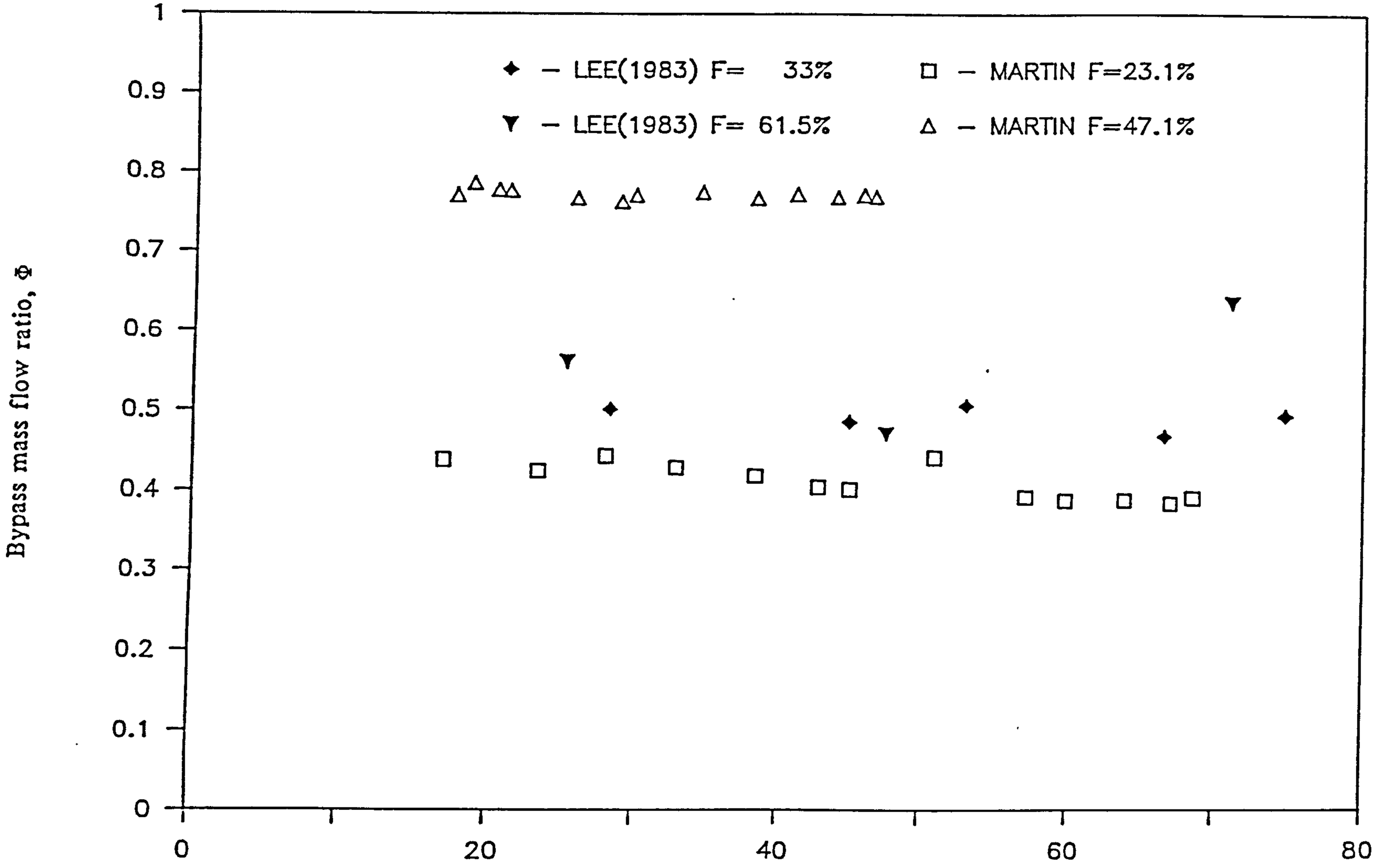

Figure 7.22 Bypass exit mass flow ratios for a 1.25 in-line square bank with bypassing, compared with the data of Lee et al. (1983).

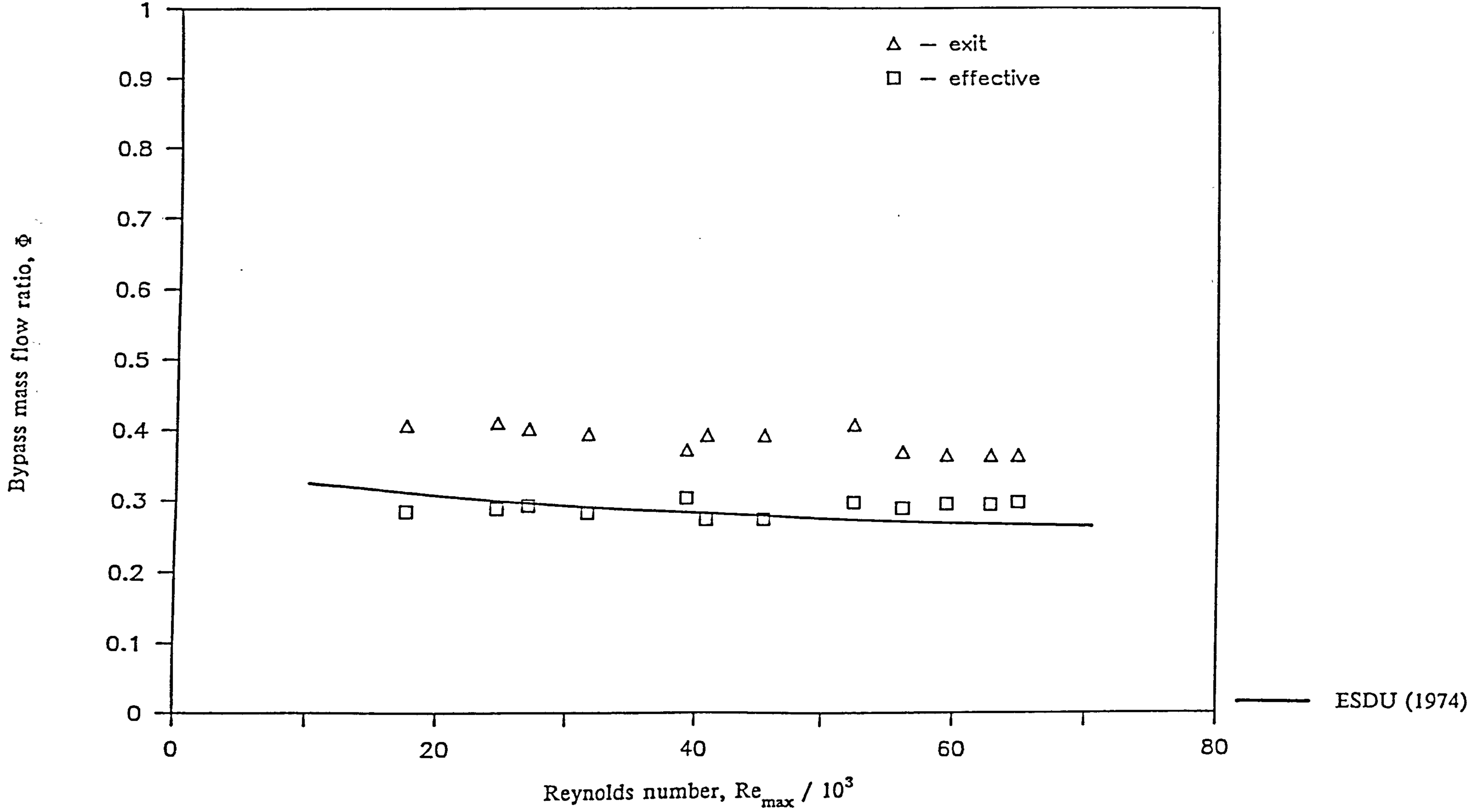

Figure 7.23 Bypass mass flow ratios for a 1.375 in-line square bank with a ½S bypass.

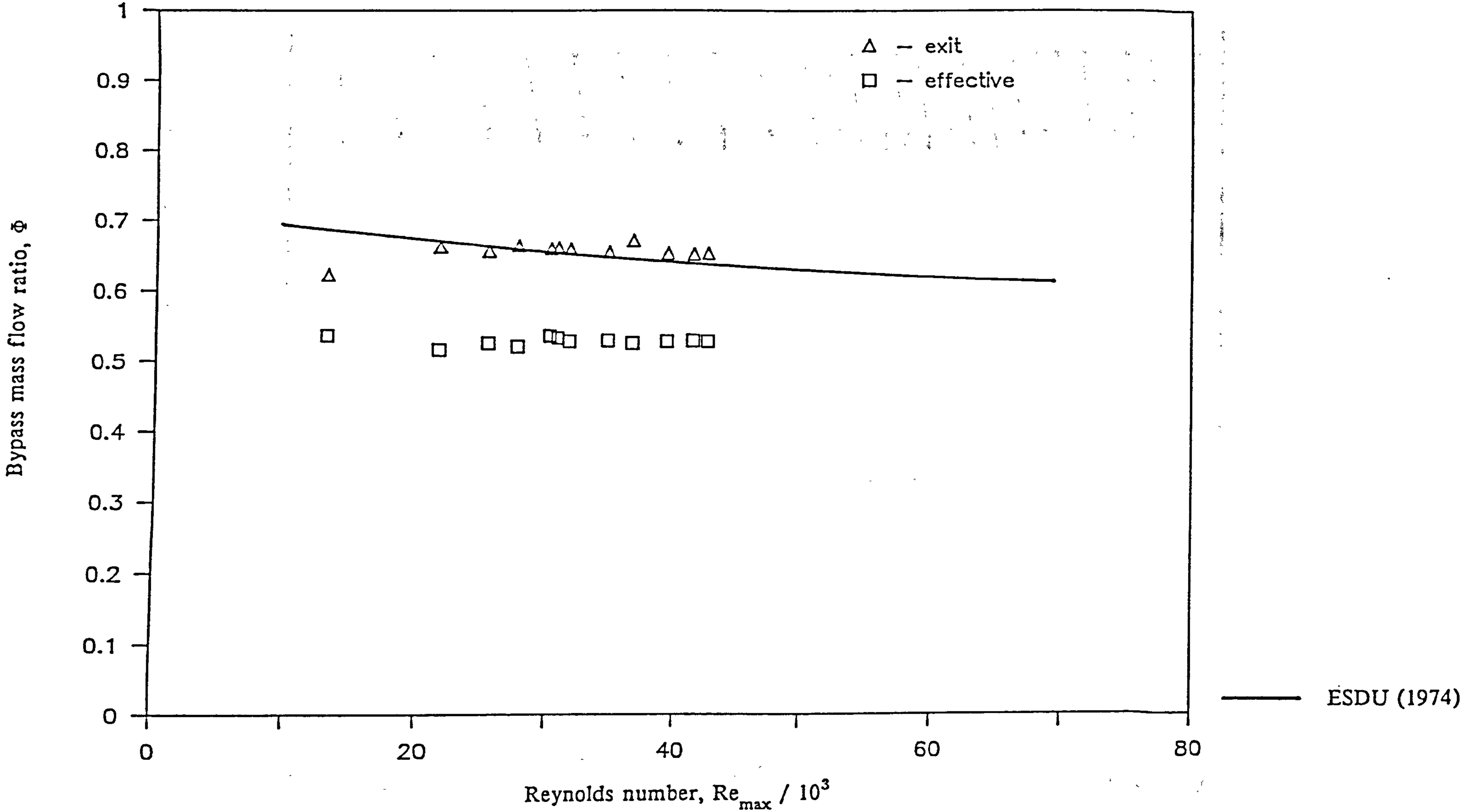

Figure 7.24 Bypass mass flow ratios for a 1.375 in-line square bank with a 1½S bypass.

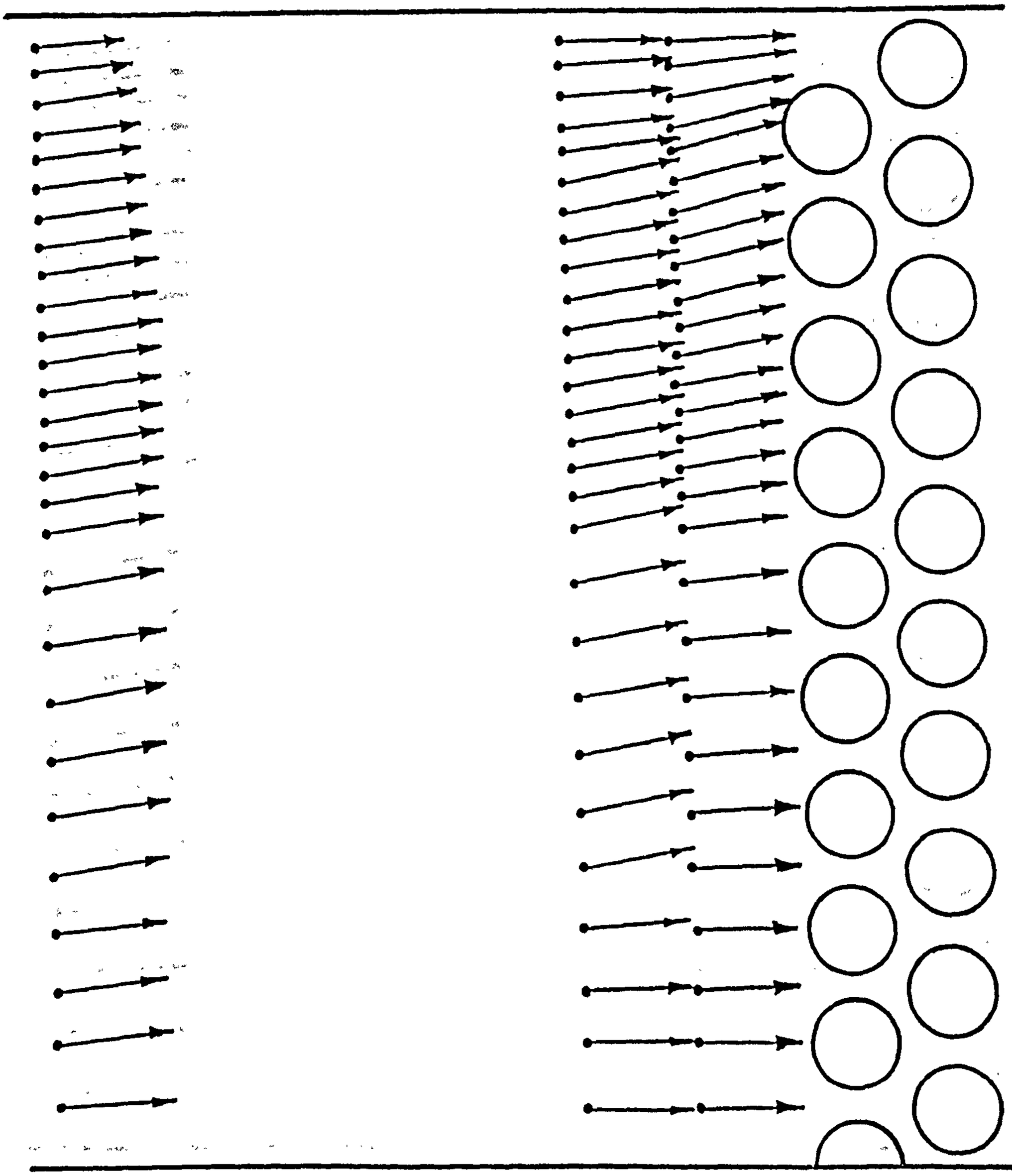

Figure 7.25 Upstream velocity profiles for a 1.25 equilateral-triangle bank with ¼T bypass.

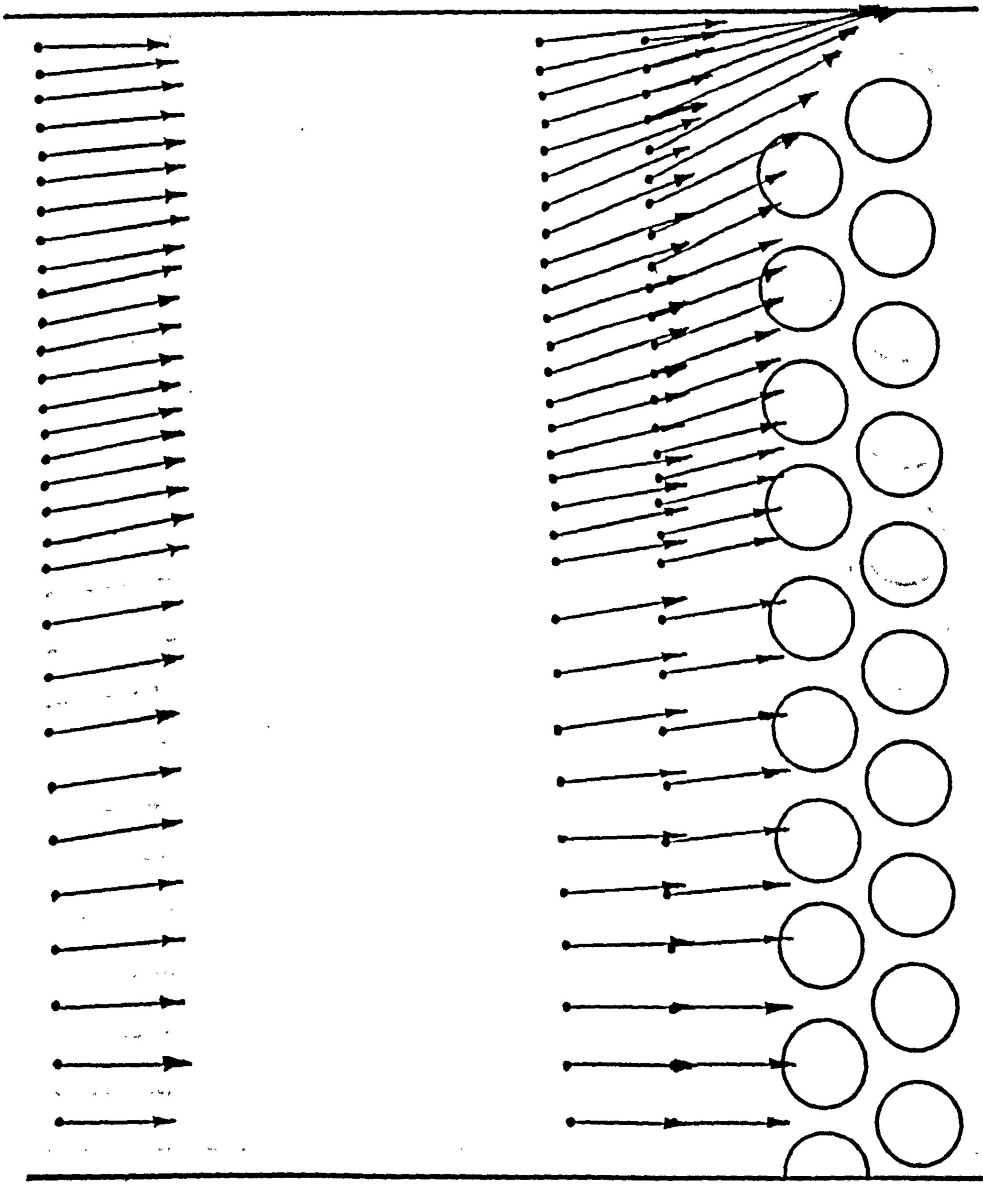

Figure 7.26 Upstream velocity profiles for a 1.25 equilateral-triangle bank with 1½T bypass.

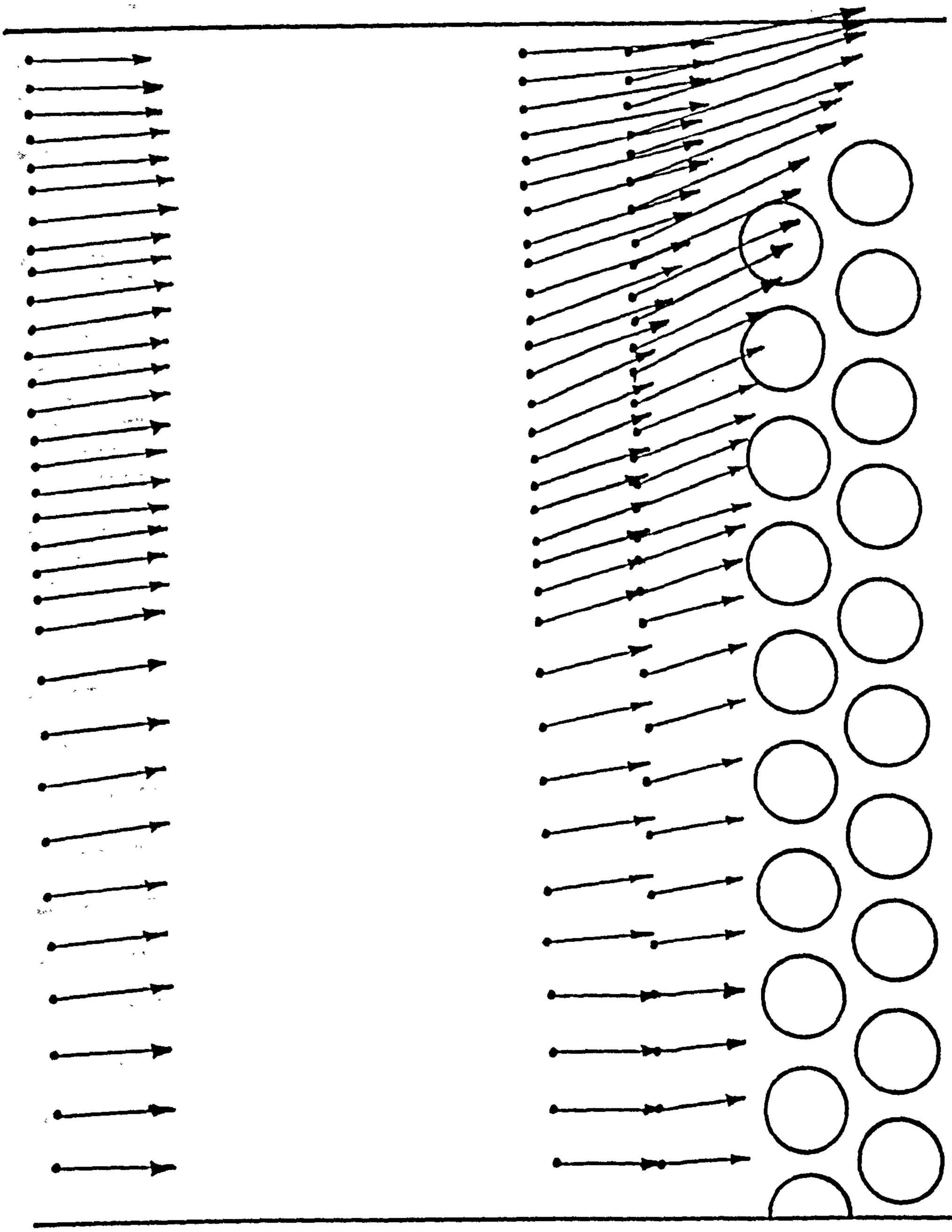

Figure 7.27 Upstream velocity profiles for a 1.25 equilateral-triangle bank with 2½T bypass.

⟵⟶ 10 m/s

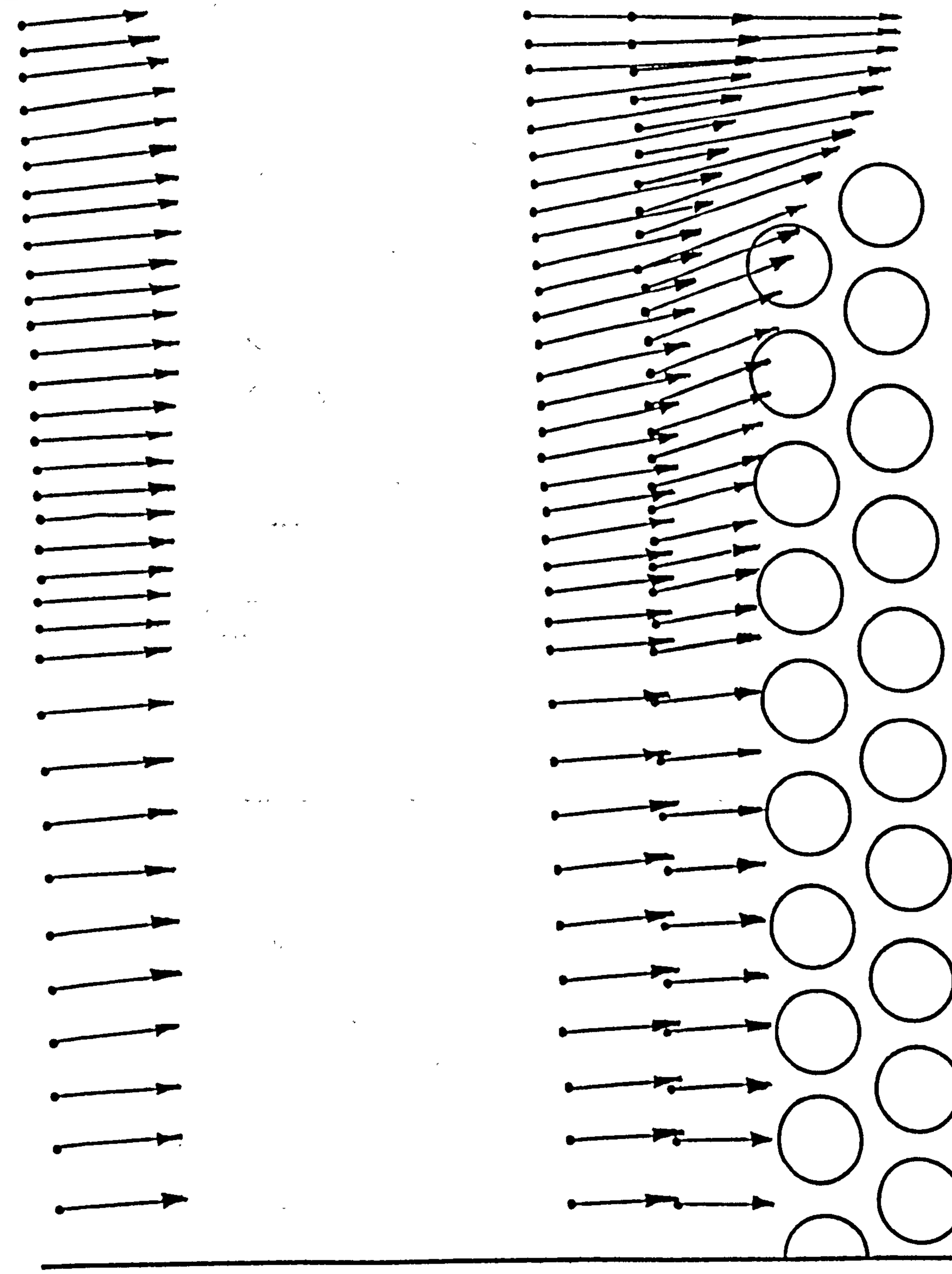

Figure 7.28 Upstream velocity profiles for a 1.25 equilateral-triangle bank with 3½T bypass. ⟵ 10 m/s

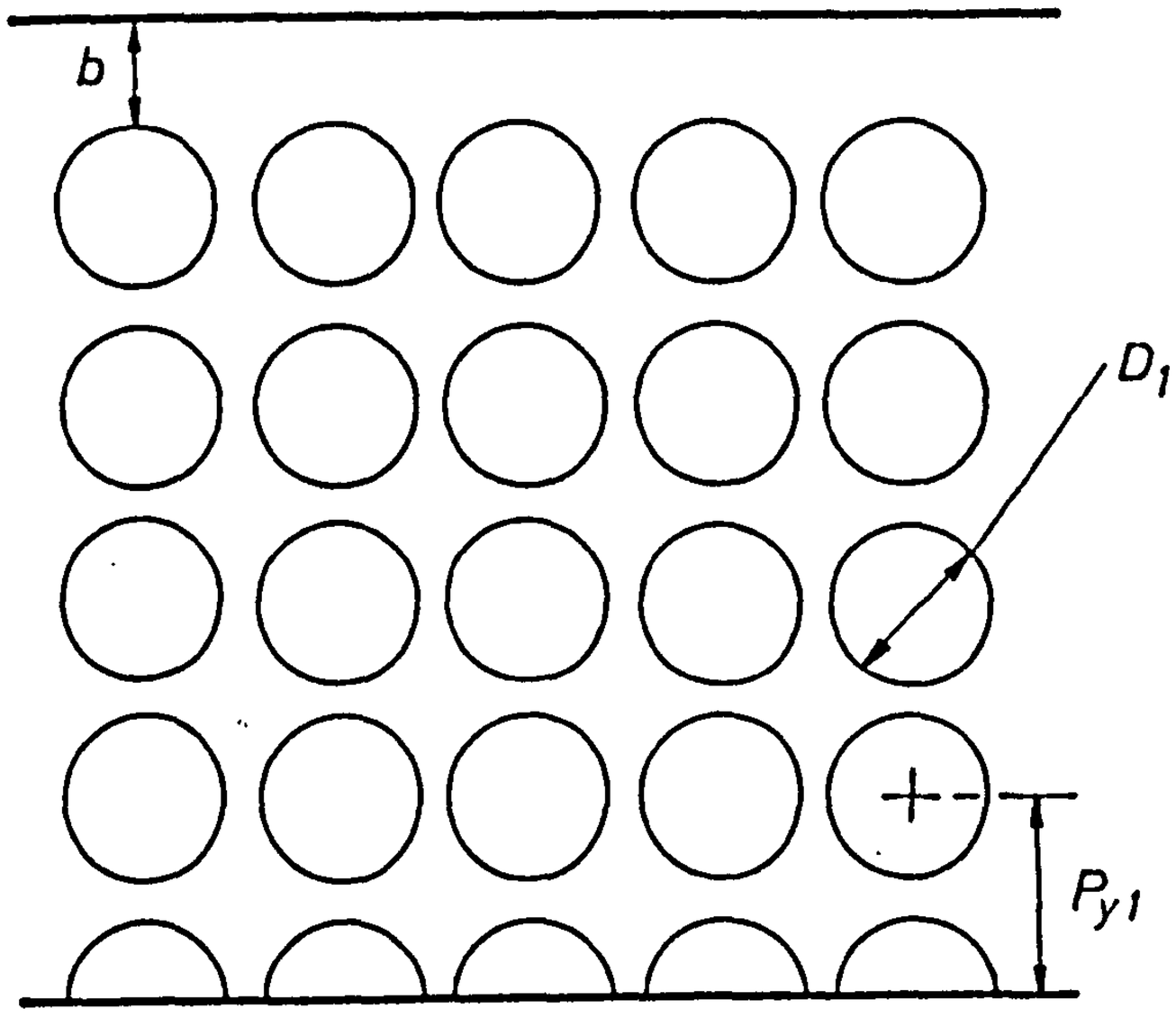

(a) Bank with b bypass clearance and $n = 4.5$ tube rows across the flow

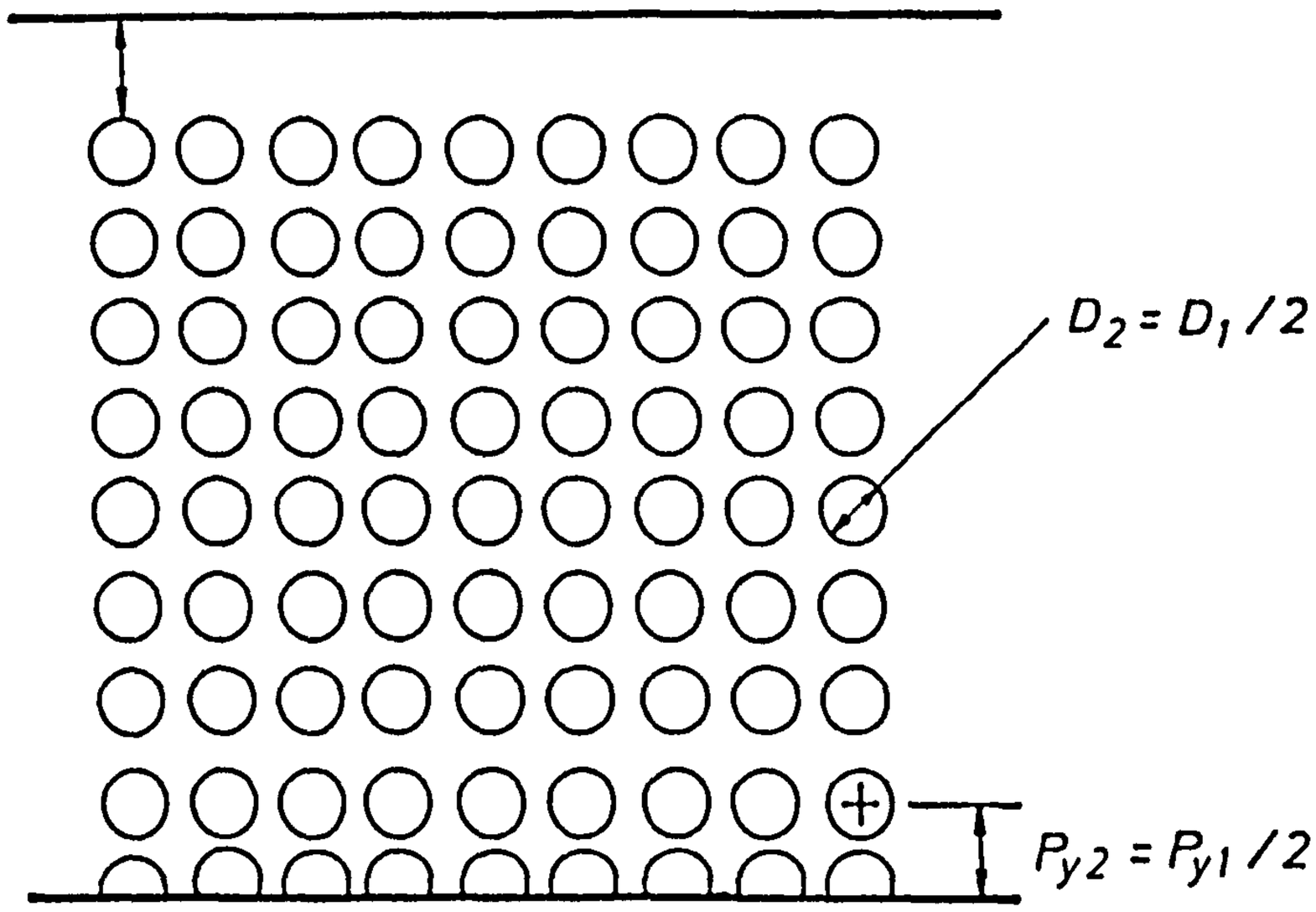

(b) Bank with b bypass clearance and $n = 8.5$ tube rows across the flow, having the same pitch/diameter ratio, and array type and for which $(n_1 - 0.5) P_{y1} = (n_1 - 0.5) P_{y1}$, hence $F_1 = F_2$

Figure 7.29 Two different bank geometries having the same value of F.

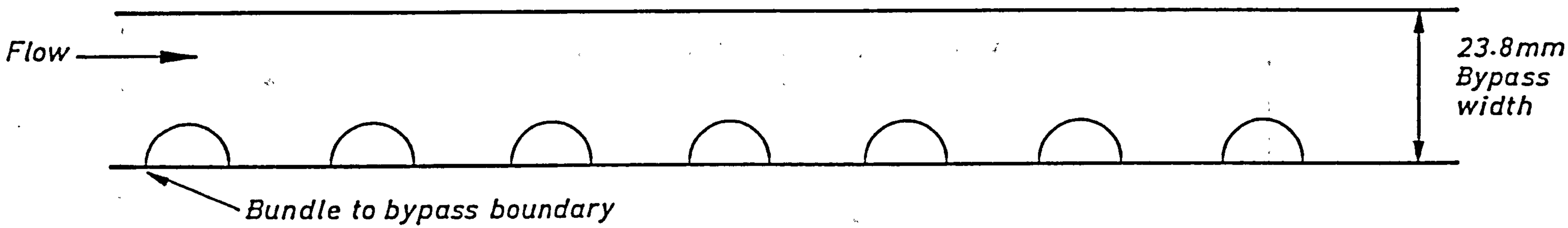

(a) Bypass lane alone, no flow transfer. Equivalent to bypass in 1.25 triangular array with 2½ T bypass.

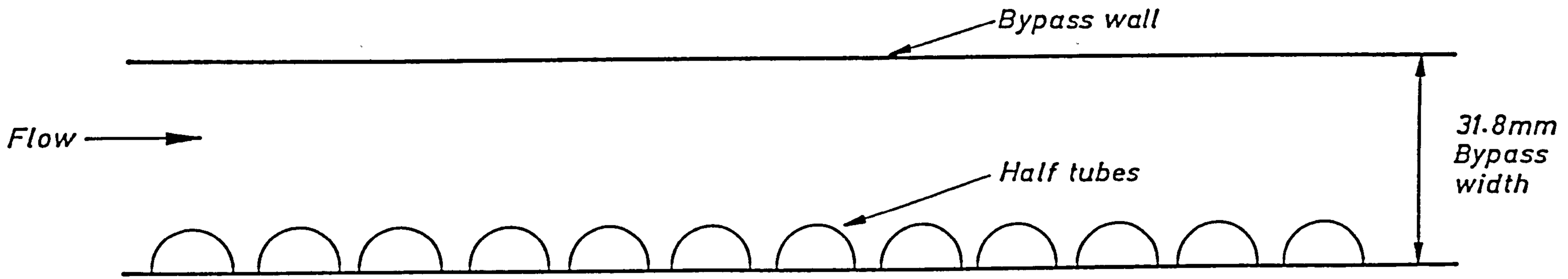

(b) Bypass lane alone, no flow transfer. Equivalent to bypass in 1.25 square array with 1½S bypass.

Figure 8.1 Typical geometries of ducts used for tests of the bypass lane alone, with no flow transfer from the bundle.

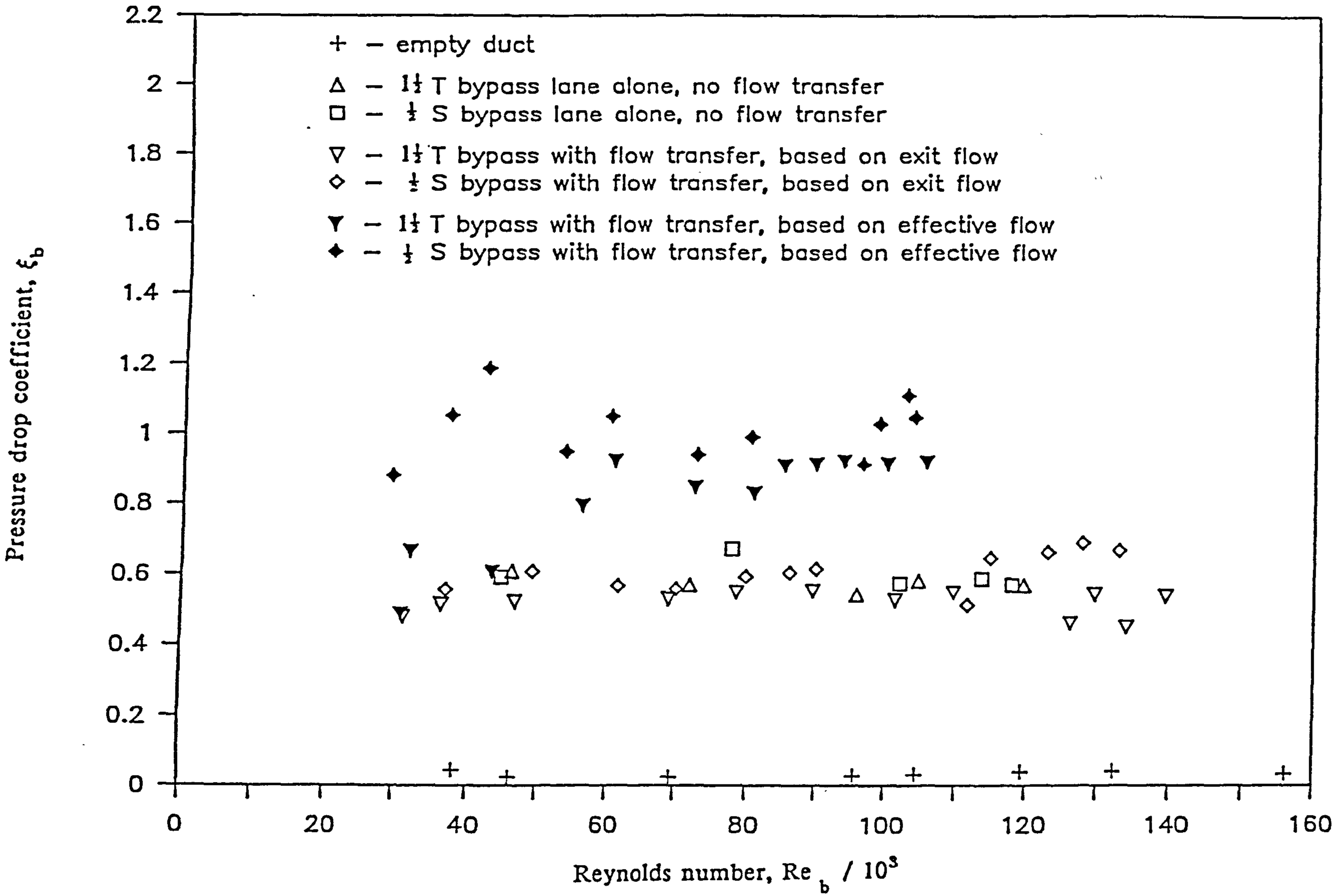

Figure 8.2 Pressure drop coefficients for a 15.9mm bypass width, with no flow transfer from the bundle.

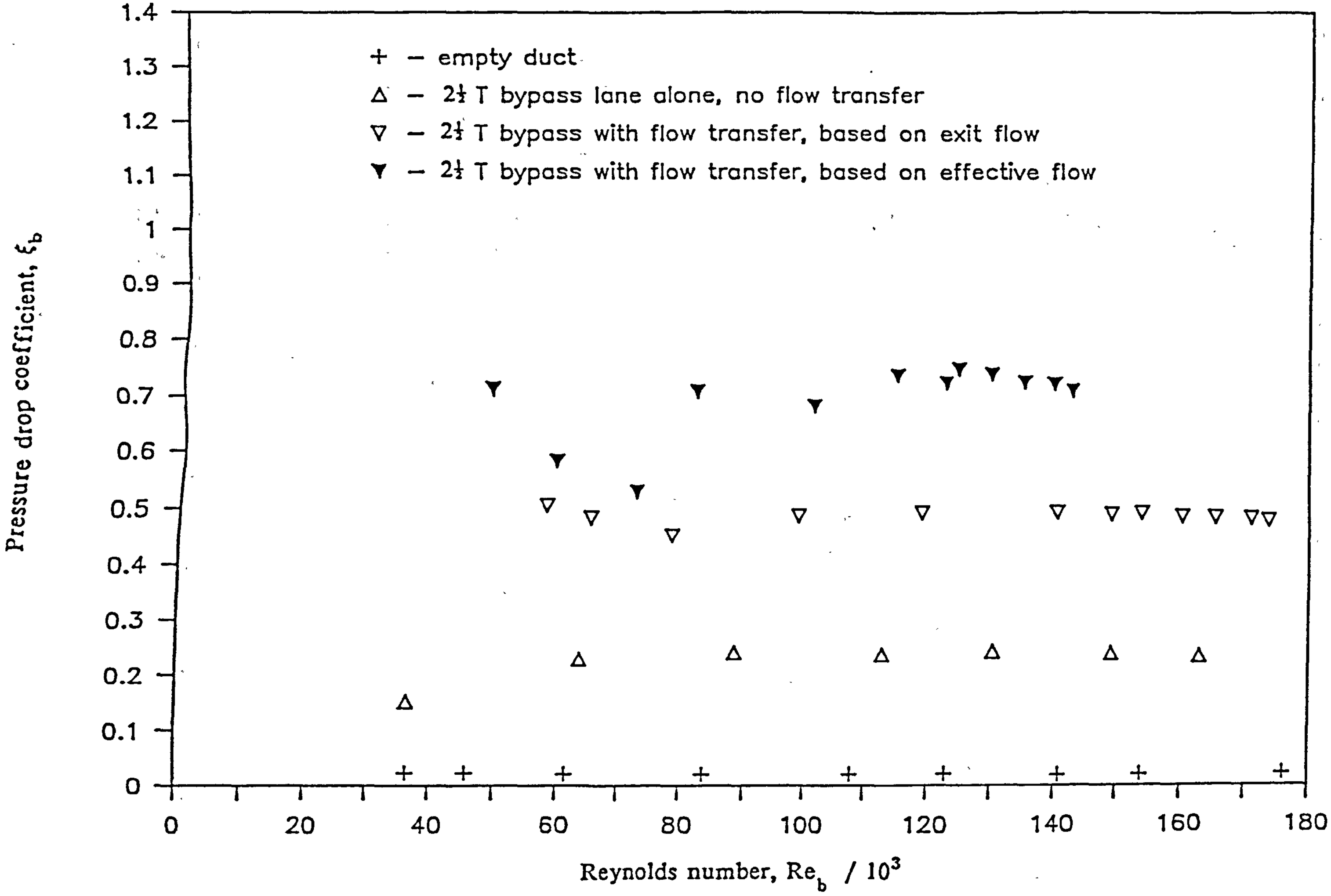

Figure 8.3 Pressure drop coefficients for a 23.8mm bypass width, with no flow transfer from the bundle.

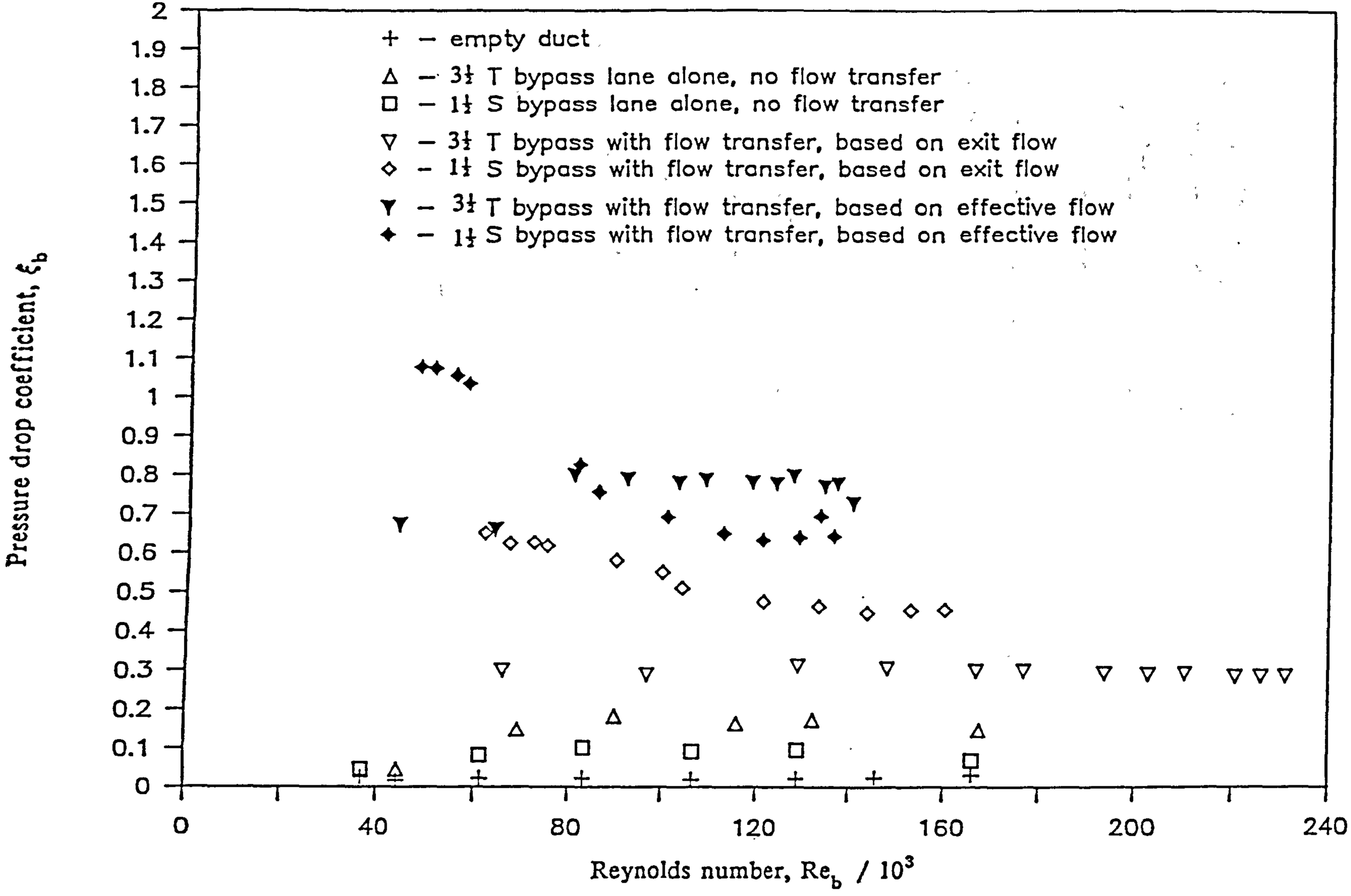

Figure 8.4 Pressure drop coefficients for a 31.8mm bypass width, with no flow transfer from the bundle.

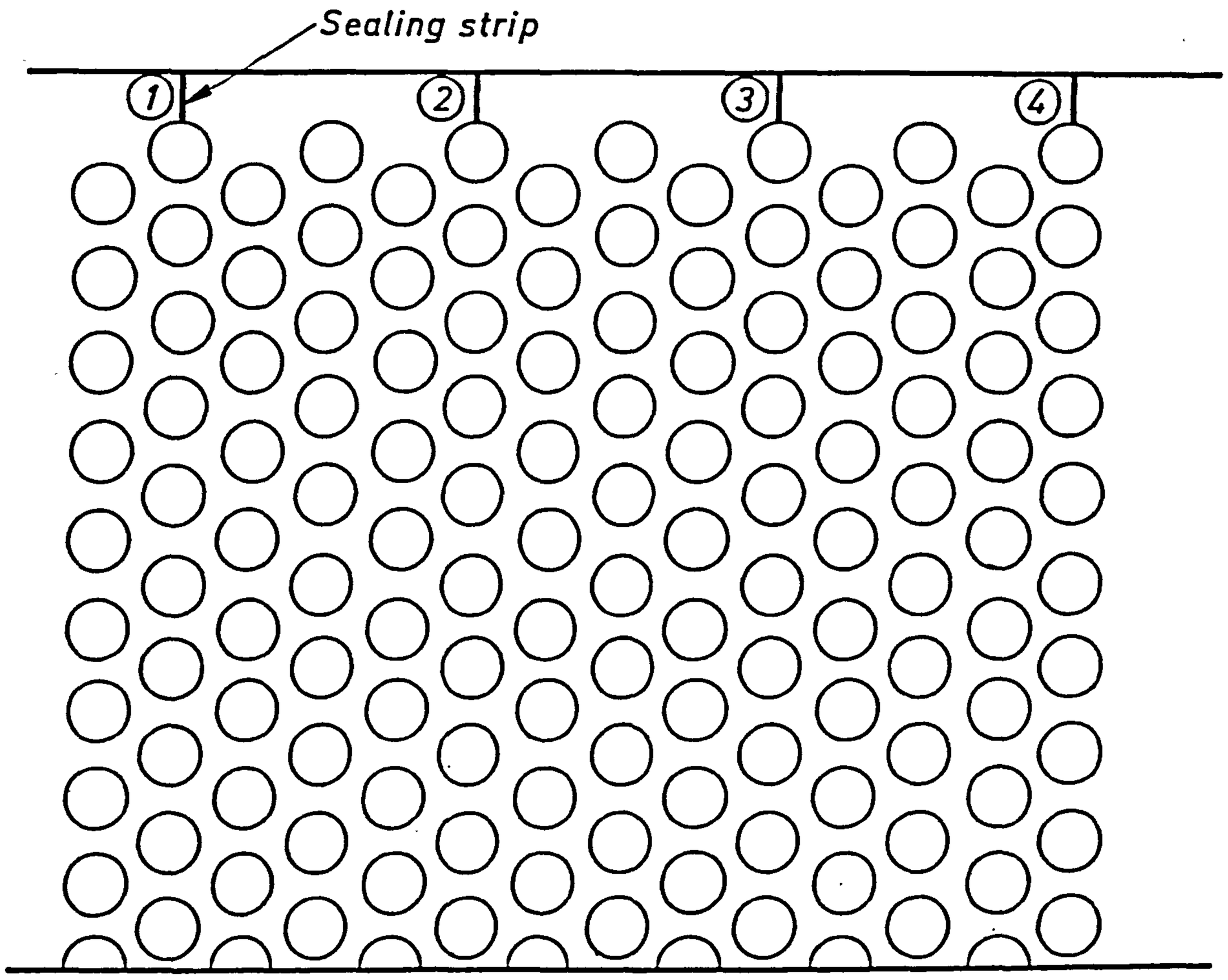

For: N_s = 1, only sealing-strip number (1) is used.

N_s = 2, only sealing-strips numbers (1) and (4) are used.

N_s = 4, sealing-strips numbers (1), (2), (3) and (4) are used.

Figure 9.1 Sealing-strip locations in rectangular tube banks.

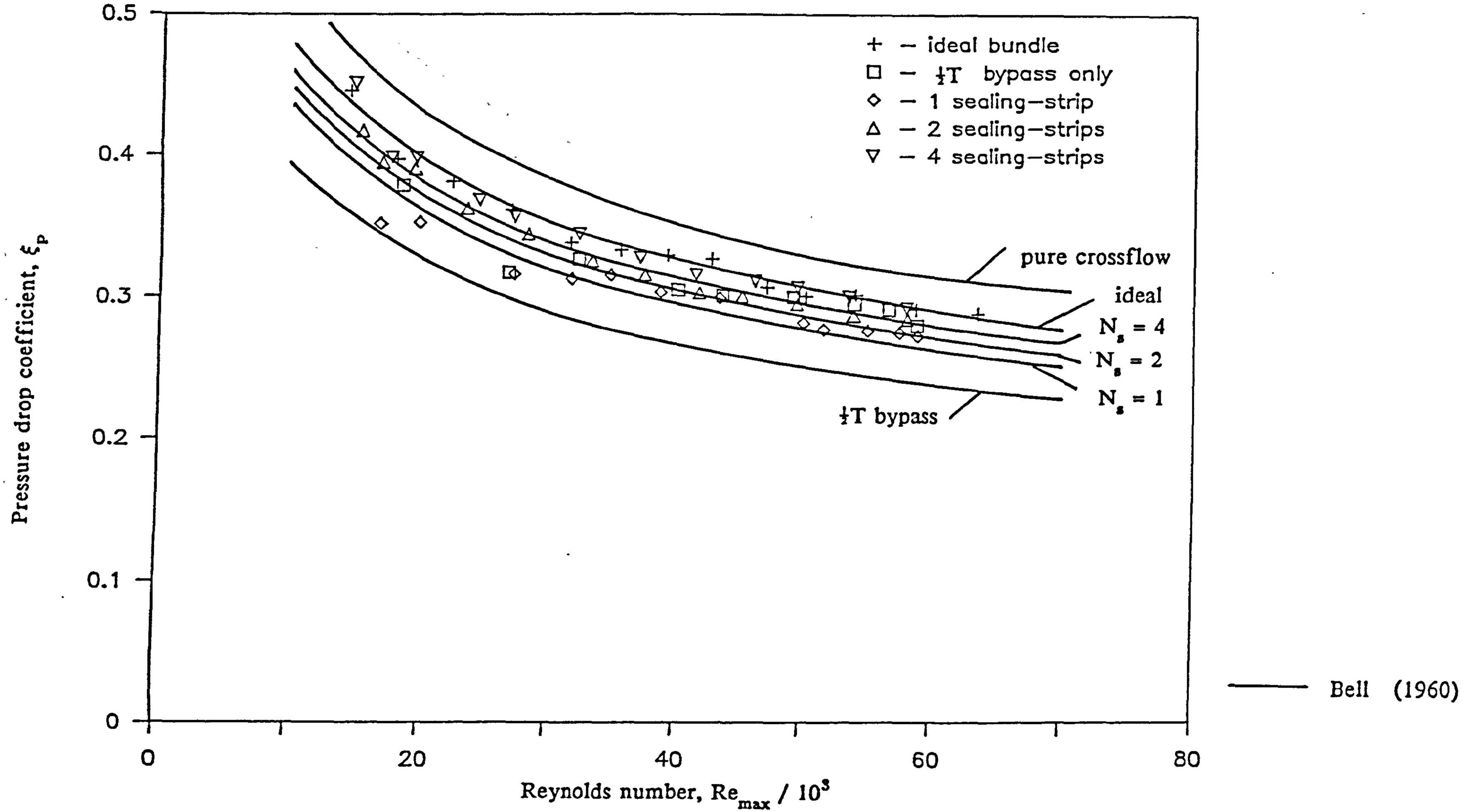

Figure 9.2 Pressure drop coefficient for a 1.25 equilateral-triangle bank having a ½T bypass and sealing-strips.

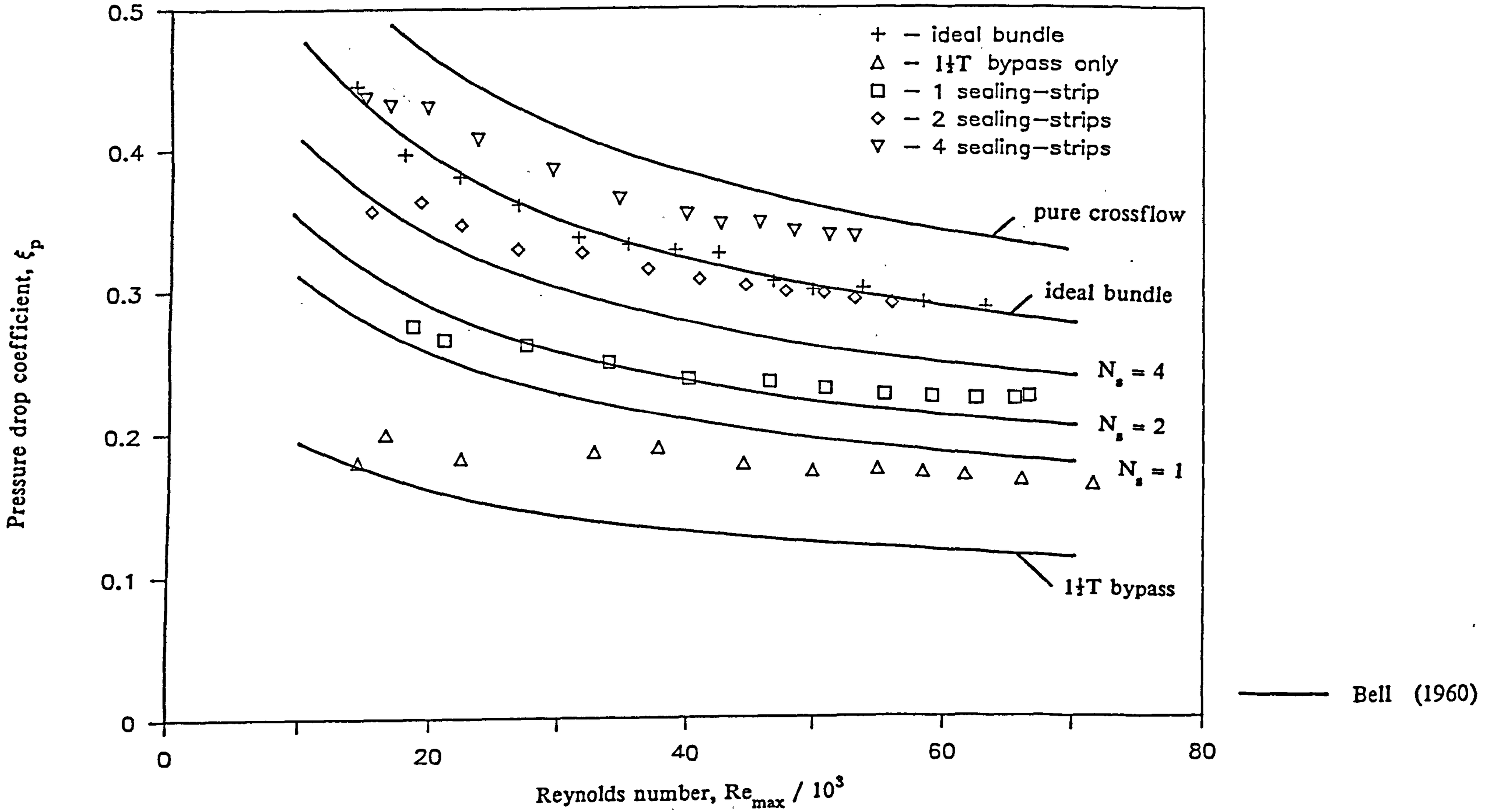

Figure 9.3 Pressure drop coefficient for a 1.25 equilateral-triangle bank having a 1½T bypass and sealing-strips.

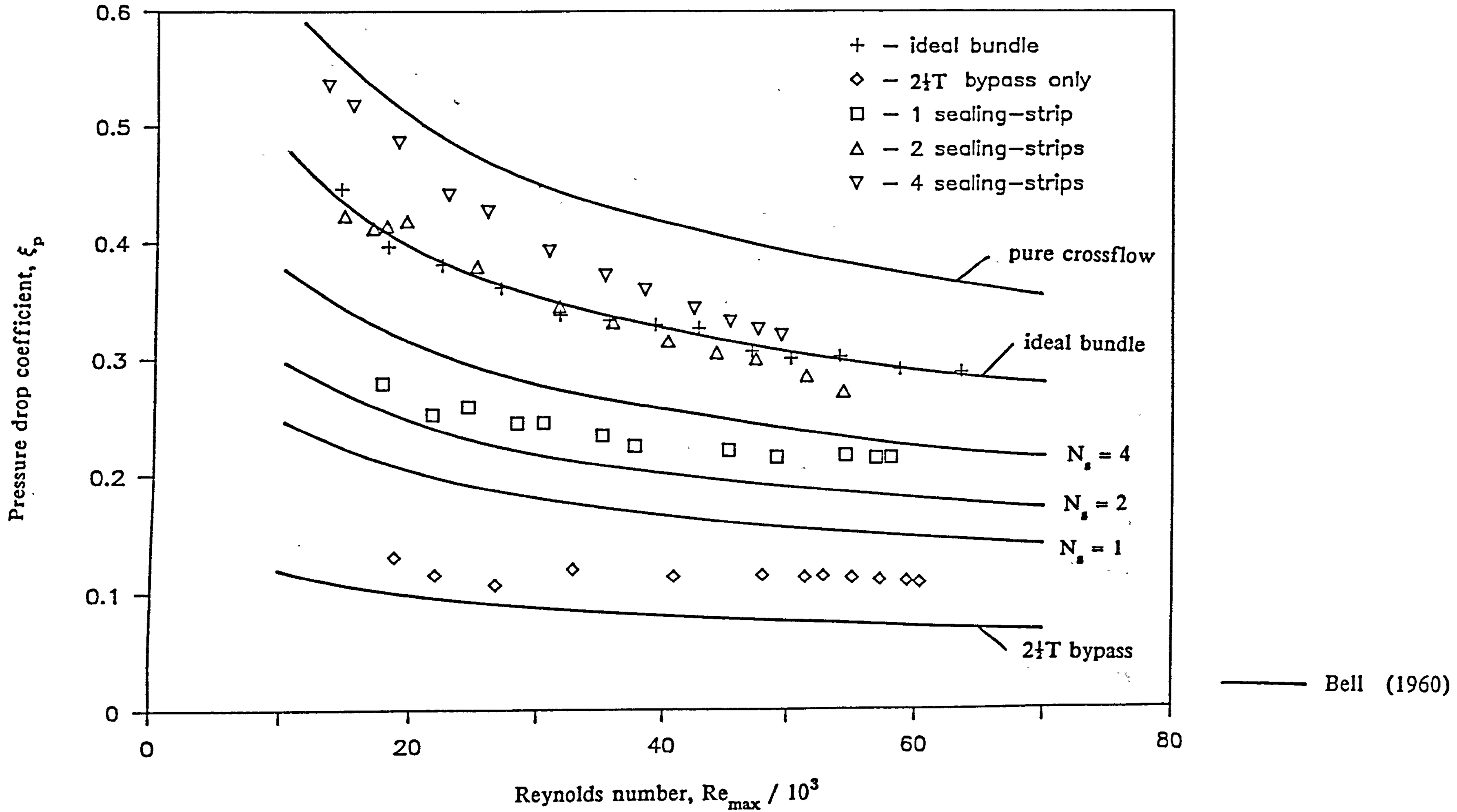

Figure 9.4 Pressure drop coefficient for a 1.25 equilateral-triangle bank having a 2½T bypass and sealing-strips.

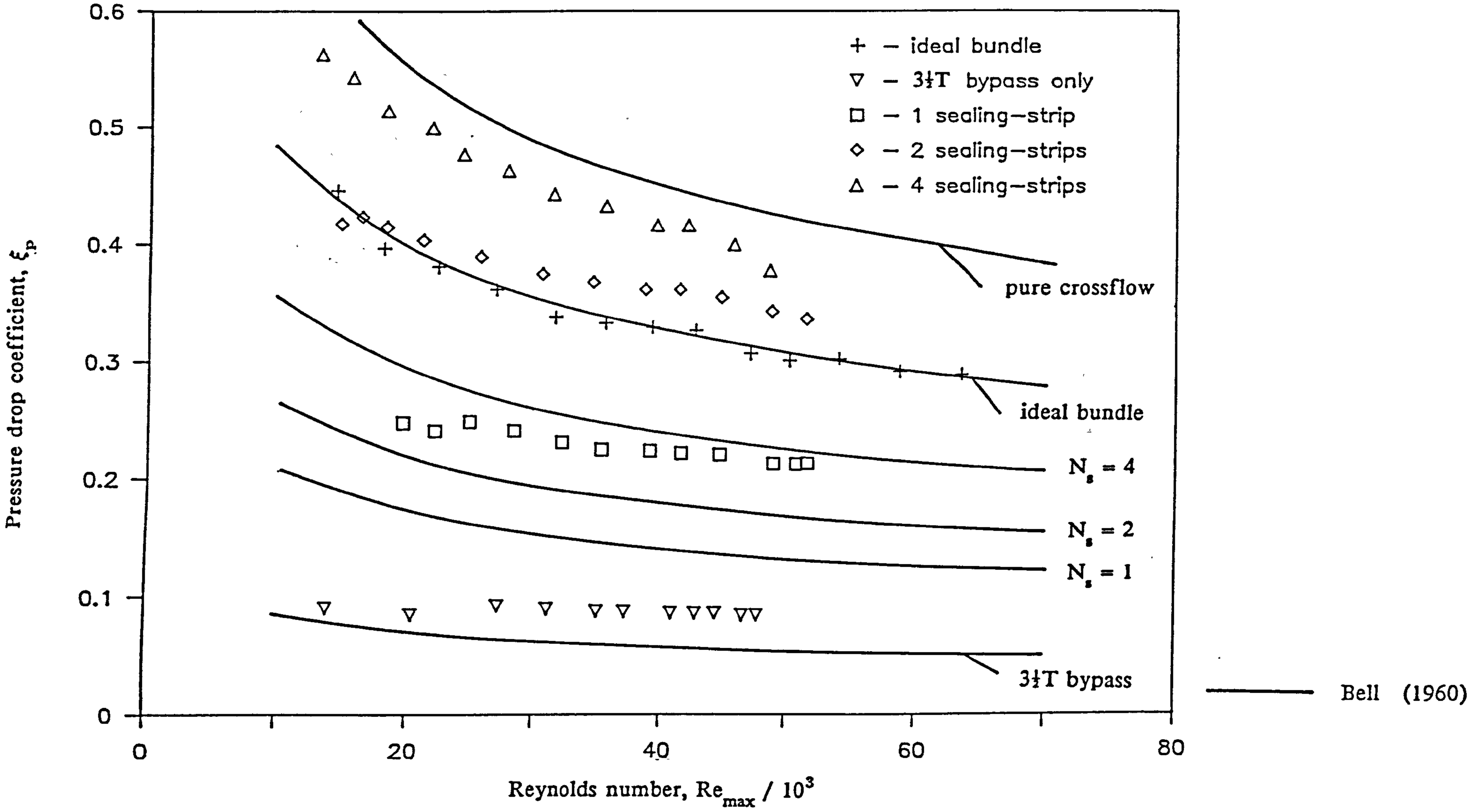

Figure 9.5 Pressure drop coefficient for a 1.25 equilateral-triangle bank having a 3½T bypass and sealing-strips.

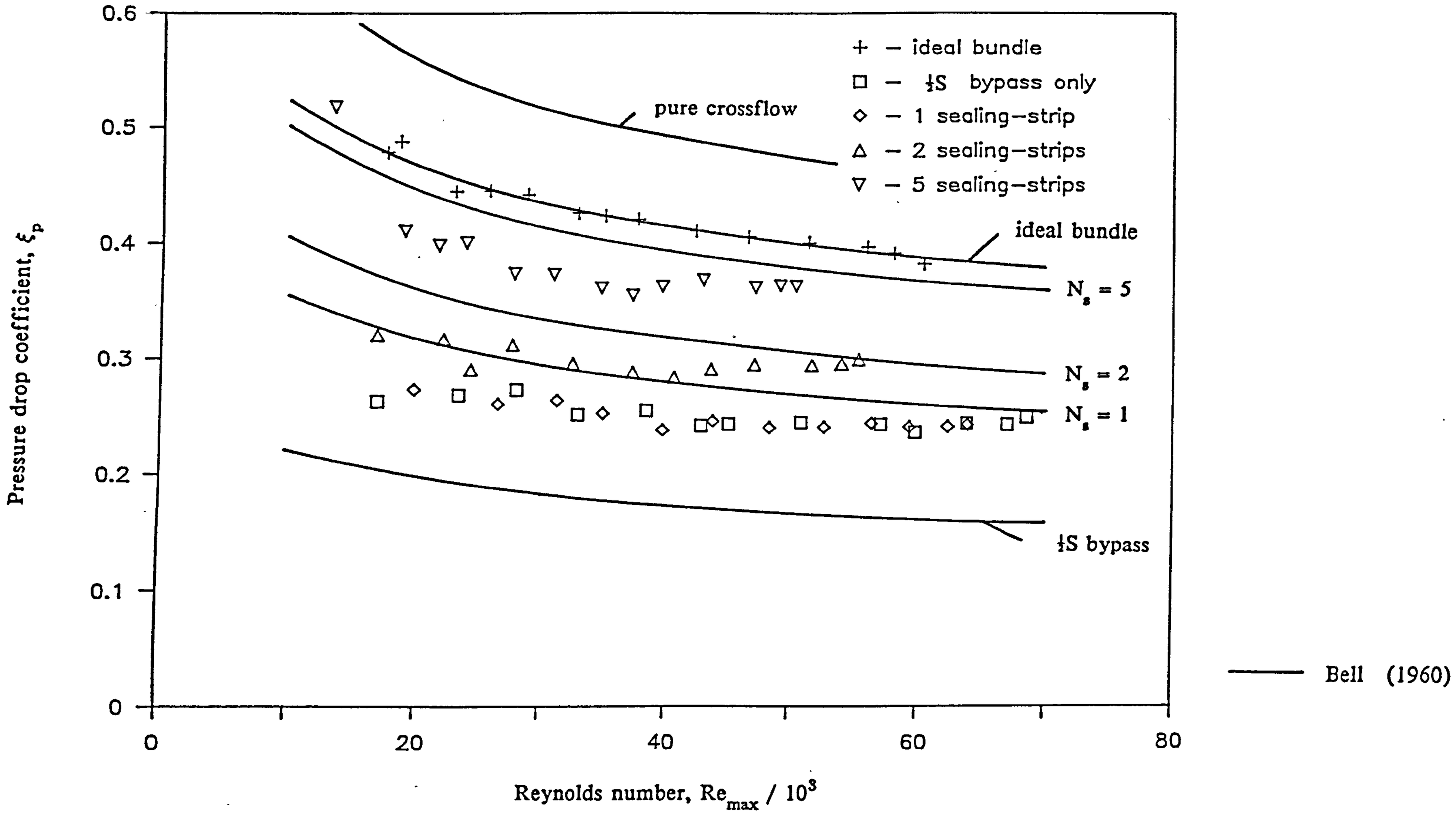

Figure 9.6 Pressure drop coefficient for a 1.25 in-line square bank having a ½S bypass and sealing-strips.

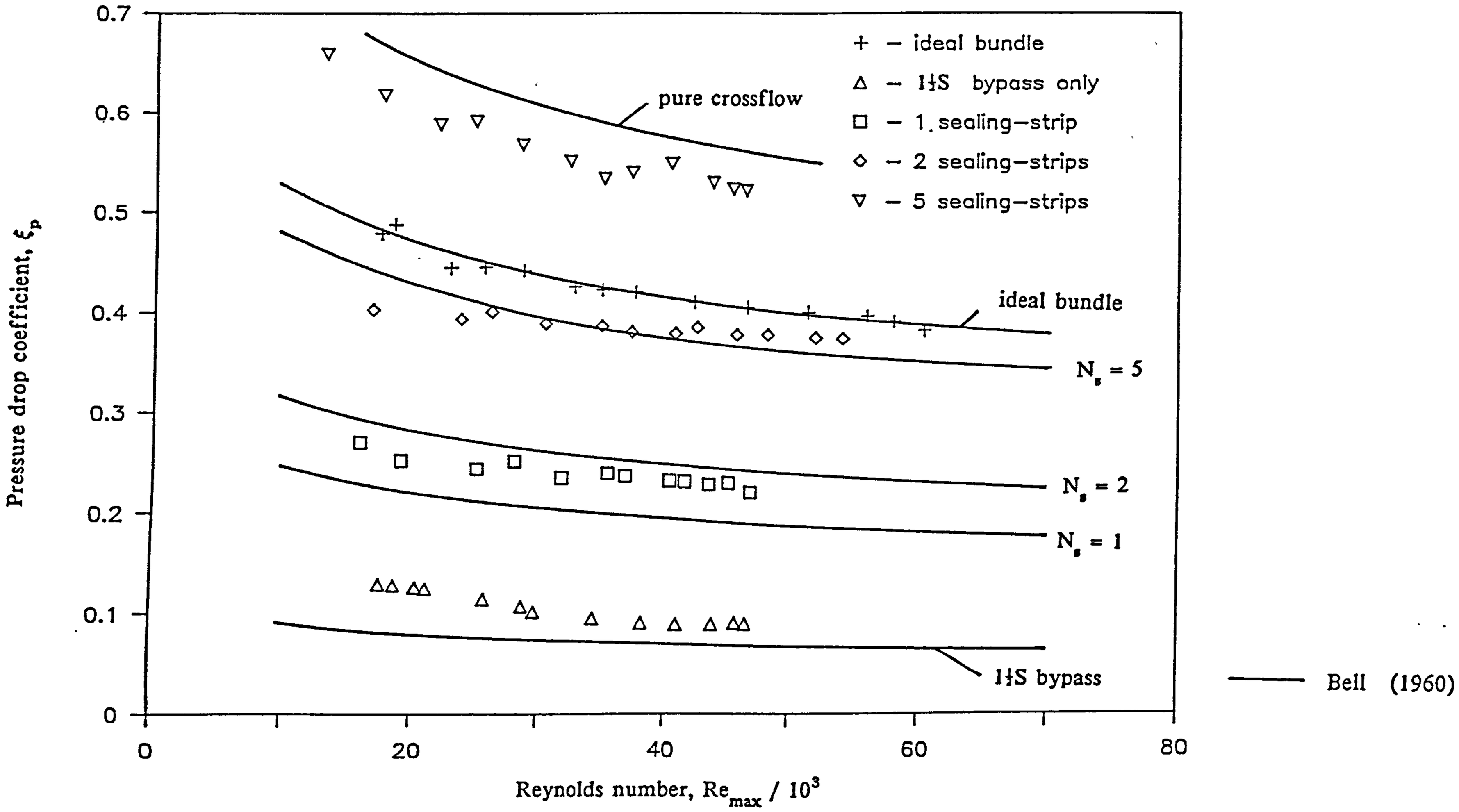

Figure 9.7 Pressure drop coefficient for a 1.25 in-line square bank having a 1½S bypass and sealing-strips.

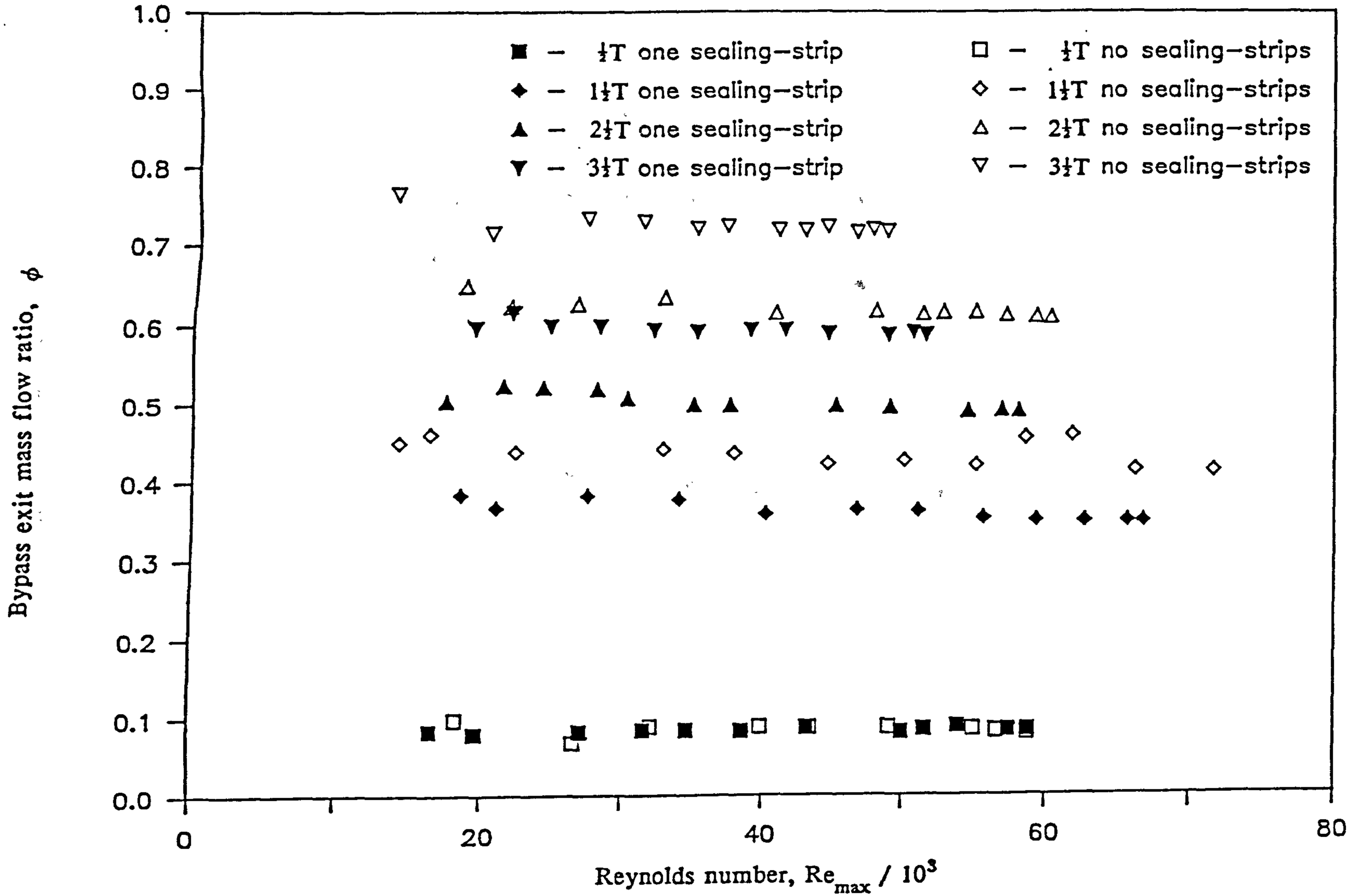

Figure 9.8 Bypass mass flow ratios for 1.25 equilateral-triangle banks having ½T, 1½T, 2½T and 3½T bypasses and one sealing-strip.

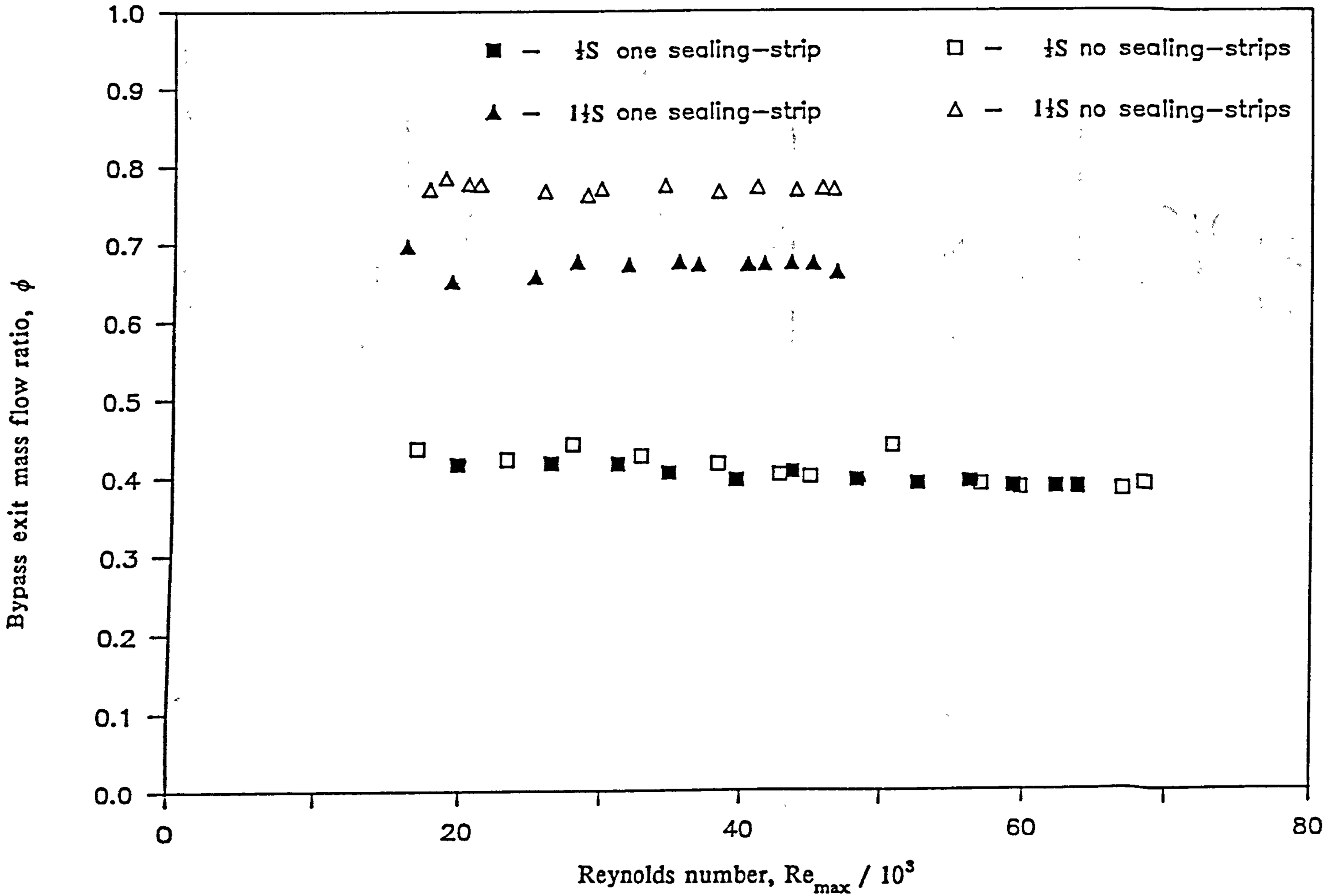

Figure 9.9 Bypass mass flow ratios for 1.25 in-line square banks having ½S and 1½S bypasses and one sealing-strip.

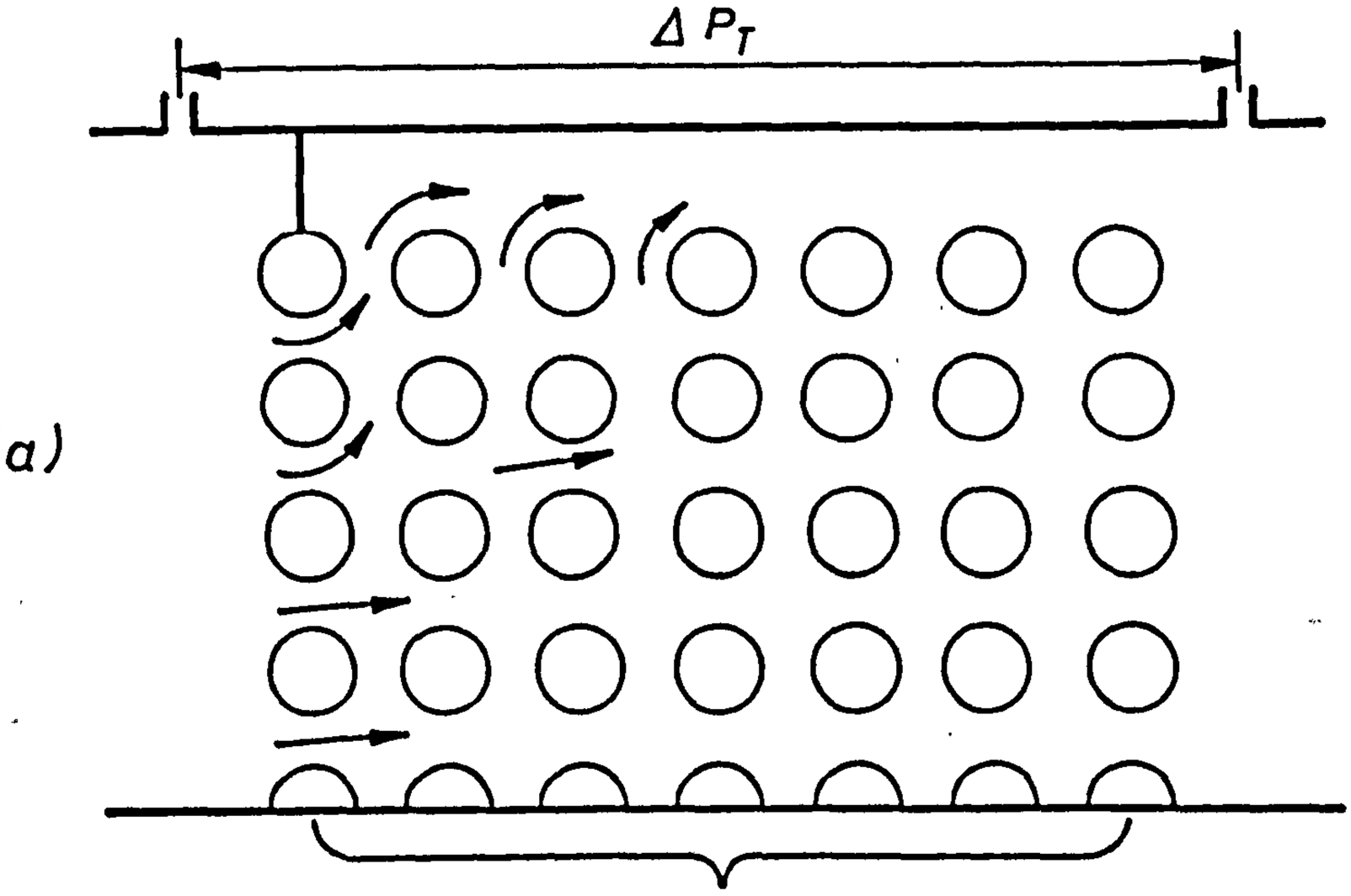

Figure 9.10 Definition of N_c, the number of rows of pure crossflow created per sealing-strip

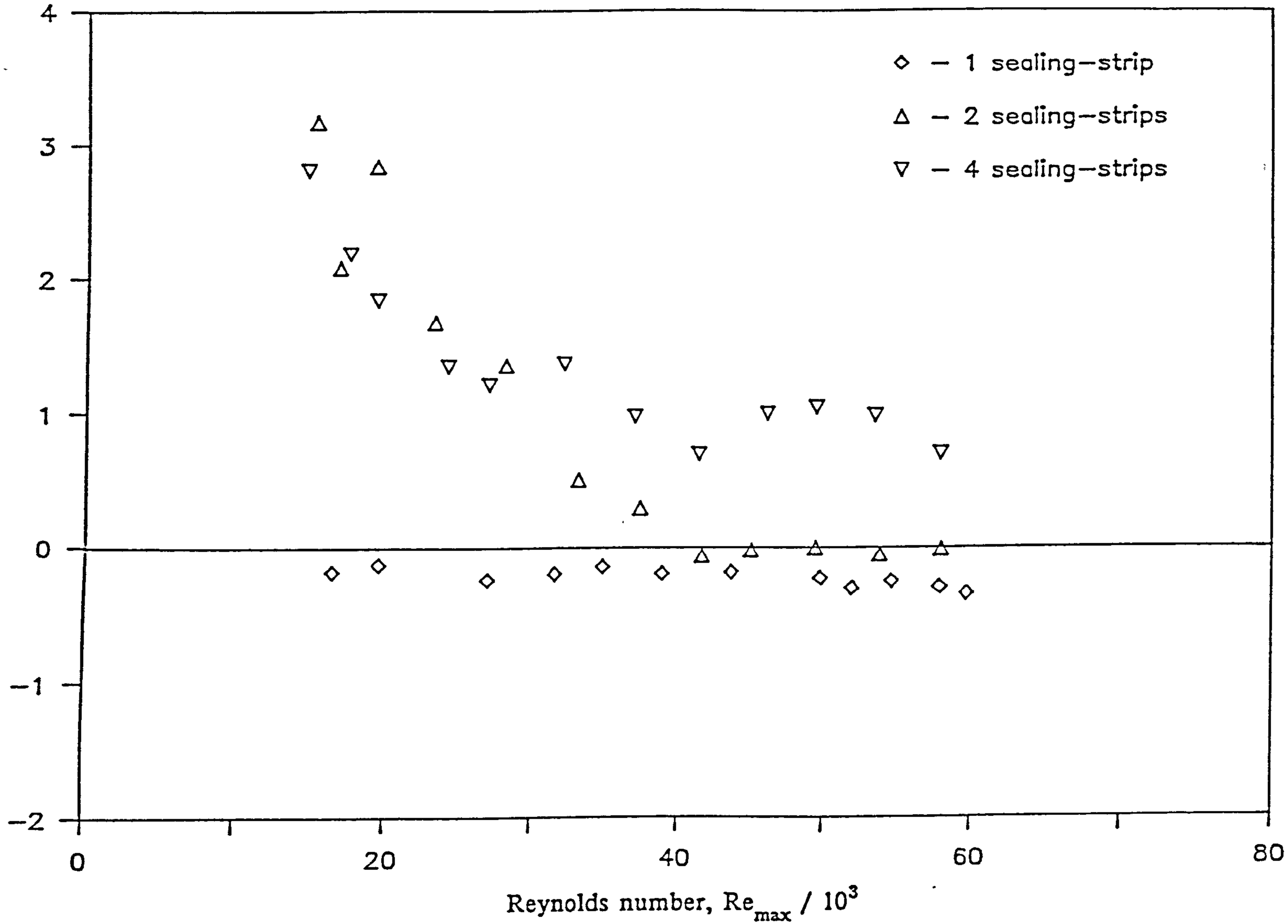

Figure 9.11 N_c for the 1.25 equilateral-triangle bank with a ¼T bypass and sealing-strips.

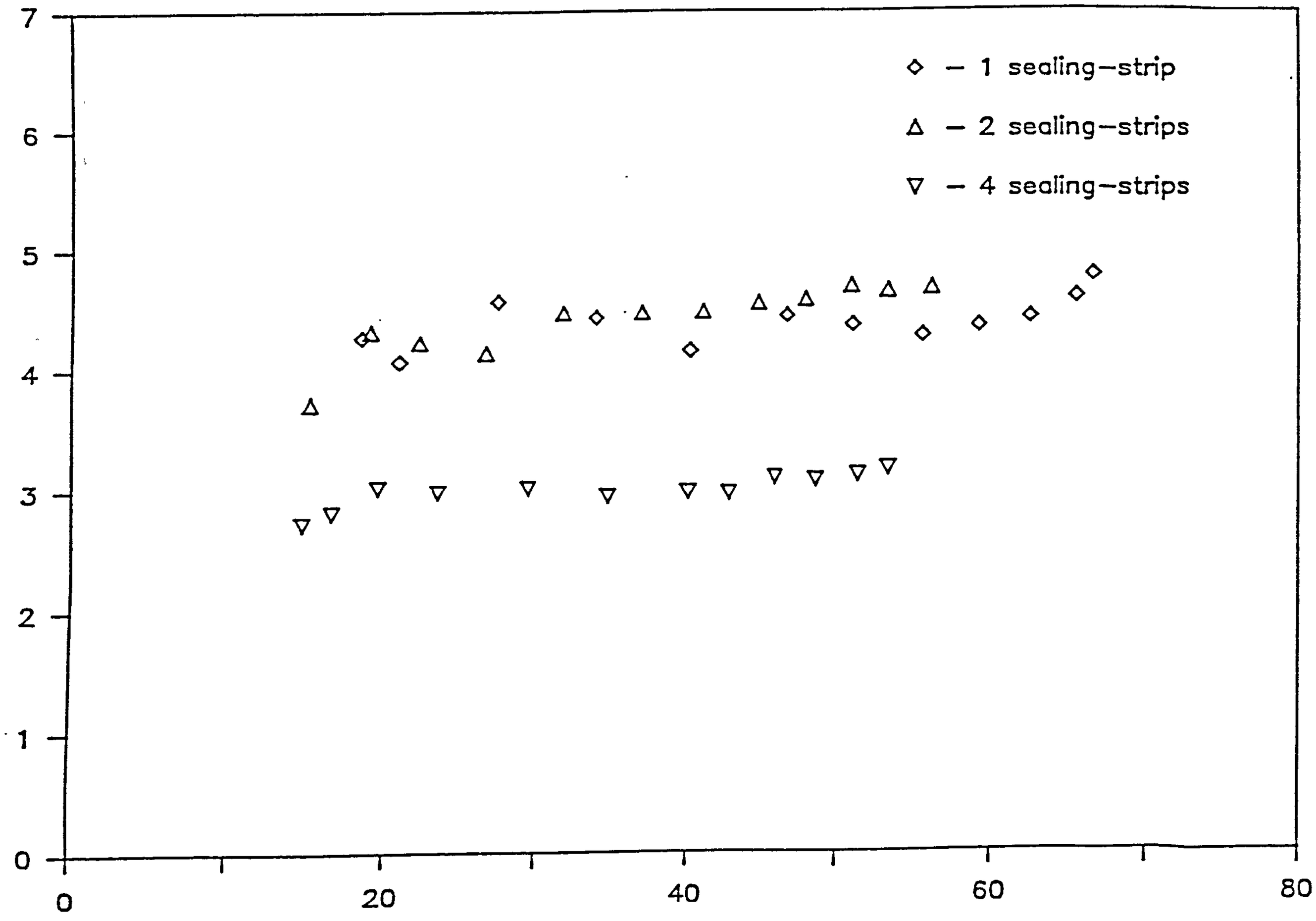

Figure 9.12 N_c for the 1.25 equilateral-triangle bank with a 1½T bypass and sealing-strips.

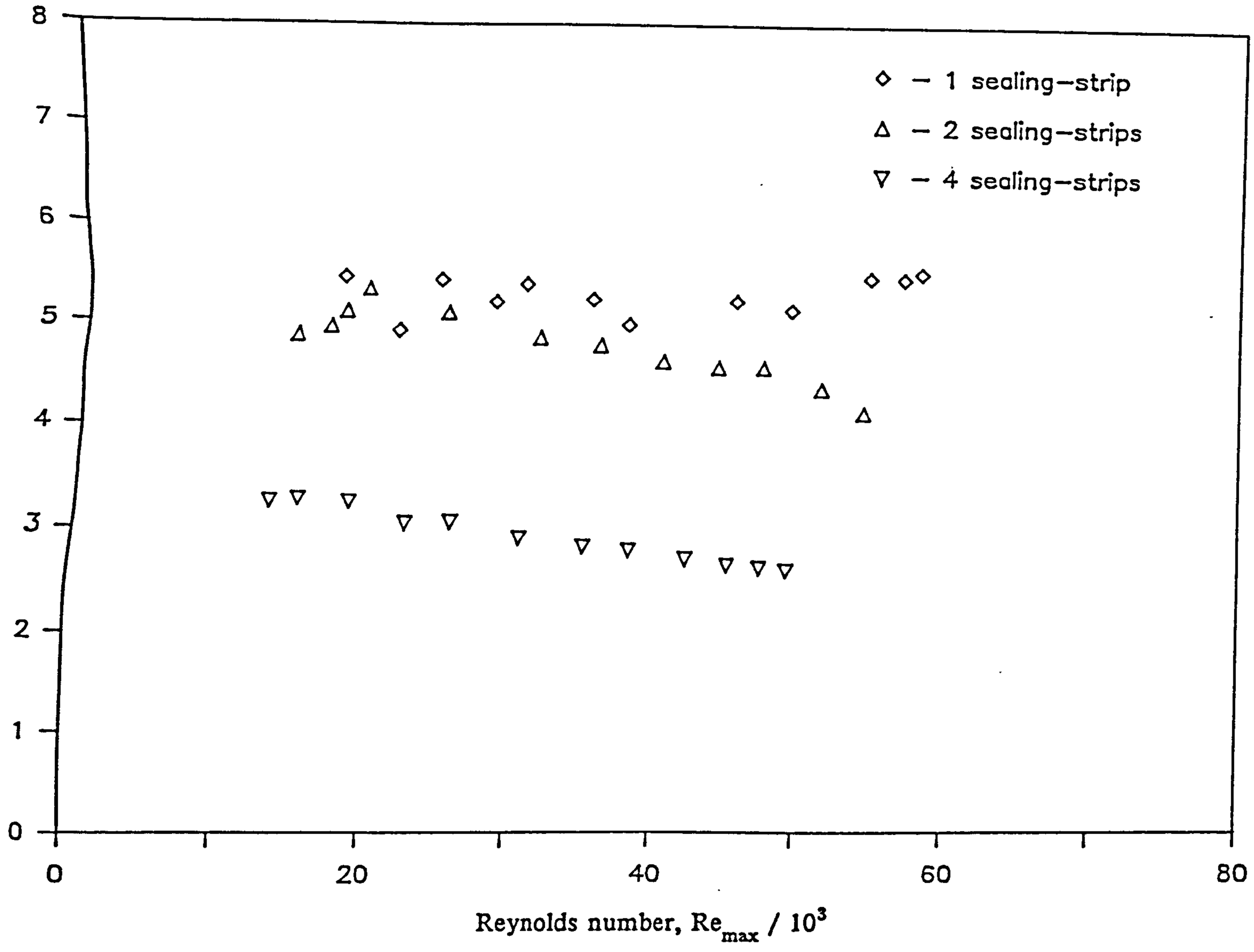

Figure 9.13 N_c for the 1.25 equilateral-triangle bank with a 2½T bypass and sealing-strips.

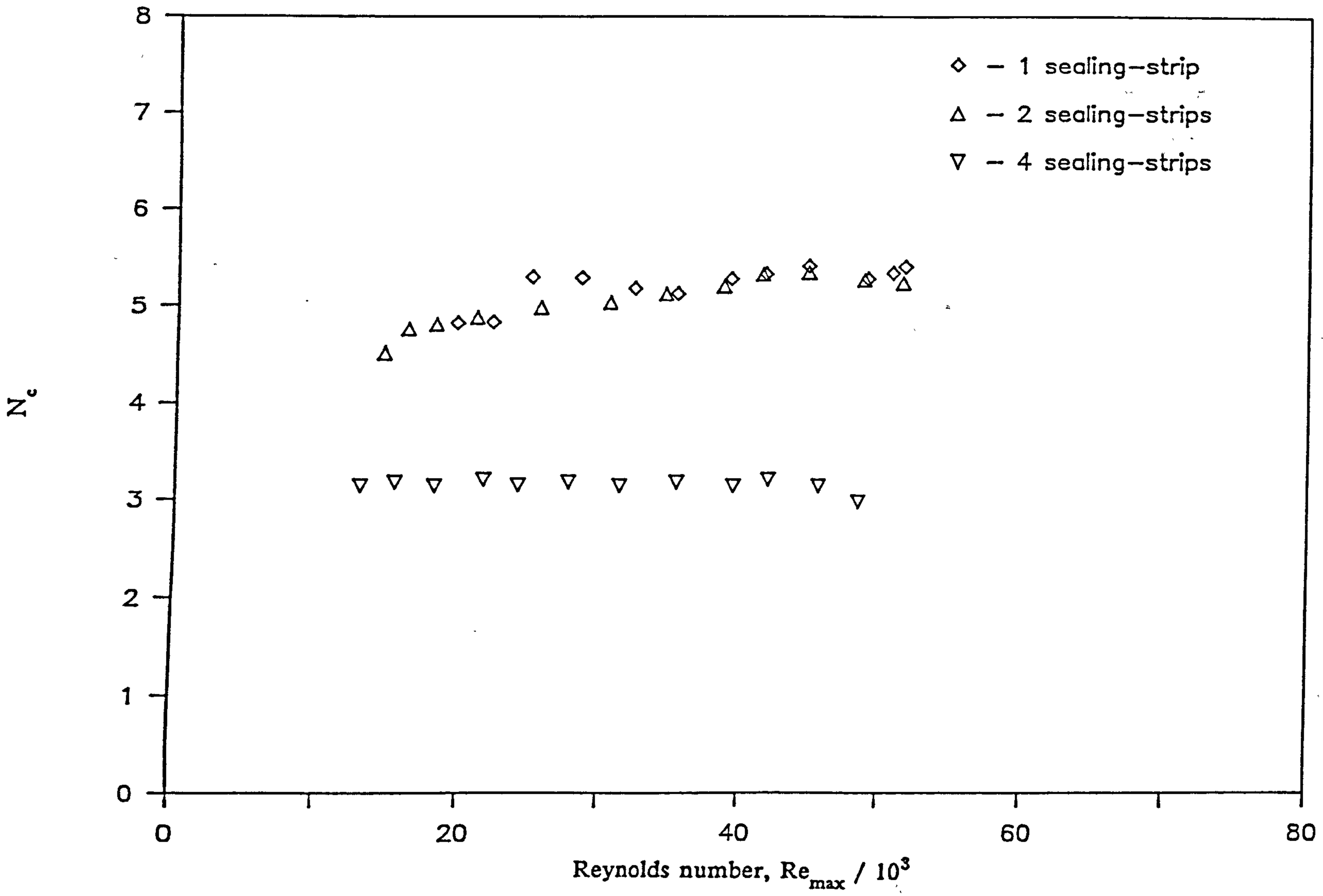

Figure 9.14 N_c for the 1.25 equilateral-triangle bank with a 3½T bypass and sealing-strips.

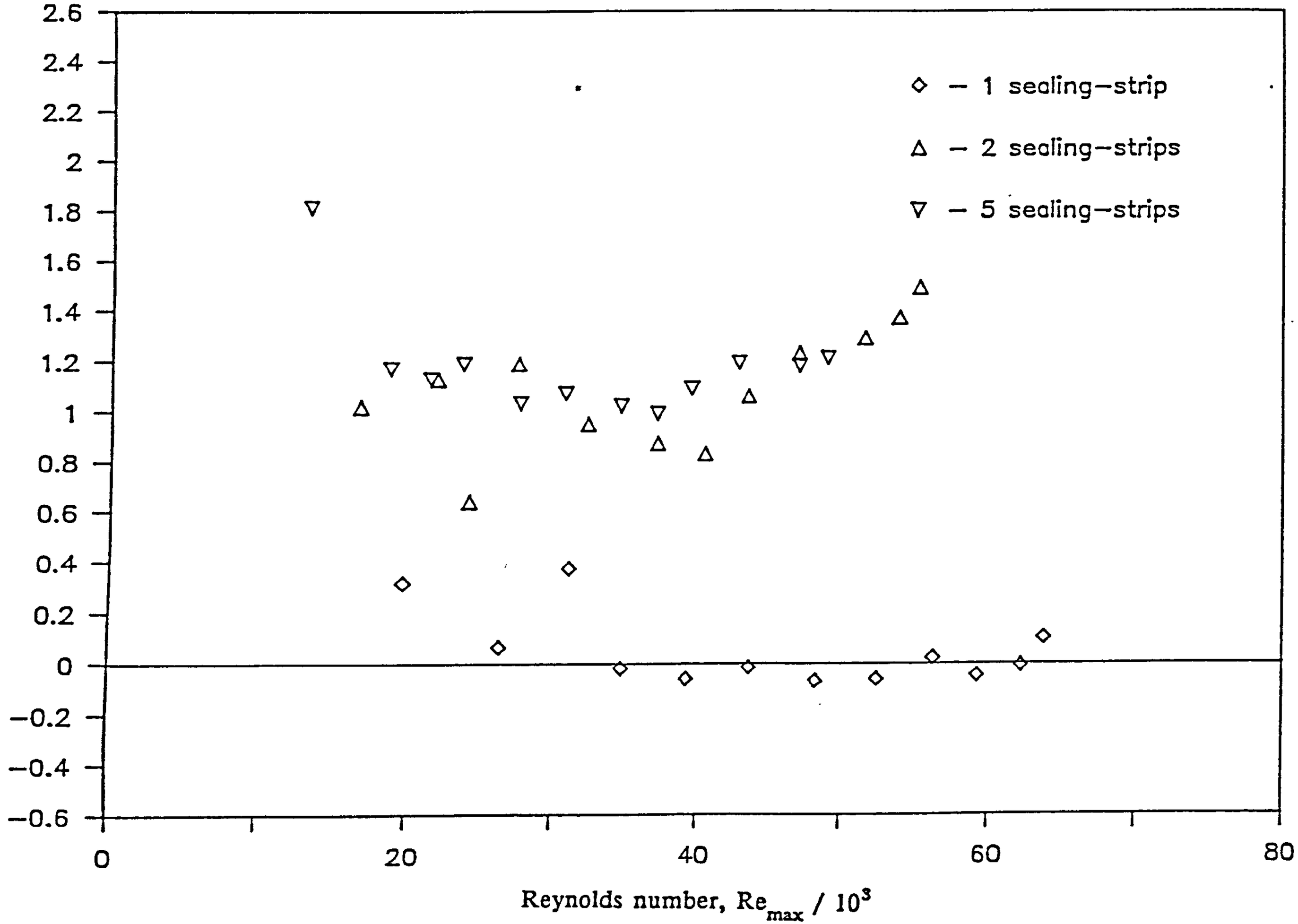

Figure 9.15 N_c for the 1.25 in-line square bank with a ½S bypass and sealing-strips.

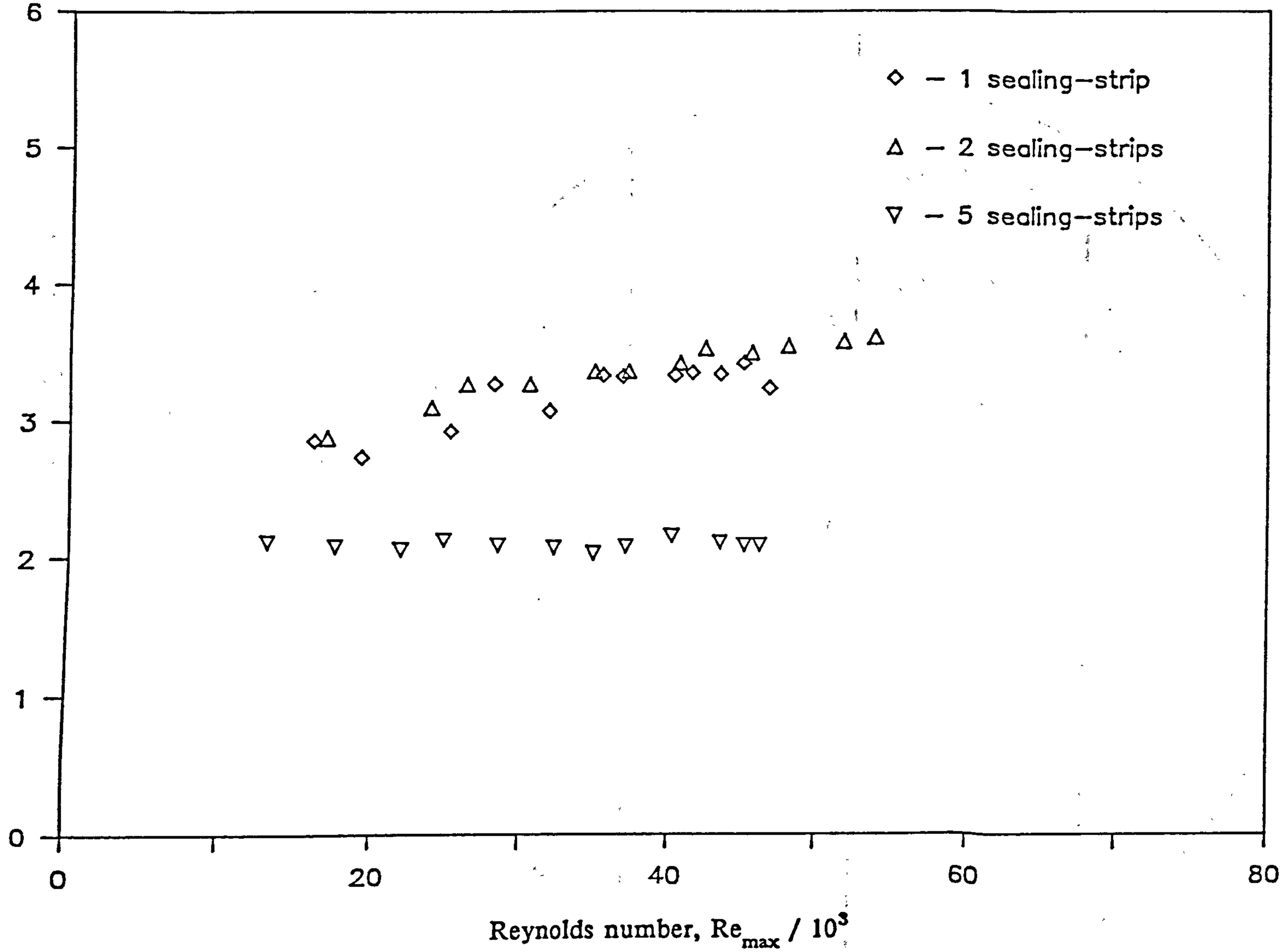

Figure 9.16 N_c for the 1.25 in-line square bank with a 1½S bypass and sealing-strips.

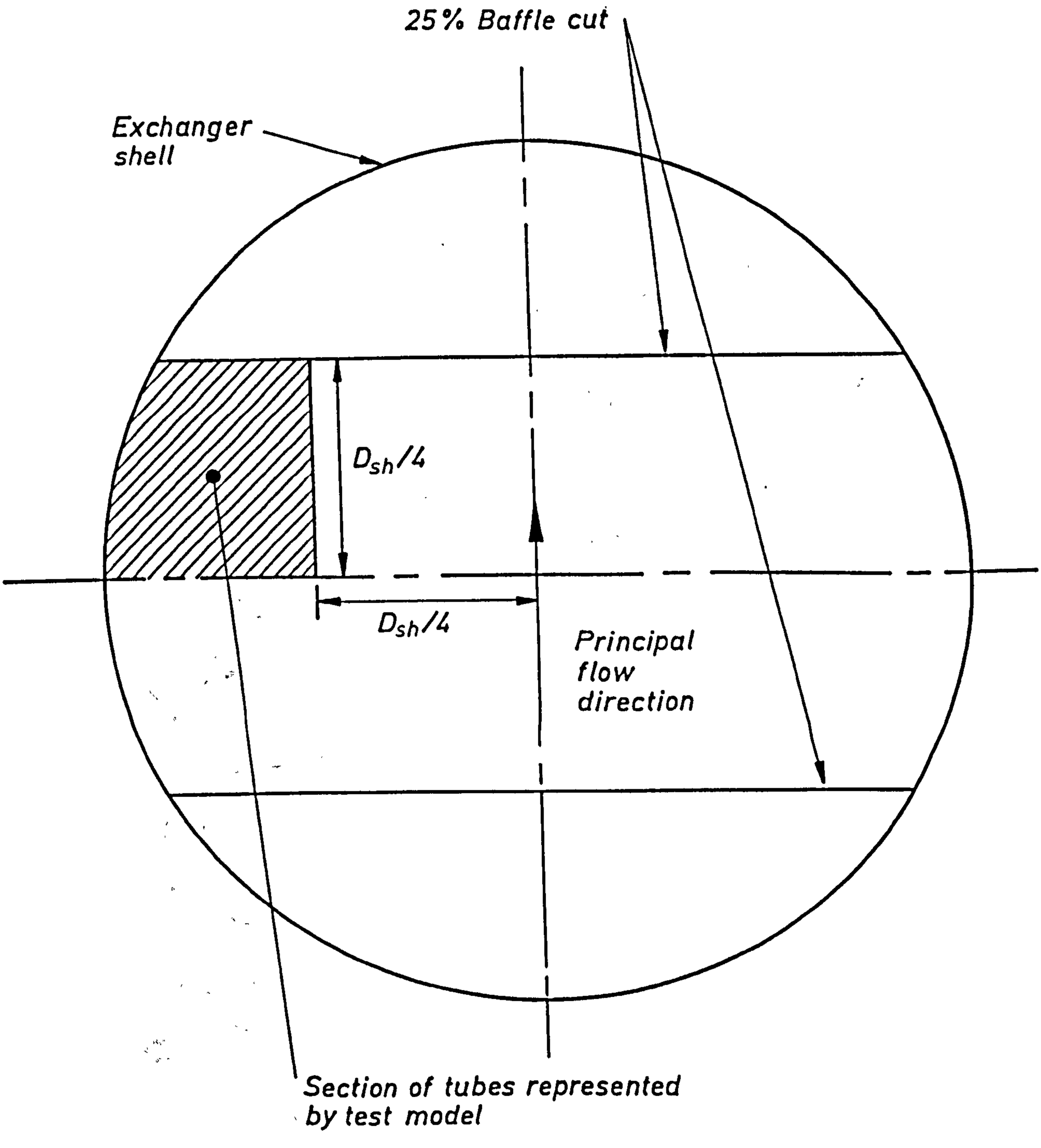

D_{sh} = Shell internal diameter

Figure 10.1 Area of exchanger cross-section represented by model.

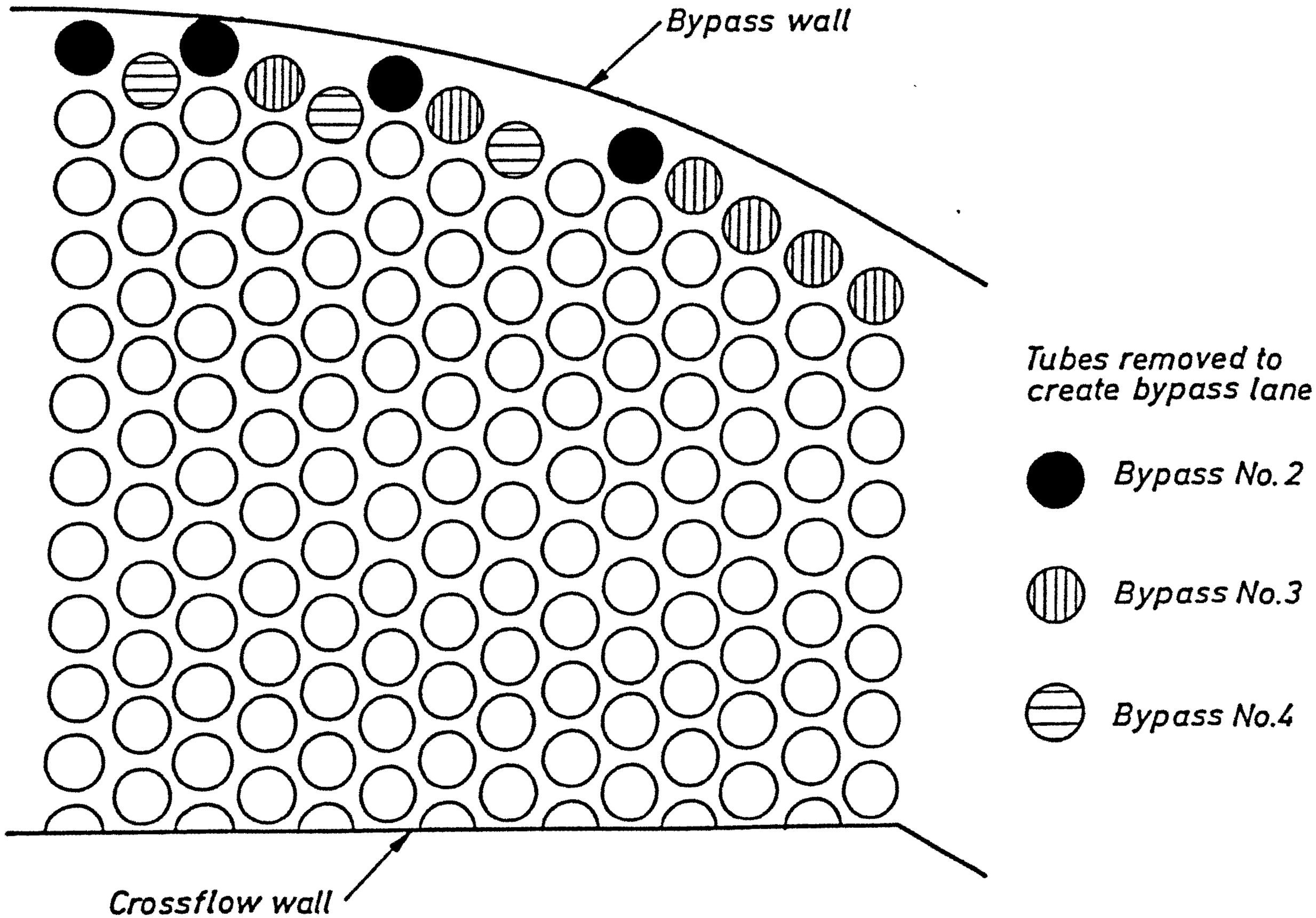

Figure 10.2 Modified test section.

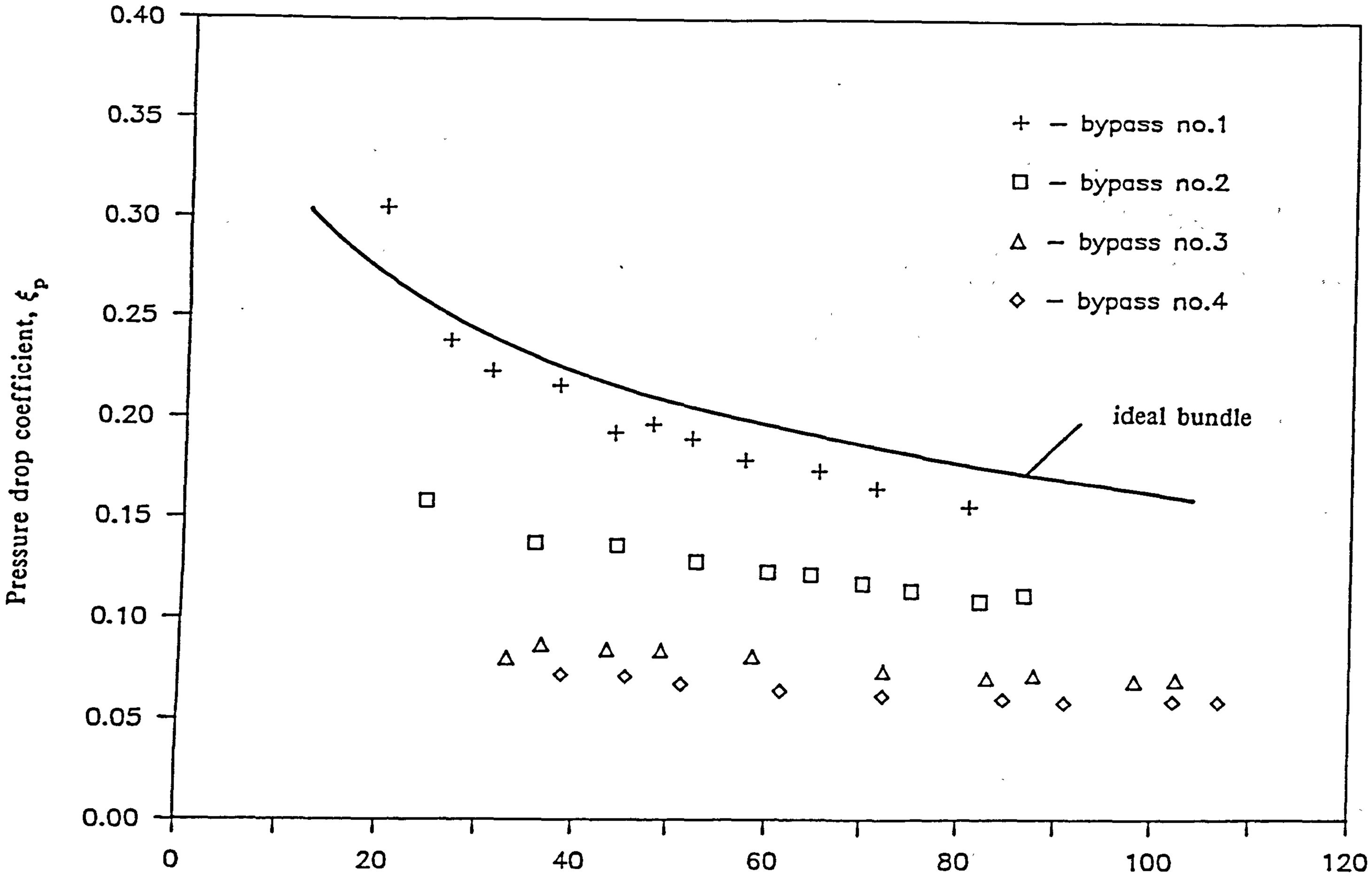

Figure 10.3 Pressure drop coefficients for cylindrical tube bundle.

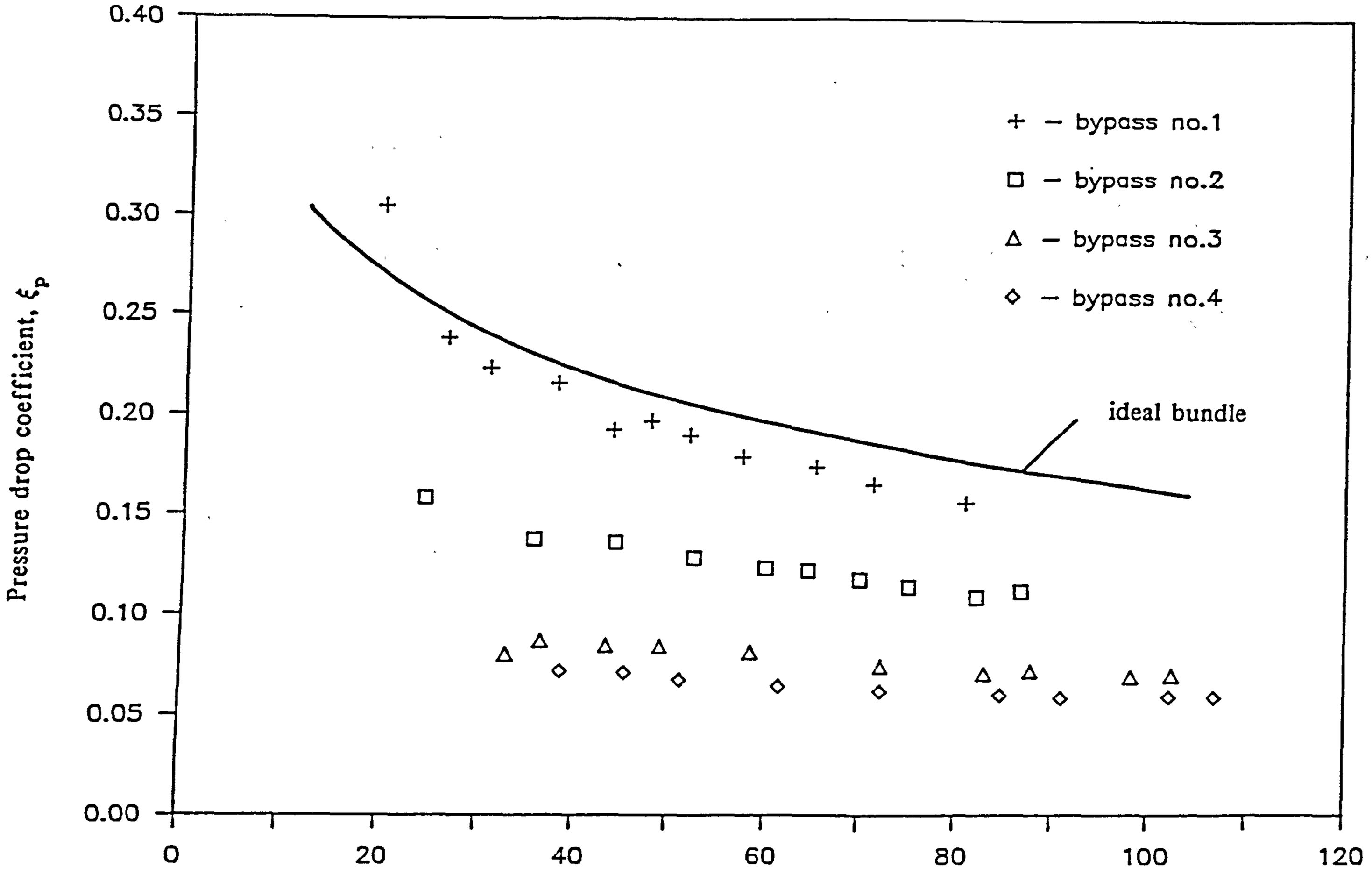

Figure 10.3 Pressure drop coefficients for cylindrical tube bundle.

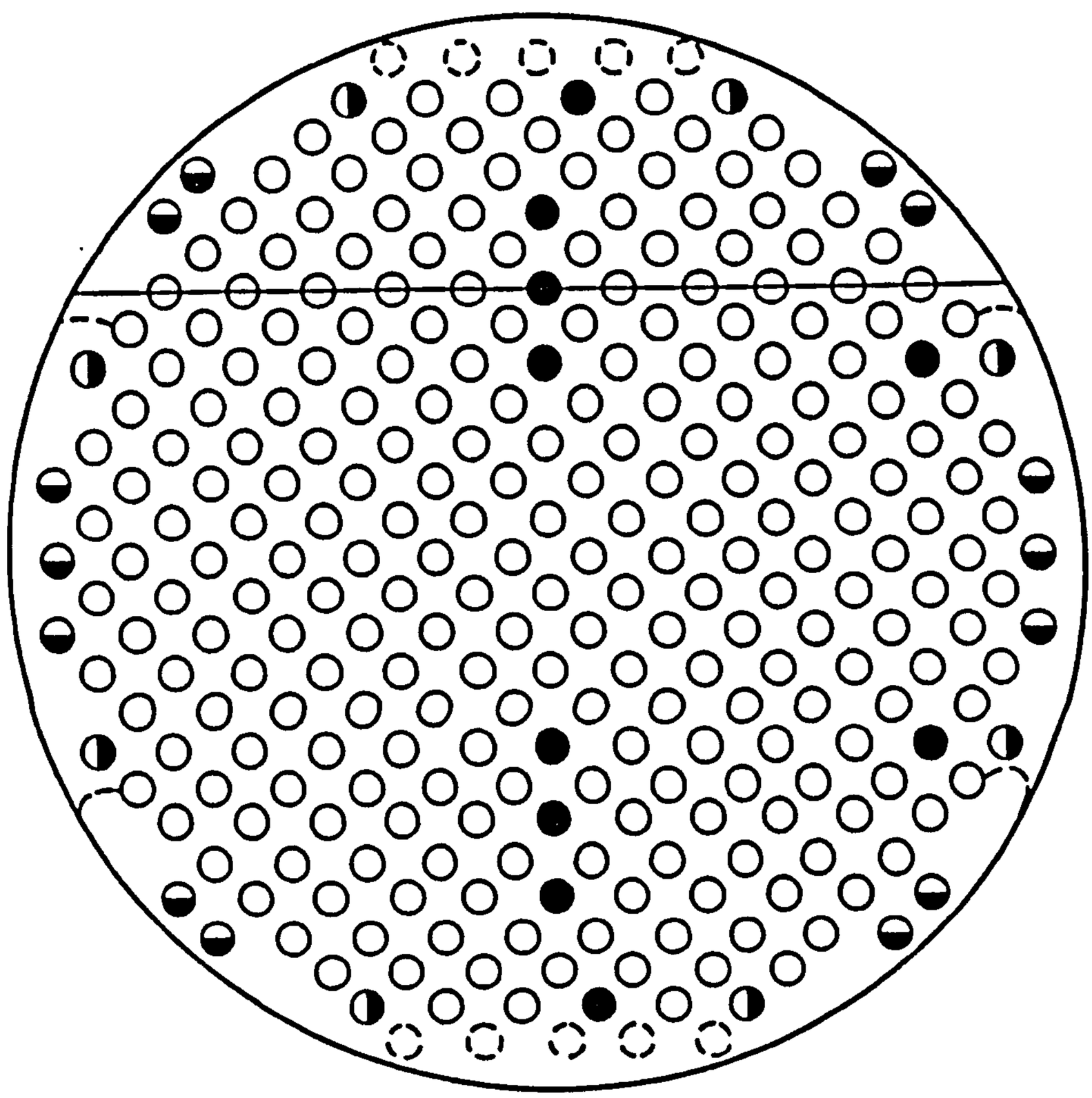

Location of sealing- strips, when used

Glass rods

Tie rods

Steel tubes, with pressure tappings

Rods removed from bundle to increase entrance area

Rods removed to create large bypass

Figure 11.1 Cross-section of tube bundle in flow visualisation rig.

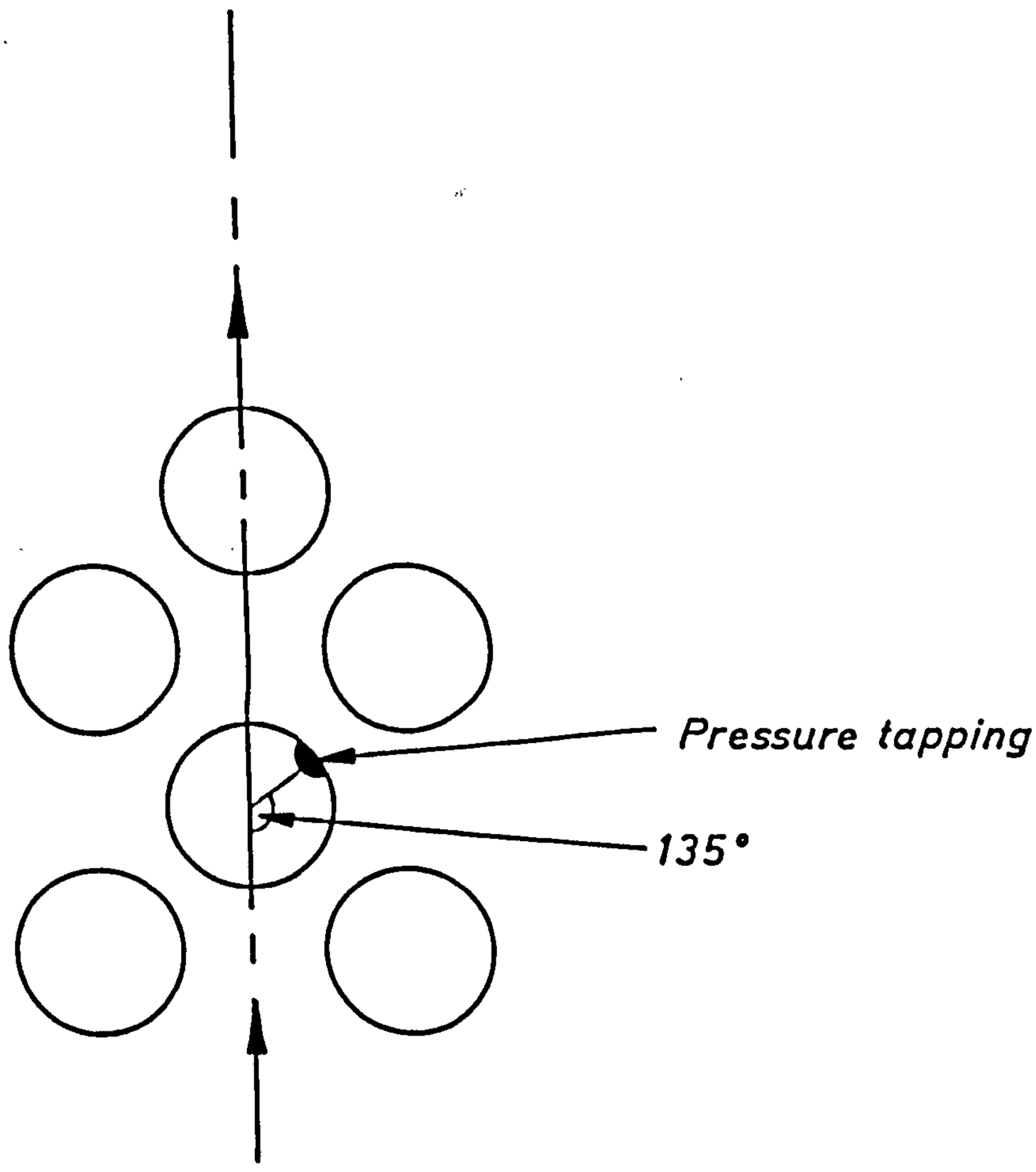

Figure 11.2 Pressure tappings.

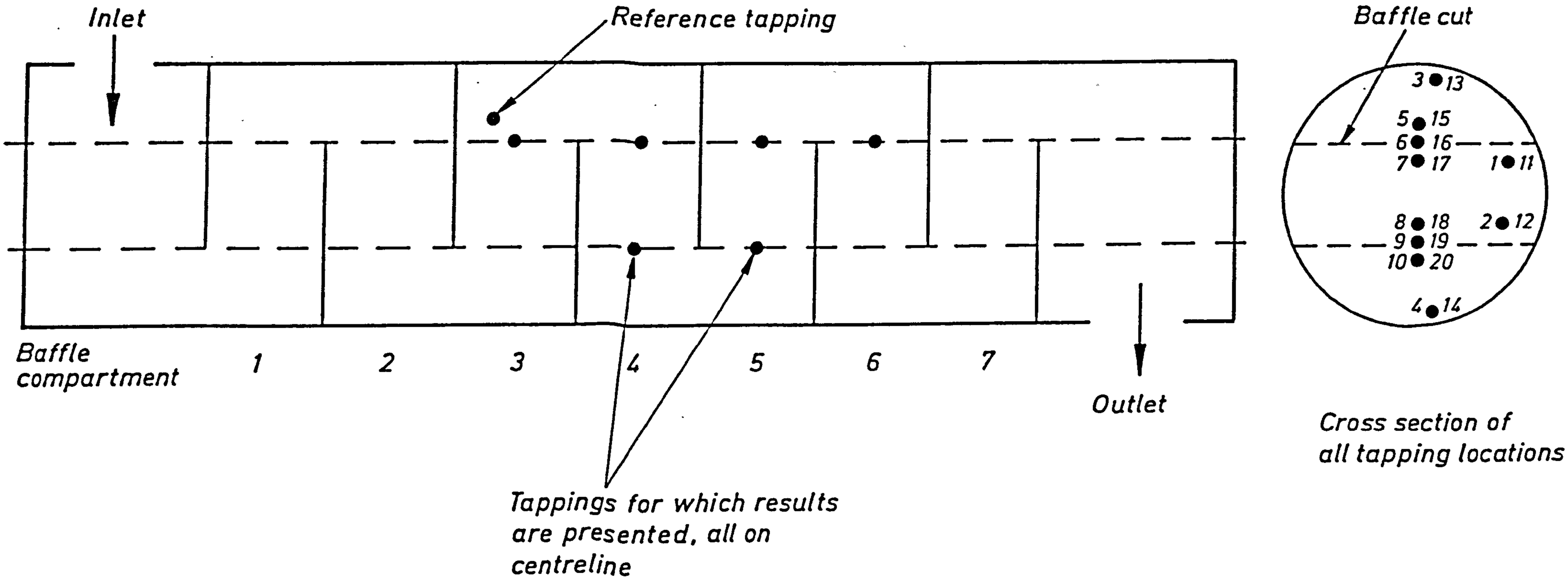

Figure 11.3 Location of pressure tappings.

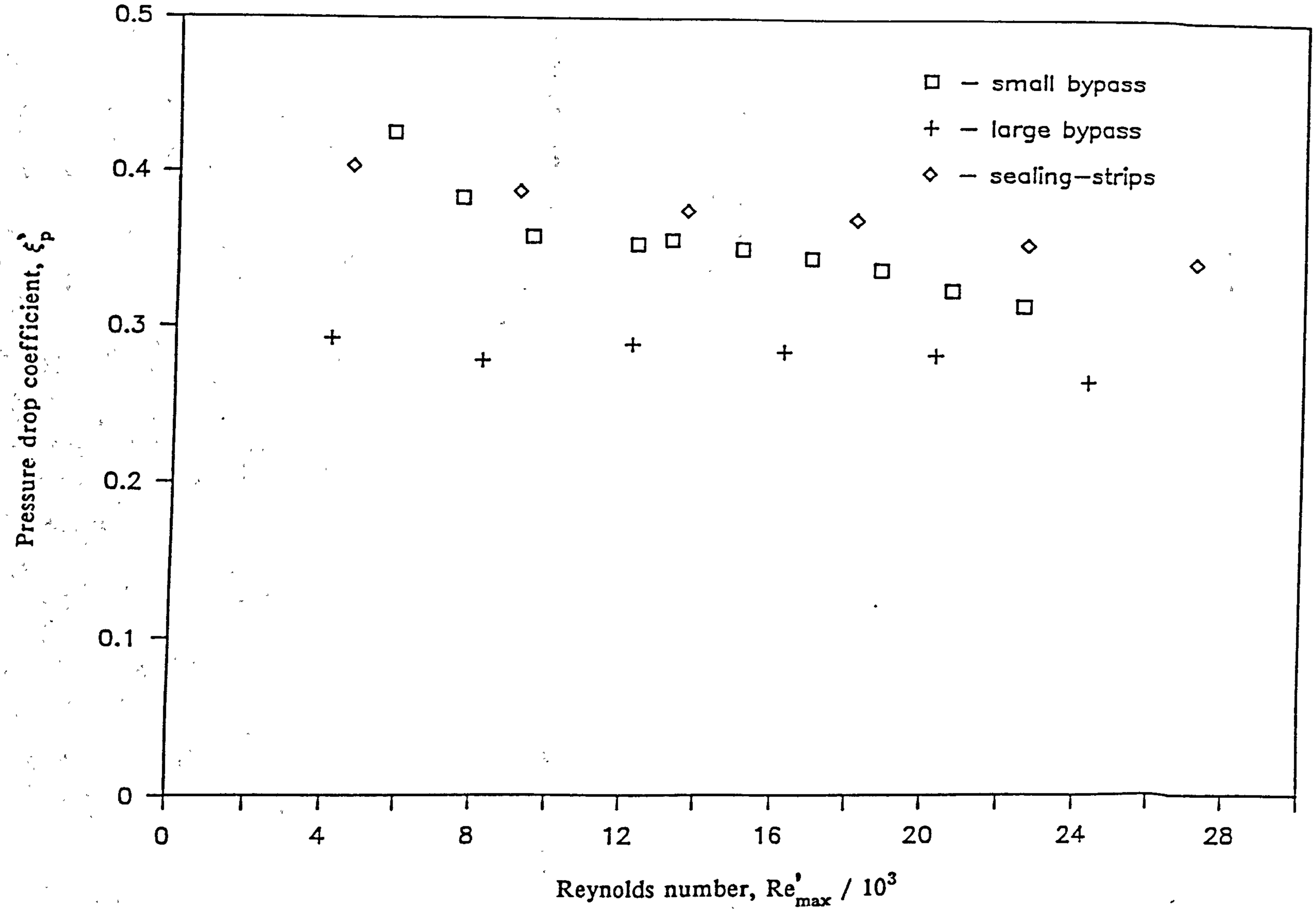

Figure 11.4 Pressure drop coefficients for flow visualisation rig.

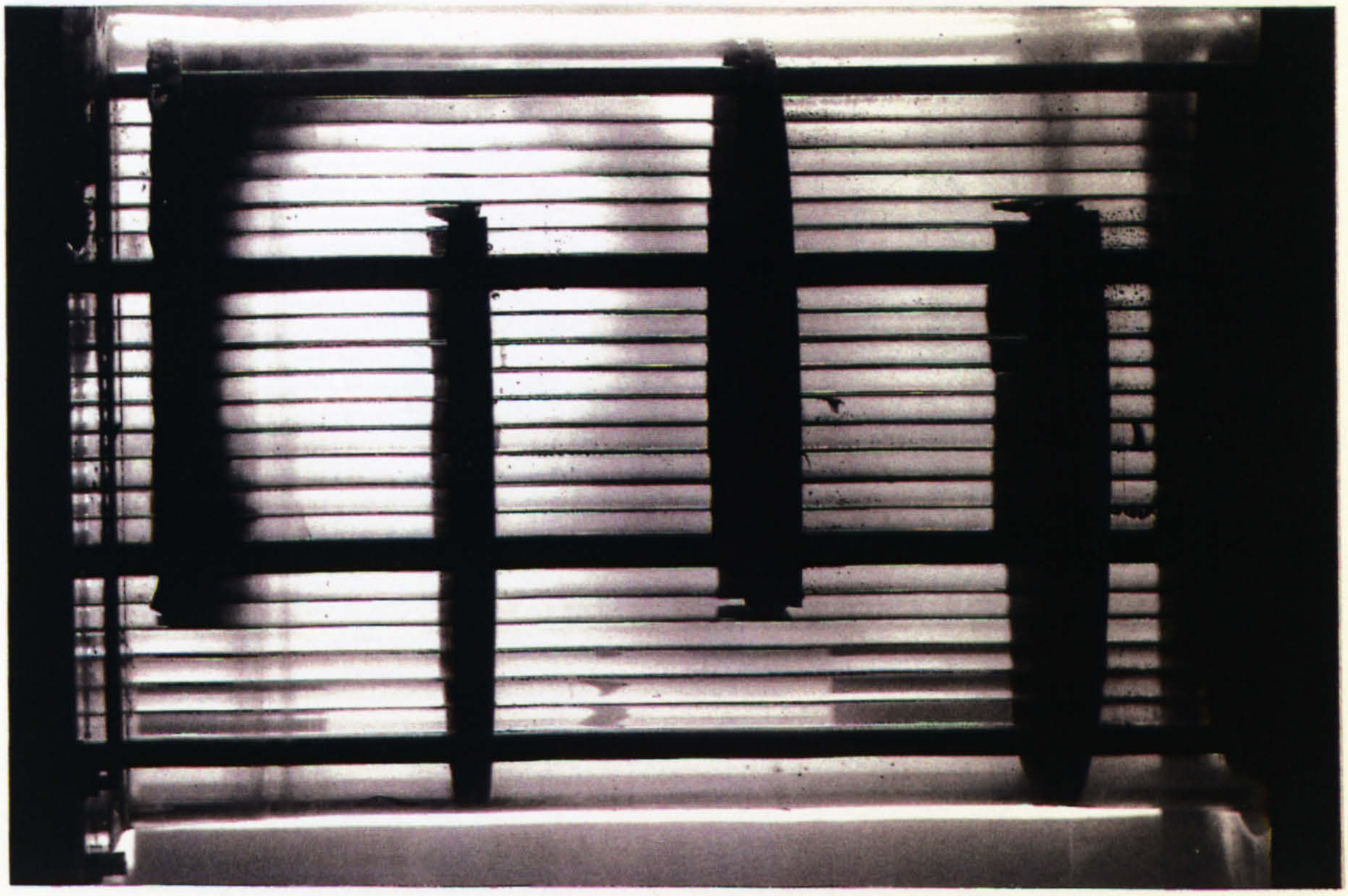

Figure 11.5 Trace produced by dye released from 10% across the baffle space at the shell centreline (exchanger with a large bypass).

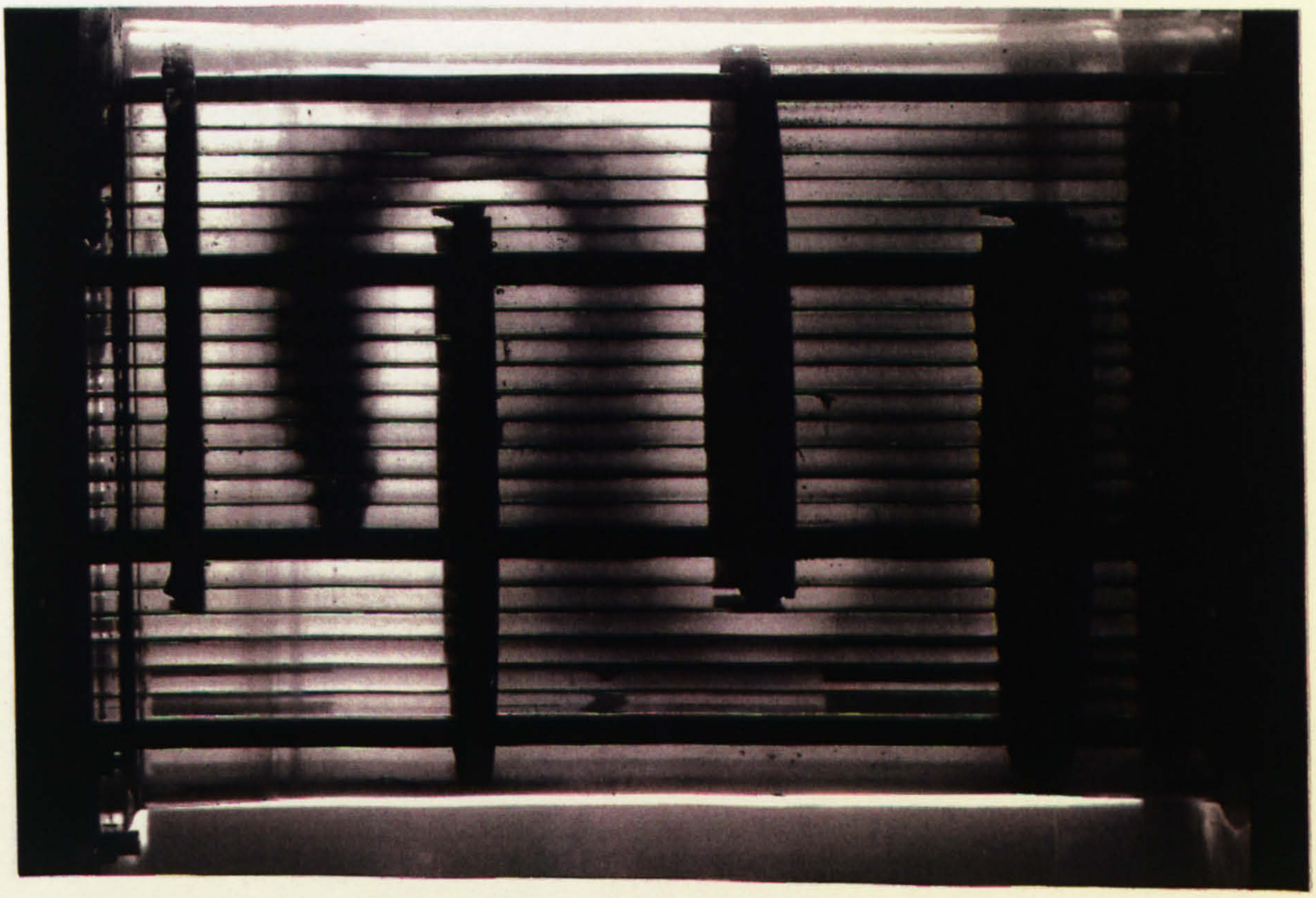

Figure 11.6 Trace produced by dye released from 50% across the baffle space at the shell centreline (exchanger with a large bypass).

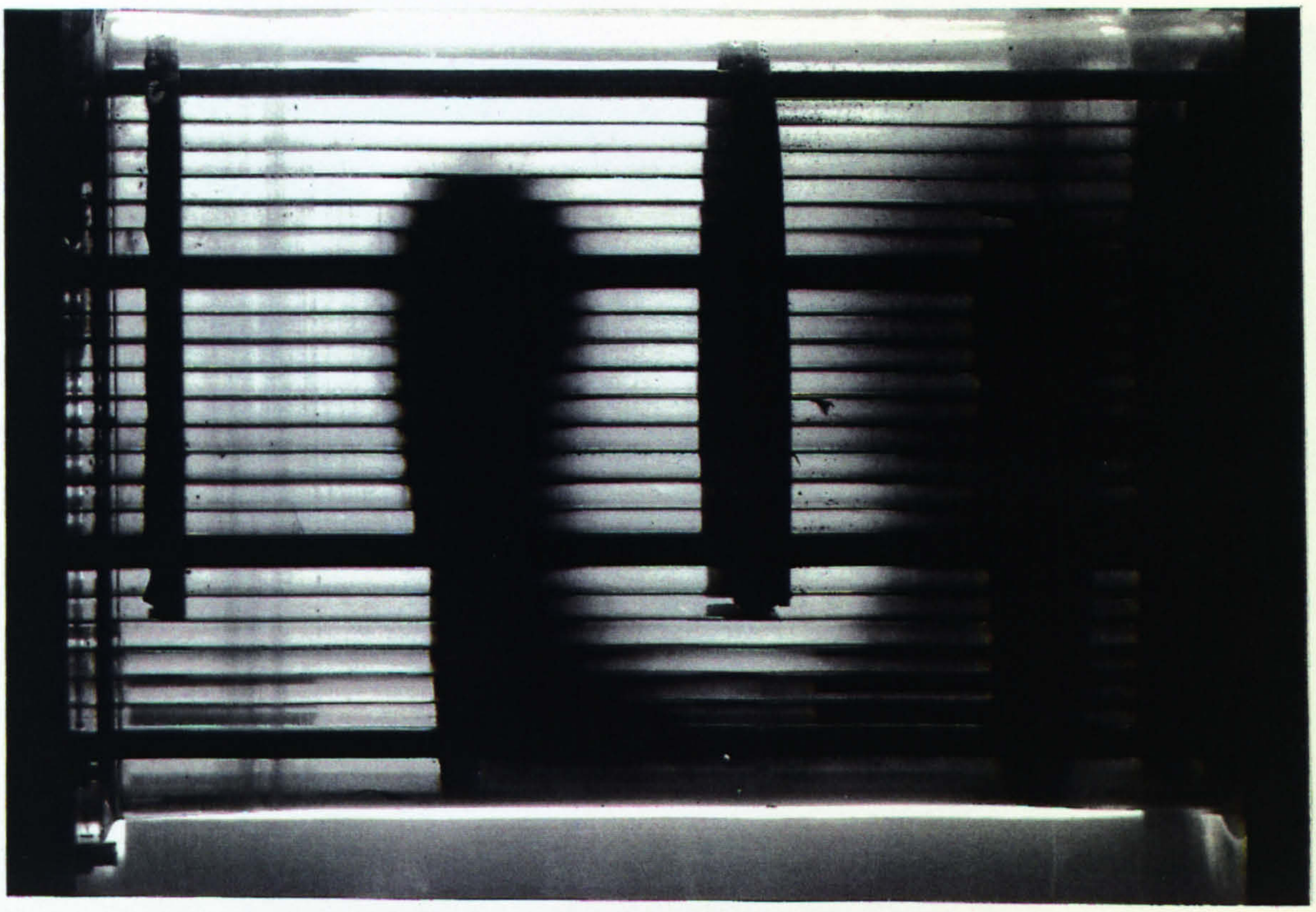

Figure 11.7 Trace produced by dye released from 90% across the baffle space at the shell centreline (exchanger with a large bypass).

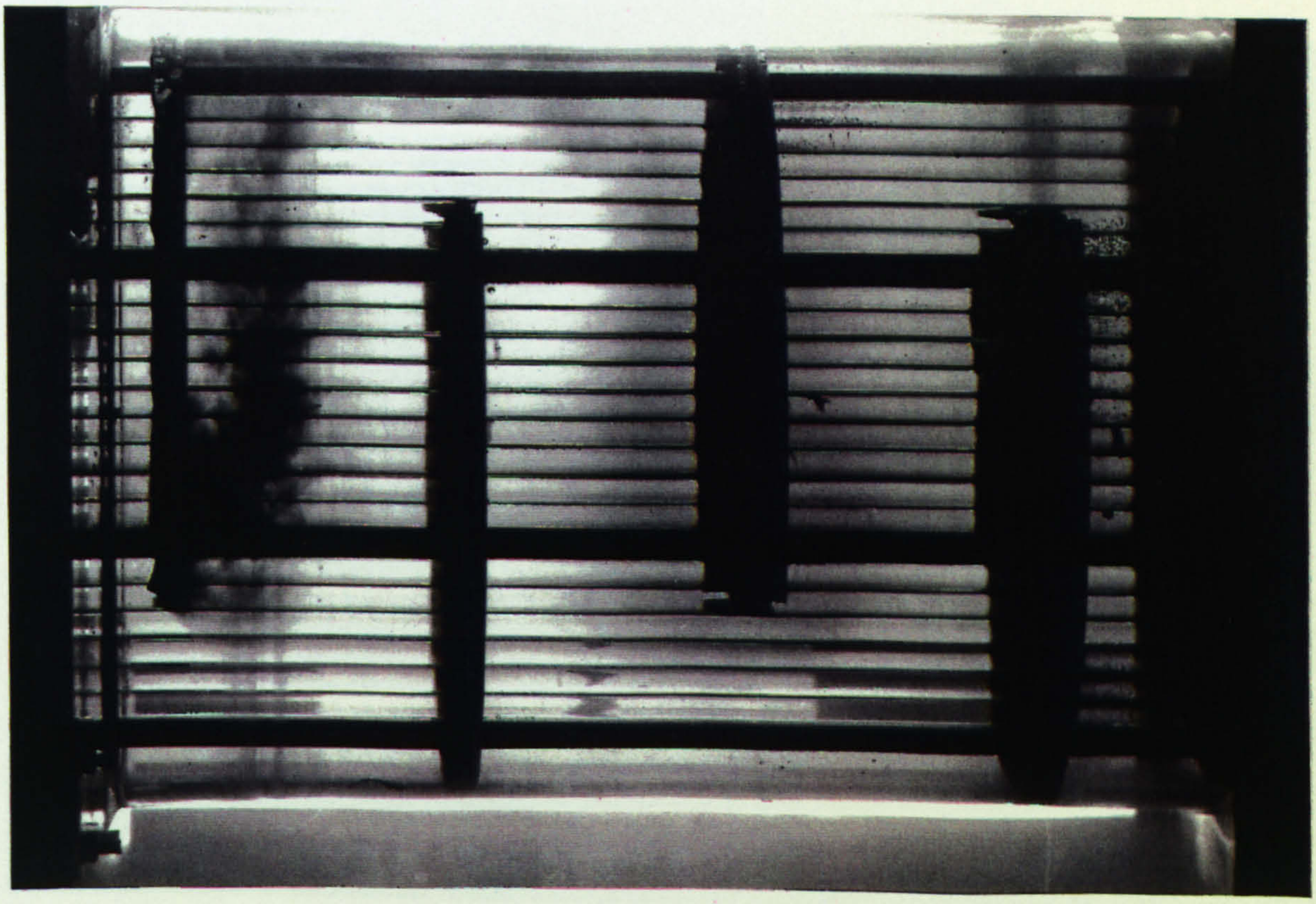

Figure 11.8 Trace produced by dye released from 10% across the baffle space at the outer edge of the tube bundle (exchanger with a large bypass).

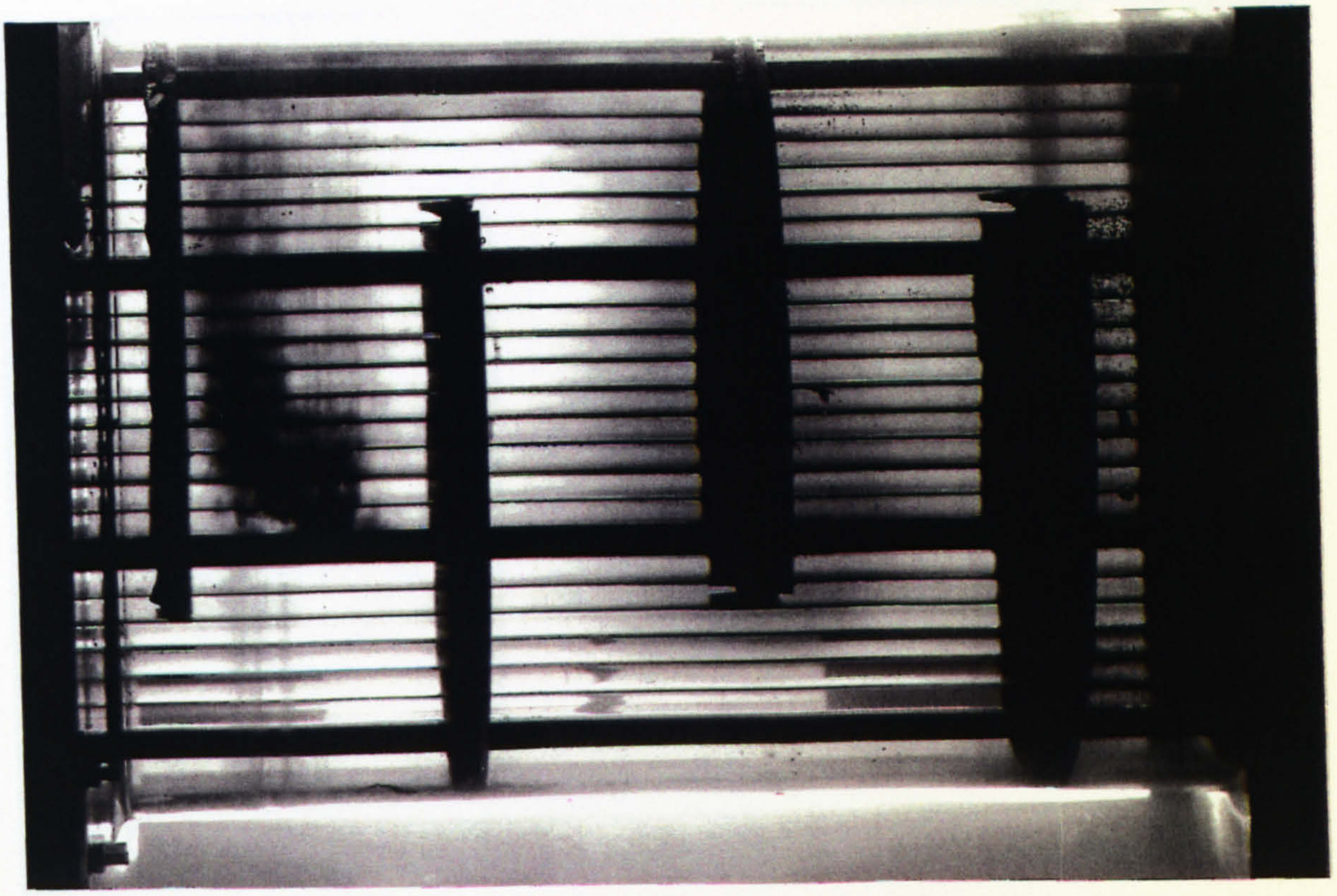

Figure 11.9 Trace produced by dye released from 50% across the baffle space at the outer edge of the tube bundle (exchanger with a large bypass).

Figure 11.10 Trace produced by dye released from 90% across the baffle space at the outer edge of the tube bundle (exchanger with a large bypass).

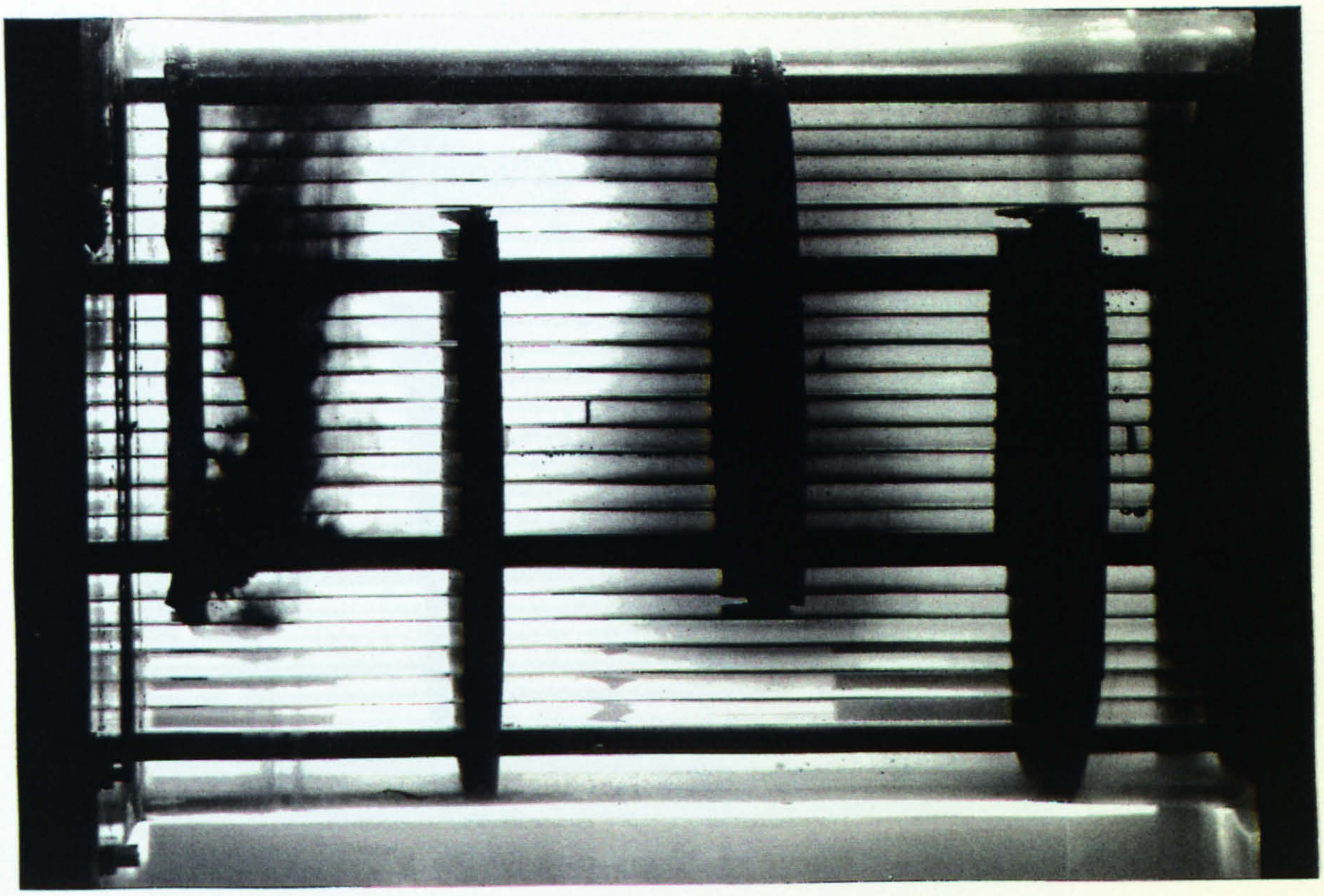

Figure 11.11 Trace produced by dye released from 10% across the baffle space within the bypass lane (exchanger with a large bypass).

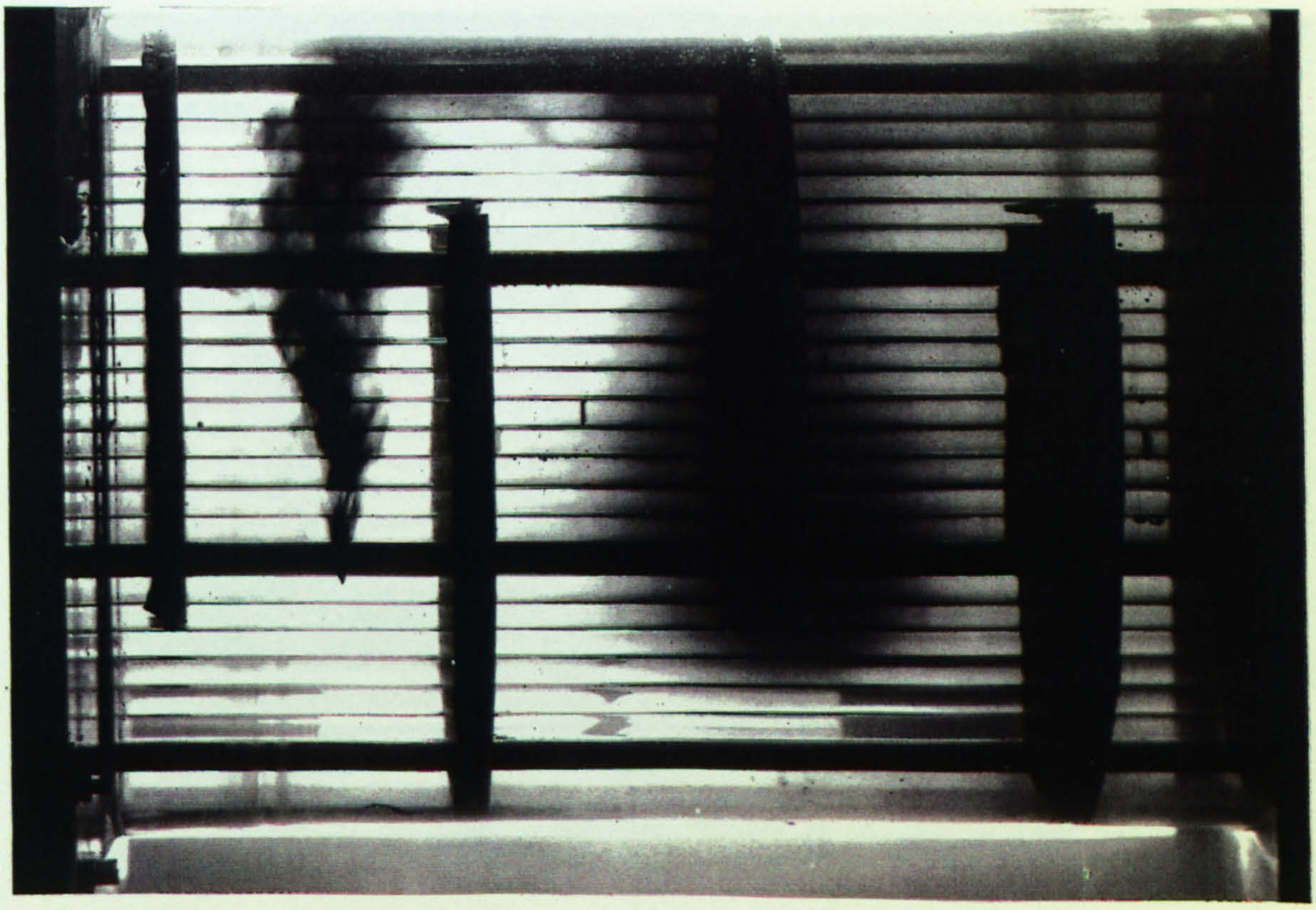

Figure 11.12 Trace produced by dye released from 50% across the baffle space within the bypass lane (exchanger with a large bypass).

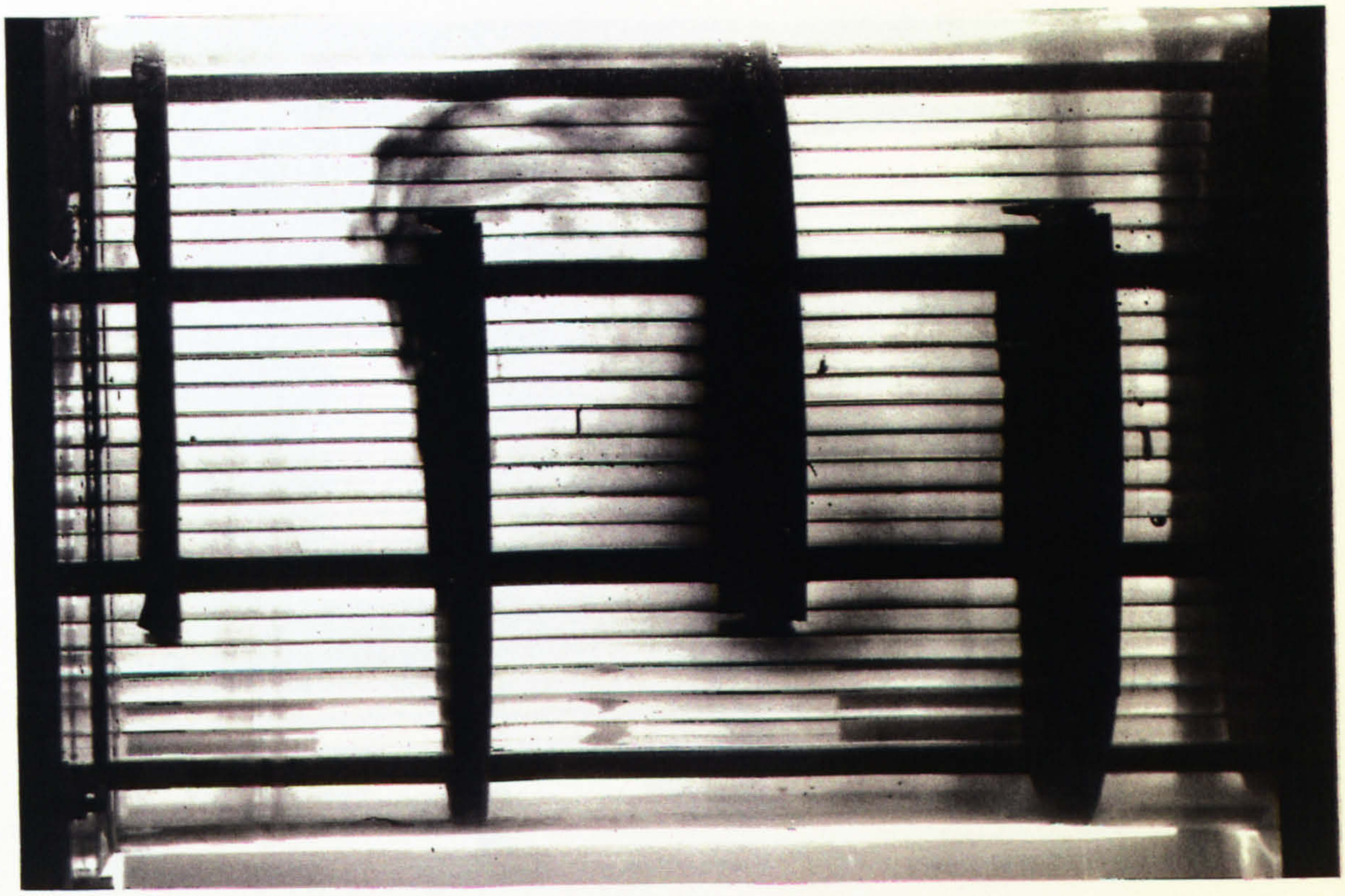

Figure 11.13 Trace produced by dye released from 90% across the baffle space within the bypass lane (exchanger with a large bypass).

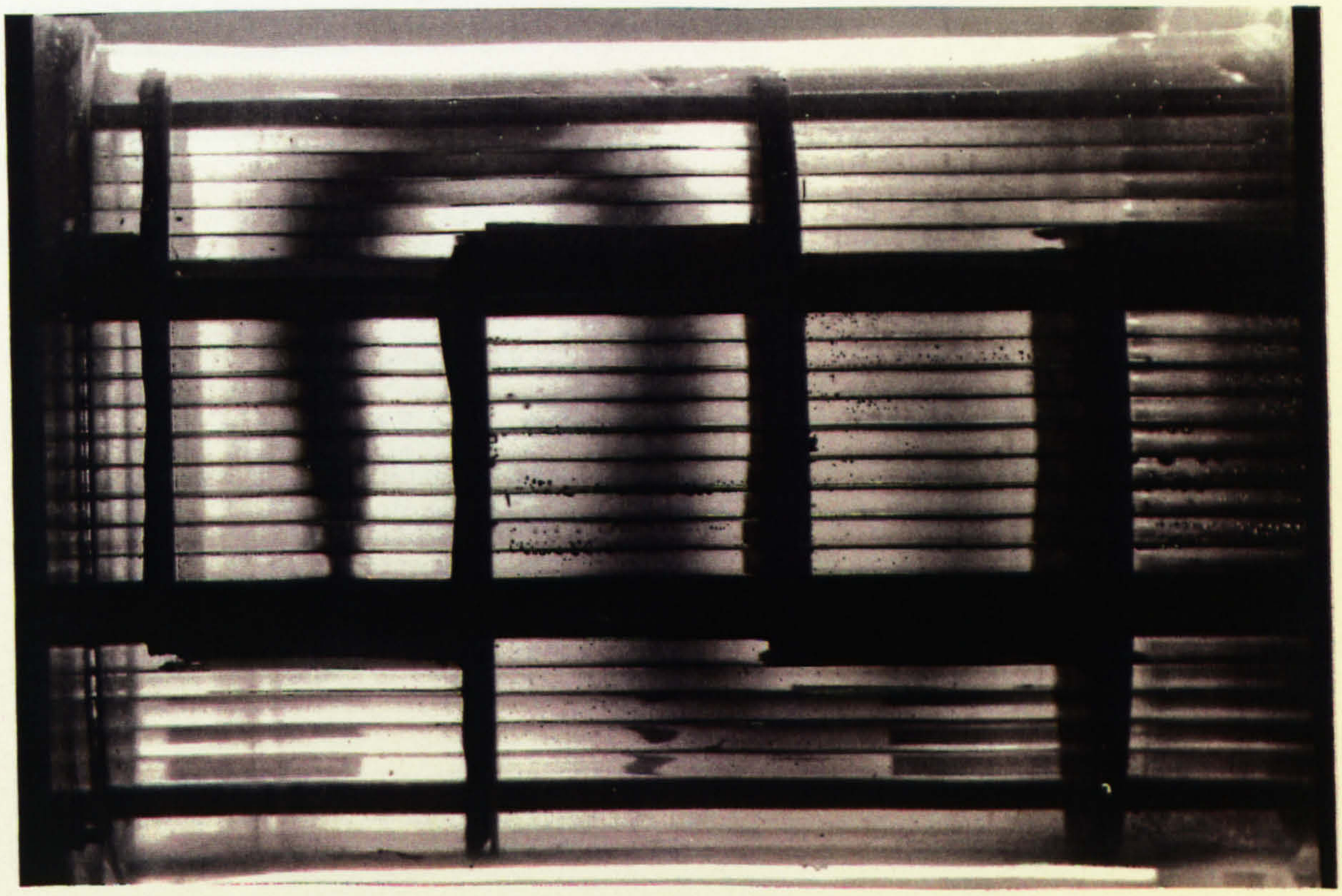

Figure 11.14 Trace produced by dye released from 50% across the baffle space at the shell centreline (exchanger with a large bypass blocked by sealing-strips).

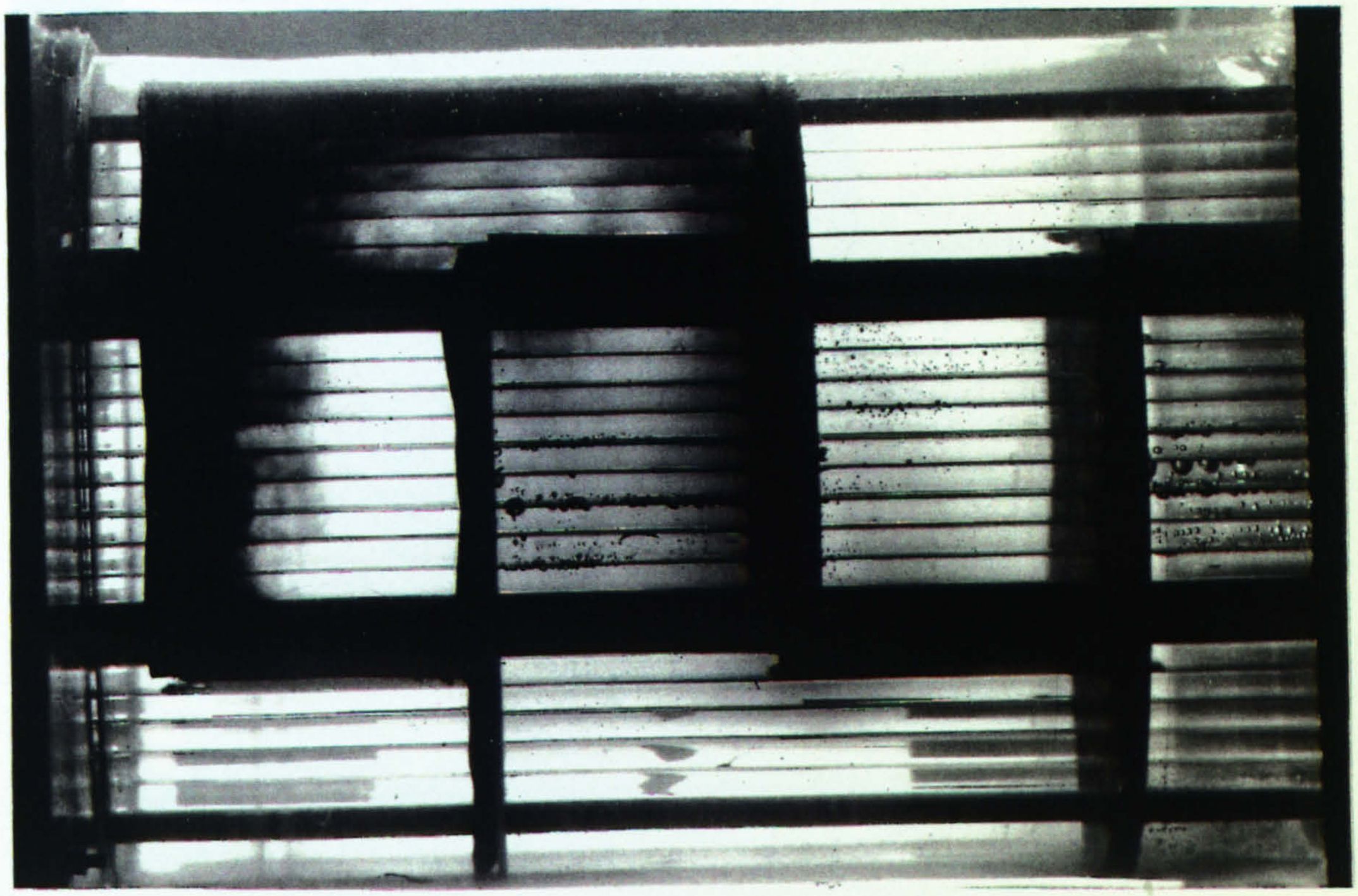

Figure 11.15 Trace produced by dye released from 10% across the baffle space at the outer edge of the tube bundle (exchanger with a large bypass blocked by sealing-strips).

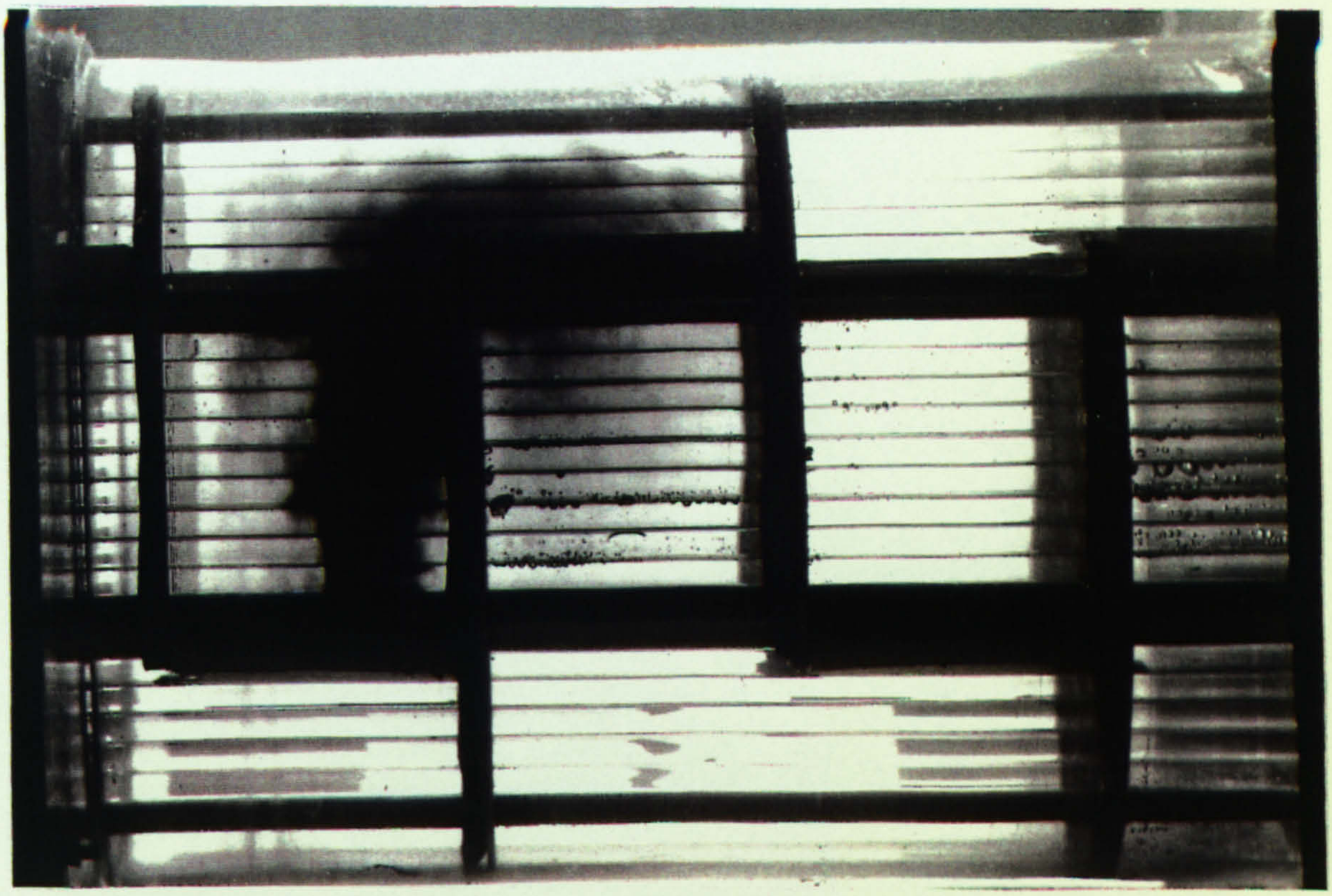

Figure 11.16 Trace produced by dye released from 50% across the baffle space at the outer edge of the tube bundle (exchanger with a large bypass blocked by sealing-strips).

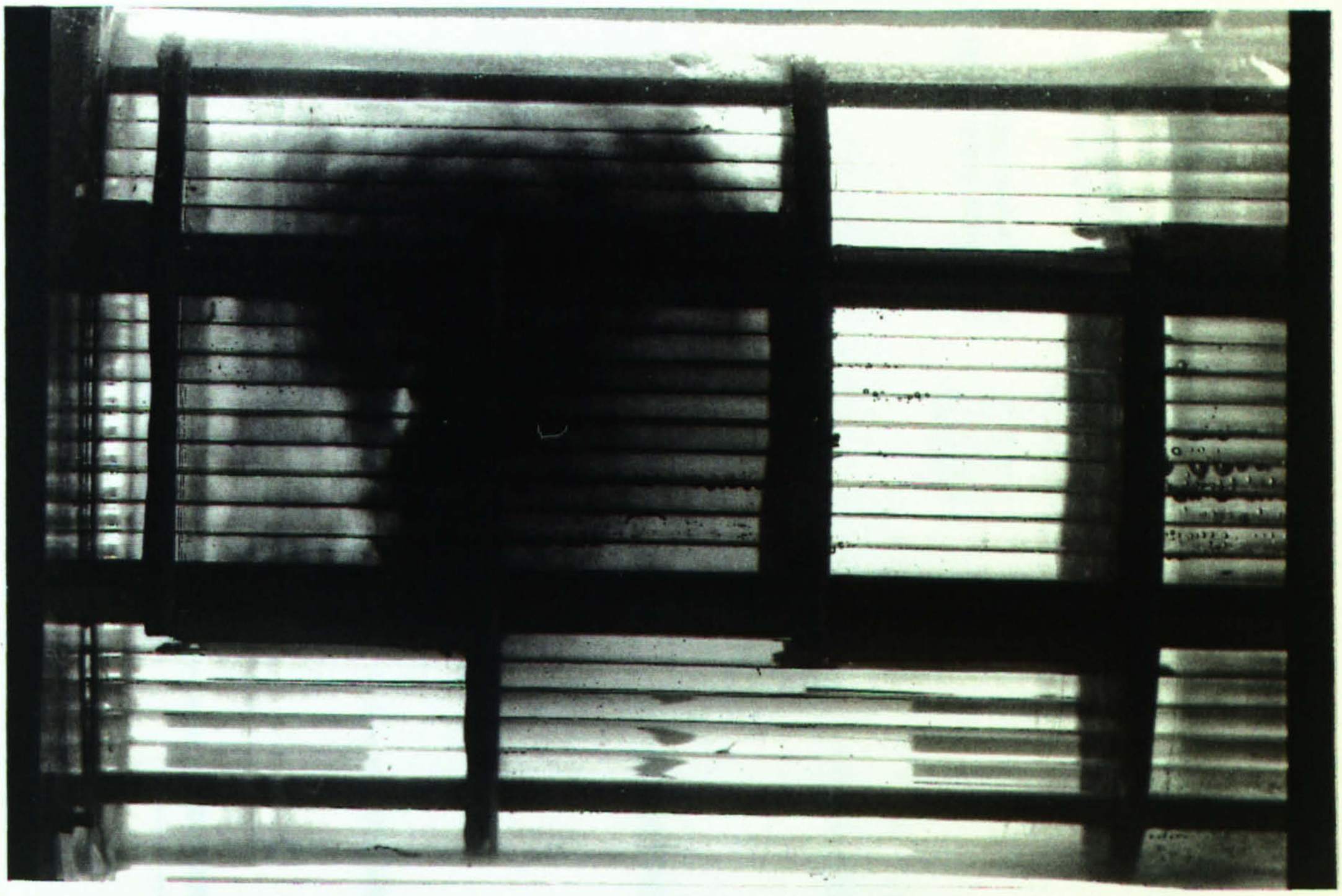

Figure 11.17 Trace produced by dye released from 90% across the baffle space at the outer edge of the tube bundle (exchanger with a large bypass blocked by sealing-strips).

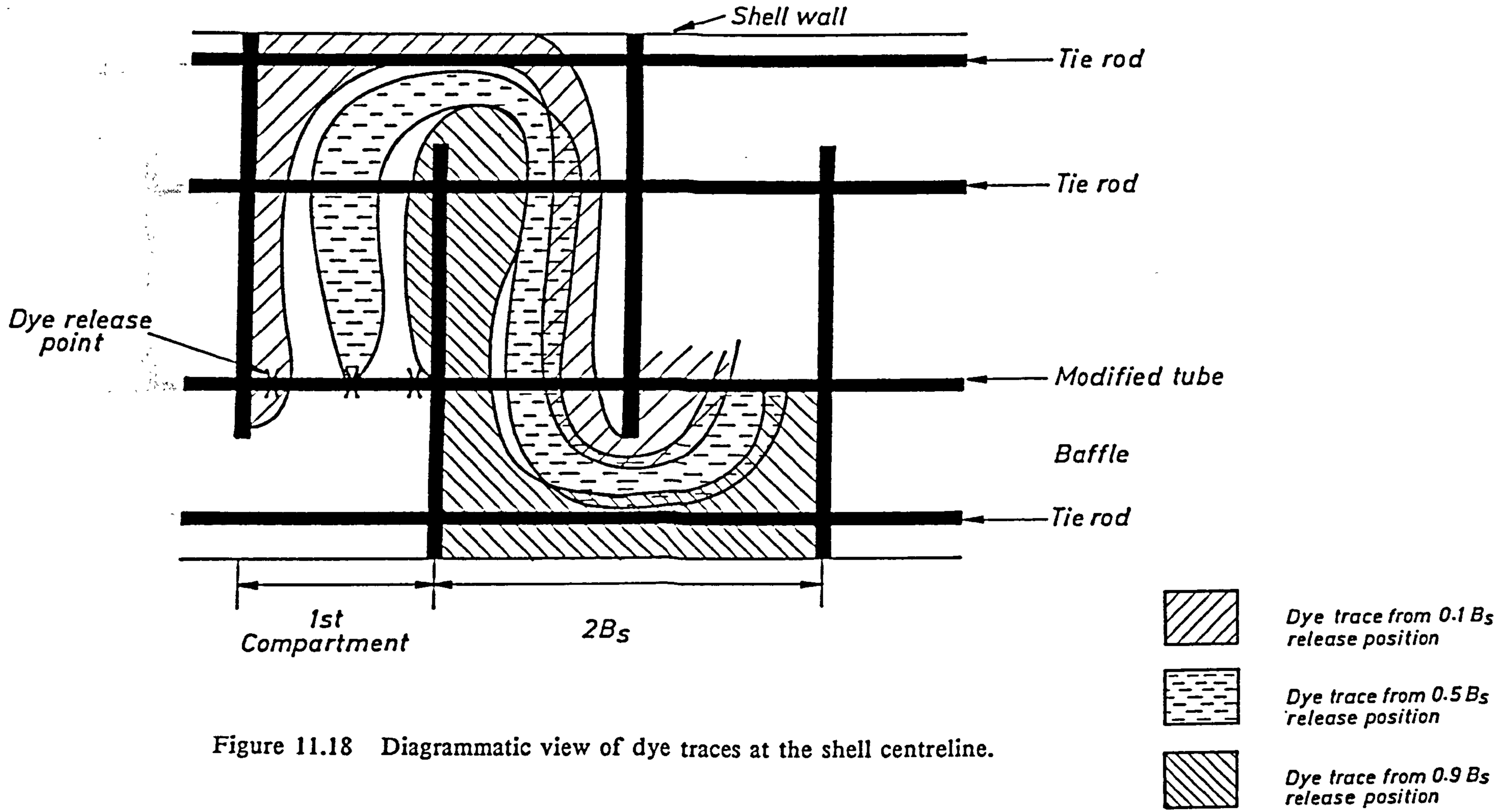

Figure 11.18 Diagrammatic view of dye traces at the shell centreline.

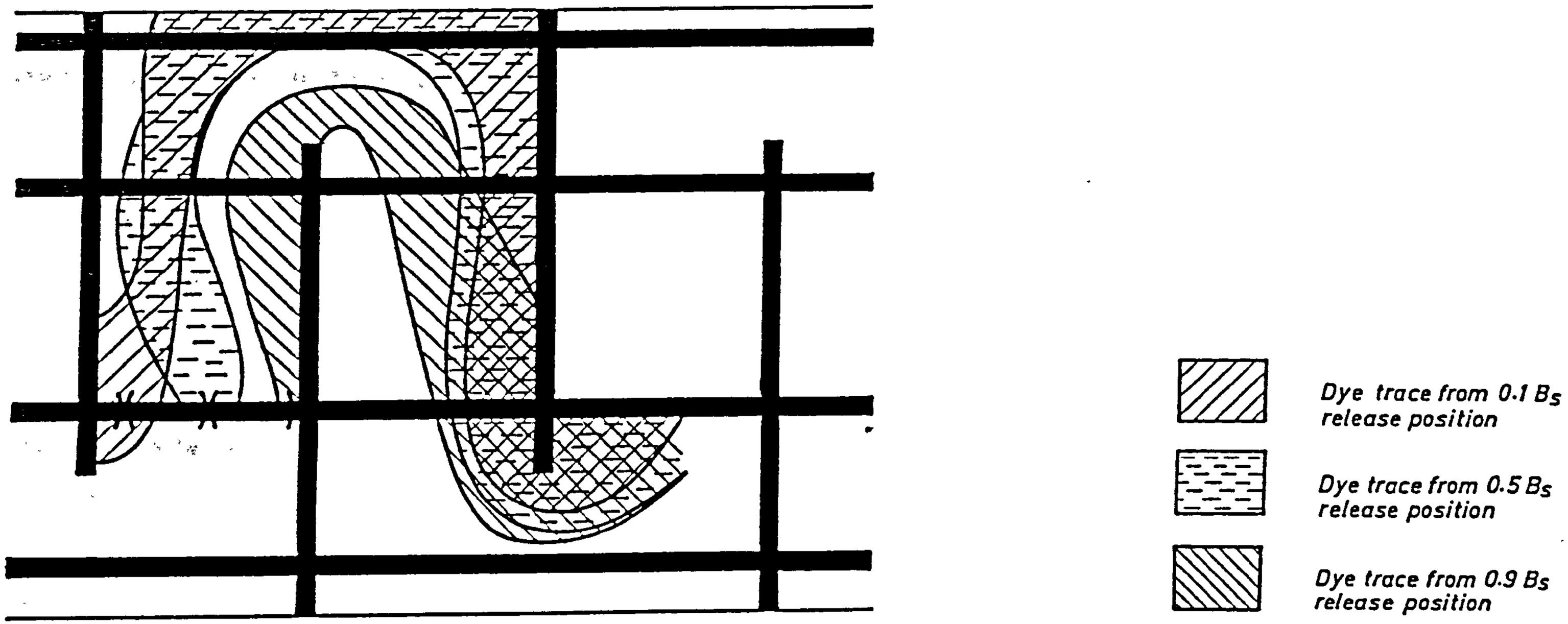

Figure 11.19 Diagrammatic view of dye traces at the outer edge of the tube bundle.

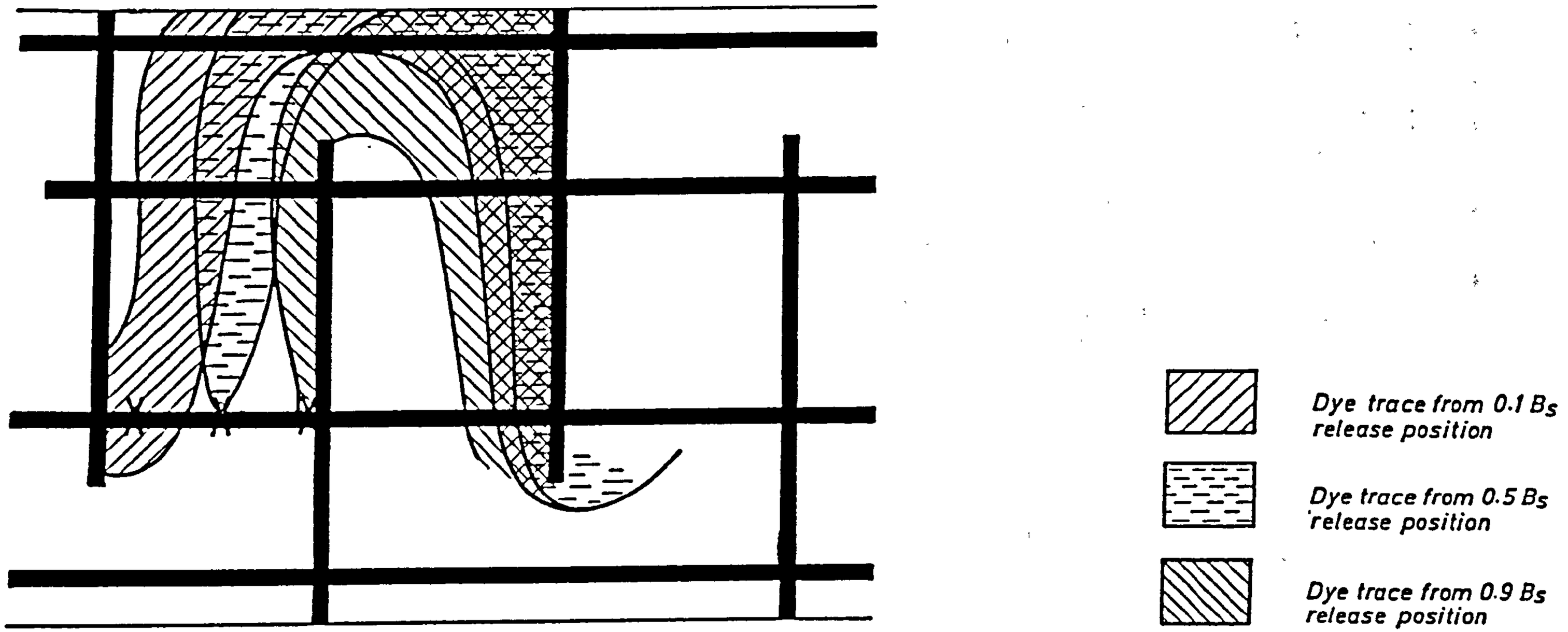

Figure 11.20 Diagrammatic view of dye traces within the bypass lane.

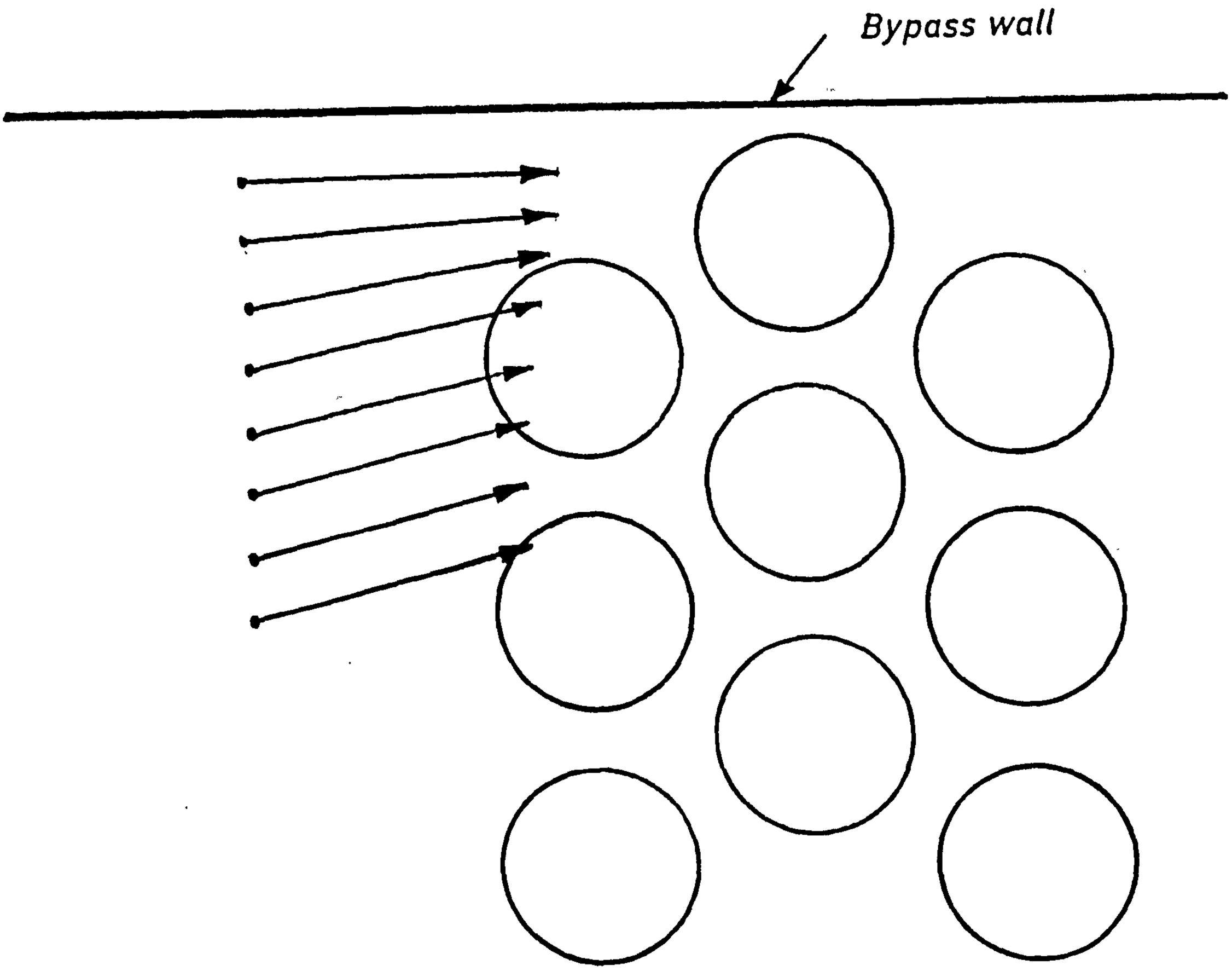

Figure C.1 Bypass inlet of ¼T bypass, 1.25 equilateral-triangle bank.

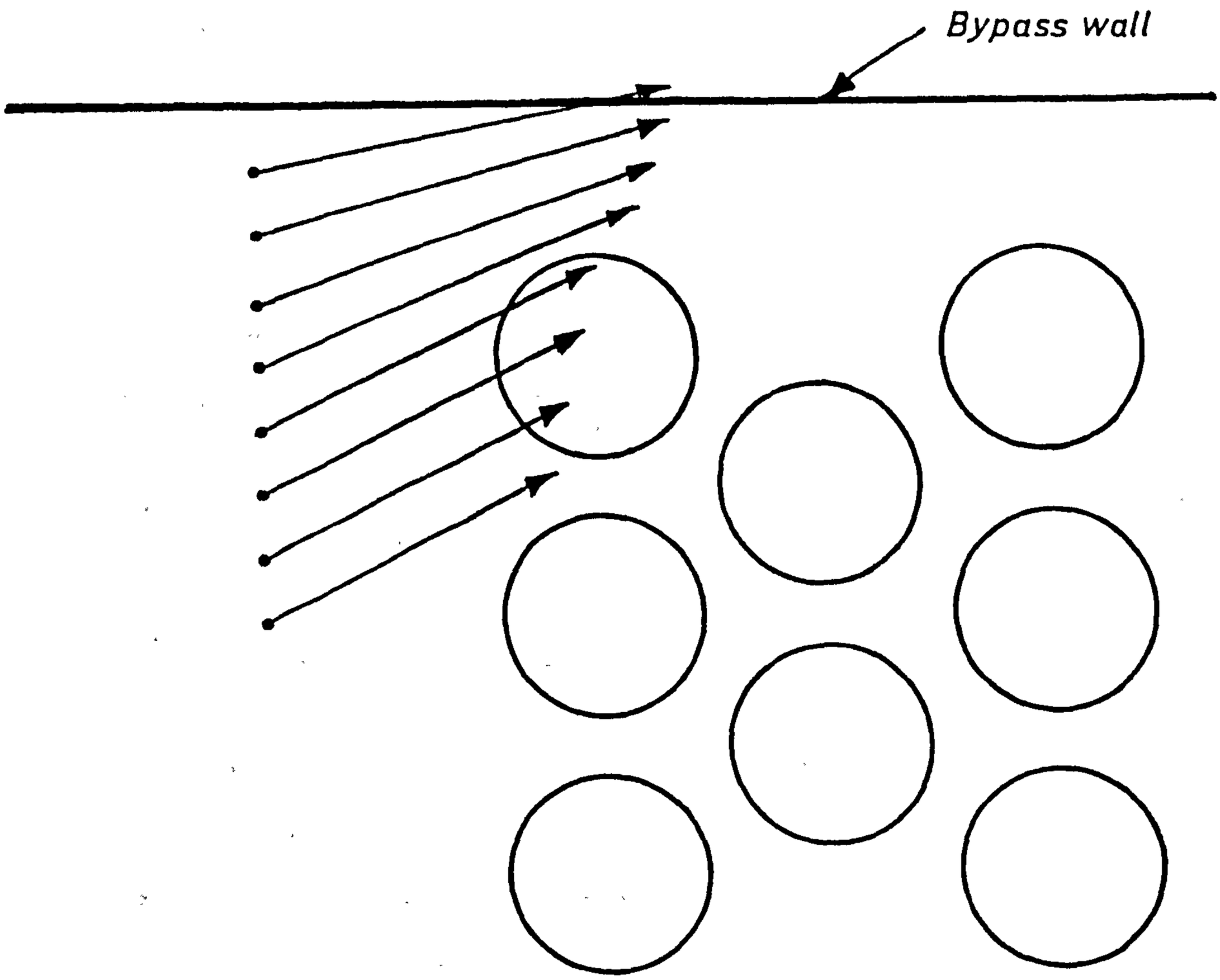

Figure C.2 Bypass inlet of 1½T bypass, 1.25 equilateral-triangle bank.

REFERENCES

Achenbach, E. (1971) *"Influence of surface roughness on the crossflow around a circular cylinder."* J. Fluid Mech., 46, pt. 2, pp 321-335.

Achenbach, E. (1971) *"Influence of surface roughness on the flow through staggered tube banks."* Wärme-und Stoffübertragung, Bd. 4, pp 120-126.

Achenbach, E. (1971) *"On the crossflow through in-line tube banks with regard to the effect of surface roughness."* Wärme-und Stoffübertragung, Bd. 4, pp 152-155.

Batham, J. P. (1973) *"Pressure distributions on in-line tube arrays in crossflow."* Int. Symp. Vibration Problems in Industry, 10-12 April, Keswick, England, paper 411.

Bell, K. J. (1960) *"Exchanger design based on the Delaware Research Program."* Petro. Chem. Eng., 32, pp C26-C40.

Bell, K. J. (1963) *"Final report of the co-operative research programme on shell-and-tube heat exchangers."* University of Delaware, Engineering Experimental Station, Bulletin No. 5, USA.

Bell, K. J. (1980) *"Delaware method for shell-side design. Heat exchangers: thermal-hydraulic fundamentals and design."* Nato. Adv. Study Inst., Istanbul, Turkey. Hemisphere Pub. Corp., ISBN-07-033284, pp 581-618.

Bergelin, O. P., Bell, K. J. and Leighton, M. D. (1959) *"Heat transfer and fluid friction during flow across banks of tubes: VII. Bypassing between tube bundle and shell."* Chem. Engng. Symp. Series, 55, No. 29, pp 45-58.

Bergelin, O. P., Brown, G. A. and Doberstein, S. C. (1952) *"Heat transfer and fluid friction during flow across banks of tubes - IV: A study of the transition zone between viscous and turbulent flow."* Trans. ASME, 74, pp 953-960.

Bergelin, O. P., Leighton, M. D., Lafferty, W. L. and Pigford, R. L. (1958) *"Heat transfer and pressure drop during viscous and turbulent flow across baffled and unbaffled tube banks."* University of Delaware, Engineering Experimental Station, Bulletin No. 4, USA.

Boucher, D. F. and Lapple, C. E. (1948) *"Pressure drop across tube banks: A critical comparison of available data and the proposed method of correlation."* Chem. Eng. Prog., 44, pp 117-134.

Bryce, C. A. (1957) *"The effect of tube bundle bypassing on pressure drop and heat transfer in laminar and turbulent regions."* MChE Thesis, University of Delaware, USA.

Butterworth, D. (1978) *"The development of a model for three dimensional flow in tube bundles."* Int. J. Heat Mass Trans., 21, pp 253-256.

Butterworth, D. (1979) *"The correlation of crossflow pressure drop by means of the permeability concept."* UKAEA Harwell Report, AERE-R9435.

Cernik, R. J. (1955) *"Velocity distribution across banks of tubes."* MChE Thesis, University of Delaware, USA.

Cheers, F. (1945) *"Note on wind tunnel contractions."* *Aero. Research Council,* Reports and Memoranda, No. 2137.

Chilton, T. H. and Genereaux, R. P. (1933) *"Pressure drop across tube banks."* Trans. AIChE, 29, pp 161-173.

Destremps, E. A. (1956) *"The effect of tube bundle bypassing on pressure drop and heat transfer in the laminar region."* MChE Thesis, University of Delaware, USA.

Emerson, W. H. (1962) *"Shell-side heat transfer and pressure drop with turbulent flow in segmentally baffled shell-and-tube heat exchangers - a survey"* Nat. Engng. Lab., U.K., Report No. 45.

Engineering Sciences Data Unit (ESDU, 1974) *"Pressure loss during crossflow of fluid with heat transfer over plain tube banks without baffles."* Item No. 74040, 251-9, Regent Street, London.

Engineering Sciences Data Unit (ESDU, 1979) *"Crossflow pressure loss over banks of plain tubes in square and triangular arrays including the effects of flow directions."* Item No. 79034, 251-9, Regent Street, London.

Fritzsch, A. F. (1951) *"Discussion of Tinker's paper."* Gen. Discussion Heat Trans., I.Mech.E. and ASME, pp 217-219.

George, P. T. (1967) *"Crossflow pressure loss characteristics of closely pitched in-line tube banks at high Reynolds numbers.."* Proc. I.Mech.E., 182, pp 52-57.

Gram, A. J., Mackey, C. O. and Monroe, E. S. (1958) *"Convection heat transfer and pressure drop of air flowing across in-line tube banks. (II - correlation of data for ten-row-deep tube banks)."* Trans. ASME, 80, pp 25-35.

Grant, I. D. R., Finlay, I. C. and Harris, D. (1974) *"Flow and pressure drop during vertically upward 2-phase flow past a tube bundle."* I.Ch.E. Symp. No. 38, April, University of Strathclyde.

Grimison, E. D. (1937) *"Correlation of new data on flow resistances and heat transfer for crossflow of gases over tube banks."* Trans. ASME, 59, pp 583-594.

Gunter, A. Y. and Shaw, W. A. (1945) *"A general correlation of friction factors for various types of surfaces in crossflow."* Trans. ASME, 65, pp 643-660.

Heat Exchanger Design Handbook (HEDH, 1983) *Part 3: "Thermal and hydraulic design of heat exchangers."* Hemisphere Pub. Corp.

Huge, E. C. (1937) *"Experimental investigation of the effects of equipment size on convection of gases over tube banks."* Trans. ASME, 59, pp 573-581.

Jakob, M. (1938) *Discussion of Pierson, Huge and Grimison papers.* Trans. ASME, 60, pp 384-386.

Kays, W. M. and London, A. L. (1955) *"Compact heat exchangers."* The National Press, Palo Alto, California.

Kern, D. Q. (1950) *"Process heat transfer."* McGraw-Hill, New York.

Lee, N. K. (1981) *"Simulation of condenser pressure losses by porous tubes with suction."* Ph.D. Thesis, University of Bristol.

Lee, N. K., Mayhew, Y. R. and Hollingsworth, M. A. (1983) *"Effect of pitch-diameter ratio and bypass lanes on pressure loss in condenser tube banks."* Condensers: Theory and Practice, I.Chem.E. Symp. Ser., No. 75, pp 323-341, Pergamon.

Monrad, C. C. (1932) *"Heat transmission in convection sections of pipe stills."* Ind. Eng. Chem., 24, pp 505-9.

Murray, P. W. (1988) *"Flow and pressure drop on the shell-side of cylindrical heat exchangers."* Ph.D. Thesis, University of Aston in Birmingham.

Murray, P. W., Martin, D. J. and Haseler, L. E. (1988) *"Flow pattern and pressure drop measurements in a shell-and-tube heat exchanger with bundle bypass."* HTFS research symposium paper 747, AERE-R13151.

Palen, J. W. and Taborek, J. (1969) *"Solution of shell-side flow pressure drop and heat transfer by stream analysis method."* Chem. Eng. Prog. Symp. Ser., 65, No. 92, pp 53-63.

Pearce, M. R. (1973)) *"Noise and vibration in heat exchangers."* D.Phil. Thesis, University of Oxford.

Pierson, O. L. (1937) *"Experimental investigation of the influence of tube arrangement on convection heat transfer and flow resistance in crossflow of gases over tube banks."* Trans. ASME, 59, pp 536-572.

Pigott, R. S. J. (1933) *"The flow of fluids in closed conduits."* Mech. Eng., 55, pp 497-501 and 513.

Prandtl, L. (1904) *"On fluid motions with very small frictions."* Proc. 3rd Int. Math. Cong., Heidelberg.

Reiher, H. (1925)) *"Wärmeübergangströmender Luft an Rohr im Kreuzstrom."* Forschungsarbeiten, V.D.I., Heft 269.

Taborek, J. (1983) *"Shell-and-tube heat exchangers: single phase flow."* Heat Exchanger Design Handbook, Sec. 3.3, Hemisphere Pub. Corp.

TEMA (1978) *"Standard of tubular exchanger manufacturers association."* 5th edition, Tubular Exchanger Manufacturers Association Inc., New York.

Tinker, T. (1948) *"Shell-side characteristics of shell-and-tube heat exchangers."* Trans. ASME, 70, pp 89-116.

Tinker, T. (1958) *"Shell-side characteristics of shell-and-tube heat exchangers - a simplified rating system for commercial heat exchangers."* Trans. ASME, 80, pp 37-52.

Wallis, P. R. and White, C. M. (1938) *"Resistance to flow through nests of tubes."* Engineering, 146, pp 605-607, pp 665-667 and pp 723-725.

Walker, H. W., Lewis, W. K. and McA, W. H. (1927) *"Principles of chemical engineering."* McGraw-Hill, New York.

Whitley, D. L. (1961) *"Calculating heat exchanger shell-side pressure drop."* Chem. Eng. Prog., 57, No. (, pp 59-65.

Zukauskas, A. (1972) *"Heat transfer from tubes in crossflow."* Adv. Heat Trans., 8, pp 93-160.

Zukauskas, A., Poskas, P. S. and Survila, V. J. (1979) *"Hydraulic drag and pattern of air flow in crossflow over different rows of bundles of high Re."* Fluid Mech. - Soviet Research, 8, No. 4, pp 1-16.

Zukauskas, A. and Ulinskas, R. (1983) *"Banks of plain and finned tubes."* Heat Exchanger Design Handbook, Sec. 2.2.4, Hemisphere Pub. Corp.